Development of biomaterial self-assembling based platforms to obtain human cartilage tissue in vitro

Lourdes Georgina Recha Sancho

Universitat Ramon Llull

DOCTORAL THESIS

Title	Development of biomaterial self-assembling based platforms to obtain human cartilage tissue *in vitro*
Presented by	Lourdes Recha Sancho
Centre	IQS School of Engineering
Department	Bioengineering
Directed by	Dr. Carlos E. Semino

C. Claravall, 1-3
08022 Barcelona
Tel. 936 022 200
Fax 936 022 249
E-mail: urlsc@sec.url.es
www.url.es

A la meva família

ACKNOWLEDGEMENTS

Quan vaig començar la tesi veia el final molt llunyà i ara escriure els agraïments significa que això realment s'acaba. Es tanca una etapa plena d'alts i baixos, de fortes emocions i vivències, d'aprenentatge constant i de creixement personal. Els dubtes sempre envolten qualsevol decisió, però decidir fer el doctorat ha estat de les millors que he pres a la meva vida. Mai oblidaré aquests 4 anys que m'han passat volant i per això vull agrair a tots els que hi heu format part i d'alguna manera o altra m'heu ajudat a tirar endavant i heu estat al meu costat.

Primer de tot vull donar les gràcies al meu director de tesi, el Dr. Carlos Semino. *Carlos, al terminar la tesis de master no tuve ninguna duda que quería continuar en tu laboratorio haciendo el doctorado y hiciste lo posible para que así fuera. Gracias por la gran oportunidad que me ofreciste y por involucrarme en un proyecto de estas características. Gracias por tu entusiasmo, positivismo, grandes ideas y, sobretodo, por toda la confianza que has depositado en mi durante estos 5 años.*

Per una altra banda, vull agrair a l'entitat que ha finançat el projecte Biocart, l'AO Foundation, i als diferents integrants que formen el programa *Acute Cartilage Injury Collaborative Research Program (ACI CRP)*. La meva estada al AO Research Institute (Davos, Suïssa) va ser molt enriquidora tant en l'àmbit professional com personal. Agrair al Dr. David Eglin i a tots els integrants del seu grup la seva acollida i atenció durant tota l'estada. A l'Olly per la seva paciència i per tot el que em va ensenyar en un laboratori nou per mi. I com no, agrair a Marina, Dalila, Ana Maria, Gert-Jan, Lucas i a la resta d'integrants del "Lunch Group" per tots els riures, soparets, excursions i, en definitiva, perquè em fessin sentir com a casa. Gràcies també al Dr. Frank Moutos i al Dr. Farsh Guilak (Cytex Therapeutics, Durham, USA) per sintetitzar i enviar-nos tots els scaffolds de PCL que hem necessitat i han permès realitzar part del treball d'aquesta tesi.

També agrair a tots els que han fet possible amb la seva contribució molts dels treballs desenvolupats en aquesta tesi. Moltes gràcies a la Dra. Maria Pilar Armengol del servei de genòmica del IGTP de l'Hospital Germans Tries i Pujol de Badalona per tota la seva ajuda i paciència en ensenyar-me i resoldre dubtes de PCR. Al Dr. Salvador Borrós del laboratori de Materials del IQS per les facilitats prestades en l'ús dels seus equips. En especial he d'agrair a la Núria Agulló per ajudar-nos a trobar les millors condicions per mesurar les propietats mecàniques amb el DMA i a la Marina per les fotos obtingudes amb el microscopi de força atòmica (AFM). Al Dr. Jordi Abellà del laboratori de Mètodes Electromètrics del IQS per la seva ajuda en l'obtenció d'imatges amb el microscopi electrònic (SEM). Finalment, també agrair a Centres Científics i Tecnològics de la UB pels serveis de microscòpia electrònica (SEM).

Durant aquests anys han estat molts els moments viscuts al laboratori, de riures, frustracions, celebracions, treball fins a les tantes... i vull agrair a tots els que d'una manera o altra n'han format part. A les meves companyes de Teixits: Mireia, Tere, Cris, Patri i Cate perquè sense vosaltres res hagués estat igual. Pels consells, per escoltar-me, per tot el que he après de vosaltres i, en definitiva, per tots els bons moments que trobaré molt a faltar! Mireia, no tinc

prou paraules per agrair-te tot el que has fet per mi tant en l'àmbit professional com personal, haurien d'haver-hi més persones al món amb la teva bondat i entusiasme. Tot i la distància que ara ens separa, és com si no haguessis marxat mai i sé que sempre et tindré al meu costat. Cris, amb tu em vaig introduir al món de les hamburgueses, gràcies per ensenyar-me i perquè sempre hi ets i estàs disposada a ajudar. *Tere, heparin power nos unió y a ello tengo que agradecer gran parte de los resultados de esta tesis, gracias por tu constante apoyo*. També agrair als membres de teixits que s'han anat incorporant en diferents moments: Alex, Javi, Melva, Oscar, Anna, Juli, Gerard... Heu aportat aire fresc al grup i les estones al laboratori han estat molt més divertides amb vosaltres. Als companys de saleta i biomaterialistes: Pere, Leti, Sejin, Robert, Sara, Anna, Victor, Oscar... i tots els que em deixo. El laboratori de Teixits seria molt avorrit sense vosaltres! Als companys de Bioquímica: Cristina, Estela, Victòria, Teresa, Hugo, Ellen... que sempre hi heu estat per deixar-nos tot el que hem necessitat. I també agrair a la Magda per estar sempre disposada a resoldre dubtes i ajudar-me amb el que necessités. En definitiva, ha estat un plaer treballar amb tots vosaltres i compartir tots aquests anys.

Com diu la dita "el roce hace el cariño" i del treball diari, dinars i estones al solet han sorgit des de cervesetes improvisades després de dures jornades fins a *destruction parties* molt ben organitzades. Gràcies als *Menudos*: Alex, Mireia i Pere, perquè tot i ser molt diferents la sinergia dels 4 ha creat moments màgics i inoblidables. A la Jenny i l'Aitor que sou maquíssims, sempre tan atents, m'ha encantat conèixer-vos més aquest últim any. A l'Estela, per les xerradetes de desfogament als banquets i per preocupar-te sempre tant pels altres. Especialment agrair a la Cris, perquè passar juntes aquesta última etapa de redacció ha alleujat el camí. *Gracias por todas las comidas, confidencias y consejos que me han hecho descubrir una gran amiga, ya nos queda nada para abandonar nuestras mochilas!*

Durant aquesta etapa també m'han acompanyat les amigues del poble: Imma, Ari i Gemma, amb les seves xerrades i quedadetes. Imma, mil gràcies per escoltar-me quan més ho necessitava, ha estat molt guay viure amb tu aquest any i Ari, un plaer les teves visitetes a Barcelona que ens han servit d'excusa per muntar bons plans. A les *biotecs* Ari i Sonia que tot i veure'ns poc quan ho fem es com si no hagués passat el temps. A l'Anna pels bons consells entre quedades, soparets i sortides. *A Alba porque des de Madrid, Asturias o desde donde sea siempre estas para animarme.* No em vull oblidar d'agrair als salseros: Mireia, Jordi, Manel, Alba, Cris, Xavi... Les estones amb vosaltres m'han fet oblidar els problemes i en aquesta darrera etapa el ball ha estat una gran teràpia que m'ha ajudat en l'empenta final.

Finalment, agrair a la meva família, perquè si he arribat fins aquí és gràcies a vosaltres. Als meus pares per tota la confiança que han dipositat en mi, per tots els sacrificis que fa anys que fan i perquè, en definitiva, m'ho han donat tot, sou un model a seguir. Als meus germans, Rebeca i Bruno, i a Beni, que també el sento com un germà, per ajudar-me, escoltar-me i per tots els vostres consells. I de forma molt especial, al petit rei de la casa, Pau, que dia rere dia ens fas descobrir nous sentiments i ens transmets l'alegria i la il·lusió per tirar endavant. Moltes gràcies per ser-hi sempre i us dedico aquesta tesi doctoral.

Lourdes, 29 de juny del 2016

Aquesta tesi ha estat possible gràcies a la beca pre-doctoral FI-DGR (2013-2015) de la Secretaria d'Universitats i Recerca del Departament d'Economia i Coneixement de la Generalitat de Catalunya i de Fons Socials Europeus, el projecte Biocart finançat per l' AO Foundation i el pressupost del IQS pel Laboratori d'Enginyeria de Teixits.

SUMMARY

Adult articular cartilage has a limited capacity for growth and regeneration and, after injury, treatments to restore tissue function remain poorly understood by the medical community. Therefore, there is currently great interest in finding practical and patient-friendly strategies for cartilage repair. Tissue engineering has emerged to restore damaged tissue by using new cellular or biomaterial-based therapeutic platforms. These approaches aim to produce cartilage-like structures that reproduce the complex mechanical and biological properties found *in vivo*. To this end, the use of biomimetic scaffolds that recreate structurally and functionally the native cell microenvironment has become of increasing interest in the field. Self-assembling peptides are attractive candidates to create artificial cellular niches, because their nanoscale network and biomechanical properties are similar to those of the natural extracellular matrix (ECM).

In the present thesis, new composite synthetic biomaterials were developed for cartilage tissue engineering (CTE). They were based on the non-instructive self-assembling peptide RAD16-I and decorated with bioactive motifs, aiming to emulate the native cartilage ECM. We employed a simple mixture of the self-assembling peptide RAD16-I with either heparin, chondroitin sulfate or decorin molecules, taking advantage of the versatility of RAD16-I. The bi-component scaffolds presented good structural and chemical stability at a physiological pH and the capacity to bind and gradually release growth factors. Then, these composite scaffolds were characterized using two different *in vitro* assessments: re-differentiation of human articular chondrocytes (ACs) and induction of human adipose derived stem cells (ADSCs) to a chondrogenic commitment. Both native chondrocytes and adult mesenchymal stem cells (MSCs), either bone marrow or adipose-tissue derived, are considered good cell sources for CTE applications. The results presented in this work revealed differences in cellular behavior, expression patterns and mechanical properties between cell types and culture conditions (scaffolds and media). Remarkably, both cell types underwent into chondrogenic commitment under inductive media conditions and 3D constructs presented mechanical properties compatible to a system undergoing chondrogenesis. Interestingly, as a consequence of the presence of heparin moieties in the scaffold cell survival of ADSCs was enhanced. Altogether, the new bi-component scaffolds represent a promising "easy to prepare" material for promoting chondrogenic differentiation.

Finally, part of this thesis was focus on developing a composite scaffold by infiltrating a three-dimensional (3D) woven microfiber poly (ε-caprolactone) (PCL) scaffold with the RAD16-I self-assembling peptide and cells. This new combination resulted into a multi-scale functional and biomimetic tissue-engineered structure providing mechanical support by PCL scaffold and facilitating cell attachment and growth by RAD16-I hydrogel. The *in vitro* 3D culture of dedifferentiated human ACs evidenced that the new composite supports cell survival and promotes the reestablishment of the chondrogenic lineage commitment. Overall, the synergistic properties of the novel composite scaffold may provide an ideal therapeutic platform to assist cartilage repair.

RESUMEN

El cartílago articular tiene una capacidad limitada de crecimiento y regeneración y, los tratamientos para restaurar la función del tejido, después de una lesión, son limitados y poco entendidos por la comunidad médica. Existe, por tanto, un gran interés en encontrar una solución práctica y agradable para el paciente que consiga la reparación del cartílago. La ingeniería de tejidos surgió para restaurar tejidos dañados usando nuevas plataformas terapéuticas basadas en células y/o biomateriales. Estas nuevas terapias pretenden crear estructuras similares al cartílago que imiten las propiedades mecánicas y biológicas que se dan *in vivo*. En este sentido, el uso de matrices biomiméticas que reproduzcan estructural y funcionalmente el microambiente nativo ha generado gran interés en este campo. Los péptidos auto-ensamblantes representan candidatos ideales para crear nichos celulares dado que, sus nanofibras y propiedades biomecánicas son similares a las de la matriz extracelular.

En esta tesis, se han desarrollado nuevos biomateriales sintéticos con gran potencial para la reparación de cartílago. Éstos, están basados en el péptido auto-ensamblante RAD16-I decorado con motivos bioactivos, tratando de reproducir la matriz del cartílago. Dada la versatilidad del hidrogel RAD16-I, las nuevas matrices se formaron por simple mezcla del péptido RAD16-I con moléculas de heparina, condroitin sulfato y decorina. Estas matrices bi-compuestas presentan buena estabilidad química y estructural a pH fisiológico y son capaces de unir y liberar, gradualmente, factores de crecimiento. La evaluación de estas matrices se llevó a cabo mediante dos estrategias *in vitro* diferentes: la rediferenciación de condrocitos articulares humanos y, la inducción del linaje condrogénico en células madre derivadas de tejido adiposo. Ambos tipos celulares son considerados una buena fuente de células para obtener constructos que reparen defectos en el cartílago. Los resultados presentados en este trabajo muestran diferencias a nivel de comportamiento celular, patrones de expresión y propiedades mecánicas entre los dos tipos celulares y las diferentes condiciones de cultivo (matrices y medios). Cabe destacar que, ambos tipos celulares se diferencian a un linaje condrogénico en medio de inducción y que los constructos presentan propiedades mecánicas compatibles con un sistema condrogénico. Además, se ha determinado que la presencia de moléculas de heparina en la matriz promueve la supervivencia de las células madre derivadas de tejido adiposo. En conjunto, las nuevas matrices bi-compuestas representan un material fácil de preparar y prometedor para promover la diferenciación condrogénica.

Por último, parte de esta tesis se ha centrado en el desarrollo de una nueva matriz compuesta mediante la infiltración del péptido RAD16-I con células en microfibras de policaprolactona (PCL). Se ha demostrado que esta nueva combinación ofrece una estructura funcional y biomimética, dado que, proporciona soporte mecánico por las fibras PCL y a su vez, facilita la adhesión y el crecimiento celular debido al hidrogel RAD16-I. El cultivo *in vitro* de condrocitos humanos desdiferenciados demuestra que la nueva matriz compuesta promueve la supervivencia celular y el restablecimiento del linaje condrogénico. En general, las propiedades sinérgicas de la nueva matriz compuesta proporcionan una plataforma terapéutica ideal para ayudar a la reparación del cartílago.

RESUM

El cartílag articular té una capacitat limitada de creixement i regeneració i, els tractaments per restaurar la funció del teixit, després d'una lesió, són limitats i poc entesos per la comunitat mèdica. Existeix, per tant, un gran interès en trobar una solució pràctica i agradable pel pacient que aconsegueixi la reparació del cartílag. La enginyeria de teixits va sorgir per restablir teixits danyats usant noves plataformes terapèutiques basades en cèl·lules i/o biomaterials. Aquestes noves teràpies pretenen crear estructures similars al cartílag que imiten les propietats mecàniques i biològiques que trobem *in vivo*. En aquest context, l'ús de matrius biomimètiques que reprodueixin estructural i funcionalment el microambient natiu han despertat gran interès en aquest camp. Els pèptids auto-ensamblants representen candidats ideals per crear nínxols cel·lulars, ja que les seves nanofibres i propietats biomecàniques son similars a les de la matriu extracel·lular.

En aquesta tesi, s'ha desenvolupat nous biomaterials sintètics amb gran potencial per la reparació de cartílag. Aquests estan basats en el pèptid auto-ensamblant RAD16-I decorat amb motius bioactius, amb l'objectiu de reproduir la matriu del cartílag. Donada la versatilitat del hidrogel RAD16-I, les noves matrius es van formar per simple mescla del pèptid RAD16-I amb molècules d'heparina, condroitin sulfat i decorina. Aquestes matrius bi-composades presenten bona estabilitat química i estructural a pH fisiològic i son capaces d'unir i alliberar, gradualment, factors de creixement. L'avaluació d'aquestes matrius es va dur a terme mitjançant dues estratègies *in vitro* diferents: la rediferenciació de condròcits articulars humans i la inducció del llinatge condrogènic en cèl·lules mare derivades de teixit adipós. Ambdós tipus cel·lulars son considerats una bona font cel·lular per obtenir constructes que reparin defectes al cartílag. Els resultats presentats en aquest treball mostren diferencies a nivell de comportament cel·lular, patrons d'expressió i propietats mecàniques entre els dos tipus cel·lulars i les diferents condicions de cultiu (matrius i medis). Cal destacar que els dos tipus cel·lulars es diferencien a un llinatge condrogènic en medi d'inducció i que els constructes presenten propietats mecàniques compatibles amb un sistema condrogènic. A més s'ha determinat que la presencia de molècules d'heparina a la matriu promou la supervivència de les cèl·lules mare derivades de teixit adipós. En conjunt, les noves matrius bi-composades representen un material fàcil de preparar i prometedor per promoure la diferenciació condrogènica.

Finalment, part d'aquesta tesi s'ha centrat en el desenvolupament d'una nova matriu composta mitjançant la infiltració del pèptid RAD16-I amb cèl·lules en microfibres de policaprolactona (PCL). S'ha demostrat que aquesta nova combinació ofereix una estructura funcional i biomimètica, ja que proporciona suport mecànic per les fibres de PCL i a la vegada, facilita l'adhesió i el creixement cel·lular per l'hidrogel RAD16-I. El cultiu *in vitro* de condròcits humans desdiferenciats demostra que la nova matriu composada promou la supervivència cel·lular i el restabliment del llinatge condrogènic. En general, les propietats sinèrgiques de la nova matriu composada proporcionen una plataforma terapèutica ideal per ajudar a la reparació del cartílag.

LIST OF CONTENTS

LIST OF FIGURES

CHAPTER 1

CHAPTER 2

CHAPTER 3

CHAPTER 5

CHAPTER 6

LIST OF TABLES

CHAPTER 1

CHAPTER 2

LIST OF ABBREVIATIONS

2D	two-dimensional
3D	three-dimensional
ACAN	aggrecan
ACI CRP	acute cartilage injury collaborative research program
ACI	autologous chondrocyte implantation
ACs	articular chondrocytes
ACT	autologous cell transplantation
ADSCs	adipose-derived stem cells
AFM	atomic force microscopy
AM	acetoxymethyl
ARI	AO Research Institute
ASCs	adult stem cells
BB	blocking buffer
Biocart	bioactive and biomimetic scaffolds for cartilage regeneration
BMP	bone morphogenetic protein
BSA	bovine serum albumin
CD	circular dichroism
cDNA	complementary DNA
COL1	collagen type I
COL10	collagen type X
COL2	collagen type II
CS	chondroitin sulfate
CTE	cartilage tissue engineering
DAPI	4’,6-diamidino-2-phenylindole
DMA	dynamic mechanical analysis
DMEM	dulbecco’s modified eagle medium
DMSO	dimethyl sulfoxide
ECM	extracellular matrix
ESCs	embryonic stem cells
EthD-1	ethidium homodimer-1
FBS	fetal bovine serum
FGF	fibroblast growth factor
G*	complex modulus
G’	storage modulus
G’’	loss modulus
GAGs	glycosaminoglycans
GalNAc	N-acetylgalactosamine
GDF5	growth and differentiation factor 5
GF	growth factor
GlcA	glucuronic acid
HA	hyaluronan
HBD	heparin binding domain
HDMECs	human dermal microvascular endothelial cells
hNDFs	human normal dermal fibroblasts
HUVECs	human umbilical vein endothelial cells
IGF-1	insulin-like growth factor-1
IPN	interpenetrating network

iPSCs	induced pluripotent stem cells
LRR	leucine rich repeats
MSCs	mesenchymal stem cells
MTT	3-[4,5-dimethylthiazol-2-yl]-2,5-diphenyl tetrazolium bromide
PBS	phosphate buffer saline
PBST	PBS with Tween-20
PCL	poly (ε-caprolactone)
PCL/RAD	PCL scaffold-RAD16-I peptide composite scaffold
PCR	polymerase chain reaction
PDGF	platelet-derived growth factor
PEG	poly(ethylene glycol)
PFA	p-formaldehyde
PGA	poly(glycolic acid)
PGs	proteoglycans
PLA	poly(lactic acid)
PLGA	poly(lactic-co-glycolicacid)
PNIPAM	poly(N-isopropylacrylamide)
PVDF	polyvinylidene difluoride
RT-PCR	reverse transcriptase PCR
RAD/CS	RAD16-I peptide-chondroitin sulfate bi-component scaffold
RAD/Decorin	RAD16-I peptide-Decorin bi-component scaffold
RAD/Hep	RAD16-I peptide-heparin bi-component scaffold
RPL22	ribosomal protein L22
SEM	scanning electron microscopy
SLRP	small leucine-rich proteoglycan
subATDPCs	subcutaneous adipose tissue-derived progenitor cells
TE	tissue engineering
TGF β	transforming growth factorβ
TRITC	tetramethylrhodamine B isothiocyanate
VEGF	vascular endothelial growth factor
WB	western blot

CHAPTER 1

Introduction to cartilage tissue engineering

1.1 BACKGROUND

1.1.1 OVERVIEW

Adult articular cartilage lacks intrinsic capacity to repair or regenerate itself after injury due to its avascular nature and limited healing potential. A variety of factors can originate cartilage lesions, including traumatic injuries or age-related degenerative diseases, such as osteoarthritis. Consequently, cartilage defects proceeds toward degeneration, resulting in significant symptomatology and join disability for patients[1,2]. Current clinical methods rely mostly on surgery; with cell-based therapies such as autologous chondrocyte implantation (ACI) and bone marrow-stimulating procedures (microfracture technique)[3–5]. They are invasive procedures, expensive and have unsatisfactory results in restoring the structure and functionality of cartilage tissue, since these treatments often induce the formation of fibrocartilage tissue with inferior biomechanically properties compared to the original cartilage[6]. There is, therefore, an unmet medical need for the treatment of cartilage defects and the development of novel therapeutic approaches with long-term functionality. Tissue engineering (TE) strategies are emerging as a powerful toolbox to create functional substitutes to address cartilage defects. To accomplish this goal, understanding the biology of articular cartilage and its formation is critical for developing cartilage tissue engineering (CTE) strategies.

1.1.2 CARTILAGE TISSUE: CHONDROGENESIS

Cartilage is an avascular connective tissue composed of only one type of specialized cells known as chondrocytes. They are embedded in a complex extracellular matrix (ECM), characterized by highly hydrated network of collagen fibrils and proteoglycans (PGs). The molecular composition and organization of the ECM varies within the three different types of cartilage: hyaline, fibrocartilage and elastic cartilage[7]. Basically, each of them has different amount of fibers produced and accumulated in the ECM by chondrocytes making the tissue more or less elastic. Therefore, the resulting mechanical properties and their occurrence in the human body differ[8]. Hyaline cartilage is the most widespread type of cartilage and it is found covering bone surfaces in joints (articular cartilage), nose, trachea, bronchi, larynx and within the rib cage (costal cartilage). Additionally, it is the most studied, because it is involved in bone formation through the process of endochondral ossification[9]. Fibrocartilage is typically present in the intervertebral discs, meniscus and pubic symphysis. Finally, elastic cartilage is found in the external ear, larynx and epiglottis[10].

Regardless of cartilage type, chondrogenesis is the dynamic cellular process that leads to the formation of cartilage tissue and maturation of chondrocytes. It proceeds via a stepwise process that includes the following events: mesenchymal stem cell migration, condensation,

proliferation and differentiation towards chondrogenic phenotype and, finally, maturation (Figure 1.1.1)[11]. Each step depends on the step before and is subjected to different genetic control that involves the expression of different sets of transcription factors, cell adhesion molecules and ECM components.

First, mesenchymal stem cells (MSCs) start to gather in the skeletal site, where they initially reside as a dispersed population of progenitor cells. Under proper signaling, prechondrogenic cells undergo mesenchymal condensation which consists in a physical compaction of the cells mediated by paracrine factors, such as fibroblast growth factor (FGF), transforming growth factorβ (TGFβ), bone morphogenetic protein (BMP) and Wnt[12]. As a result, chondroprogenitor cells increase cell-cell and cell-matrix interactions and start to synthesize new matrix components such as collagen type I, fibronectin and short PGs (versican, perlecan or syndecan). Condensed cells differentiate to chondroblasts and express the transcription factor Sox9 that promotes the upregulation of Sox5, Sox6 and collagen type II. In turn, Sox5 and Sox6 induce the synthesis of collagen type IX and aggrecan[13]. In this process, cells change their fibroblastic-like shape for the chondroblastic spherical morphology. Finally, mature chondrocytes are embedded and sparsely distributed within a rich matrix in collagens and PGs leading to an increased rigidity typical of cartilage stiffness[14].

At this stage, the fate of hyaline chondrocytes has two possibilities: they can remain chondrocytes and maintain the ECM or proceed to terminal differentiation to hypertrophy[7]. This transition is regulated by the balance between Sox9 and the osteogenic transcription factor Runx2. Hypertrophic chondrocytes activate the expression of collagen type X and metalloproteases resulting in matrix remodeling and angiogenesis to convert cartilage to bone via endochondral ossification[15].

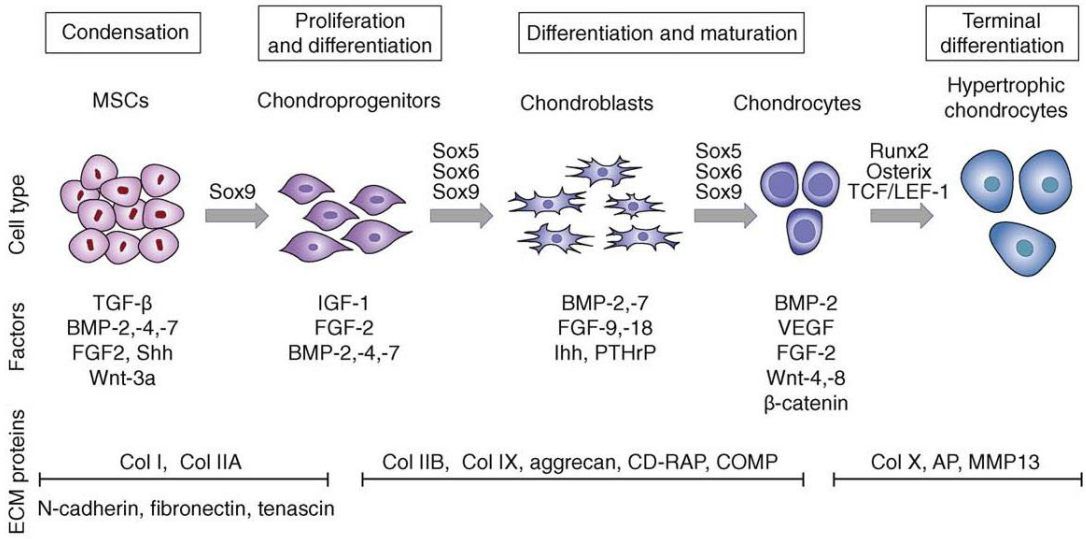

Figure 1.1.1. Schematic representation of different stages of chondrogenesis. Mesenchymal stem cells (MSCs) condense and differentiate to chondroblasts, under the regulation of Sox9, to finally become mature chondrocytes. They can further undergo to terminal differentiation to hypertrophy, under the regulation of Runx2. The main transcription factors involved in each step are indicated and the temporal

expression profiles of the different growth factors and extracellular matrix (ECM) components are shown in the lower part of the figure. Abbreviations: AP, alkaline phosphatase; CD-RAP, cartilage-derived retinoic acid-sensitive protein; Col, collagen; COMP, cartilage oligomeric protein; MMP, matrix metalloprotease; VEGF, vascular endothelial growth factor. Image from Vinatier *et al.*[16]

1.1.3 ARTICULAR CARTILAGE: COMPOSTION, STRUCTURE AND FUNCTION

Articular cartilage provides a low-friction, wear-resistant joint surface that transmits and distributes stress to the underlying bone. The specific mechanical properties are determined by the intimate relation between the tissue constituents[17]. Basically, articular cartilage is a hypocellular tissue that mainly consists of highly organized ECM structural components. Chondrocytes contribute to only 1-5% of tissue volume and are found as single, isolated cells, or in a chondron, an aggregate of several chondrocytes[8]. They are highly metabolically active in order to maintain the integrity of the vast surrounding matrix. Since articular cartilage is avascular, the supply of oxygen and nutrients and the removal of waste products are slow and mediated by simple diffusion between synovial fluid and cartilage matrix, facilitated during joint movement[18]. In particular, the oxygen tension in cartilage may be as low as 1% to 3%, compared with 21% in normal atmosphere[19].

The cartilage ECM is principally composed of a network of collagens and proteoglycans (PGs) (Figure 1.1.2 A). Type II collagen is the predominant collagen (90–95%) and forms a highly cross-linked and interconnected network of fibrils providing tensile strength to the articular cartilage[20]. Other types of collagen molecules, in particular types V, VI, IX, X and XI, are also found in cartilage tissue in smaller amounts[21,22]. Regarding PGs, cartilage displays a wide variety, but they can be classified in two major classes: large aggregating PGs monomers (aggrecans) and small PGs molecules (decorin, biglycan and fibromodulin). Aggrecan is the most abundant PGs and is composed of highly negative charged glycosaminoglycans (GAGs) side chains (chondroitin and keratin sulfate) bound to a core protein[23,24]. Remarkably, aggrecan does not exist in monomeric form in the extracellular space, but its normal organization is assembling into large aggregates with hyaluronan (HA). The interaction between aggrecan core protein and HA is non-covalent and stabilized with a link protein (Figure 1.1.2 B)[7]. These aggregates are embedded within the mesh of collagen type II fibers resulting in densely packed negative charged structures capable of interacting with water via hydrogen bond and causing osmotic potential. Nevertheless, the PGs ability to swell is limited by compressive forces from the outside and by the collagen network inside the ECM that resists the tensile forces caused by swelling[8]. This key feature enables cartilage tissue to resist deformation under compression and to withstand and redistribute mechanical loads[25].

Furthermore, other PGs expressed during chondrogenesis and in cartilage are also critical for the structure and function of cartilage. They include the cell surface syndecans and glypican, the small leucine-rich PGs decorin, biglycan, fibromodulin, lumican and epiphycan and the basement membrane PG, perlecan. These PGs may sequester growth factors (GFs), mediate

critical events during prechondrogenic condensation, and organize the fine structure of the ECM thus regulating the expression of the chondrocyte phenotype[26].

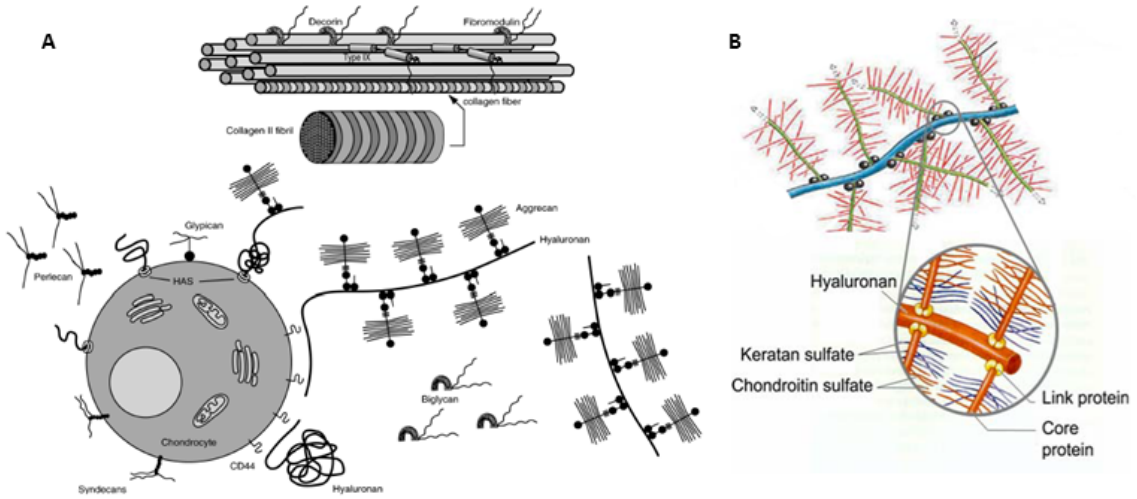

Figure 1.1.2. Scheme of the extracellular matrix of mature chondrocytes. (A) Articular cartilage ECM is basically composed of an intricate network of collagen fibrils (primarily collagen type II) and proteoglycans (mostly aggregates of aggrecan with hyaluronan). Other proteoglycans such as decorin, biglycan, perlecan and fibromodulin are also present within cartilage. (B) The most relevant proteoglycans in articular cartilage consist of aggrecan monomers non-covalently attached to hyaluronan and stabilized by the link protein. Aggrecan is composed of glycosaminoglycans, keratan sulfate and chondroitin sulfate, covalently bound to a central core protein. Image adapted from Knudson and Knudson[27] and Schulz and Bader[8].

1.1.3.1 Mechanotransduction

The unique blending and organization of collagens and PGs within the ECM determine the stiffness and viscoelastic properties of cartilage tissue. Any remodeling and turnover of ECM components must be carefully regulated in order to keep the normal tissue homeostasis and the biomechanical function[27]. Chondrocytes maintain the matrix reacting to external biochemical and biophysical stimuli in an orchestrated microenvironment. In particular, they are subjected to a variety of mechanical forces and flows that affect their phenotypic expressions through a process called mechanotransduction (Figure 1.1.3)[28,29]. It is based on cell sensing from their surrounding matrix through cellular mechanosensors, such as integrins and other cell surface receptors, that convert biomechanical stimulation into intracellular signal[8]. The mechanism relies on the connection of the ECM with the actin-myosin cytoskeleton of cells through mechanosensors. By this bidirectional interaction cells “feel” mechanical changes and respond to the resistance sensed by adjusting its adhesions, cytoskeleton, the distribution of cell surface integrin receptors and overall state[30]. Hence, chemical and mechanical signals are strongly coupled enabling mechanical information to be transduced into morphological changes and, as a result, cells were directly influenced by rigidity or elasticity of their local microenvironment[31].

The induction of biochemical changes by mechanical stimuli is not limited to chondrocytes. Mechanical forces regulate cell physiology and modulate ECM synthesis and organization of many tissues, including musculoskeletal and cardiovascular[32]. Finally, it is possible that the deformation of chondrocytes itself caused by external mechanical loads or compression may also participate in the mechanical signal transduction pathway[33,34]. Altogether, the effects of mechanical signals are essential in the control of chondrocyte metabolic behavior and, consequently, tissue maintenance.

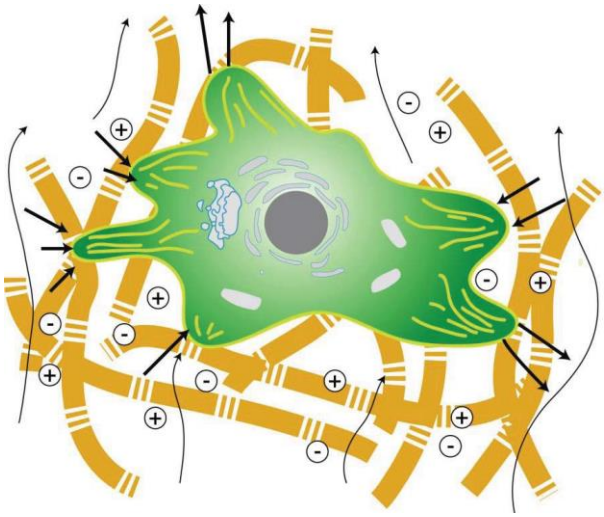

Figure 1.1.3. Schematic representation of mechanotransduction process in chondrocytes. It can be originated from a variety of biophysical forces and flows via pulling, compressing, and shearing the cells (bold arrows) and other types of stimuli, such as streaming potentials (fine arrows). Image from Kyriacos *et al.* [35]

1.1.4 TISSUE ENGINEERING

Cartilage function and tissue integrity are compromised after traumatic lesions or osteoarthritis and their repair is limited by the low intrinsic regeneration potential of cartilage. Thus, medical treatments are required and tissue engineering (TE) strategies could help to recover cartilage tissue and function. Langer and Vacanti defined TE in 1993 as a new field that applies the principles of biology and engineering to the development of functional substitutes for damaged tissue[36]. This definition is still applied today and significant progress has been accomplished in the field since then[37]. Initially, TE emerged as a possible alternative to tissue or organ transplantation, due to the limited number of available organs and the increasing number of patients on the waiting list[38,39]. During the last two decades, TE has become a growing scientific area with broad application in regenerative medicine. The main objective of TE is to create functional substitutes in order to restore, maintain or enhance a damaged tissue which function has been lost or compromised by disease, injury or aging[40,41]. Ideally, the engineered tissue should functionally integrate into the host tissue, remodel in response to environmental factors and provide good durability *in vivo*.

The basic approach of TE involves the isolation of cells from the patient, their expansion *in vitro* and their seeding within scaffolds to generate engineered constructs (Figure 1.1.4). The addition of signaling molecules to these constructs could help to specifically guide the course of differentiation in the desired direction for further re-implantation into the patient[42]. Therefore, TE involves three key constituents: cells, scaffolds and signaling factors that should be properly combined for each specific application[43].

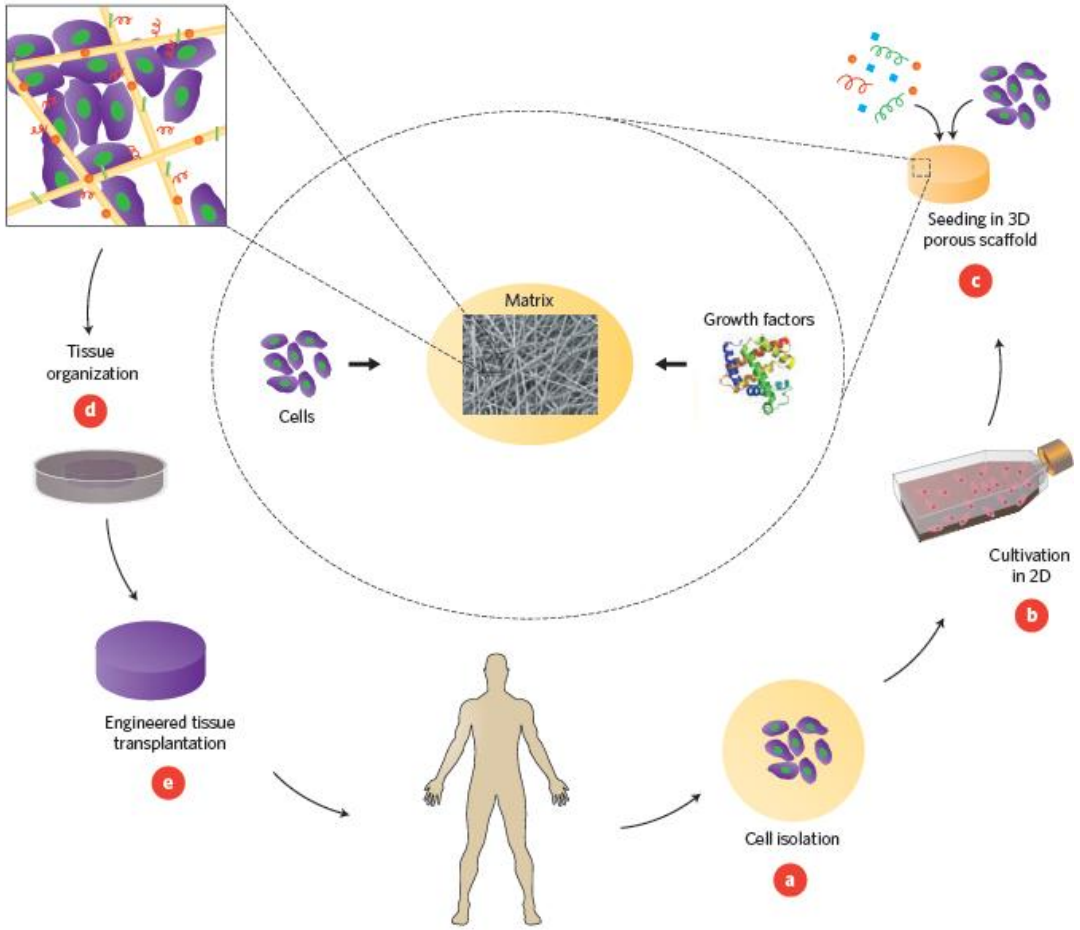

Figure 1.1.4. An example of a tissue engineering concept that involves seeding cells within porous biomaterial scaffolds. (a) Cells are isolated from the patient and may be cultivated (b) *in vitro* on two-dimensional (2D) surfaces for efficient expansion. (c) Next, the cells are seeded in porous scaffolds together with growth factors, small molecules, and micro- and/or nanoparticles. The scaffolds serve as a mechanical support and a shape-determining material, and their porous nature provides high mass transfer and waste removal. (d) The cell constructs are further cultivated in bioreactors to provide optimal conditions for organization into a functioning tissue. (e) Once a functioning tissue has been successfully engineered, the construct is transplanted on the defect to restore function. Adapted from Dvir *et al.*[44]

Moreover, apart from the development of tissue and organ substitutes, TE has also become a useful tool for the study of complex physiological and pathophysiological processes *in vitro*[45]. 3D cultures can be developed as models for fundamental research, since they can help to study the cellular and molecular mechanisms underlying human diseases and test the safety and efficacy of drugs. The idea is to bridge the gap between 2D cultures and animal models by recreating some of the complex features of the *in vivo* microenvironment (Figure 1.1.5)[46]. 3D cultures are more complex cellular systems than monolayer cultures, while simpler than *in vivo* environment in living organisms. Therefore, they can represent an intermediate stage in fundamental research.

In mammalian tissues, cells are continuously interacting with neighboring cells and with the ECM through physical, biochemical and mechanical cues. In particular, cell-cell and cell-matrix interactions create a 3D network that defines the architecture, signaling and biomechanics of the cellular microenvironment. Given this complex interplay, it has been shown that 2D cultures limit to predict cellular responses *in vitro*, since essential cellular functions present in the tissues are missed[47]. Culturing cells in 3D versus 2D environments give another dimension for mechanical properties and cell communications, where integrins have a key role on how cells interpret biochemical cues from their immediate surroundings and traduce to intracellular signals[45]. Hence, there is high interest in the development of *in vitro* models that better mimic biological complexity than traditional 2D cultures. Thus, providing the appropriate cues through 3D cultures will better resemble *in vivo* systems and basic questions could be answered before having to turn to animal research, reducing their use in experimentation[48].

In this thesis, the experimental outcome is focused on the development of tissue engineered substitutes and, in particular, in the field of cartilage tissue engineering (CTE).

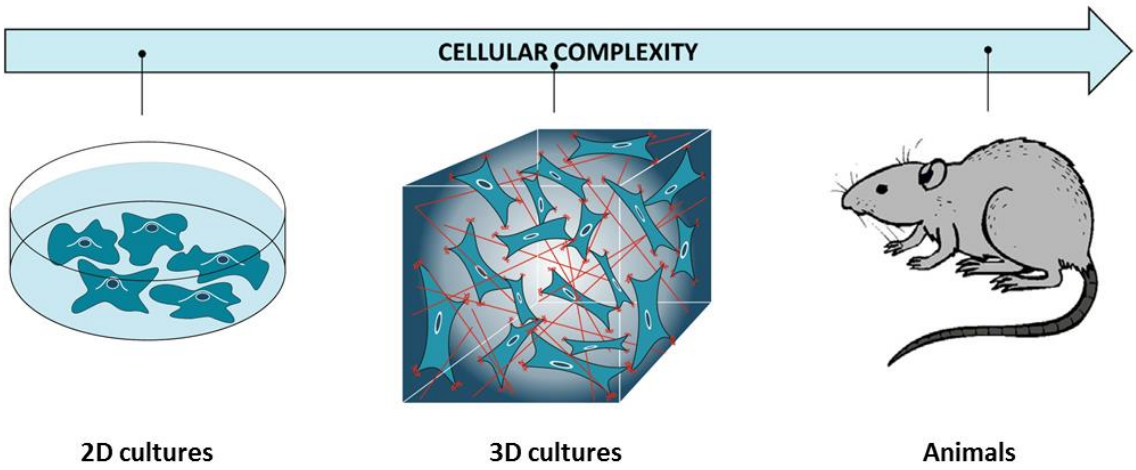

Figure 1.1.5. 3D cultures models as intermediate step between 2D cultures and animal models. Tissue engineering provides 3D cultures that recreate the complex cellular microenvironment more precisely than traditional 2D cultures, due to the incorporation of multiple physical, mechanical and chemical cues that arise from ECM-cell and cell-cell interactions. At the opposite end of the experimental continuum, animals do not capture important facets of human behaviour. Therefore, 3D cultures can bridge the gap between 2D cultures and animal models. Adapted from Alemany-Ribes and Semino[49].

1.1.4.1 Cartilage Tissue Engineering

The field of cartilage tissue engineering (CTE) aims to develop structurally and functionally competent cartilage grafts by using cells, scaffolds and stimulating factors, such as soluble factors (GFs, chondroitin sulfate, hyaluronic acid, genes…) or mechanical stimulation[50]. The proper combination of them could provide specific culture conditions that may help to

stimulate the proliferation and chondrogenesis of the selected cell source and enhance the synthesis and deposition of ECM components. Particularly, ECM *in vitro* deposition may increase the mechanical functionality of the cell-seeded construct to withstand loading forces encountered after implantation[51].

However, there are a number of challenges that remain to be accomplished due to the complex biological environment that is necessary to mimic. Future directions for CTE are related to the integration of engineered construct with existing cartilage, since cartilage is a tissue that acts as one entity to distribute applied loads[52]. Moreover, if implanted or injected immediately, the scaffold should maintain its shape and possess robust mechanical characteristics similar to native cartilage to match the loading environment. However, *in vitro* culturing systems do not require scaffolds with these strict properties, since during the culture period new tissue forms and acquires slowly the chondrogenic commitment[43].

Given the importance of the selection of cell source, scaffolds and stimulatory factors in CTE, they are reviewed in detail in the following sections.

1.1.4.2 Cell sources for cartilage regeneration

Determining the optimal cell source for CTE is still a challenge. A variety of cell sources are potentially applicable, including terminally differentiated chondrocytes, adult stem cells (ASCs), embryonic stem cells (ESCs), induced pluripotent stem cells (iPSCs) or even fibroblasts. Ideally, cells should be easy to isolate, expand and culture *in vitro* and have a good and reliable performance (Table 1.1.1)[50].

Chondrocytes represent an ideal cell source for CTE, because they are found in native cartilage and have the original chondrogenic phenotype[53]. Since they are isolated from patients, the main drawback is to obtain a sufficient cell number for their use in clinics. For this reason, an *ex vivo* expansion is often required to overcome the limited supply[54]. Once they are isolated from their natural surrounding matrix and cultured in monolayer, they undergo dedifferentiation losing their ability to express articular cartilage ECM specific markers including collagens and GAGs[55–57]. Therefore, the recovery of the chondrogenic phenotype is an essential step prior to further application. Promising results were obtained with different 3D culture platforms to restore and maintain the chondrogenic phenotype *in vitro*[58–60].

ASCs persist in organism to preserve tissue maintenance and regeneration. They have the ability to produce more stem cells maintaining a constant pool and to differentiate into mature cells in order to replace the ones that have been lost because of physiological turnover, injury, or disease. Self-renewal and differentiation are regulated by stem cell intrinsic factors and signals from the surrounding microenvironment in which they reside, called stem cell niche[61,62]. Mesenchymal stem cells (MSCs) are a multipotent progenitor cells with high proliferative capacity *in vitro* that can be obtained from different adult tissues such as bone marrow, muscle, adipose tissue and umbilical cord[63,64]. In particular, adipose origin provides an

easy and abundant supply of cells with minimally invasive surgery[65]. MSCs have the capability to differentiate into mesodermal lineages, such as osteogenic, adipogenic or chondrogenic when cultured under specific growth conditions[66,67]. Thus, an appropriate biochemical and biomechanical microenvironment is required to guide MSCs into chondrogenic commitment and promote stable cartilaginous tissue formation[68]. For all these reasons, the plasticity of MSCs provides a promising source of ASCs in CTE purposes[69].

ESCs are derived from the inner cell mass of the blastocyst stage embryos. They can give rise to any cell type in the human body and exhibit ceaseless proliferation *in vitro*[70]. Therefore, they have a broader potential than ASCs, since, apart from mesodermal lineage, they can differentiate into cells from endoderm and ectoderm. Nevertheless, undifferentiated ESCs may cause teratoma formation *in vivo*, due to their highly proliferative capacity. For this reason, efficient differentiation protocols to derive tissue-specific progenitor cells are critical prior to transplantation[71,72]. ESCs chondrogenic differentiation for clinical applications is limited, in part, due to regulatory and ethical issues. Hence, their use has been mainly focus on understanding more fundamental biological questions[73].

Table 1.1.1. Advantages and disadvantages of various cell sources. Adapted from Keeney *et al*[74] and Johnstone *et al*[73].

Cell types	Advantages	Disadvantages
Autologous chondrocytes	• Native phenotype • Minimal risk immunological problem	• Low initial cell number • Dedifferentiation *in vitro*
Mesenchymal Stem Cells (MSCs)	• Potential to produce large number • Various harvest sites • Capacity to differentiate into mesodermal lineages	• Potential for hypertrophy • Differentiation unstable and non-reproducible
Embryonic Stem Cells (ESCs)	• Multipotency • High proliferative capacity *in vitro*	• Ethical controversy • Risk of teratoma formation • Differentiation unstable and non-reproducible
Induced Pluripotent Stem Cells (iPSCs)	• Multipotency • No ethical controversy	• Risk of teratoma formation • Differentiation unstable and non-reproducible
Fibroblasts	• Abundant and easy obtaining • Source of patient specific cells	• Low differentiation capacity

Recent advances in stem cell biology have enabled the generation of pluripotent cell populations called iPSCs. They are derived from adult fibroblasts by introducing four transcription factors (Oct3/4, Klf4, Sox2 and c-Myc)[75]. In this way, differentiated cells can be reprogrammed to an embryonic-like stage exhibiting the morphology and growth properties of ESCs and expressing their markers. These cells can be derived from the patient's own adult cells population, avoiding immunological and ethical problems. However, the risks of tumor formation and function disruption of endogenous genes by retroviral insertion may hinder their use in clinical applications[76].

Finally, fibroblasts have been gaining interest during the last years for TE applications. Different reports showed that these cells can be redirected towards chondrocytic phenotype when cultured under the appropriate conditions[77–79]. In fact, it has not been elucidated whether this plasticity is due to transdifferentiation of committed fibroblasts or to differentiation of resident stem cells, since dermal fibroblasts comprises a heterogeneous population containing progenitor's cells. A clear advantage of fibroblasts is the cell number and availability. Skin presents a minimally invasive, relatively abundant source of fibroblasts, thus large number of cells can be extracted by a simple biopsy. Nevertheless, the main drawback is their low differentiation capacity compared to MSCs[80].

Regardless of cell type, cell sources include autologous cells from the patient, allogeneic cells from a human donor who is not immunologically identical to the patient, or even xenogeneic cells from a different species[81]. Moreover, the quality of cells can vary depending on age, disease or other parameters of the donor affecting the maintenance and differentiation potential[6].

1.1.4.3 Scaffolds for CTE

The identification of the appropriate biomaterials that support cellular attachment, proliferation and lineage-specific differentiation is crucial for TE applications. As previously mentioned, ECM provides structural integrity and regulatory signaling that play a key role in controlling cellular behavior[82]. Hence, the development of tailored *in vitro* cell culture environment that recapitulates biological properties of ECM is desirable to guarantee to cells the proper signals and information for tissue development[83]. In this regard, the major challenge in TE is designing scaffolds that are essentially inspired on the native ECM to recreate the *in vivo* milieu.

A wide variety of biomaterials have been used for CTE and they are often classified into natural or synthetic depending on their origin (Table 1.1.2). Moreover, different parameters should be carefully considered in the selection of scaffolds: composition, viscoelasticity, porosity, degradation and chemical and physical cues between others[84]. Natural scaffolds can be easily obtained and may provide efficient adhesion sites for cell attachment and a wide range of biological signals. However, the diversity of the (often unknown) signals makes difficult to isolate the effect of specific factors and could induce immune system response. In addition,

the extraction and purification techniques used in the industrial manufacturing lead to variability in composition and mechanical properties from batch to batch. Therefore, reproducibility and possible modifications to improve them are limited. Examples of natural materials that have been studied for their application in cartilage repair are: collagen[85], fibrin[86], hyaluronan[87], agarose[88], alginate[89], gelatin[90] or chondroitin sulfate[91]. Nowadays, naturally-derived biomaterials are often limited to *in vitro* studies due to their weak mechanical properties and regulatory/manufacturing difficulties[70].

On the other hand, synthetic scaffolds can be well-defined and molecularly tailored in their properties –mechanical strength, chemistry, porosity, degradation profile and biologically active sites –. Thus, controllable and reproducible cellular microenvironments can be obtained with this type of biomaterials[83]. However, their main drawbacks include toxicity due to degradation byproducts and low cell-scaffold interactions. Several synthetic scaffolds are being widely used in CTE: poly(α-hydroxy esters)[92–95], polyurethane[96], poly(ethylene glycol) (PEG)[97], poly(N-isopropylacrylamide) (PNIPAM)[98], elastin-based polymers[99] and self-assembling peptides, such as KLD-12[100] and RAD16-I[79,101–103]. Interestingly, these biomaterials can be tuned with adhesion peptides or molecular cues that better recreate cartilage ECM to recapitulate or induce developmental processes. Up to date, peptide sequences such as RGD moieties to stimulate cell adhesion[104] and decorin moieties to bind and release GFs[105] have been reported to enhance chondrogenesis and reach the same levels of differentiation obtained with natural scaffolds. Additionally, composites consisting of two or more materials incorporated in a single scaffold are also under development. This group can include a mixture of fibres from different natural materials and a synthetic or naturally derived hydrogel infused into a synthetic mesh. For instance, coatings of collagen and fibronectin are used for cartilage applications in order to improve cell adhesion, based on the cell-integrin receptors. This combination is an interesting approach to replicate the complex structure to provide the functional *in vivo* properties[35]. The development of new well-defined biomaterials with controllable properties is constantly improving CTE field.

Table 1.1.2. Examples of types of biomaterials used in cartilage tissue engineering (CTE).

Natural materials	**Synthetic materials**
Collagen[85]	Poly(α-hydroxy esters) - Poly(glycolic acid) (PGA)[92] - Poly(lactic acid) (PLA)[93] - Poly(lactic-co-glycolicacid) (PLGA)[94] - Poly(ε-caprolactone) (PCL)[95]
Fibrin[86]	Polyurethane[96]
Hyaluronan[87]	Poly(ethylene glycol) (PEG)[97]
Agarose[88]	Poly(N-isopropylacrylamide) (PNIPAM)[98]

Alginate[89]	Elastin-based polymers[99]
Gelatin[90]	Self-assembling peptides - KLD-12[100] - RAD16-I[79,101–103]
Chondroitin sulfate[91]	

1.1.4.4 Self-assembling peptides: RAD16-I

Among synthetic materials, self-assembling peptides constitute a relatively new class of biomaterials. They have the capacity to form stable hydrogels and encapsulate cells for potential therapeutic applications[106,107]. They consist of short peptide sequences with alternating hydrophilic and hydrophobic residues. Under exposure to physiological pH and ionic strength, they form water-soluble β-sheet structures driven by a self-assembling process. Consequently, nanometer-sized structures are formed, showing biomechanical properties similar to native ECM and, therefore, being ideal candidates as cell culture scaffolds for TE applications[108]. Cells can be easily embedded in a truly 3D environment during the self-assembling process, which may promote cell adhesion, spreading, migration, growth and differentiation[61].

In the most basic form, self-assembly consists of the spontaneous organization of molecules into structurally stable arrangements under thermodynamic equilibrium conditions by the driving force of non-covalent interactions, including hydrogen bonds, ionic bonds, electrostatic interaction, van der Waals interaction, etc.[109]. The self-assembly of these amphiphilic peptides is facilitated by electrostatic interactions on one side and the hydrophobic interactions on the other, in addition to the β-sheet hydrogen bonds along the backbone[101,110]. Definitely, a well-organized nanostructured is formed driven by weak non-covalent interactions.

In particular, RAD16-I self-assembling peptide is used in this thesis as a cell culture scaffold. It is a 16-amino acid amphiphilic peptide (with sequence: AcN-RADARADARADARADA-$CONH_2$; where R = Arginine, A = Alanine and D= Aspartic acid) commercially available under the name of Puramatrix™ (Figure 1.1.6). After the self-assembling process, a network of interweaving fibers of around 10-nm diameter is formed and the nanofiber scaffold has an average pore size of 50-200 nm. This is particularly important in trying to imitate nature, since the native ECM is composed of an intricate interweaving of fibers ranging from 10 to several hundreds of nanometers[44]. As a result, RAD16-I environment is permeable to small molecules, metabolites and macromolecules such as gases, nutrients and GFs.

Additionally, cells anchor and pull against the ECM to sense the stiffness of the local microenvironment and respond appropriately, as previously described. The stiffer the matrix, the more difficult is for cells to contract it, which promotes certain cell functions and inhibits others[45]. Importantly, the mechanical strength of RAD16-I can be controlled and modulated for

each different study by changing peptide concentration, as the nanofiber density correlates with the concentration of peptide solution[111,112]. The nanofiber network promotes cell–cell and cell–matrix interactions allowing cells to freely grow, proliferate, migrate, and differentiate under specific experimental conditions. Furthermore, it can be defined as "non-instructive" environment from the point of view of cell receptor recognition/activation, since it does not contain specific motifs in their native sequence[113]. Nevertheless, a key factor of RAD16-I is its versatility to incorporate specific signaling motifs or cues and, thus, be functionalized to promote different cellular responses[114,115]. Finally, it shows good biocompatibility and biodegradability and it is stable at room temperature for long period of time, which makes it very convenient for storage and distribution purposes[116]. The material has also been shown to be non-toxic *in vivo* [117].

Finally, RAD16-I hydrogel peptide has been successfully used to promote *in vitro* maintenance, growth and differentiation of a variety of cell types including hepatocytes[118], neuronal cells[119], osteoblasts[120,121], endothelial cells[122], mesenchymal stem cells[123,124] and fibroblasts[79,103].

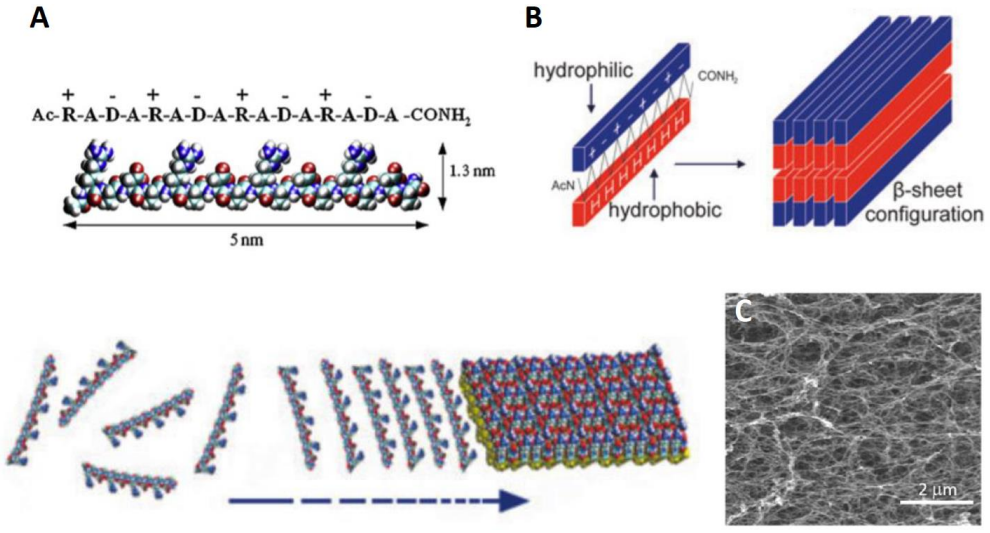

Figure 1.1.6. RAD16-I self-assembling peptide. (A) Molecular model of RAD16-I self-assembling peptide (R=Arg, A=Ala, D=Asp Acid). (B) Schematic model of self-assembling process. RAD16-I is an amphiphilic 16-amino acid peptide that presents alternatively repeating units of positively charged and negatively charged side groups. Under the appropriate conditions (strong ionic or neutral medium), the hydrogel spontaneously self-assembled into a β-sheet configuration, forming a network of interweaving nanofibers, in which cells experienced a truly 3D microenvironment. This process is driven by electrostatic interactions in addition to conventional β-sheet backbone hydrogen bonding. (C) Scanning electron microscopy of the nanofiber network. Adapted from Alemany-Ribes *et al*.[125] and Genové *et al* [115].

1.1.4.5 Stimulatory factors

Besides cells and scaffolds, the third component of TE is stimulating factors that are required to induce, accelerate, and/or enhance cartilage formation. They can be divided into three groups: (*i*) biological stimuli, such as GFs and cytokines; (*ii*) biophysical stimuli, which include oxygen tension and (*iii*) mechanical stimulation, as matrix stiffness.

Regarding biological factors, a plethora of soluble GFs, cytokines and small cell-permeable molecules have been long recognized as important candidates to work in concert in the enhancement of chondrogenesis[53]. They are typically added to the culture medium to drive cell growth and differentiation *in vitro*. A number of GFs like TGFβ, BMP, FGF, insulin-like growth factor-1 (IGF-1), platelet-derived growth factor (PDGF) and Wnt families have been proposed to play a crucial role on chondrogenic lineage commitment during development[126,127]. They act via specific membrane-bound receptors and their effects are mediated by intracellular signaling pathways that regulate the expression of specific genes, leading to the induction of cell proliferation and differentiation. Of particular interest are the members of TGFβ superfamily, which also includes the BMPs, activin, and growth and differentiation factor 5 (GDF5). They have been shown to play an important role in cartilage development, enhancing matrix production and phenotype maintenance[128,129]. Moreover, chondrogenic fate can also be regulated by cell permeable small molecules such as ascorbic acid (also known as vitamin C), dexamethasone (a glucocorticoid receptor agonist), sodium pyruvate, thyroid hormones and retinoic acids[130].

On the other hand, chondrocytes reside in a low oxygen environment (approximately 1%–5%) due to the absence of blood vessels. Moreover, they are subjected to intermittent hydrostatic pressure and mechanical forces *in vivo*[65]. Attempting to mimic physiological properties of cartilage, hypoxia and mechanostimulation have demonstrated to be important regulators of chondrocytes metabolism and chondrogenic inducers of undifferentiated progenitor cells[53,131]. The explanation relies on capability of cells to respond to physical stimuli through mechanotransduction, which can affect their phenotypic expression. Therefore, controlling the physiochemical environment of engineered constructs could lead in the enhancement of tissue development and function *in vitro*. In this regard, different bioreactor systems have been devised in order to apply different mechanical stimuli such as stress, strain, compression and pressurization[132,133].

1.2 FRAMEWORK BIOCART

This thesis is framed in the Biocart project (Bioactive and biomimetic scaffolds for cartilage regeneration) funded by the AO Foundation (Switzerland). The AO Foundation is a medically guided nonprofit organization led by an international group of scientists and surgeons specialized in the investigation and treatment of trauma and disorders of the musculoskeletal system.

Biocart is part of Acute Cartilage Injury Collaborative Research Program (ACI CRP) composed of an international, interdisciplinary network of research teams (Table 1.2.1). ACI CRP is aimed at assessing problems of acute cartilage injury and at developing solutions for treatment, which is a field of great interest due to the current limited surgical treatments for traumatic articular lesions. The ultimate objective is to achieve a pre-clinical proof of concept study testing the consortium developed repair technique/device. Team partners work on collaborative projects towards the consortium goal. To ensure proper function of the network, members from the AO Research Institute (ARI) are responsible for the scientific coordination.

Table 1.2.1. Projects of Acute Cartilage Injury Collaborative Research Program (ACI CRP). From *www.aofoundation.org.*

Project Acronym	Project Title	Investigators
STEMCART	*In vitro* recapitulation of the *in vivo* stem cell niche	- Mauro Alini - Martin Stoddart AO Research Institute, Davos (Switzerland)
CARTHA	Controlling the degradation of hyaluronan hydrogel for cartilage repair	- David Eglin - Martin Stoddart - Mauro Alini AO Research Institute, Davos (Switzerland)
JANUSCAF II	Biphasic Elastomeric Scaffold	- David Eglin - Martin Stoddart - Mauro Alini AO Research Institute, Davos (Switzerland)
STEMLOAD	The effect of mechanical stimulation and biological factors on human MSCs chondrogenesis	- Mauro Alini - Martin Stoddart AO Research Institute, Davos

	and hypertrophy	(Switzerland)
INJURAAV	Gene transfer of chondrogenic factors combined with mechanical loading of MSCs to enhance articular cartilage repair	- Henning Madry - Magali Cucchiarini Saarland University, Homburg (Germany)
BIOCART	Bioactive and biomimetic scaffolds for cartilage regeneration	- Alvaro Mata Queen Mary, University of London, London (UK) - Carlos Semino IQS-School of Engineering, Barcelona (Spain)
OSTEOCHON3D	Multifunctional 3D woven scaffolds for osteochondral repair	- Farshid Guilak Washington University and Shriners Hospitals for Children – St. Louis, St. Louis, MO (USA) - Franklin Moutos Cytex Therapeutics Inc., Durham NC, (USA)
HICARTIA	High throughput cartilage analysis A novel platform for optimizing material design for cartilage tissue engineering and enabling drug discovery for cartilage restoration	- Robert Mauck - George Dodge University of Pennsylvania, Philadelphia (USA)

In particular, Biocart research project proposed to develop bioactive, easy-to-use, biodegradable, and ECM-like materials capable of promoting regeneration of articular cartilage lesions. Biomimetic materials constitute a highly valuable strategy with practical applications in cartilage regeneration. Therefore, the project pursued the design of scaffolds incorporating both structural and functional elements of cartilage, such as specific bioactive signals to attract and stimulate chondrogenic differentiation. Moreover, biodegradability of the material is required to be replaced by the natural cartilage and become a practical off-the-shelf potential strategy for treating cartilage defects. Considering this, we were interested in the combination of building blocks with the intention of developing hydrogels with different properties and functionalities. The initial approach was to combine an amphiphilic self-assembling peptide with other molecular entity naturally present in cartilage ECM, such as heparin (Chapters 3 and 4), chondroitin sulfate and decorin (Chapter 5). The new synthetic scaffolds are expected to

provide a regenerative alternative repair of cartilage lesions, as well as a material platform for the rest of consortium partners.

Furthermore, a collaboration with a consortium member opened the possibility to explore new strategies for cartilage repair. In Osteochon3D project, a custom-designed 3D woven PCL scaffold was developed possessing biomimetic properties of articular cartilage. The basis of this scaffold is a woven matrix structure that recreates the mechanical properties of native articular cartilage and supports cell growth and differentiation. The scaffold is a reinforced 3D meshwork of resorbable fibers, which can be infiltrated with other biomaterials and cells. The design is highly versatile and can be customized using virtually any combination of fibers and matrix gel. Therefore, we were interested in combining with Biocart biomaterials and testing their chondrogenic potential. As a result, part of the work developed in this thesis comes from this collaboration (Chapter 6).

1.3 MOTIVATIONS AND GENERAL AIMS

This thesis was based on exploring different biomaterials as scaffolds for CTE and testing their chondrogenic potential at *in vitro* level. Our working hypothesis was that the use of 3D matrices mimicking the native ECM could promote the chondrogenic differentiation process. With this aim, the non-instructive self-assembling peptide RAD16-I was functionalized with different motifs naturally present in the cartilage ECM such as heparan sulphate (in form of heparin), chondrointin sulphate and decorin. Moreover, as a collaborative project in the context of Biocart, the combination of PCL scaffolds with the RAD16-I hydrogel was explored to create a new composite scaffold with enhanced properties for CTE.

To corroborate our hypothesis two different scenarios were evaluated: the chondrogenic differentiation of adipose-derived stem cells (ADSCs) and the redifferentiation of expanded dedifferentiated articular chondrocytes (ACs), both cell types from human origin. Therefore, the general aims of this thesis are the following:

- To evaluate the chondrogenic potential of the RAD/Heparin bi-component scaffold by inducing ADSCs into cartilage commitment (Chapter 3).

- To evaluate the chondrogenic potential of the RAD/Heparin bi-component scaffold in the redifferentiation process of expanded human ACs (Chapter 4).

- To develop two new bi-component scaffolds (RAD/CS and RAD/Decorin) and evaluate their potential to foster chondrogenic commitment of ADSCs and dedifferentiated ACs (Chapter 5).

- To develop a new composite biomaterial by combining the PCL scaffold with the RAD16-I hydrogel to promote the redifferentiation process of expanded human ACs (Chapter 6).

1.4 REFERENCES

1. Hunziker, E. B. Articular cartilage repair: basic science and clinical progress. A review of the current status and prospects. *Osteoarthr. Cartil.* **10,** 432–463 (2002).
2. Jeng, L., Ng, F. & Spector, M. *Chapter 42 - Articular Cartilage*. *Principles of Regenerative Medicine* (Elsevier Inc., 2011). doi:10.1016/B978-0-12-381422-7.10042-2
3. Madry, H., Grün, U. W. & Knutsen, G. Cartilage repair and joint preservation: medical and surgical treatment options. *Dtsch. Arztebl. Int.* **108,** 669–77 (2011).
4. Chiang, H. & Jiang, C. Repair of articular cartilage defects: review and perspectives. *J. Formos. Med. Assoc.* **108,** 87–101 (2009).
5. Hunziker, E. B., Lippuner, K., Keel, M. J. B. & Shintani, N. An educational review of cartilage repair: precepts & practice - myths & misconceptions - progress & prospects. *Osteoarthritis Cartilage* **23,** 334–350 (2014).
6. Cucchiarini, M. *et al.* A vision on the future of articular cartilage repair. *Eur. Cell. Mater.* **27,** 12–6 (2014).
7. Bobick, B. E., Chen, F. H., Le, A. M. & Tuan, R. S. Regulation of the chondrogenic phenotype in culture. *Birth Defects Res. Part C - Embryo Today Rev.* **87,** 351–371 (2009).
8. Schulz, R. M. & Bader, A. Cartilage tissue engineering and bioreactor systems for the cultivation and stimulation of chondrocytes. *Eur. Biophys. J.* **36,** 539–568 (2007).
9. Reddi, A. H. Bone and cartilage differentiation. *Curr. Opin. Genet. Dev.* **4,** 737–744 (1994).
10. Ross, M. & Pawlina, W. in *Histology: A Text and Atlas* **39,** 184–191 (2004).
11. Onyekwelu, I., Goldring, M. B. & Hidaka, C. Chondrogenesis, joint formation, and articular cartilage regeneration. *J. Cell. Biochem.* **107,** 383–392 (2009).
12. Hall, B. K. & Miyake, T. All for one and one for all: Condensations and the initiation of skeletal development. *BioEssays* **22,** 138–147 (2000).
13. Zuscik, M. J., Hilton, M. J., Zhang, X., Chen, D. & O'Keefe, R. J. Regulation of chondrogenesis and chondrocyte differentiation by stress. *J. Clin. Invest.* **118,** 429–438 (2008).
14. Quintana, L., zur Nieden, N. I. & Semino, C. E. Morphogenetic and regulatory mechanisms during developmental chondrogenesis: new paradigms for cartilage tissue engineering. *Tissue Eng. Part B. Rev.* **15,** 29–41 (2009).
15. Goldring, M. B. Chondrogenesis, chondrocyte differentiation, and articular cartilage metabolism in health and osteoarthritis. *Ther. Adv. Musculoskelet. Dis.*

4, 269–285 (2012).

16. Vinatier, C., Mrugala, D., Jorgensen, C., Guicheux, J. & Noël, D. Cartilage engineering: a crucial combination of cells, biomaterials and biofactors. *Trends Biotechnol.* **27,** 307–14 (2009).

17. Kim, Y. J., Bonassar, L. J. & Grodzinsky, A. J. The role of cartilage streaming potential, fluid flow and pressure in the stimulation of chondrocyte biosynthesis during dynamic compression. *J. Biomech.* **28,** 1055–1066 (1995).

18. Archer, C. W., McDowell, J., Bayliss, M. T., Stephens, M. D. & Bentley, G. Phenotypic modulation in sub-populations of human articular chondrocytes in vitro. *Journal of cell science* **97 (Pt 2),** 361–371 (1990).

19. Ulrich-Vinther, M., Maloney, M. D., Schwarz, E. M., Rosier, R. & O'Keefe, R. J. Articular cartilage biology. *J. Am. Acad. Orthop. Surg.* **11,** 421–430 (2003).

20. Bruckner, P. & Van der Rest, M. Structure and function of cartilage collagens. *Microsc. Res. Tech.* **28,** 378–384 (1994).

21. Eyre, D. Collagen of articular cartilage. *Arthritis Res.* **4,** 30–35 (2002).

22. Eyre, D. R. Collagens and cartilage matrix homeostasis. *Clin. Orthop. Relat. Res.* S118–S122 (2004). doi:10.1097/01.blo.0000144855.48640.b9

23. Dean, D., Han, L., Grodzinsky, A. J. & Ortiz, C. Compressive nanomechanics of opposing aggrecan macromolecules. *J. Biomech.* **39,** 2555–2565 (2006).

24. Athanasiou, K. A., Darling, E. M., DuRaine, G. D., Hu, J. C. & Reddi, A. H. in *Articular Cartilage* 1–50 (CRC Press/Taylor & Francis Group, 2013). doi:10.1201/b14183

25. Robi, K., Jakob, N. & Matevz, K. The Physiology of Sports Injuries and Repair Processes. *Curr. Issues Sport. Exerc. Med.* 43–86 (2013).

26. Roughley, P. J. The structure and function of cartilage proteoglycans. *Eur. Cell. Mater.* **12,** 92–101 (2006).

27. Knudson, C. B. & Knudson, W. Cartilage proteoglycans. *Semin. Cell Dev. Biol.* **12,** 69–78 (2001).

28. Fitzgerald, J. B., Jin, M. & Grodzinsky, A. J. Shear and compression differentially regulate clusters of functionally related temporal transcription patterns in cartilage tissue. *J. Biol. Chem.* **281,** 24095–103 (2006).

29. Szafranski, J. D. *et al.* Chondrocyte mechanotransduction: Effects of compression on deformation of intracellular organelles and relevance to cellular biosynthesis. *Osteoarthr. Cartil.* **12,** 937–946 (2004).

30. Discher, D. E., Janmey, P. & Wang, Y.-L. Tissue cells feel and respond to the stiffness of their substrate. *Science* **310,** 1139–43 (2005).

31. Engler, A. J., Sen, S., Sweeney, H. L. & Discher, D. E. Matrix elasticity directs stem cell lineage specification. *Cell* **126,** 677–89 (2006).

32. Burdick, J. A. & Vunjak-novakovic, G. Review : Engineered Microenvironments for Controlled Stem Cell Differentiation. **14,** (2008).

33. Guilak, F., Meyer, B. C., Ratcliffe, A. & Mow, V. C. The effects of matrix compression on proteoglycan metabolism in articular cartilage explants. *Osteoarthritis Cartilage* **2,** 91–101 (1994).

34. Guilak, F., Jones, W. R., Ting-Beall, H. P. & Lee, G. M. The deformation behavior and mechanical properties of chondrocytes in articular cartilage. *Osteoarthritis Cartilage* **7,** 59–70 (1999).

35. Athanasiou, Kyriacos A., Darling, Eric M., Hu, J. C. *Articular Cartilage Tissue Engineering*. (2009).

36. Langer, R. & Vacanti, J. P. Tissue Engineering. *Science (80-.).* **260,** 920–926 (1993).

37. Furth, M. E. & Atala, A. *Chapter 6 – Tissue Engineering: Future Perspectives*. *Principles of Tissue Engineering* (Elsevier, 2014). at <http://dx.doi.org/10.1016/B978-0-12-398358-9.00006-9>

38. Nerem, R. M. Tissue engineering: confronting the transplantation crisis. *Proc. Inst. Mech. Eng. H.* **214,** 95–99 (2000).

39. Khademhosseini, A., Langer, R., Borenstein, J. & Vacanti, J. P. Microscale technologies for tissue engineering and biology. *Proc. Natl. Acad. Sci. U. S. A.* **103,** 2480–7 (2006).

40. Lavik, E. & Langer, R. Tissue engineering: current state and perspectives. *Appl. Microbiol. Biotechnol.* **65,** 1–8 (2004).

41. Lanza, Robert P., Langer, Robert, Vacanti, J. *Principles of Tissue Engineering*. (2007).

42. Hunziker, E. B. & Mu, M. E. Articular cartilage repair : basic science and clinical progress . A review of the current status and prospects. 432–463 (2002). doi:10.1053/joca.2002.0801

43. Castells-Sala, C. *et al.* Current Applications of Tissue Engineering in Biomedicine. *J. Biochip Tissue Chip* **S2,** 1–14 (2013).

44. Dvir, T., Timko, B. P., Kohane, D. S. & Langer, R. Nanotechnological strategies for engineering complex tissues. *Nat. Nanotechnol.* **6,** 13–22 (2011).

45. Griffith, L. G. & Swartz, M. a. Capturing complex 3D tissue physiology in vitro. *Nat. Rev. Mol. Cell Biol.* **7,** 211–24 (2006).

46. Yamada, K. M. & Cukierman, E. Modeling Tissue Morphogenesis and Cancer in 3D. *Cell* **130,** 601–610 (2007).

47. Pampaloni, F., Reynaud, E. G. & Stelzer, E. H. K. The third dimension bridges the gap between cell culture and live tissue. *Nat. Rev. Mol. Cell Biol.* **8,** 839–45 (2007).

48. Abbott, A. Biology ' s new dimension. **424,** (2003).

49. Alemany-Ribes, M. & Semino, C. E. Bioengineering 3D environments for cancer models. *Adv. Drug Deliv. Rev.* **79-80,** 40–49 (2014).

50. Chung, C. & Burdick, J. Engineering Cartilage Tissue. *Adv Drug Deliv Rev.* **60,** 243–62 (2008).

51. Kisiday, J. D., Jin, M., DiMicco, M. a., Kurz, B. & Grodzinsky, A. J. Effects of dynamic compressive loading on chondrocyte biosynthesis in self-assembling peptide scaffolds. *J. Biomech.* **37,** 595–604 (2004).

52. Iwamoto, M., Ohta, Y., Larmour, C. & Enomoto-Iwamoto, M. Toward regeneration of articular cartilage. *Birth Defects Res. Part C - Embryo Today Rev.* **99,** 192–202 (2013).

53. Freyria, A.-M. & Mallein-Gerin, F. Chondrocytes or adult stem cells for cartilage repair: The indisputable role of growth factors. *Injury* **43,** 259–265 (2012).

54. Brittberg, M. *et al.* Treatment of deep cartilage defects in the knee with autologous chondrocyte transplantation. *N Engl J Med* **331,** 889–895 (1994).

55. Darling, E. M. & Athanasiou, K. A. Rapid phenotypic changes in passaged articular chondrocyte subpopulations. *J. Orthop. Res.* **23,** 425–432 (2005).

56. Lefebvre, V., Peeters-Joris, C. & Vaes, G. Production of collagens, collagenase and collagenase inhibitor during the dedifferentiation of articular chondrocytes by serial subcultures. *Biochim Biophys Acta* **1051,** 266–275 (1990).

57. Hong, E. & Reddi, a H. Dedifferentiation and redifferentiation of articular chondrocytes from surface and middle zones: changes in microRNAs-221/-222, -140, and -143/145 expression. *Tissue Eng. Part A* **19,** 1015–22 (2013).

58. Girotto, D. *et al.* Tissue-specific gene expression in chondrocytes grown on three-dimensional hyaluronic acid scaffolds. *Biomaterials* **24,** 3265–3275 (2003).

59. Miot, S. *et al.* Effects of scaffold composition and architecture on human nasal chondrocyte redifferentiation and cartilaginous matrix deposition. *Biomaterials* **26,** 2479–2489 (2005).

60. Grad, S., Ph, D., Gogolewski, S. & Sci, D. Effects of Simple and Complex Motion Patterns on Gene Expression of Chondrocytes Seeded in 3D Scaffolds. **12,** (2006).

61. Semino, C. E. Can we build artificial stem cell compartments? *J. Biomed. Biotechnol.* **3,** 164–169 (2003).

62. Sharma, M. B., Limaye, L. S. & Kale, V. P. Mimicking the functional hematopoietic stem cell niche in vitro: recapitulation of marrow physiology by hydrogel-based three-dimensional cultures of mesenchymal stromal cells. *Haematologica* **97,** 651–60 (2012).

63. Kolf, C. M., Cho, E. & Tuan, R. S. Mesenchymal stromal cells. Biology of adult

mesenchymal stem cells: regulation of niche, self-renewal and differentiation. *Arthritis Res. Ther.* **9,** 204 (2007).

64. Eslaminejad, M. B. & Poor, E. M. Mesenchymal stem cells as a potent cell source for articular cartilage regeneration. **6,** 344–354 (2014).

65. Guilak, F., Estes, B. T., Diekman, B. O., Moutos, F. T. & Gimble, J. M. 2010 Nicolas Andry Award: Multipotent adult stem cells from adipose tissue for musculoskeletal tissue engineering. *Clin. Orthop. Relat. Res.* **468,** 2530–2540 (2010).

66. Pittenger, M. F. Multilineage Potential of Adult Human Mesenchymal Stem Cells. *Science* **284,** 143–147 (1999).

67. Sharma, B. & Elisseeff, J. H. Engineering structurally organized cartilage and bone tissues. *Ann. Biomed. Eng.* **32,** 148–159 (2004).

68. Chen, W.-H. *et al.* In vitro stage-specific chondrogenesis of mesenchymal stem cells committed to chondrocytes. *Arthritis Rheum.* **60,** 450–9 (2009).

69. Boeuf, S. & Richter, W. Chondrogenesis of mesenchymal stem cells: role of tissue source and inducing factors. *Stem Cell Res. Ther.* **1,** 31 (2010).

70. Hwang, N. S., Varghese, S. & Elisseeff, J. Controlled differentiation of stem cells ☆. **60,** 199–214 (2008).

71. Craft, A. M. *et al.* Specification of chondrocytes and cartilage tissues from embryonic stem cells. *Development* **140,** 2597–610 (2013).

72. Craft, A. M. *et al.* Generation of articular chondrocytes from human pluripotent stem cells. *Nat. Biotechnol.* **33,** 638–645 (2015).

73. Johnstone, B. *et al.* Tissue engineering for articular cartilage repair--the state of the art. *Eur. Cell. Mater.* **25,** 248–67 (2013).

74. Keeney, M., Lai, J. H. & Yang, F. Recent progress in cartilage tissue engineering. *Curr. Opin. Biotechnol.* **22,** 734–740 (2011).

75. Takahashi, K. & Yamanaka, S. Induction of pluripotent stem cells from mouse embryonic and adult fibroblast cultures by defined factors. *Cell* **126,** 663–76 (2006).

76. Sun, N., Longaker, M. T. & Wu, J. C. Human iPS cell-based therapy: Considerations before clinical applications. *Cell Cycle* **9,** 880–885 (2010).

77. Rakar, J., Lönnqvist, S., Sommar, P., Junker, J. & Kratz, G. Interpreted gene expression of human dermal fibroblasts after adipo-, chondro- and osteogenic phenotype shifts. *Differentiation* **84,** 305–313 (2012).

78. Junker, J. P. E., Sommar, P., Skog, M., Johnson, H. & Kratz, G. Adipogenic, chondrogenic and osteogenic differentiation of clonally derived human dermal fibroblasts. *Cells Tissues Organs* **191,** 105–118 (2010).

79. Bianca M. Bussmann, Sven Reiche, Núria Marí-Buyé, Cristina Castells-Sala, H. J.

M. and C. E. S. Chondrogenic potential of human dermal fibroblasts in a contractile, soft, self-assembling, peptide hydrogel. *J. Tissue Eng. Regen. Med.* (2013). doi:10.1002/term

80. Yan, H. & Yu, C. Repair of Full-Thickness Cartilage Defects With Cells of Different Origin in a Rabbit Model. **23,** 178–187 (2007).

81. Griffith, L. G. Tissue Engineering--Current Challenges and Expanding Opportunities. *Science (80-.).* **295,** 1009–1014 (2002).

82. Geckil, H., Xu, F., Zhang, X., Moon, S. & Demirci, U. Engineering hydrogels as extracellular matrix mimics. *Nanomedicine (Lond).* **5,** 469–484 (2010).

83. Lutolf, M. P. & Hubbell, J. a. Synthetic biomaterials as instructive extracellular microenvironments for morphogenesis in tissue engineering. *Nat. Biotechnol.* **23,** 47–55 (2005).

84. Liao, J. *et al.* Recent Developments in Scaffold-Guided Cartilage Tissue Regeneration. *J. Biomed. Nanotechnol.* **10,** 3085–3104 (2014).

85. Chajra, H. *et al.* Collagen-based biomaterials and cartilage engineering. Application to osteochondral defects. *Biomed. Mater. Eng.* **18,** S33–45 (2008).

86. Deponti, D. *et al.* Fibrin-Based Model for Cartilage Regeneration : Tissue Maturation from In Vitro to In Vivo. **18,** (2012).

87. Kim, I. L., Khetan, S., Baker, B. M., Chen, C. S. & Burdick, J. A. Fibrous hyaluronic acid hydrogels that direct MSC chondrogenesis through mechanical and adhesive cues. *Biomaterials* **34,** 5571–5580 (2013).

88. Mauck, R. L., Yuan, X. & Tuan, R. S. Chondrogenic differentiation and functional maturation of bovine mesenchymal stem cells in long-term agarose culture. *Osteoarthr. Cartil.* **14,** 179–189 (2006).

89. Xu, J. *et al.* Chondrogenic differentiation of human mesenchymal stem cells in three-dimensional alginate gels. *Tissue Eng. Part A* **14,** 667–680 (2008).

90. Shin, H., Olsen, B. D. & Khademhosseini, A. The mechanical properties and cytotoxicity of cell-laden double-network hydrogels based on photocrosslinkable gelatin and gellan gum biomacromolecules. *Biomaterials* **33,** 3143–3152 (2012).

91. Coburn, J. M., Gibson, M., Monagle, S., Patterson, Z. & Elisseeff, J. H. Bioinspired nanofibers support chondrogenesis for articular cartilage repair. *Proc. Natl. Acad. Sci. U. S. A.* **109,** 10012–7 (2012).

92. Zhu, L. *et al.* Engineered cartilage with internal porous high-density polyethylene support from bone marrow stromal cells: A preliminary study in nude mice. *Br. J. Oral Maxillofac. Surg.* **48,** 462–465 (2010).

93. Hsu, S. H. *et al.* Evaluation of biodegradable polyesters modified by type II collagen and Arg-Gly-Asp as tissue engineering scaffolding materials for cartilage regeneration. *Artif. Organs* **30,** 42–55 (2006).

94. Uematsu, K., Hattori, K., Ishimoto, Y., Yamauchi, J. & Habata, T. Cartilage regeneration using mesenchymal stem cells and a three-dimensional poly-lactic-glycolic acid (PLGA) scaffold. **26,** 4273–4279 (2005).

95. Moutos, F. T., Freed, L. E. & Guilak, F. A biomimetic three-dimensional woven composite scaffold for functional tissue engineering of cartilage. *Nat. Mater.* **6,** 162–167 (2007).

96. Chia, S.-L., Gorna, K., Gogolewski, S. & Alini, M. Biodegradable elastomeric polyurethane membranes as chondrocyte carriers for cartilage repair. *Tissue Eng.* **12,** 1945–1953 (2006).

97. Bryant, S. J., Bender, R. J., Durand, K. L. & Anseth, K. S. Encapsulating chondrocytes in degrading PEG hydrogels with high modulus: Engineering gel structural changes to facilitate cartilaginous tissue production. *Biotechnol. Bioeng.* **86,** 747–755 (2004).

98. Mortisen, D., Peroglio, M., Alini, M. & Eglin, D. Tailoring Thermoreversible Hyaluronan Hydrogels by ‘ Click ’ Chemistry and RAFT Polymerization for Cell and Drug Therapy. (2010).

99. MacEwan, S. R. & Chilkoti, A. Elastin-like polypeptides: biomedical applications of tunable biopolymers. *Biopolymers* **94,** 60–77 (2010).

100. Kisiday, J. *et al.* Self-assembling peptide hydrogel fosters chondrocyte extracellular matrix production and cell division: implications for cartilage tissue repair. *Proc. Natl. Acad. Sci. U. S. A.* **99,** 9996–10001 (2002).

101. Zhang, S. Fabrication of novel biomaterials through molecular self-assembly. *Nat. Biotechnol.* **21,** 1171–8 (2003).

102. Quintana, L. *et al.* Early tissue patterning recreated by mouse embryonic fibroblasts in a three-dimensional environment. *Tissue Eng. Part A* **15,** 45–54 (2009).

103. Fernández-Muiños, T., Suárez-Muñoz, M., Sanmartí-Espinal, M. & Semino, C. E. Matrix dimensions, stiffness, and structural properties modulate spontaneous chondrogenic commitment of mouse embryonic fibroblasts. *Tissue Eng. Part A* **20,** 1145–55 (2014).

104. Salinas, C. N. & Anseth, K. S. The enhancement of chondrogenic differentiation of human mesenchymal stem cells by enzymatically regulated RGD functionalities. *Biomaterials* **29,** 2370–2377 (2008).

105. Salinas, C. N. & Anseth, K. S. Decorin moieties tethered into PEG networks induce chondrogenesis of human mesenchymal stem cells. *J. Biomed. Mater. Res. - Part A* **90,** 456–464 (2009).

106. Matson, J. B. & Stupp, S. I. Self-assembling peptide scaffolds for regenerative medicine. *Chem. Commun.* **48,** 26 (2012).

107. Zhang, S. Designer Self-Assembling Peptide Nanofiber Scaffolds for Study of 3-D

Cell Biology and Beyond. *Adv. Cancer Res.* **99,** 335–362 (2008).

108. Gelain, F., Horii, A. & Zhang, S. Designer self-assembling peptide scaffolds for 3-D tissue cell cultures and regenerative medicine. *Macromol. Biosci.* **7,** 544–551 (2007).

109. Whitesides, G. M. & Grzybowski, B. Self-assembly at all scales. *Science* **295,** 2418–21 (2002).

110. Lin, Y. & Mao, C. Bio-inspired supramolecular self-assembly towards soft nanomaterials. *Front. Mater. Sci.* **5,** 247–265 (2011).

111. Zhang, S. & Semino, C. E. Design peptide scaffolds for regenerative medicine. *Adv. Exp. Med. Biol.* **534,** 147–63 (2003).

112. Sieminski, a. L., Was, a. S., Kim, G., Gong, H. & Kamm, R. D. The Stiffness of Three-dimensional Ionic Self-assembling Peptide Gels Affects the Extent of Capillary-like Network Formation. *Cell Biochem. Biophys.* **49,** 73–83 (2007).

113. Semino, C. E. Self-assembling Peptides: From Bio-inspired Materials to Bone Regeneration. *J. Dent. Res.* **87,** 606–616 (2008).

114. Genové, E. *et al.* Functionalized self-assembling peptide hydrogel enhance maintenance of hepatocyte activity in vitro. *J. Cell. Mol. Med.* **13,** 3387–97 (2009).

115. Genove, E., Shen, C., Zhang, S. & Semino, C. E. The effect of functionalized self-assembling peptide scaffolds on human aortic endothelial cell function. *Biomaterials* **26,** 3341–3351 (2005).

116. Marí-buyé, N., Fernández Muiños, M. T. & Semino, C. E. in *Methods in Bioengineering: 3D Tissue Engineering* 21–42 (2011).

117. Dégano, I. R. *et al.* The effect of self-assembling peptide nanofiber scaffolds on mouse embryonic fibroblast implantation and proliferation. *Biomaterials* **30,** 1156–65 (2009).

118. Wu, J. *et al.* Nanometric self-assembling peptide layers maintain adult hepatocyte phenotype in sandwich cultures. *J. Nanobiotechnology* **8,** 29 (2010).

119. Semino, C. E., Kasahara, J. & Hayashi, Y. Entrapment of Migrating Hippocampal Neural Cells in Three-Dimensional Peptide Nanofiber Scaffold. *Tissue Eng Part* **10,** (2004).

120. Garreta, E., Genové, E., Borrós, S. & Semino, C. E. Osteogenic Differentiation of Mouse Embryonic Stem Cells and Mouse Embryonic Fibroblasts in a Three-Dimensional. *Tissue Eng Part A* **12,** 2215–2227 (2006).

121. Marí-Buyé, N., Luque, T., Navajas, D. & Semino, C. Development of a three-dimensional bone-like construct in a soft self-assembling peptide matrix. *Tissue Eng Part A* **19,** 870–881 (2013).

122. Sieminski, a L., Semino, C. E., Gong, H. & Kamm, R. D. Primary sequence of ionic

self-assembling peptide gels affects endothelial cell adhesion and capillary morphogenesis. *J. Biomed. Mater. Res. A* **87,** 494–504 (2008).

123. Fernández-Muiños, T. *et al.* Bimolecular based heparin and self-assembling hydrogel for tissue engineering applications. *Acta Biomater.* **16,** 35–48 (2015).

124. Castells-Sala, C. *et al.* Three-Dimensional Cultures of Human Subcutaneous Adipose Tissue-Derived Progenitor Cells Based on RAD16-I Self-Assembling Peptide. *Tissue Eng. Part C. Methods* **22,** 1–12 (2016).

125. Alemany-Ribes, M., García-Díaz, M., Busom, M., Nonell, S. & Semino, C. E. Toward a 3D Cellular Model for Studying In Vitro the Outcome of Photodynamic Treatments: Accounting for the Effects of Tissue Complexity. *Tissue Eng. Part A* (2013). doi:10.1089/ten.TEA.2012.0661

126. Gaissmaier, C., Koh, J. L. & Weise, K. Growth and differentiation factors for cartilage healing and repair. *Injury* **39,** 88–96 (2008).

127. Fortier, L. A., Barker, J. U., Strauss, E. J., McCarrel, T. M. & Cole, B. J. The role of growth factors in cartilage repair. in *Clinical Orthopaedics and Related Research* **469,** 2706–2715 (2011).

128. Baugé, C., Girard, N., Lhuissier, E., Bazille, C. & Boumediene, K. Regulation and Role of TGFβ Signaling P athway in Aging and Osteoarthritis Joints. *Aging Dis.* **5,** 394–405 (2014).

129. van der Kraan, P. M., Blaney Davidson, E. N. & van den Berg, W. B. A role for age-related changes in TGFbeta signaling in aberrant chondrocyte differentiation and osteoarthritis. *Arthritis Res. Ther.* **12,** 201 (2010).

130. Ding, S. & Schultz, P. G. Small molecules and future regenerative medicine. *Curr. Top. Med. Chem.* **5,** 383–95 (2005).

131. Kelly, D. J. & Jacobs, C. R. The role of mechanical signals in regulating chondrogenesis and osteogenesis of mesenchymal stem cells. *Birth Defects Res. Part C - Embryo Today Rev.* **90,** 75–85 (2010).

132. Grad, S., Eglin, D., Alini, M. & Stoddart, M. J. Physical stimulation of chondrogenic cells in vitro: A review. *Clin. Orthop. Relat. Res.* **469,** 2764–2772 (2011).

133. Neumann, A. J., Gardner, O. F. W., Williams, R. & Alini, M. Human Articular Cartilage Progenitor Cells Are Responsive to Mechanical Stimulation and Adenoviral-Mediated Overexpression of. 1–17 (2015). doi:10.1371/journal.pone.0136229

CHAPTER 2

Materials and methods

2.1 MATERIAL CHARACTERIZATION

2.1.1 BI-COMPONENT SCAFFOLDS

2.1.1.1 Sample preparation for staining

The bi-component scaffolds RAD/Heparin, RAD/CS and RAD/Decorin were prepared by combining 95 µL of RAD16-I 0.5% (w/v) (PURAMATRIX™; 354250, Corning) and 5 µL of heparin sodium salt (H3149, Sigma), chondroitin sodium salt (C3788, Sigma) or Decorin (D8428, Sigma) in a concentration range between 0.01% and 1% (w/v). Control RAD16-I samples were prepared with a final concentration of 0.5% (w/v). First, 100 µL of each sample was loaded into a cell culture insert (PICM-1250, Millipore) in a 6-well culture plate, and 500 µL of phosphate buffer saline (PBS) (D8537, Sigma) were added under the insert to start the self-assembly process. Samples were incubated for 30 minutes at room temperature to allow gelation. Then, 200 µL of PBS was added at the inner wall of the insert, allowing it to slowly slide to the gel, and 2.5 mL of PBS was added outside the insert.

2.1.1.2 Toluidine blue staining

Toluidine blue staining was performed to evaluate the presence of highly negative charges provided by the heparin, CS or Decorin molecules. Samples were incubated with toluidine blue 0.05% (w/w) (T3260, Sigma) in water for 20 minutes and then washed several times with Milli-Q water. Finally, stained samples were analyzed under a stereoscopic microscope (Nikon SMZ660).

2.1.1.3 Congo red staining

Congo red staining was performed to evaluate the presence of β-sheet structural characteristics of the self-assembling peptide RAD16-I. Thus, a wide range of blending ratios of the bi-component scaffolds was analyzed by visual inspection, from very low to very high quantities of heparin. Samples were incubated with 0.1% (w/v) congo red (75768, Sigma) in Milli-Q water for 5 minutes and washed several times with PBS. Samples were analyzed under a stereoscopic microscope (Nikon SMZ660).

2.1.1.4 Atomic force microscopy (AFM)

The bi-component scaffolds RAD/Heparin, RAD/CS and RAD/Decorin were prepared by combining 95 µL of RAD16-I 0.15% (w/v) and 5 µL of Heparin, CS or Decorin at a concentration 0.2% (w/v). The mixture was then diluted to a final concentration of 0.005% (w/v) RAD16-I with Milli-Q water. 10 µL of each composite and the control RAD16-I peptide were then placed

onto a mica surface of 9.9 mm diameter. Images were obtained at a resolution of 256 x 256 pixels, using a XE-100 Atomic force microscope (AFM) (Park Systems, Suwon, Korea), operating in non-contact mode. A silicon cantilever (ACTA 10M, Park Systems, Suwon, Korea), resonance frequency of 300 KHz, force constant 40 N/m, tip curvature radius < 10 nm, and 125 µm were used to perform the analysis.

2.1.1.5 ELISA quantification of growth factor (GF) release

RAD/Heparin, RAD/CS and RAD/Decorin composite gels were prepared by combining 95 µL of RAD16-I 0.5% (w/v) and 5 µL of 0.2% (w/v) of the corresponding molecule (CS, Decorin or Heparin). Exceptionally, 0.01% (w/v) heparin was used in the first ELISA test (Chapter 3). Control RAD16-I samples were prepared at a final concentration of 0.5% (w/v). All gels were prepared in triplicate and incubated with a solution of 500 ng/ml TGFβ1 in binding buffer (DMEM, High Glucose, GlutaMAX with 0.1% BSA) for 3 hours at 37ºC and 5% CO_2. Then, the GF solution was removed, and the gels were incubated with binding buffer to allow for the release of TGFβ1 (Figure 2.1.1). Noncumulative measurements were taken at 12, 24, 36, 60 and 84 hours, which required removing the excess binding buffer containing free GF and adding fresh binding buffer to the gels. Samples were analyzed with ELISA kit for TGFβ1 (ab100647, Abcam) according to the manufacturer's protocol.

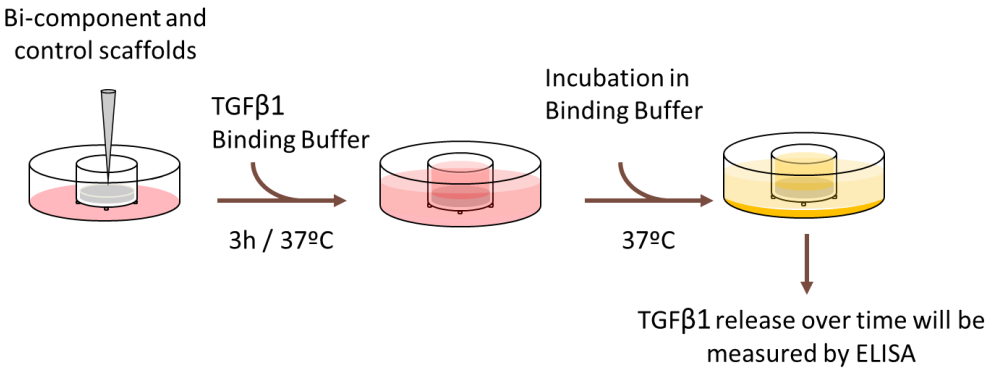

Figure 2.1.1. Schematic representation of TGFβ1 release protocol for ELISA quantification. Bi-component scaffolds (RAD/Heparin, RAD/CS and RAD/Decorin) and control scaffold (RAD16-I) were prepared at final concentration of 0.5% (w/v) RAD16-I and incubated with TGFβ1 in binding buffer for 3 hours at 37ºC. Then, the GF solution was removed, and the gels were incubated with binding buffer to allow for the release of TGFβ1. Samples were taken at 12, 24, 36, 60 and 84 hours and analyzed with ELISA kit.

2.1.2 PCL SCAFFOLD

2.1.2.1 PCL scaffold production

PCL scaffolds were produced and kindly provided by Farshid Guilak, PhD and Franklin T. Moutos, PhD from Washington University and Shriners Hospitals for Children – St. Louis, St. Louis, MO (USA) and Cytex Therapeutics Inc., Durham NC (USA). Scaffolds were woven from multifilament PCL yarns (EMS-Griltech, Domat, Switzerland) as previously described[1]. For this study, 11 layers of yarns were axially oriented in alternating x and y directions with a third set of fibers passing through the thickness of the structure (z-direction). The result is a 0.75 mm thick structure with a total internal void space of ~45% comprised of interconnected rectangular pores measuring approximately 0.35 mm x 0.25 mm x 0.1 mm. Scaffolds were treated with 4N NaOH for 16 hours to clean the fibers and increase surface hydrophilicity, rinsed in deionized water, and dried. Scaffolds were subsequently heat set for 10 minutes at 57°C in deionized H_2O. Dried scaffolds were then punched using a trephine to obtain uniform 5 mm disks. For tissue engineering experiments, disks were ethylene-oxide sterilized in 24 well ultra-low attachment plates (Corning, NY) prior to use.

2.1.2.2 Contact angle measurements

Contact angles of water and RAD16-I drops over the surface of PCL scaffold were measured in a goniometer (DSA 100, Kruss). 2 µL drop of Milli-Q water or RAD16-I 0.5% (w/v) was placed over the surface of the scaffold and a camera immediately acquired an image. Measurements were made at room temperature and three repetitions per each condition were performed.

2.1.2.3 Scanning Electron Microscopy (SEM)

The topographies of PCL scaffolds and PCL/RAD composite scaffolds were examined under field emission SEM (JOEL JSM-5310) at an accelerating voltage of 20 kV. Previously, the surface of the scaffolds were gold-coated (thickness ~150Å) using a Polaron SC7620 Sputter Coater. For this analysis, PCL/RAD composites scaffolds were prepared by lyophilizing 0.5% (w/v) RAD16-I within the PCL scaffolds.

2.1.2.4 Scaffold surface morphology evaluation

The wettability and fiber architecture of PCL scaffolds were evaluated with a stereoscopic microscope (Leica M165 C). 20 µL drop of Milli-Q water or RAD16-I 0.5% (w/v) was placed over the surface of the scaffold and then, they were inspected in a stereoscopic microscope which allows 3D view.

2.2 2D CELL CULTURE

2.2.1 CULTURE OF ADIPOSE-DERIVED STEM CELLS (ADSCs)

ADSCs (PT-5006, Lonza) were cultured at the recommended seeding density (5,000 cells/cm^2) from passage 2 to passage 6 in 175 cm^2 culture flasks. The medium was composed of ADSC Basal Medium (ADSC-BM) (PT-3273, Lonza) supplemented with ADSC Growth Medium (ADSC-GM) SingleQuots (PT-4503, Lonza) containing FBS, L-glutamine and gentamicin/amphotericin-B. Cultures were maintained in a humidified incubator at 37ºC and 5% CO_2.

2.2.2 CULTURE OF HUMAN ARTICULAR CHONDROCYTES (ACs)

ACs cells (CC-2550, Lonza) were cultured at the recommended seeding density (10,000 cells/cm^2) from passage 2 to passage 6 in 25, 75 and 175 cm^2 culture flasks. The expansion medium was composed of Chondrocyte Basal Medium (CBM) (CC-3217, Lonza) plus SingleQuots of Growth Supplements (CC-4409, Lonza) containing R3-IGF-1, bFGF, transferrin, insulin, FBS and gentamicin/amphotericin-B. Cultures were maintained in a humidified incubator at 37ºC and 5% CO_2.

2.2.3 CELL HARVESTING AND SUBCULTURE FROM TISSUE CULTURE FLASKS

Cells were detached using Trypsin-EDTA 0.05 % - 0.02 % (25300-062, Invitrogen) at 37ºC when they are just sub-confluent (approximately 90% confluent). Trypsinization time was usually 5 min or until cells detached from the flask. Then, trypsin's activity was inhibited adding medium containing serum and the solution was dispersed by pipetting over the cell layer surface several times. Cells were centrifuged, resuspended in a minimal volume of medium and counted to be seeded at the corresponding density. Viability was assessed using trypan blue. Cultures were fed every 2 to 3 days after plating until the cells were subcultured or used for 3D cultures.

2.2.4 FREEZING AND THAWING CELLS

Cells were frozen at a final concentration of 1 million cells/0.5 ml. The freeze medium was based on fetal bovine serum (FBS) (DE14-801F; Lot 1SB003, Lonza) with 5% of dimethyl sulfoxide (DMSO) tissue culture tested (D2650, Sigma). DMSO acts as a cryoprotector in order to avoid cellular fracture by reducing the formation of intracellular water crystals. The freezing process is performed slowly by decreasing the temperature of the cells suspended in freezing medium from 4 ºC to -80 ºC in several hours (24 hours) by incubating the freezing tubes into an ice container that is immediately located into a -80 ºC freezer. The following step is to store

the cryotube submerged in liquid nitrogen until the moment of the next programmed culture. The thaw process must be performed quickly. As the cryotube is taken out of the nitrogen tank it is directly submerged in a bath at 37 ºC until only a little part of froze media remains in the cell suspension. Then, the cell suspension is mixed carefully with 10 ml of the corresponding culture medium pre-warmed at 37 ºC. The fast thawing process avoids the osmotic exchanges through the plasmatic membrane between the cells and the medium.

2.3 3D CELL CULTURE

2.3.1 RAD-BASED 3D CULTURES

To obtain 3D cultures, RAD16-I and the composite RAD/Heparin, RAD/CS and RAD/Decorin were prepared at a final concentration of 0.3% (w/v) RAD16-I. The composites were prepared by combining 95 µL of RAD16-I 0.5% (w/v) and 5 µL of CS, Decorin or Heparin at the corresponding concentration. In the case of RAD/Heparin composites, heparin concentration was ranging 0.01-0.1% (w/v), corresponding to ratios mg RAD16-I/mg Heparin 950/1-95/1. RAD/CS and RAD/Decorin composite scaffolds were prepared with 0.2% (w/v) of CS or Decorin, corresponding to ratio mg RAD16-I/mg CS or Decorin 47.5/1. The mixtures were then diluted to a final concentration of 0.3% (w/v) RAD16-I.

The peptide solution was mixed with an equal volume of cell suspension at 4 x 10^6 cells/mL in 10% (w/v) sucrose (S0389, Sigma) to obtain a final concentration of 2 x 10^6 cells/mL in 0.15% (w/v) of RAD16-I and 10% (w/v) sucrose. Then, 80 µL of the cell-peptide mixture (160,000 cells) was loaded into individual wells of a 48-well culture plate previously equilibrated with 150 µL of medium (Figure 2.3.1). Control medium was prepared with DMEM, High Glucose, GlutaMAX (61965, Gibco), ITS+Premix 100x (354352, BD Bioscience), 100 U/mL Penicillin/ 100 µg/mL Streptomycin (P11-010, PAA), 40 µg/mL L-Proline (P5607, Sigma) and 1 mM Sodium Pyruvate (11360, Life Technologies). Upon loading the mixture, the medium induced the self-assembly of RAD16-I, and cells were homogenously distributed in the scaffold. Then, plates were incubated for 20 minutes at 37°C and 5% CO_2. 650 µL of fresh medium were added to the 3D cell cultures, which were then maintained at 37°C and 5% CO_2 for 4 weeks. The medium was changed every second day by removing 400 µL from the well and adding 400 µL of fresh medium. Cultures for chondrogenic differentiation were induced at day 2 with chondrogenic medium (control medium supplemented with 10 ng/mL TGFβ1 (GF111, Millipore), 25 µg/mL L-Ascorbic Acid 2-phosphate (A8960, Sigma) and 100 nM dexamethasone (D8893, Sigma).

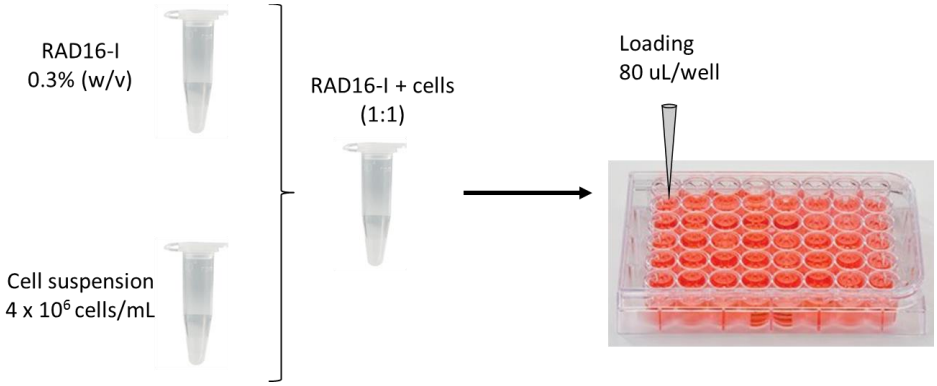

Figure 2.3.1. Schematic representation of cell encapsulation protocol in RAD16-I peptide. RAD16-I 0.3 % (w/v) was mixed with cell suspension ($4 \cdot 10^6$ cells/mL in sucrose 10% (w/v)) in a blend ratio of 1:1. The mixture was loaded inside 48-well plates previously filled with 150 µL of medium.

Cultures were maintained for 4 weeks in the described serum-free media under control or chondrogenic conditions (in the presence of stimulating factors to induce chondrogenic differentiation)[2,3]. After 4 weeks of culture, 3D constructs were analyzed for morphology, viability, gene and protein expression, structural characteristics and mechanical properties.

2.3.2 PCL-BASED 3D CULTURES

ACs at passage 6 were seeded into three different scaffold systems: woven PCL scaffold, RAD16-I self-assembling peptide (described above, in section 2.3.1.) and its combination: the composite PCL/RAD.

In the case of PCL scaffold alone, the procedure consisted on seeding a cell suspension of 25 million cells/mL of ACs in expansion medium (described in section 2.2.2.) onto the surface of 5mm x 0.75mm woven PCL scaffolds (500,000 cells/scaffold). After 2 hours, 100µL of expansion or control medium (described in section 2.3.1.) were slowly added into the well and, after 4 hours, 700 µL were finally added.

The composites PCL/RAD were performed by mixing a cell suspension of 50 million cells/mL of ACs in 10% (w/v) sucrose with 1% (w/v) RAD16-I peptide (1:1). The homogeneous mixture was seeded onto the woven PCL scaffold disks (500,000 cells/scaffold). Then, 40 µL of expansion or control medium were added and the gel was spontaneously formed inside the PCL scaffolds embedding cells. After 30 minutes, 60 µL of medium were added in the well and, after 2 hours, 700 µL were finally added.

3D cell cultures were maintained in the incubator at 37°C and 5% CO_2 during 4 weeks. The medium was changed every second day by removing 400 µL of medium from the well and adding 400 µL of fresh medium. Cultures for chondrogenic differentiation were induced at day 2 with chondrogenic medium (described in section 2.3.1.). After 4 weeks of culture, 3D

constructs were analyzed for morphology, viability, gene and protein expression, staining and mechanical characterization.

2.4 3D CELL CULTURE CHARACTERIZATION

2.4.1 CELL AND CONSTRUCT MORPHOLOGY EVALUATION

Cell morphology into the constructs was directly visualized under Nikon Eclipse TE2000-1 microscope along the culture. The shape of constructs was monitored with the stereoscopic microscope Nikon digital Slight DS-2M. For fluorescence staining, 3D cultures were fixed with p-formaldehyde (PFA) 1% (w/v) (P6148, Sigma) for 1 hour and treated with 0.1% (w/v) Triton X-100 (X100, Sigma) for 30 minutes to permeabilize the cell membrane. Then, they were incubated during 25 minutes with phalloidin-tetramethylrhodamine B isothiocyanate (phalloidin-TRITC) (7418, Sigma) and 5 minutes with 4',6-diamidino-2-phenylindole (DAPI) (D9542, Sigma), both reagents at a final concentration of 0.1 µg/ml in PBS. DAPI is a blue fluorescent probe that fluoresces brightly upon selectively binding to the minor groove of double stranded DNA, where its fluorescence is approximately 20-fold greater than in the unbound state[4]. When the complex DAPI-DNA is formed, DAPI is excited at 364 nm and emits at 454 nm (blue region). Phalloidin binds polymeric F-actin, revealing the distribution of actin filaments and thus enables the visualization of the cytoskeleton. Phalloidin inhibits microfilament de-polymerization and in this case, is attached to TRITC that has its maximum excitation at 540-545 nm and emission at 570-573 nm (red region).

Finally, after 3 washes with PBS, entire constructs were examined under a fluorescence microscope (Zeiss Axiovert 200M inverted microscope with coupled ApoTome system).

2.4.2 CELL VIABILITY ASSESSMENT

2.4.2.1 Live and dead staining

Cell viability was qualitatively assessed by fluorescence using the LIVE/DEAD® Viability/Cytotoxicity kit for mammalian cells (L3224; Invitrogen). It is a two-color fluorescence assay composed of calcein acetoxymethyl (calcein AM) and ethidium homodimer-1 (EthD-1) that simultaneously determines live (green) and dead (red) cells. Calcein AM is a cell-permeable compound which in contact with intracellular esterases is cleaved and becomes intensely fluorescent (in the green spectrum zone). Therefore, only cells with intracellular esterase activity (live cells) will produce green fluorescence. EthD-1 appears fluorescent when bound to nucleic acids and produces a bright red fluorescence in dead cells as they have damaged the plasmatic membrane, which allows the entrance of the compound.

Both compounds (calcein AM and EthD-1) were freshly prepared at a final concentration of 2 µM in PBS and keep it in the dark. Samples were washed previously with PBS and then incubated with the solution for 15 minutes. Then, they were washed again in order to remove any excess of fluorescent compounds (3 times with PBS for 30 minutes) and analyzed under the fluorescent microscope (Zeiss Axiovert 200M inverted microscope with coupled ApoTome system). To detect live cells (green fluorescence) the blue excitation filter (420-495 nm) is used and for dead cells (red fluorescence) the green excitation filter (510-560 nm).

2.4.2.2 MTT assay

Cell viability was quantitatively assessed by MTT assay. MTT (3-[4,5-dimethylthiazol-2-yl]-2,5-diphenyl tetrazolium bromide) (M5655,Sigma) is a water soluble tetrazolium salt yielding a yellowish solution when prepared in media. Dissolved MTT is converted to an insoluble purple formazan by cleavage of the tetrazolium ring by dehydrogenase enzymes (Figure 2.4.1). The conversion only takes place when mitochondrial dehydrogenases are active and, consequently, only in living cells, so this conversion is used as a measure of viable cells. Formazan crystals were solubilized using DMSO (D8418, Sigma) and the dissolved material is measured spectrophotometrically at 550 nm yielding absorbance as a function of concentration of converted dye.

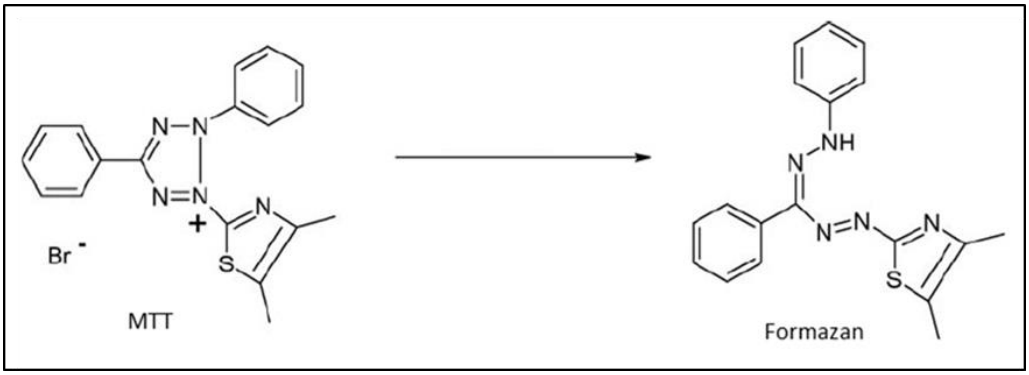

Figure 2.4.1. Reduction of MTT to formazan by dehydrogenase enzymes.

First, a MTT stock solution (10 mg/ml) was prepared with tissue culture water, filtered through a 0.2 µm filter and stored at 2-8 ºC. Each day of the experiment, MTT stock solution was dissolved with culture medium at a final concentration of 0.5 mg/ml, then added covering the samples and incubated for 3 hours at 37 ºC in the dark. After incubation, MTT solution was removed and constructs were lysed with DMSO to solubilize formazan crystals. Samples were prepared in triplicate. Absorbance was read at 550 nm in a microplate reader (Biotek ELX808).

2.4.3 SCANNING ELECTRON MICROSCOPY (SEM)

After 4 weeks of culture, constructs were fixed in 2% (w/v) PFA and dehydrated in successive ethanol washes. Once dehydrated, samples were dried using a CO_2 critical point dryer (Emitech K850). Dried samples were subsequently coated with a thin layer of graphite (approximately 40-50 nm) (Emitech K950X). Finally, samples were examined under a JEDL J-7100 field emission scanning electron microscope (Cathodeluminiscence spectrometer GATAN MONO-CL4, EDS detector, retroscattered electron detector) at an accelerating voltage of 15 and 20 kV.

2.4.4 TOLUIDINE BLUE STAINING

Toluidine blue staining was performed to detect glycosaminoglycans (GAGs) in the 3D cultures thanks to its ability to form complexes with anionic glycoconjugates such as proteoglycans (PGs) and GAGs[5]. Samples were washed with PBS and fixed with 2% (w/v) PFA in PBS for 1 hour at room temperature. Fixed samples were incubated with 0.05% (w/v) Toluidine Blue (T3260, Sigma) in water during 20 minutes and then washed several times with Milli-Q water. Finally, samples were analyzed under a stereoscopic microscope (Leica M165 C).

2.4.5 VON KOSSA STAINING

Von Kossa staining was performed to detect matrix mineralization. 3D constructs were washed with PBS and fixed with PFA 2% (w/v) in PBS for 1 hour at room temperature. Then, cultures were washed several times with Milli-Q water to completely remove the PBS to prevent precipitation with the silver nitrate solution. Then, cultures were incubated for 1 hour with a solution of 5% (w/v) silver nitrate (209139, Sigma) in a dark chamber. The culture was then washed several times with distilled water and placed under a bright light source for 10 minutes. Finally, samples were analyzed under a stereoscopic microscope (Leica M165 C).

2.5 GENE EXPRESSION BY REAL TIME RT-PCR

Real time reverse transcription polymerase chain reaction (real time RT-PCR) was performed in order to analyze gene expression in 2D and 3D cultures. The first step was RNA extraction, followed by complementary DNA (cDNA) synthesis and real time PCR. Finally, the results were confirmed with agarose gels.

2.5.1 RNA EXTRACTION AND PURIFICATION

2D and 3D cultures were washed with PBS and lysed with RNA lysis buffer (12-6834-02, Peqlab) with immediate inactivation of endogenous and exogenous RNases. Constructs were disrupted by pipetting up and down with the micropipette or a pestle and stored at -80ºC. RNA was isolated and purified with PeqGold Total RNA kit (12-6834-02, Peqlab), according to the manufacturer's instructions. The kit provides a quick isolation of total RNA using the reversible binding characteristics of PerfectBind silica filters in centrifugation columns. RNA binds selectively to the silica matrix and can be washed easily before eluting in RNase-free water.

The amount and purity of RNA was determined by measuring its absorbance at 230 nm, 260 nm, 280 nm and 320 nm with the spectrophotometer. Their absorption at 260 UV wavelength is because of the double bonds of the nitrogenous bases. The quantification by this technique may be affected by scattering of light and some impurities such as protein, phenol or other contaminants that absorb near 260 nm. For this reason, some correction parameters should be used. A_{320} corrects for light scattering due to dust particles, which affects the reading at 260 nm. In an optically homogeneous medium, the light progresses in a straight line. Any change of the optical properties by an obstacle will deflect the ray of light from its path. This physical process is called scattering of light by particles. So, the value obtained at 320 nm is subtracted from the corresponding value at 260 nm. This effect is especially noticeable for readings in small volumes. A_{230} gives information about contamination by chemicals: alcohol, phenol, guanidinium from lysis buffer and so on. That can cause overestimation of RNA concentration. So, A_{260}/A_{230} ratio can be calculated as indicated in Equation 2.5.1 and to ensure a good RNA quantification, the ratio value should be in the range 2-2.4.

$$A_{260}/A_{230} = (A_{260} - A_{320}) / (A_{230} - A_{320})$$

Equation 2.5.1. Relationship between nucleic acids and chemical impurities.

A_{280} gives information about protein contamination, because the aromatic amino acids (Phe, Tyr, Trp) absorb UV light at the maximum absorbance of 280 nm. It can also cause an overestimation of RNA concentration, for this reason A_{260}/A_{280} ratio is used to assess the purity of RNA (Equation 2.5.2). A ratio between 1.8 and 2.1 is generally accepted as "pure" for RNA.

$$A_{260}/A_{280} = (A_{260} - A_{320}) / (A_{280} - A_{320})$$

Equation 2.5.2. Relationship between nucleic acids and proteins.

The concentration of nucleic acid can be determined using Lambert-Beer's law, which predicts a linear change in absorbance with concentration (Equation 2.5.3).

$$A = \varepsilon \cdot l \cdot C$$

Equation 2.5.3. Lambert-Beer's law.

Where A is absorbance, Ɛ is the molar extinction coefficient, l is the light path traversed (1 cm with a standard cuvette), and C is the concentration of the absorbent substance. Although the extinction coefficient of nucleic acids depends on the particular sequence of nucleotides, some values can be estimated depending on nucleic acids type (see Table 2.5.1).

Table 2.5.1. Extinction coefficients of different nucleic acids

Nucleic acids	Extinction coefficient ($cm^{-1} \cdot M^{-1}$)
double stranded DNA	0.02
single stranded DNA	0.03
RNA	0.025

Consequently, the RNA amount was calculated as follows (Equation 2.5.4):

$$[RNA] / \mu g \cdot ml^{-1} = (A_{260} - A_{320}) \times \frac{1}{0.025} \times \text{dilution factor}$$

Equation 2.5.4. RNA concentration.

2.5.2 cDNA SYNTHESIS

First, RNA was treated for an effective genomic DNA elimination with the Turbo DNA-free kit (AM1907, Applied Biosystems), according to manufacturer's instructions. Briefly, TURBO DNase Buffer and TURBO DNase were added to RNA sample and mixed gently. Then, samples were incubated at 37°C for 20–30 minutes. DNase Inactivation Reagent was added and incubated during 5 minutes at room temperature. Samples were centrifuged and transferred to a fresh tube.

cDNA was synthesized using a reverse transcriptase enzyme with the High Capacity cDNA Reverse Transcription Kit (4368814; Applied Biosystems), according to manufacturer's instructions. First, a master mix was prepared mixing MultiScribe™ Reverse Transcriptase, Reverse Transcriptase Buffer, dNTPs Mix and Primer Mix. Then, RNA was mixed with the corresponding volume of master mix. The reaction for cDNA synthesis was performed at 42°C and was then inactivated at 95°C. Primer Mix contained a specially optimized mix of oligo-dT and random primers that enable cDNA synthesis from all regions of RNA transcripts, even from 5' regions.

2.5.3 REAL TIME PCR

Real Time PCR reactions were performed with LightCycler® 480 Real-Time PCR System (Roche), using the iQ™ SYBR® Green Supermix (170-8882, Bio-Rad) as fluorescent reporter. SYBR® Green binds to double-stranded DNA and upon excitation emits fluorescence. Primers were designed using Primer Blast software from National Center for Biotechnology Information (NCBI). The following considerations were taken: a melting temperature around 60ºC, maximum of CG content of 60% (optimum between 40-50%), ending with cytosine or guanine bases, maximum of 3-4 dimmers and hairpins, 15-30 base pair of primer length and 200-80 base pair of PCR product length. Primers sequences are shown in ¡Error! No se encuentra el origen de la referencia..

Table 2.5.2. List of primer sequences. Primers from ribosomal protein L22 *(RPL22),* collagen type I *(COL1),* collagen type II *(COL2),* collagen type X *(COL10),* aggrecan *(ACAN), SOX9* and *RUNX2* (all human).

Gene	F/R	Primer sequence (5' to 3')	Length (bp)	Tm (ºC)
RPL22	F	TGACATCCGAGGTGCCTTTC	20	60
	R	GTTAGCAACTACGCGCAACC	20	60
COL1	F	AGACGGGAGTTTCTCCTCGG	20	60
	R	CGGAGGTCCACAAAGCTGAA	20	60
COL2	F	ATGACAATCTGGCTCCCAAC	20	55
	R	CTTCAGGGCAGTGTACGTGA	20	55
COL10	F	CCAATGCCGAGTCAAATGGC	20	60
	R	GGGGGAAGGTTTGTTGGTCT	20	60
ACAN	F	TGGTGATGATCTGGCACGAG	20	64
	R	CGTTTGTAGGTGGTGGCTGT	20	64
SOX9	F	CAGACGCACATCTCCCCCAA	20	62

	R	GCTTCAGGTCAGCCTTGCC	19	62
RUNX2	F	GGTTCAACGATCTGAGATTTGTGGG	25	55
	R	CACTGAGGCGGTCAGAGAACAAACTAG	27	55

Real-time PCR was carried out under the following conditions: 1 cycle of 10 minutes at 95ºC in order to activate the hot-start iTaq™ DNA polymerase, followed by 40 cycles of 15 seconds at 94ºC for denaturation of the double stranded cDNA, 30 seconds at 55ºC (COL2 and RUNX2) or 60ºC (RPL22, COL1 and COL10) or 62ºC (SOX9) or 64ºC (ACAN) for primer annealing and 30 seconds at 72ºC for extension. Finally, a melting step was performed from 58ºC to 95ºC to obtain the melting curve. Relative gene-fold variations were determined according to the 2-ΔΔCt method using the ribosomal protein L22 as a housekeeping gene[6].

2.5.4 AGAROSE GEL ELECTROPHORESIS

Samples from real time RT-PCR were run in a 4% (w/v) agarose gel in order to estimate their size. To prepare the gel, 6 g agarose (A9539, Sigma) were dissolved in 150 mL TAE buffer 1X (from a stock solution TAE 50X: 252 g Tris-Base, 57,1 mL AcOH glacial, 100 mL 18,5 g solid EDTA and deionized H_2O up to 1 L), by heating until complete dissolution. Then, 12 µL of EtBr (10 µg/mL) were added to the agarose solution. 16 µL of the DNA sample were mixed with 4 µL loading buffer 5X (G2526, Sigma), and these 20 µL were loaded into the agarose gel-wells. DNA ladder was also run to estimate DNA fragments size (10821705001 or 11062590001, Roche). The gel was run at 150 V during 1 hour. Finally, the gel was observed using a UV lamp.

2.6 PROTEIN EXPRESSION BY WESTERN BLOT

2D and 3D cultures were lysed in RIPA buffer (R0278, Sigma) with protease inhibitor cocktail (Complete Mini) (11836153001, Roche). Constructs were disrupted by pipetting up and down with the micropipette or a pestle and stored at -20ºC. Protein content of samples was determined using Micro BCA™ Protein assay kit (23225, Pierce-Thermo Scientific). Equal amounts of total protein (5 µg) were denatured using SDS (L5750, Sigma) and β-mercaptoethanol at 95 ºC during 10 minutes. Acrylamide gels were prepared according to the size of the proteins, generally at concentrations of 7.5% or 10% (w/v). Cell lysates were run by applying 150 V for 90 minutes. After migration through the gel, proteins were transferred to a polyvinylidene difluoride (PVDF) membrane (LC 2005, Invitrogen) by applying 40 V for 2 hours at RT. The membrane was incubated at RT for 2 hours in blocking buffer (BB) consisting of 4% (w/v) nonfat milk powder in PBS (18912-014, Gibco) complemented with Tween-20 (P-1379, Sigma) (PBST). Membranes were incubated for 1 hour at room temperature with primary

antibodies at a final concentration of 1 mg/mL in PBST. Then, a species-specific immunoglobulin G-horseradish peroxidase (IgG-HRP) secondary antibody was added, at a final concentration of 1 mg/mL, and incubated at room temperature for 1 hour. Finally, the membrane was evaluated for HRP detection with SuperSignal West Pico Chemiluminescent Substrate (34080; Thermo Scientific). Chemiluminescent images were taken in the ImageQuant™ LAS 4000 mini (GE HealthCare). Anti-Actin (sc-1615; SCBT), anti-Collagen I (ab138492; Abcam), anti-Collagen II (ab3092; Abcam) and anti-Collagen X (ab182563; Abcam) were used as primary antibodies. Anti-goat IgG-HRP (ab97100; Abcam), anti-mouse IgG-HRP (ab97023; Abcam) and anti-rabbit IgG-HRP (ab97051; Abcam) were used as secondary antibodies.

2.7 MECHANICAL CHARACTERIZATION

The mechanical properties of 3D cultures were analyzed by Dynamic Mechanical Analysis (DMA) at the end of the culture. A compression assay with *DMA Multi-Frequency-Strain* mode was applied to each construct and PCL-based scaffolds with a DMA Q800 (TA Instruments). The conditions of the assay were as follows: Amplitude = 1 μm, Preload force = 0.01 N and Frequency = 1 Hz. The frequency was selected based on the standard working frequency historically used in this type of experiment, and the amplitude was selected based on a range of amplitude values wherein the sample remained constant. Construct diameter and thickness were measured for each sample. Under the same conditions, calf and chicken native cartilage could also be measured. However, the soft nature of the 3D constructs cultured in control medium, constructs cultured for only a few days or the RAD16-I scaffold alone did not allow mechanical measurements under the same conditions. Therefore, only chondrogenic 3D constructs could be compared to native cartilage under the experimental conditions described.

Results were obtained with *TA Instrument Explorer* software and analyzed with *TA Universal analysis* software. The storage modulus (G'), loss modulus (G''), complex modulus (G*) and tan(delta) values were obtained and presented in separate graphics. G' is the measure of the sample's elastic behavior, G'' measures the viscous response of the material, G* is the sum of both components and tan(delta) is the ratio of the loss to the storage, representing a measure of the energy dissipation of the material.

2.8 STATISTICS

Samples were prepared in triplicate for the conditions analyzed. All values were expressed as the mean ± SD. Significant differences were analyzed using GraphPad Prism 6. Statistical analysis was carried out by one-way or two-way ANOVA, as appropriate, followed by Tukey

post-hoc analysis. N refers to independent experiments and n to samples per group in each experiment.

Samples were prepared in triplicate for the conditions analyzed. All values were expressed as the mean ± SD. Significant differences were analyzed using GraphPad Prism 6. Statistical analysis was carried out by one-way or two-way ANOVA, as appropriate, followed by Tukey post-hoc analysis. N refers to independent experiments and n to samples per group in each experiment.

2.9 REFERENCES

1. Moutos, F. T. & Guilak, F. Functional properties of cell-seeded three-dimensionally woven poly(epsilon-caprolactone) scaffolds for cartilage tissue engineering. *Tissue Eng. Part A* **16,** 1291–1301 (2010).
2. Cals, F. L. J., Hellingman, C. A., Koevoet, W., Baatenburg de Jong, R. J. & van Osch, G. J. V. M. Effects of transforming growth factor-β subtypes on in vitro cartilage production and mineralization of human bone marrow stromal-derived mesenchymal stem cells. *J. Tissue Eng. Regen. Med.* **6,** 68–76 (2012).
3. Baugé, C., Girard, N., Lhuissier, E., Bazille, C. & Boumediene, K. Regulation and Role of TGFβ Signaling P athway in Aging and Osteoarthritis Joints. *Aging Dis.* **5,** 394–405 (2014).
4. Kubista, M., Akerman, B. & Nordén, B. Characterization of interaction between DNA and 4',6-diamidino-2-phenylindole by optical spectroscopy. *Biochemistry* **26,** 4545–4553 (1987).
5. Terry, D. E., Chopra, R. K., Ovenden, J. & Anastassiades, T. P. Differential use of Alcian blue and toluidine blue dyes for the quantification and isolation of anionic glycoconjugates from cell cultures: application to proteoglycans and a high-molecular-weight glycoprotein synthesized by articular chondrocytes. *Anal. Biochem.* **285,** 211–9 (2000).
6. Livak, K. J. & Schmittgen, T. D. Analysis of relative gene expression data using real-time quantitative PCR and the 2^- ΔΔCT Method. *Methods* **25,** 402–8 (2001).

CHAPTER 3

EVALUATION OF THE CHONDROGENIC POTENTIAL OF THE RAD/HEPARIN BI-COMPONENT SCAFFOLD BY INDUCING ADIPOSE-DERIVED STEM CELLS INTO CARTILAGE COMMITMENT

Fernández-Muiños T*, Recha-Sancho L*, Lopez-Chicon P, Castells-Sala C, Mata A, Semino CE. Bimolecular based heparin and self-assembling hydrogel for tissue engineering applications. *Acta Biomaterialia*. **16**, 35-48 (2015).

*Both authors contributed equally to this work

3.1 INTRODUCTION

Nowadays, self-assembling peptides have been widely used as scaffolds for tissue engineering applications due to their similarity to the natural extracellular matrix (ECM) in terms of mechanical properties and nanoscale network. These peptides self-assemble under physiological conditions into a network of interweaving nanofibers of around 10-nm diameter, forming a hydrogel scaffold with pores sizes of 50–200 nm and over 99% water content[1]. Moreover, mechanical properties can be modulated by changing the peptide sequence and concentration[2,3] and can be defined as ''non-instructive'' from the point of view of cell receptor recognition/activation[1]. Several *in vitro* studies have shown their ability to support cell attachment, growth, maintenance and differentiation of a variety of mammalian cells[4–11]. Other characteristics of self-assembling peptides are: ease synthesis, injectability, biocompatibility, biodegradability and suitability for the incorporation of bioactive motifs or molecules[4,12].

To emulate natural ECM better, both structurally and functionally, growth factors (GFs) can be covalently or non-covalently coupled to the self-assembling peptides[13]. The native ECM binds a wide variety of soluble GFs and cytokines, which slows their diffusion allowing a fine tune of its local concentration and gradients[14]. Moreover, GF-ECM complex favors the interaction with it specific cell receptor promoting better signaling transduction. Trying to increase the local concentration of these molecules in tissue engineered constructs, efforts have been focused on recapitulating their electrostatic interactions with heparan sulphate proteoglycans, which act as GFs reservoir as well as presenter[15] (Figure 3.1.1).

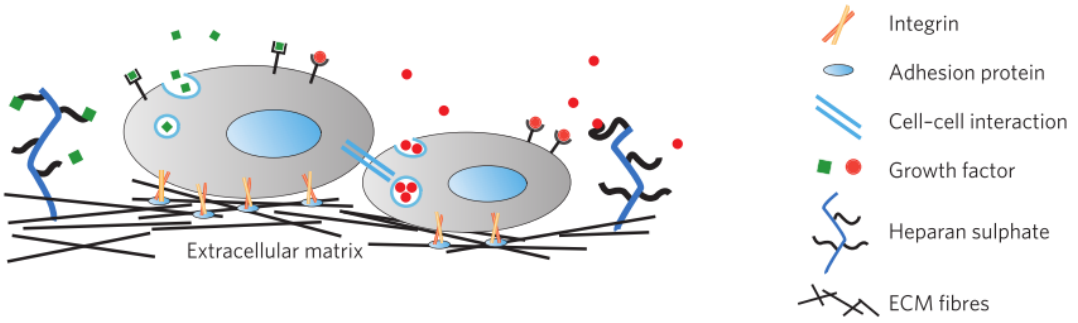

Figure 3.1.1. Information provided to cells by the extracellular matrix (ECM). ECM fibers provide cells with topographical features that trigger morphogenesis. Adhesion proteins such as fibronectin and laminin located on the fibers interact with the cells through their transmembrane integrin receptors to initiate intracellular signaling cascades, which affect most aspects of cell behavior. Polysaccharides such as hyaluronic acid and heparan sulphate act as a compression buffer against the stress, or serve as a growth factor depot. Image from Dvir *et al.*[15]

With this aim, previous work from other groups have designed self-assembling peptides containing a heparin binding domain (HBD) to obtain a strong binding affinity for heparin, which can also bind a wide variety of heparin-binding GFs including $VEGF_{165}$ and FGFβ[13,16–18].

Thus, heparin is a class of glycosaminoglycan with growth factor binding affinity sequestering GFs and localizing of their activity. As a consequence, heparin protects them from degradation and, as mentioned above, might enhance their binding to cell surface receptors[19]. Similar strategies have been used with other types of materials where heparin has been covalently linked to polymers such as alginate and collagen or entrapped within chitosan[18,20,21].

In a previous work from our group, a new injectable nanofiber scaffold with GF binding affinity was developed[22]. The material was formed by the simple combination of the commercially available self-assembling peptide RAD16-I (Puramatrix™), which confers the three-dimensional (3D) environment and heparin moieties, which would allow the binding of heparin binding containing GFs. RAD16-I peptide is soluble in water and self-assembles into nanofibers hydrogels by changing the ionic strength and/or the pH of the solution forming a soft hydrogel. The driving force of the self-assembling process is driven by weak non-covalent interactions including hydrogen bonds, ionic bonds, electrostatic interactions, van der Waals interactions, etc. This brings a unique opportunity to embed cells in a truly 3D matrix during the self-assembling process. Importantly, this nanofiber network promotes cell–cell and cell–matrix interactions allowing cells to freely grow, proliferate, migrate and differentiate under specific experimental conditions[1,10,23]. On the other hand, heparin is highly-sulfated polysaccharide consisting of alternating residues of uronic acid (either β -D-glucuronic acid or α-L-iduronic acid) and hexosamine (α-D-glucosamine) linked by 1→4-glycosidic linkages (Figure 3.1.2). It has various *O*-sulfonate, *N*-sulfonate, and *N*-acetyl substituents that are usually heterogeneously distributed along the GAG chains[24]. Consequently, heparin composition varies depending on the source it is extracted and its molecular size is heterogeneous. It constitutes a mixture of polyanion chains having molecular weights ranging from 6,000 to 30,000 Daltons, with most chains in the range of 17,000 to 19,000 Daltons. Regarding biological function, apart from being a naturally occurring anticoagulant, heparin can interact and modulate the activities of a wide range of proteins that are essentials to important biological processes such as cell growth, differentiation, morphology and migration[25–27]. Its binding affinity properties relies on the fact that the negative charge from the sulfate group and uronic acid in heparin molecule can bind to positively charged basic amino acids through ionic interactions, thus favoring heparin-protein interactions. Therefore, polymeric growth factor delivery systems based on heparin are widely used since it can store GFs in a similar manner to the native ECM[28]. Altogether it evidences the attractive qualities that motivated the combination of the self-assembling peptide RAD16-I and heparin to obtain a new scaffold for tissue engineering applications with drug delivery capacity.

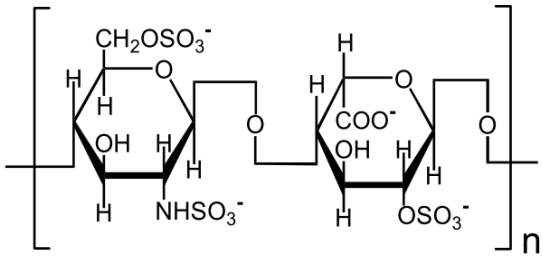

Figure 3.1.2. Chemical structure of the disaccharide repeating unit of heparin. (**left**):glucosamine (GlcN); (**right**): L-iduronic acid (IdoA). Image from Ou *et al.*[29]

In particular, in this thesis, the functionality and potentiality of the new biomaterial was evaluated from the point of view of chondrogenic differentiation. Other tissue engineering strategies were previously successfully addressed, such as vascular tissue formation and cardiogenic differentiation, demonstrating the versatility of the new material[22,30,31].

As mentioned in chapter 1, cartilage is an avascular tissue with limited capacity of regeneration. Thus, treatments to restore function of cartilage defects due to injure or tissue diseases -such as osteoarthritis- is a challenge topic in therapeutic medicine[32]. Application of autologous cell transplantation (ACT) using patient chondrocytes or mesenchymal stem cells (MSCs) are currently under development to assist cartilage repair. Patient isolated chondrocytes dedifferentiate rapidly after expansion and therefore they need to be redifferentiated[33]. MSCs are a population of multipotent cells able to differentiate into chondrogenic, osteogenic and adipogenic lineages[34]. They can be isolated from the bone marrow and adipose tissue which provides an abundant supply of cells. Many studies have demonstrated the potential of MSCs to differentiate into bone and cartilage[35]. For these reasons, MSCs from the adipose tissue were selected to test the chondrogenic potential of the new bi-component hydrogel. In addition to cell sources, the microenvironment has a crucial role in the determination of cells to the chondrogenic lineage. An important factor to be considered is the capacity of the differentiated cells to be transplanted in maintaining a good chondrogenic phenotype since it is common for the cells to become hypertrophic and induce mineralization at the transplanted site. The use of biomimetic material-based platforms, which recreates the natural environment of the chondrocytes, seems to enhance the differentiation process. Therefore, efforts have been focused on TE applications using biomimetic scaffolds to improve the conventional treatments for cartilage injury[36]. In particular, the advantages of the new bi-component RAD/Heparin hydrogel include: the commercial availability of both components, which eliminates the need of synthesis as compared to previous studies[13,16,17]; and the availability of clinical grade components, which facilitates its future use in *in vivo* pre-clinical and clinical studies.

3.2 PREVIOUS RESULTS

3.2.1 DEVELOPMENT AND CHARACTERIZATION OF A NEW BI-COMPONENT MATERIAL

A new biomaterial for TE applications based on the self-assembling peptide RAD16-I was previously developed by Dra. Maria Teresa Fernández-Muiños[22]. It is basically a hydrogel scaffold consisting in two components: the RAD16-I self-assembling nanofiber matrix and the heparin polysaccharide. First, in order to obtain a biomaterial with good mechanical, structural and biological properties, the possibility of combining the self-assembling peptide RAD16-I with heparin in different blended ratios was evaluated. Thus, the chemical and structural stability of the mix (RAD16-I and heparin) without conjugation was tested, in order to assess the degree of interaction between both molecules. For this purpose, different composites were prepared with blending ratios of RAD16-I and heparin (RAD/Heparin), ranging from 950/1 to 9.5/1. Interestingly, the combination was structurally very stable at physiological pH and developed a nanofiber composite self-assembling peptide–heparin. The permanent blue/purple color observed after staining with toluidine blue indicated the presence of highly negative charges provided by the heparin molecules associated with the self-assembling nanofiber network in a dose dependent manner (Figure 3.2.1 A)[37]. In addition, congo red, which stained β-sheet structures characteristic of the self-assembled RAD16-I[38], showed that heparin was not interfering in the self-assembling process, independently of the heparin quantity (Figure 3.2.1 A).

In addition, the effect of heparin in the β-sheet secondary structure characteristic of the peptide RAD16-I was studied by Circular Dichroism (CD)[39,40]. CD is a spectroscopy technique that refers to the differential absorption of the left and right circularly polarized components of plane-polarized radiation[40]. It is a useful tool for the structural characterization of proteins and peptides. A typical CD spectrum for a β-sheet structure shows a minimum molar ellipticity around 218 nm, which represents the β-sheet content and a maximum at 195 nm which corresponds to the backbone twist of the peptide in b-sheet configuration[41]. First, RAD16-I was analyzed separately and as expected, it showed a typical CD spectrum for a β-sheet structure showing a minimum molar ellipticity (deg cm^2/decimole) around 216 nm and a maximum at 195 nm (Figure 3.2.1 B). Subsequently, the secondary structures of the composites were similarly studied to elucidate whether the addition of heparin was affecting the β-sheet secondary structure. Three types of composites were prepared with ratios of RAD/Heparin equal to: 950/1, 95/1 and 9.5/1. The addition of heparin was translated into weaker β-sheet structures, represented by a decrease in the intensity of molar ellipticity with a minimum at 216 nm and the maximum at 198 nm. This effect was observed in a dose dependent trend: the higher the concentration of heparin, the weaker the β-sheet structure (Figure 3.2.1 C).

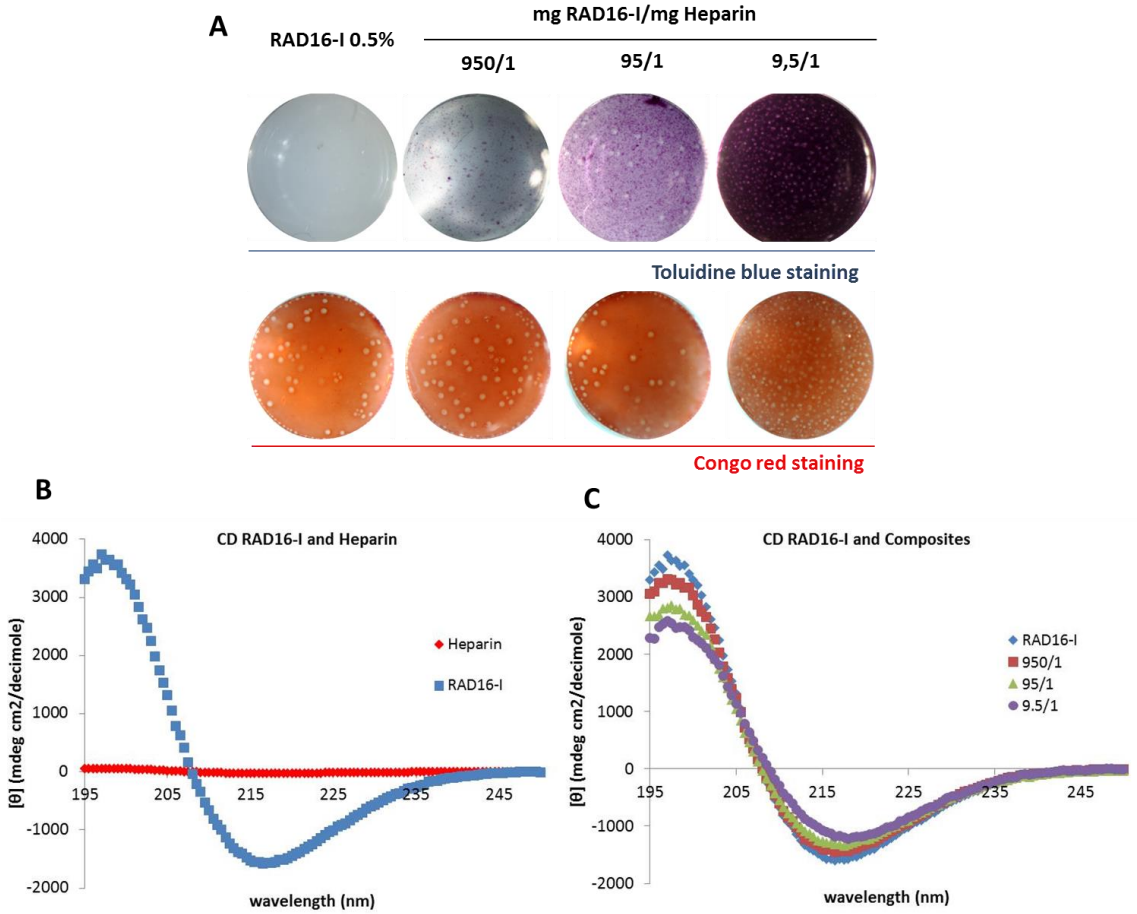

Figure 3.2.1. Influence of heparin in the RAD16-I self-assembling process. (A) Toluidine blue and congo red staining of RAD16-I and composites with increasing quantities of heparin. Ratios mg RAD16-I/mg Heparin from 950/1 to 9.5/1. (B) Circular Dichroism (CD) of RAD16-I and Heparin. (C) CD of RAD16-I and composites with ratios mg RAD16-I/mg Heparin from 950/ 1 to 9.5/1.

Then, Scanning Electron Microscopy (SEM) imaging was used to visualize and characterize the morphology of the nanofibers (Figure 3.2.2). As expected due to the CD analysis, a network of interweaving nanofibers was observed when the composite (950/1) and the control RAD16-I were analyzed (Figure 3.2.2 A&C). Interestingly, areas with higher density of nanofibers, forming bundles but maintaining the nanofiber structure, were detected in a dose dependent manner in the composites with increasing quantities of heparin (Figure 3.2.2 E&G). It was speculated that during the assembly process heparin interacts with RAD16-I peptide through electrostatic interactions. Indeed, heparin is a highly sulfated anionic polysaccharide which is negatively charged at working pH and RAD16-I is an amphiphilic peptide consisting of repeating units of hydrophilic (arginine (R), and aspartic acid (D)) and hydrophobic (alanine (A)) aminoacids with alternating positive and negative charges in the hydrophilic phase. Thus, negatively charged heparin would bind electrostatically to the positively charged arginine residues at physiological pH. As a consequence, the areas with higher density of nanofibers could be formed due to the strong ionic interaction between both molecules. Moreover, it was

also speculated that these nanofiber bundles corresponded to the areas stained with toluidine blue also observed in a dose dependent manner (Figure 3.2.2 D,F&H). In view of these results, it was decided to use the lowest heparin concentration (ratio RAD/Heparin 950/1) for the subsequent analysis of growth factor delivery. The CD of this composite was slightly different from the control self-assembling peptide and it also maintained its structural properties as observed by SEM.

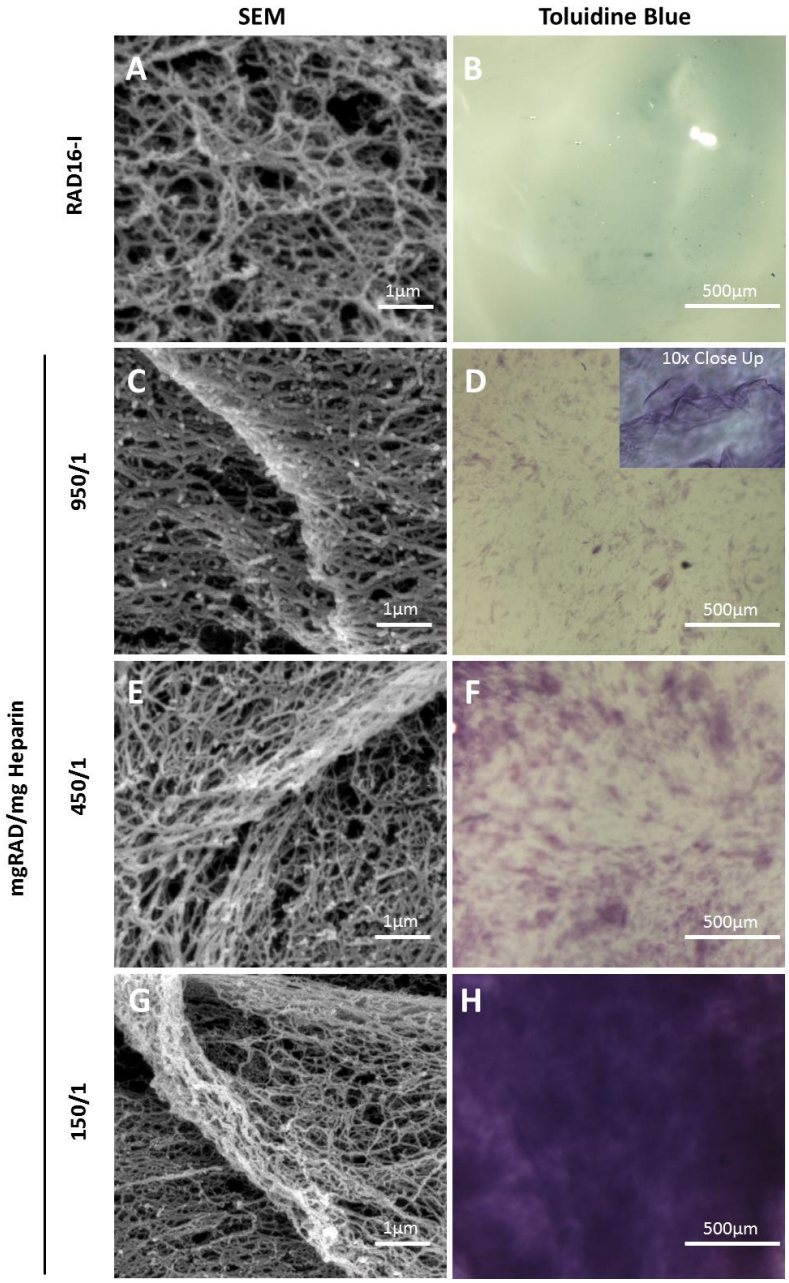

Figure 3.2.2. Scanning Electron Microscopy (SEM) of RAD16-I and composites RAD/Heparin. RAD16-I and composites with ratios mg RAD16-I/mg Heparin: 950/1, 450/1 and 150/1 were prepared at a final concentration of 0.5% (w/w) RAD16-I. (A) SEM image and (B) Toluidine blue of RAD16-I; (C) SEM image and (D) Toluidine blue of 950/1 composite; (E) SEM images and (F) Toluidine blue of 450/1 composite; (G) SEM image and (H) Toluidine blue of 150/1 composite.

3.2.2 GROWTH FACTOR DELIVERY

After analyzing the influence of heparin on the self-assembling process and the nanofiber formation, the suitability of the composite for drug delivery was assessed. For this purpose, a non-cumulative quantification of GFs containing HBDs ($VEGF_{165}$ and FGFβ) released by the composite and the control RAD16-I was performed. Thus, it was observed that the control scaffold released almost all the $VEGF_{165}$ in the first 12 h and that the amount of GFs after 24 h nearly reached zero. Nevertheless, the peptide-heparin composite gradually released $VEGF_{165}$ over the course of the experiment (36 h) (Figure 3.2.3 A). In the case of FGFβ a similar GF release was observed, however no significant differences were found between the control RAD16-I and the composite (Figure 3.2.3 B).

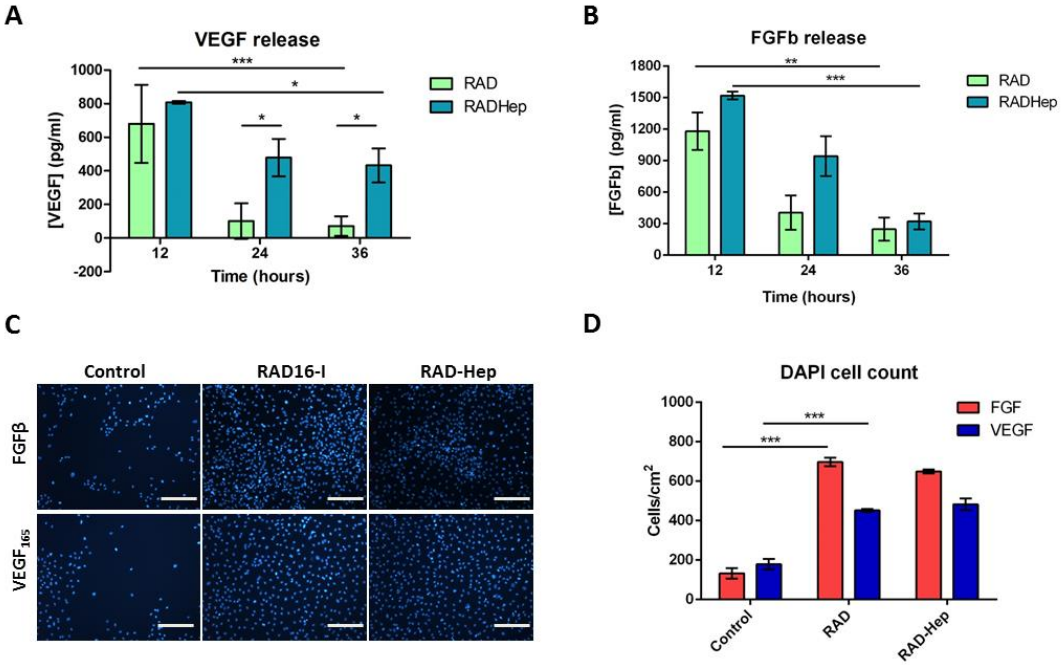

Figure 3.2.3. Characterization of RAD16-I and the composite RAD/Heparin as drug delivery hydrogels. Non-cumulative quantification of (A) VEFG, and (B) FGFβ released by RAD16-I and the composite RAD/Heparin 950/1 after 12, 24 and 36 hours of delivery. (C) DAPI staining of 2D endothelial cells cultures after 48 hours of culture with the released growth factors from RAD and RAD/Heparin composite and, (D) Cell count of 2D cultures from (C). (Statistical differences are indicated as:* for $p<0.05$, ** for $p<0.01$, and *** for $p<0.001$, Two-way ANOVA, n=3).

In order to know if the released GF was biologically active, a functional study was performed. It consisted of adding the released GF to a 2D culture of Human Umbilical Vein Endothelial Cells (HUVECs) cultured in Endothelial Basal Media-2 without any additional GF. After 48 h, cell cultures were stained with DAPI in order to count the cells of each type of culture: GF released from the control RAD16-I, GF released from the composite and the control without the addition of any GF (Figure 3.2.3 C). Results showed a clear effect of the released GFs on

HUVECs maintenance and proliferation with higher cell numbers in cases were the GF was added to the culture media than the control where almost all cells were dead (Figure 3.2.3 D). These results suggested that both, $VEGF_{165}$ and FGFβ, maintained their biological activity after being released by the hydrogels. No significant differences, in terms of cell number, were found between GFs released from RAD16-I or the composite.

3.2.3 TESTING THE NEW BIOMATERIAL FOR CELL VIABILITY

Then, the effect of heparin in cell viability was evaluated using human Normal Dermal Fibroblasts (hNDFs). Interestingly, cell viability was not affected by the presence of heparin in the scaffold as compared to the control (RAD16-I) where almost all cells were alive (Figure 3.2.4 A&B). Moreover, it was observed a similar behavior in terms of cell elongation and network development as it is shown in the DAPI-Phalloidin staining (Figure 3.2.4 C-F).

In addition, the new hydrogel was also used to culture other cellular types for different TE applications. In particular, the angiogenic and cardiogenic capacity of the RAD/Heparin composite was evaluated with Human Dermal Microvascular Endothelial Cells (HDMECs)[22] and human subcutaneous Adipose Tissue-Derived Progenitor Cells (subATDPCs)[30], respectively. The bi-component scaffold exhibited good biological properties in the growth and maintenance of the tested cellular types and potential to be used in different scenarios.

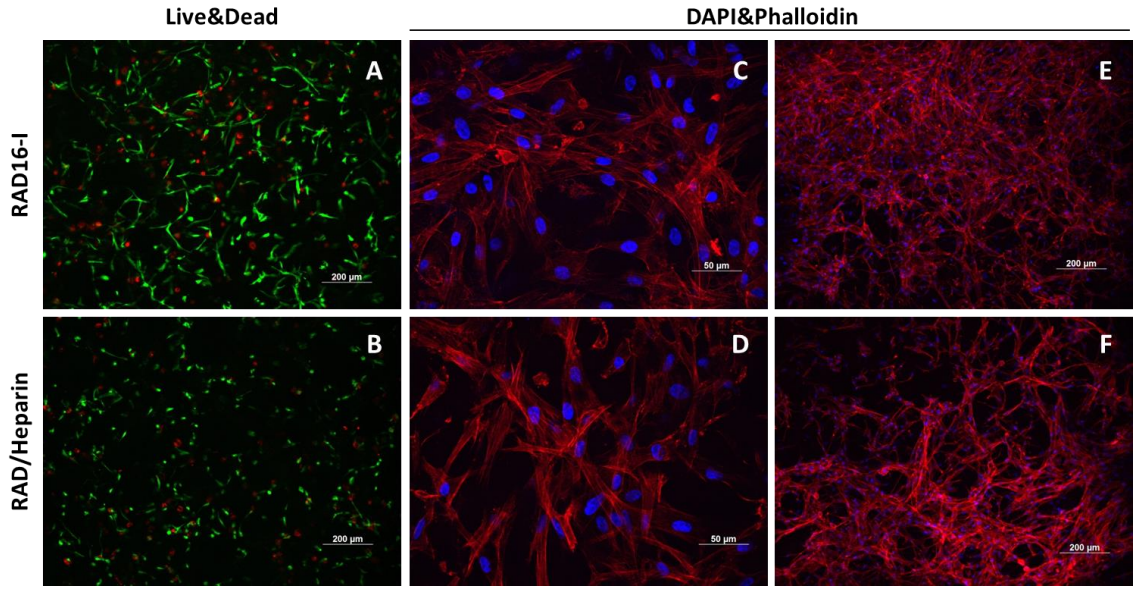

Figure 3.2.4. Human Normal Dermal Fibroblasts (hNDFs) viability and network development in RAD16-I and the composite RAD/Heparin. RAD16-I and the composite RAD16-I/Heparin 950/1 was prepared at a final concentration of 0.15% (w/w) RAD16-I. hNDFs were encapsulated in both types of materials and maintained for 8 days. (A,B) Live and dead staining showed no differences in cell viability between different types of materials. (C-F) DAPI-Phalloidin staining showed similar cell behavior in all materials with cell elongation and development of a tight network.

3.3 MOTIVATIONS AND SPECIFIC AIMS

Previous results indicated that the new composite RAD/Heparin presents good mechanical, structural and biological properties. In this regard, the main general objective of this chapter is to evaluate the chondrogenic potential of the bi-component scaffold using human Adipose-Derived Stem Cells (ADSCs). In particular, the specific aims for this chapter are the following:

(1) To assess the intrinsic potential of the bimolecular based hydrogel for the delivery of TGFβ1.

(2) To evaluate the behavior of ADSCs in the new biomaterial hydrogels at 2 and 4 weeks of culture under chondrogenic conditions.

(3) To study the expression patterns at both gene and protein level of specific chondrogenic and hypertrophic markers.

(4) To characterize mechanically the 3D constructs properties at the end of the culture comparing to native articular cartilage.

3.4 RESULTS

3.4.1 ASSESING THE INTRINSIC POTENTIAL OF THE BIMOLECULAR BASED HYDROGEL FOR TGFB1 DELIVERY

Taking advantage of the versatility of RAD/Heparin composite to be used in different applications, in the present thesis, the bi-component scaffold was studied for CTE purposes. Particularly, the chondrogenic differentiation capacity of RAD16-I and RAD/Heparin composite was evaluated using human ADSCs. First, due to the key role of TGFβ1 in the chondrogenic differentiation process, we aimed to know whether this GF presented a differential binding depending on the presence of heparin in the scaffold. Therefore, the GF binding affinity of TGFβ1 to both biomaterials, the RAD16-I self-assembling peptide with and without heparin, was tested. Considering previous results of GF delivery with $VEGF_{165}$ and FGFβ (see Figure 3.2.3 A&B), the same study of binding and release (a non-cumulative quantification) was performed for TGFβ1, but in this case the duration of the experiment was increased. A similar GF release pattern was observed between the control RAD16-I and the composite RAD/Heparin over time, indicating that TGFβ1 did not show any specific affinity to heparin in the conditions of the assay (Figure 3.4.1).

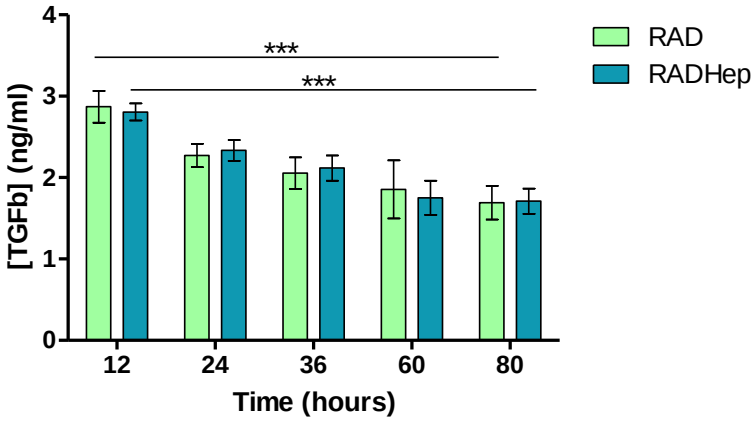

Figure 3.4.1. TGFβ1 release pattern of RAD16-I and the composite RAD/Heparin. Non-cumulative quantification of TGFβ1 released by RAD16-I and the composite RAD/Heparin 950/1 from 12 to 80 hours of delivery. (Statistical differences are indicated as:* for p<0.05, ** for p<0.01, and *** for p<0.001, Two-way ANOVA, n=3).

Subsequently, the effect of heparin concentration in the scaffold was studied in greater detail for further *in vitro* assays. With this aim, new blended ratios of RAD/Heparin composite were prepared ranging from 950/1 to 9.5/1. Their structural stability was evaluated by staining gels with toluidine blue and congo red in order to assess the presence of heparin and β-sheet structure, respectively (Figure 3.4.2). Homogeneous gels were formed in all cases and toluidine blue stained them in a dose dependent manner indicative of the presence of heparin.

Composites developed into a nanofiber network as evidenced by β-sheet structures stained by congo red. As is previously mentioned, heparin binds unspecifically to the self-assembling peptide RAD16-I through electrostatic interactions resulting into structurally stable scaffold at physiological pH. Moreover, the RAD/Heparin gels maintain positive toluidine blue staining after extensive washing, demonstrating the molecular stability of the peptide-polysaccharide interaction.

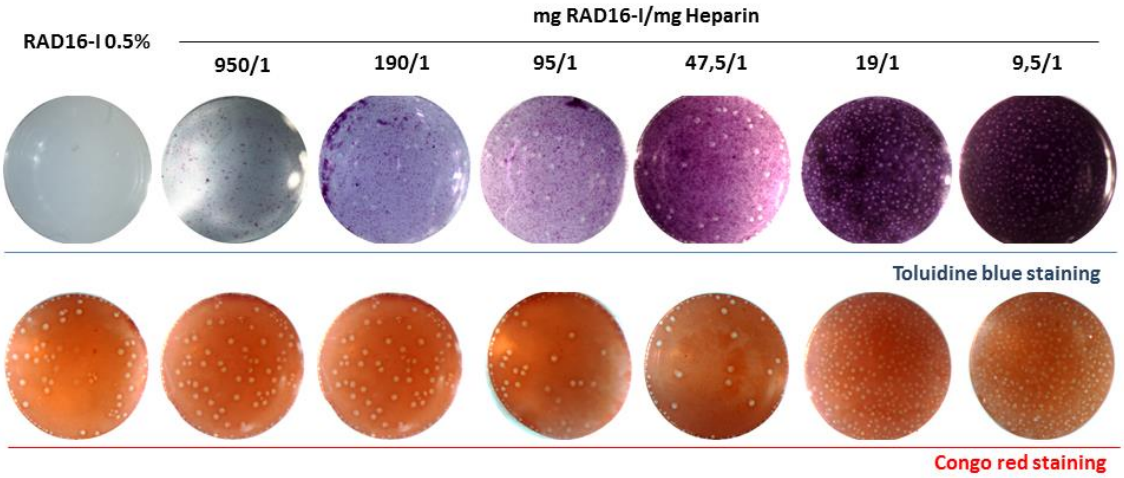

Figure 3.4.2. Toluidine blue and congo red staining of RAD16-I and RAD/Heparin composites. Ratios mg RAD16-I/mg Heparin from 950/1 to 9.5/1.

3.4.2 EVALUATION OF ADSCs BEHAVIOR IN THE NEW BIOMATERIAL

In view of these results, composites RAD16/Heparin of the lowest quantity of heparin were selected to culture ADSCs. Moreover, we aimed to chemically induce the chondrogenic differentiation process by using chondrogenic medium containing TGFβ1, L-ascorbic acid 2-phosphate and dexamethasone as inductors (described in Chapter 2, Materials and Methods)[42,43]. The same media composition without the chondrogenic inductors was used as a control medium. Remarkably, these media do not contain FBS, therefore its composition will be more controllable, reproducible and make future therapeutic applications more suitable.

The idea was to promote chondrogenesis of ADSCs by culturing them into RAD/Heparin composite scaffolds under chondrogenic conditions during 4 weeks (Figure 3.4.3). First of all, a previous study of cell morphology and viability was performed at 2 weeks of culture in order to evaluate the behavior of ADSCs in this nanofiber network environment. For this purpose, ADSCs were embedded in RAD16-I and in two different composites (RAD/Heparin 950/1 and 95/1) and maintained under control and chondrogenic media. Interestingly, a morphological change was observed macroscopically in 3D constructs cultured in chondrogenic medium (Figure 3.4.4). The diameter of the constructs was reduced around 65% after 2 weeks of culture compared to the initial diameter at day 1. As a consequence, the 3D construct resulted

in a compacted structure. This event was independent of the presence of heparin in the scaffold and no apparent construct geometry reduction was observed under control medium conditions.

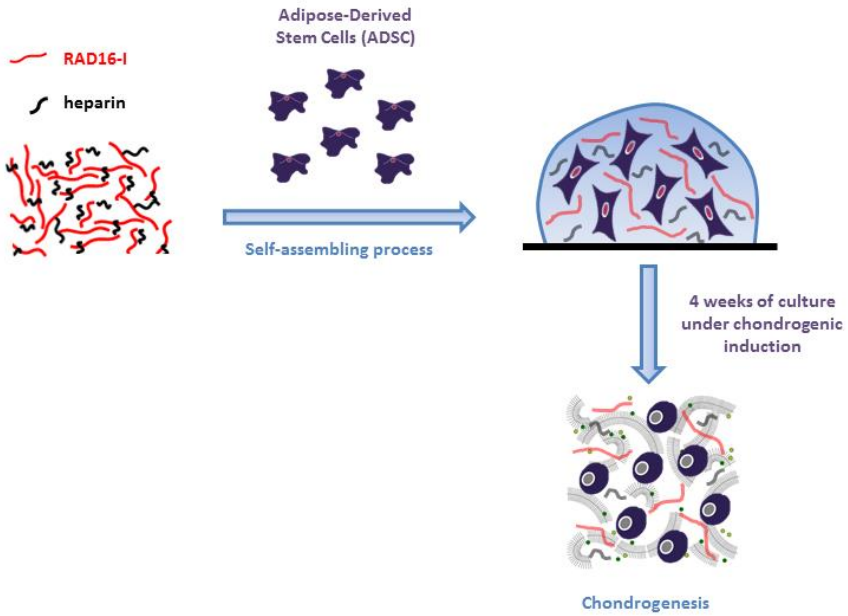

Figure 3.4.3. Schematic process to obtain 3D cultures of Adipose-Derived Stem Cells (ADSCs) in bi-component scaffolds to promote chondrogenesis. ADSCs were cultured into RAD/Heparin composite scaffolds during 4 weeks under chondrogenic conditions.

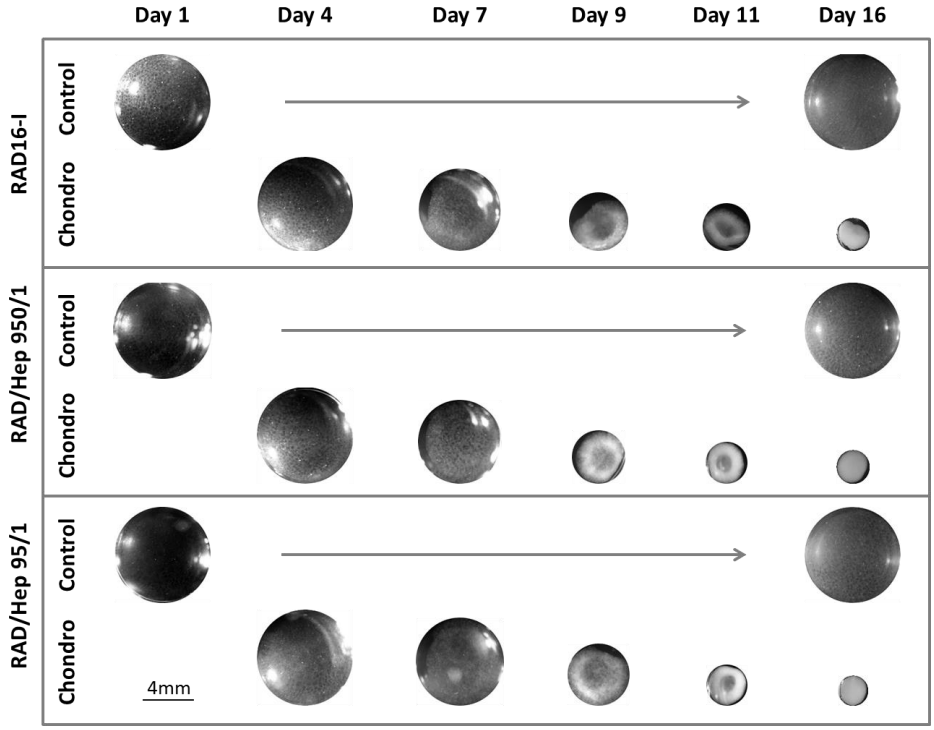

Figure 3.4.4. Morphologic assessment of Adipose-Derived Stem Cells (ADSCs) 3D constructs during the culture time. ADSCs were encapsulated in RAD16-I and in the composites RAD/Heparin 950/1 and 95/1. 3D constructs were maintained during 2 weeks in control and chondrogenic medium (added the second day of culture). Control refers to control medium and chondro to chondrogenic medium. ADSCs 3D constructs under chondrogenic medium suffered a contraction process during the culture time (diameter reduction around 65%).

In view of the fact that final compacted 3D structures were only achieved under chondrogenic conditions, it is reasonable to think that the composition of this medium was driven the contraction process. Therefore, in order to elucidate the specific components, a more detailed study was performed. Considering that the only difference between control and chondrogenic medium were the inducers (TGFβ1, L-ascorbic acid 2-phosphate and dexamethasone), they were added individually or in combination to ADSCs 3D constructs. Figure 3.4.5 shows that when the inducers where added individually, only in the case of dexamethasone the construct diameter was reduced. Then, the addition of only 2 inducers reduces the constructs diameter with all the possible combinations. Therefore, although we could initially think that dexamethasone was driving the contraction process, the synergic effect of TGFβ1 and L-ascorbic acid 2-phosphate also produced a similar effect. Importantly, this reduction was comparable in terms of diameter size to that observed with the complete chondrogenic medium.

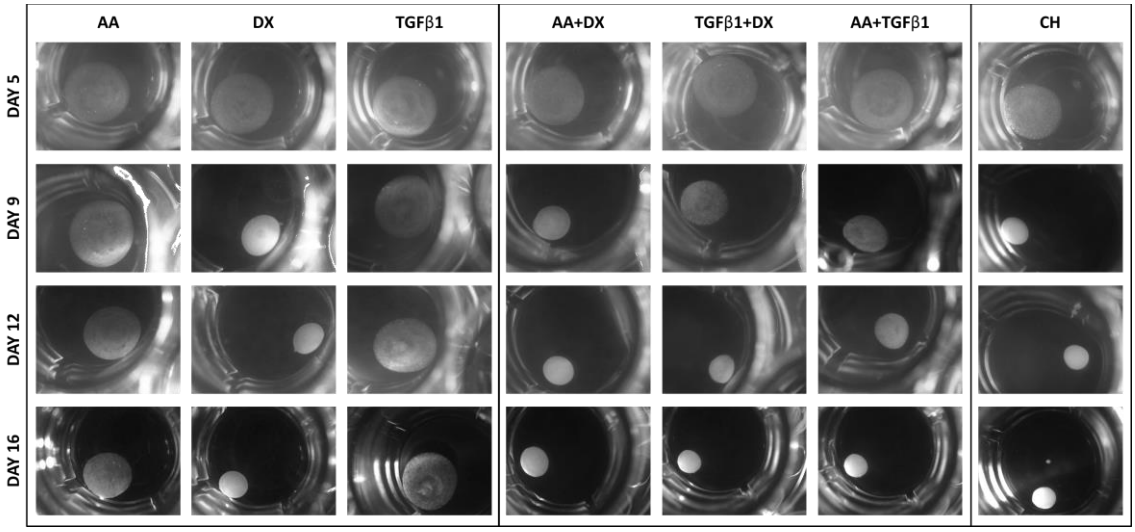

Figure 3.4.5. Effect of chondrogenic inducers in the 3D construct morphology of Adipose-Derived Stem Cells (ADSCs) over time. ADSCs were cultured in RAD16-I and 3D constructs were maintained during 2 weeks in different combinations of chondrogenic inducers (added the second day of culture). AA refers to L-ascorbic acid 2-phosphate, DX to dexamethasone, TGFβ1 to transforming growth factor beta1 and CH to chondrogenic medium.

At microscopic level, cell morphology and organization within the 3D cultures were characterized by DAPI-Phalloidin staining. In general, a similar cell behavior was observed between scaffolds types and differences were detected between culture media (Figure 3.4.6). A dense cellular network could be observed in constructs cultured under chondrogenic medium, while cells appeared more dispersed in constructs under control medium. Initially, during the first days of culture, cells exhibited a rounded shape that progressively changed to a more elongated morphology (Figure 3.4.7). Hence, during culture time, different cellular behaviors were taking place in the 3D system. Cells elongate and spread supporting intercellular connections and moreover, other complex cellular processes, such as cell migration, proliferation and differentiation, could be taking place in a dynamic microenvironment. These events were possible due to the soft nature of the peptide RAD16-I, since the non-covalent interactions between the nanometric fibers enable cells to freely interact, migrate and extend different cellular processes.

At the same time, cellular behaviors could have an effect in the 3D construct morphology as observed in this work (Figure 3.4.4). The system evolved into a compacted structure under chondrogenic conditions due to mainly forces exerted by the cells. This morphological change was previously observed in the RAD16-I milieu with other cellular types: human dermal fibroblasts[44], mouse osteoblasts[45], subATDPCs[30] and mouse embryonic fibroblasts[9,46].

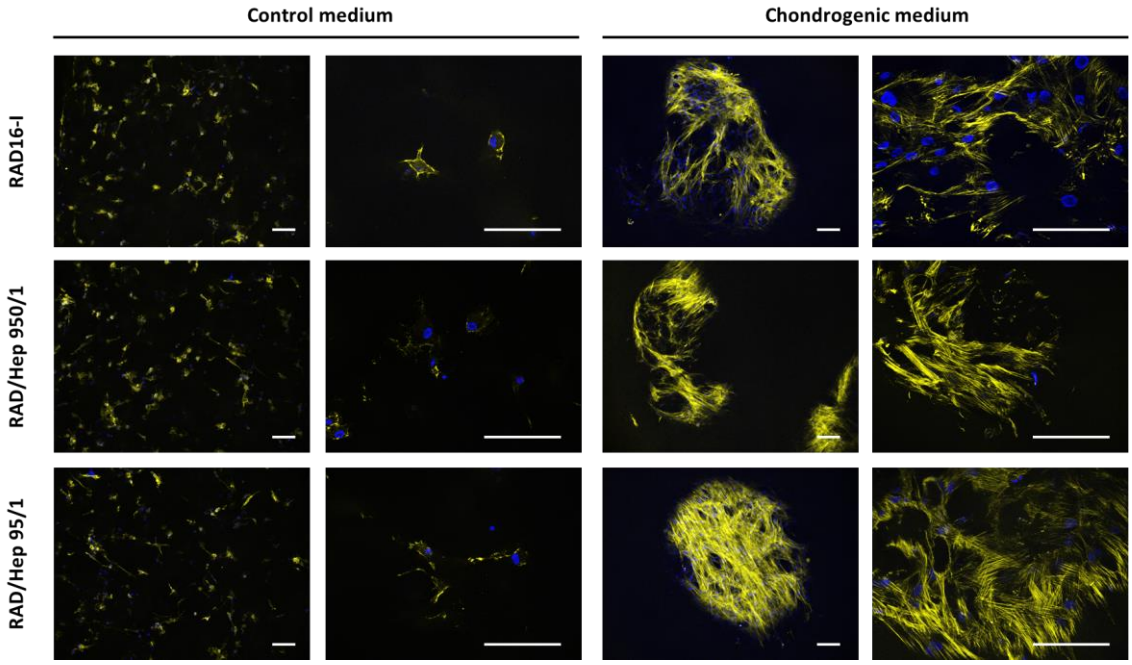

Figure 3.4.6. Adipose Adipose-Derived Stem Cells (ADSCs) morphology in RAD16-I and in RAD/Heparin composites at 2 weeks of culture. ADSCs were encapsulated in RAD16-I and in the composites RAD/Heparin 950/1 and 95/1. 3D constructs were maintained during 2 weeks in control and chondrogenic medium (added the second day of culture). DAPI stains nuclei (blue) and Phalloidin-TRITC stains actin microfilaments of the cytoskeleton (pseudo-colored in yellow). Scale bar of 100 µm.

Finally, cell viability of ADSCs 3D constructs was assessed at 2 weeks of culture (Figure 3.4.8). The majority of cells were alive in the different conditions, independently of the scaffold type and media composition. Again, compacted structures of 3D constructs under chondrogenic medium were observed.

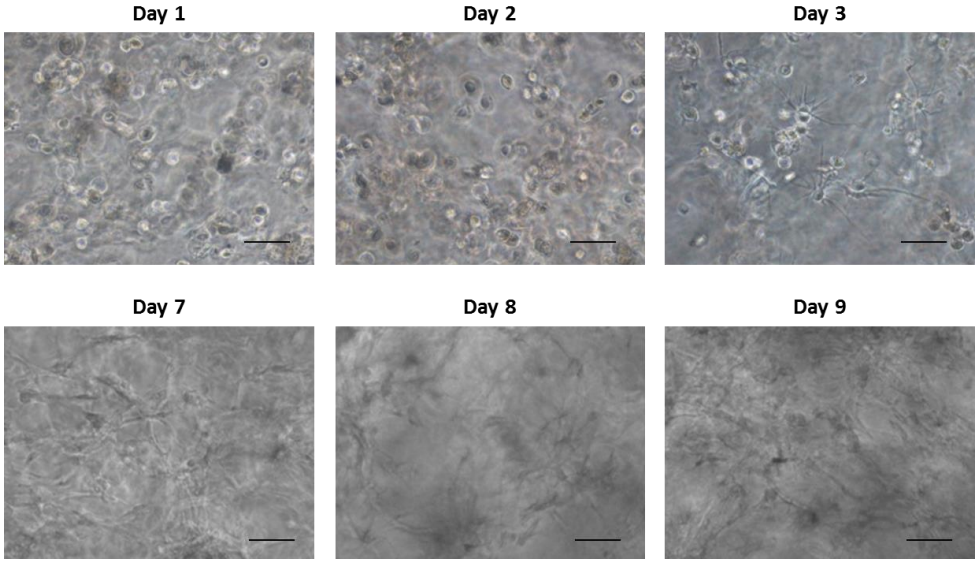

Figure 3.4.7. Adipose-Derived Stem Cells (ADSCs) morphology cultured in RAD16-I hydrogel scaffold under chondrogenic induction. ADSCs were encapsulated in RAD16-I and cultured in chondrogenic medium during 2 weeks. From day 9 of culture 3D constructs were so compacted that it was not possible to get phase images of cell morphology inside the scaffold. Scale bar of 50 µm.

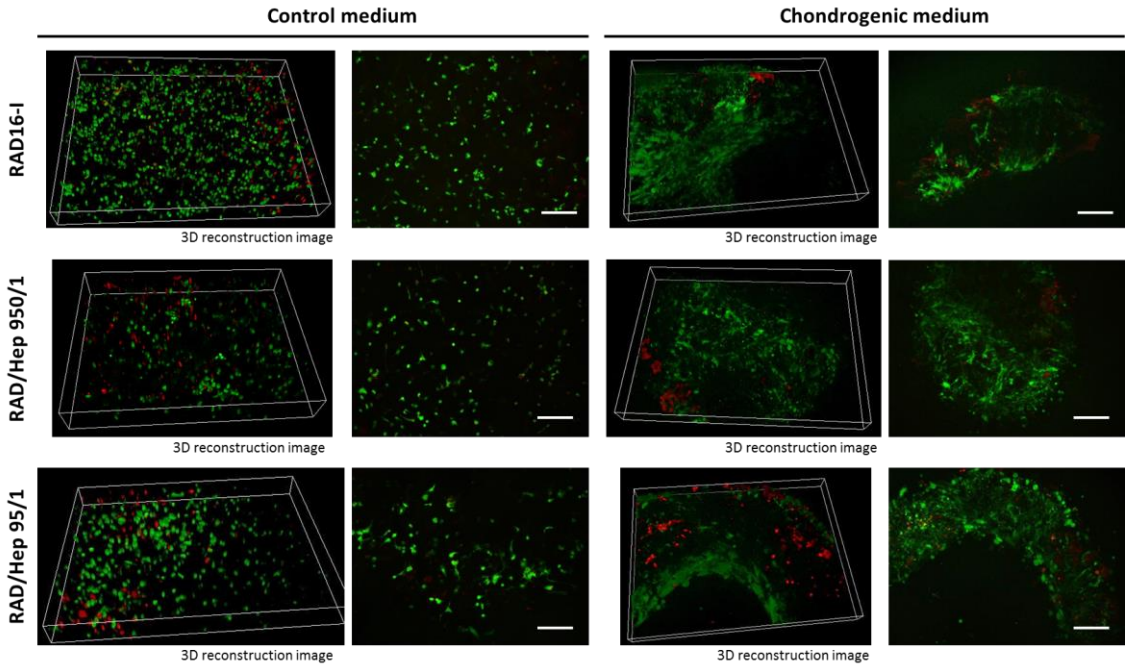

Figure 3.4.8. Adipose-Derived Stem Cells (ADSCs) viability in RAD16-I and in RAD/Heparin composites at 2 weeks of culture. ADSCs were encapsulated in RAD16-I and in the composites RAD/Heparin 950/1 and 95/1. 3D constructs were maintained during 2 weeks in control and chondrogenic medium (added the second day of culture). Control refers to control medium and chondro to chondrogenic medium. Images correspond to 3D reconstructions from optical sections taken with a semi-confocal microscope. Live cells were stained with calcein dye (green) and dead cells with ethidium homodimer-1 (red). Scale bar of 200 µm.

After corroborating good maintenance of ADSCs in the nanofiber matrix during 2 weeks of culture, we proceed to increase the culture time to 4 weeks. Moreover, a new intermediate blended ratio of the bi-component scaffold was added to the experimental setting. In this way, 3D cultures of ADSCs were prepared using RAD16-I and the three composites RAD16-I/Heparin of increasing amounts of heparin (950/1, 190/1 and 95/1). Then, they were maintained for 4 weeks and analyzed for morphology, network formation and viability (Figure 3.4.9-Figure 3.4.11).

Regarding 3D construct morphology of the different hydrogels (Figure 3.4.9 A–D), as previously observed at 2 weeks of culture, when ADSCs were cultured in chondrogenic medium independent of the scaffold used, the system underwent morphological changes that ended in a compacted structure. The construct diameter was reduced by approximately 70% after 4 weeks of culture compared to the initial diameter at day 0 and, interestingly, this reduction was already achieved at 2 weeks of culture (Figure 3.4.10). This event was consistent with the formation of a dense cellular network as evidenced by DAPI–Phalloidin staining (Figure 3.4.9 A–D). We suggest that macroscopic construct reduction was caused mainly by microscopic cell behaviors, as cell migration, proliferation and cell–cell/cell–matrix interactions, therefore, the cell microenvironment was changing and different cellular processes were taking place.

In contrast, this event did not occur so sharply in constructs maintained in the control medium which reduced less their diameter compared to chondrogenic constructs and more progressively in time (Figure 3.4.10). The diameter of RAD/Heparin composite construct was reduced around 50% after 4 weeks, while control constructs (RAD16-I) were reduced only 10%. Microscopically, a similar cell behavior was observed in composites maintained in the control medium: cells elongated and developed a network as it was evidenced by DAPI–Phalloidin staining (Figure 3.4.9 A–D). Nevertheless, cells remained round shaped in RAD16-I scaffold cultured with the control medium, indicating that cells did not migrate, form cell–cell network and therefore, contract the construct. These results showed that the presence of heparin in the scaffold promoted cell–cell interactions and the chondrogenic medium causes the 3D-system contraction.

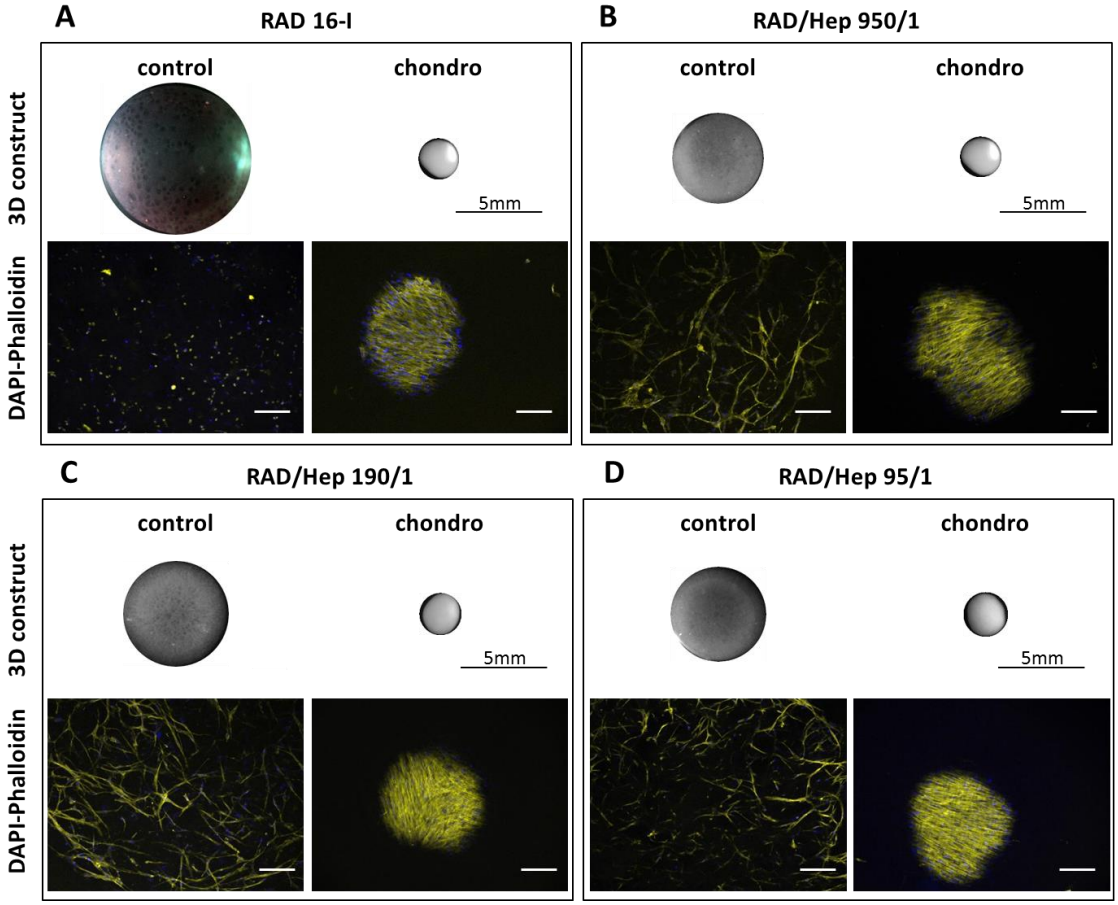

Figure 3.4.9. Adipose-Derived Stem Cells (ADSCs) cultured in RAD16-I and RAD/Heparin composites at 4 weeks of culture. RAD16-I (A), RAD/Hep 950/1 (B), RAD/Hep 190/1 (C) and RAD/Hep 95/1 (D) were prepared at a final concentration of 0.15% (w/w) RAD16-I. ADSCs were encapsulated in the different hydrogels and maintained for 4 weeks with control and chondrogenic medium. 3D constructs images by phase contrast showed a contracted structure of constructs cultured with chondrogenic medium. DAPI and phalloidin staining showed a dense cellular network in constructs cultured with chondrogenic medium and elongated cells in the composites RAD/Hep cultured with control medium. Scale bar of 200µm.

In terms of viability, when the 3D cultures were maintained in control media the majority of the cells were alive only when heparin was present in the scaffold (Figure 3.4.11). In parallel, ADSCs cultured in a monolayer with control medium did not survive, suggesting that the media composition is not enough for cell maintenance (data not shown). On the other hand, when constructs were maintained in chondrogenic medium cell viability was not affected by the presence of heparin compared to the control (RAD16-I) where almost all cells were alive. Therefore, heparin promoted cell survival during the 4 weeks of culture when chondrogenic inductors were not present in the culture medium. We speculate that the ability of heparin retaining GFs had a key role in cell survival.

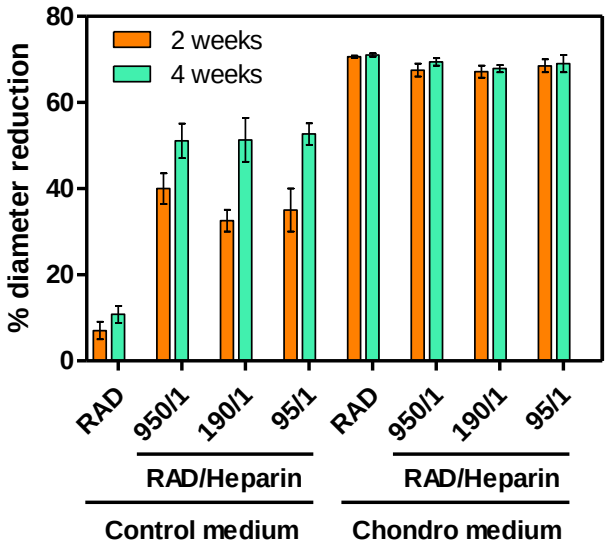

Figure 3.4.10. Adipose-Derived Stem Cells (ADSCs) constructs diameter reduction after 4 weeks of culture. ADSCs were cultured in RAD16-I and in the composites RAD/Heparin (950/1, 190/1 and 95/1) with control and chondrogenic medium. The diameter of 3D constructs were measured at 2 and 4 weeks of culture and represented relative to the initial diameter (mean±SD, n=3).

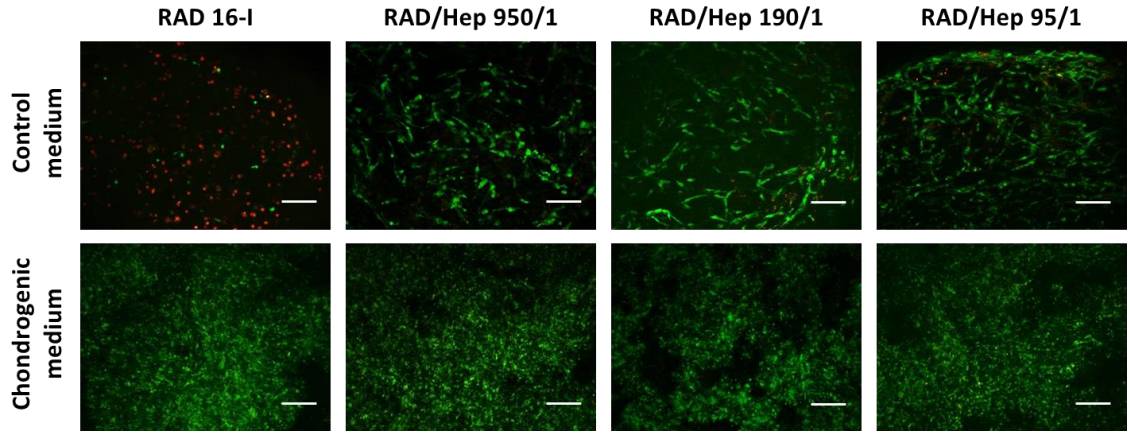

Figure 3.4.11. Adipose-Derived Stem Cells (ADSCs) viability in RAD16-I and in RAD/Heparin composites at 4 weeks of culture. ADSCs were cultured in RAD16-I and in the composites RAD/Heparin 950/1, 190/1 and 95/1. 3D constructs were maintained during 4 weeks in control and chondrogenic medium. Live and dead staining showed the majority cells dead in constructs cultured with control medium in RAD16-I and no differences in the other constructs. Live cells were stained with calcein dye (green) and dead cells with ethidium homodimer-1 (red). Scale bar of 200 µm.

3.4.3 EXPRESSION PATTERNS STUDIES OF SPECIFIC CARTILAGE MARKERS

Regarding expression pattern studies, the initial approach was to evaluate the expression of different collagens constituents of the ECM of both ADSCs and chondrogenic lineage. The study was focused on analyzing the protein expression by western blots in ADSCs cultured in monolayer (2D) and in the 3D scaffolds (Figure 3.4.12). Collagen type I (COL1) was observed in the 2D cultures and in all 3D scaffolds cultured with the chondrogenic medium; however COL1 was not detected in 3D constructs cultured with the control medium. Curiously, the bands pattern was different between 2D and 3D cultures. A band of high molecular weight (~220kDa), probably a pro-collagen intermediate, was observed in all positive samples. In addition, more bands of lower molecular weight (ranging from 180 to 130kDa) were detected in 3D cultures, which could indicate a remodeling of the 3D system after 4 weeks of culture. Interestingly, collagen type II (COL2), characteristic of chondrogenic differentiation, was only detected in 3D constructs cultured with chondrogenic medium. Therefore, the chondrogenic inductors added to the medium stimulate COL2 synthesis, since ADSCs in 2D cultures were not synthesizing this specific protein of articular cartilage ECM. Regarding collagen type X (COL10) protein expression, it was detected in 2D cultures and also after 4 weeks of culture with chondrogenic medium in the 3D system. Altogether, the combination of the 3D system and the chondrogenic medium stimulated the production of collagen types I, II and X and, importantly, collagen type II was not previously detected in 2D cultures.

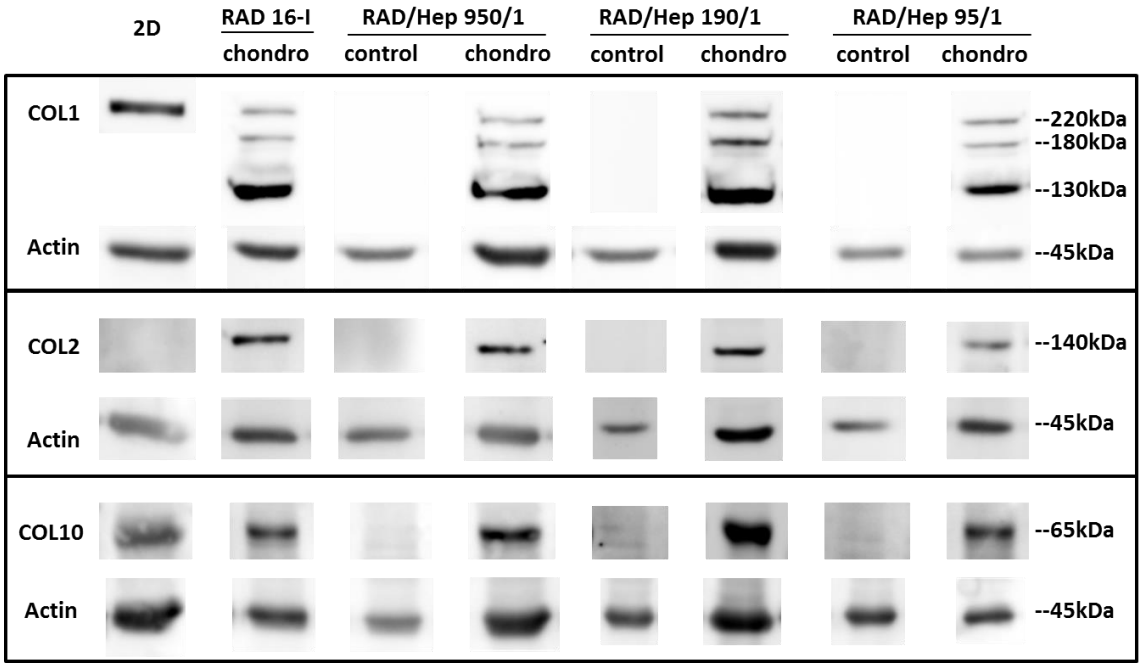

Figure 3.4.12. Protein expression characterization of ADSCs cultured in monolayer and in RAD16-I and composites scaffolds after 4 weeks of culture. Western blot results of collagen type I, II and X when ADSCs were maintained in control and chondrogenic media in RAD16-I and in the three selected RAD/Heparin composites (950/1, 190/1 and 95/1). Control medium for RAD16-I was not shown because cells were dead. Actin expression was used as an internal control. Samples were prepared in triplicate.

In terms of gene expression, different chondrogenic and hypertrophic markers were analyzed by RT-PCR in ADSCs cultured in monolayer (2D) and in the 3D scaffolds (Figure 3.4.13). *COL1* was detected in all samples, 2D and 3D cultures of ADSC. Considering previous results of protein expression, 3D cultures under control medium expressed collagen type I at gene level but not at protein level. Regarding specific ECM components of cartilage, *COL2* and aggrecan were only expressed in 3D constructs under chondrogenic induction correlating, in the case of *COL2*, with the obtained western blot results (Figure 3.4.12). The gene expression profile of *SOX9* transcription factor is positive for all samples, although a faint band was observed in ADSCs 2D cultures. Finally, hypertrophic markers, *COL10* and *RUNX2*, were detected in all samples. These results provide information about specific markers expressed by ADSCs in different culture conditions. However, we aimed to quantify the expression of positive samples, in particular the ones that expressed the chondrogenic markers. For this reason, subsequent quantitative gene expression analyses were only performed to 3D cultures maintained in chondrogenic medium.

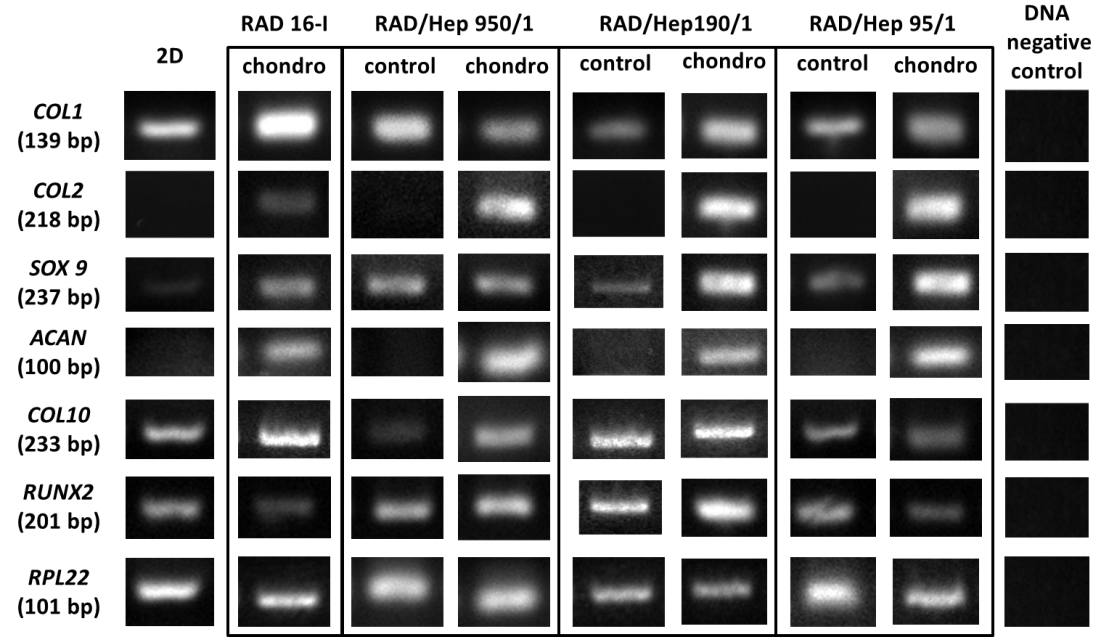

Figure 3.4.13. Gene expression of chondrogenic and hypertrophic markers of ADSCs cultured in monolayer and in RAD16-I and composites scaffolds after 4 weeks of culture. Ribosomal Protein L22 (*RPL22*), collagen type I (*COL1*), collagen type II (*COL2*), *SOX9*, aggrecan (*ACAN*), collagen type X (*COL10*) and *RUNX2* were determined through RT-PCR. Resulting PCR products were analyzed using 4% (w/v) agarose gels. ADSCs were maintained in control and chondrogenic media in RAD16-I and in the three selected RAD/Heparin composites (950/1, 190/1 and 95/1). Control medium for RAD16-I was not shown because cells were dead. *RPL22* was used as a housekeeping gene. Samples were prepared in triplicate.

In order to ascertain separately the effect of heparin itself in the same 3D environment, gene expression levels of ADSCs cultured in RAD/Heparin composites and maintained in chondrogenic medium were quantitatively compared to RAD16-I scaffold (Figure 3.4.14). *COL1*

expression was downregulated in composites with highest heparin concentration (RAD/Heparin 95/1), however it was maintained to RAD16-I levels in composites with lower heparin (Figure 3.4.14 A). Interestingly, the expression of *COL2*, one of the main components of the ECM of chondrocytes, was upregulated in composites with lower heparin content (RAD/Heparin 950/1 and 190/1) and maintained to RAD16-I cultures levels in composites with more heparin content (RAD/Heparin 95/1) (Figure 3.4.14 B). This indicates an increased *COL2* expression in scaffolds with lower heparin quantity relative to scaffolds without heparin, however no differences were observed between the scaffolds containing heparin. The expression of the transcription factor *SOX9*, which is necessary for the expression of *COL2*, was only upregulated in the RAD/Heparin 190/1 (Figure 3.4.14 C). In the case of aggrecan (*ACAN*), the expression was downregulated in composite RAD/Heparin 95/1, nonetheless no differences exist between composites of lower concentration of heparin and RAD16-I (Figure 3.4.14 D). Regarding hypertrophic markers, *COL10* expression was downregulated in the presence of low quantities of heparin in the scaffold and maintained at highest heparin concentration (Figure 3.4.14 E). Finally, *RUNX2* was downregulated in all composites RAD/Heparin (Figure 3.4.14 F), these results together with *COL10* indicate that the presence of heparin in the scaffold system reduce hypertrophy.

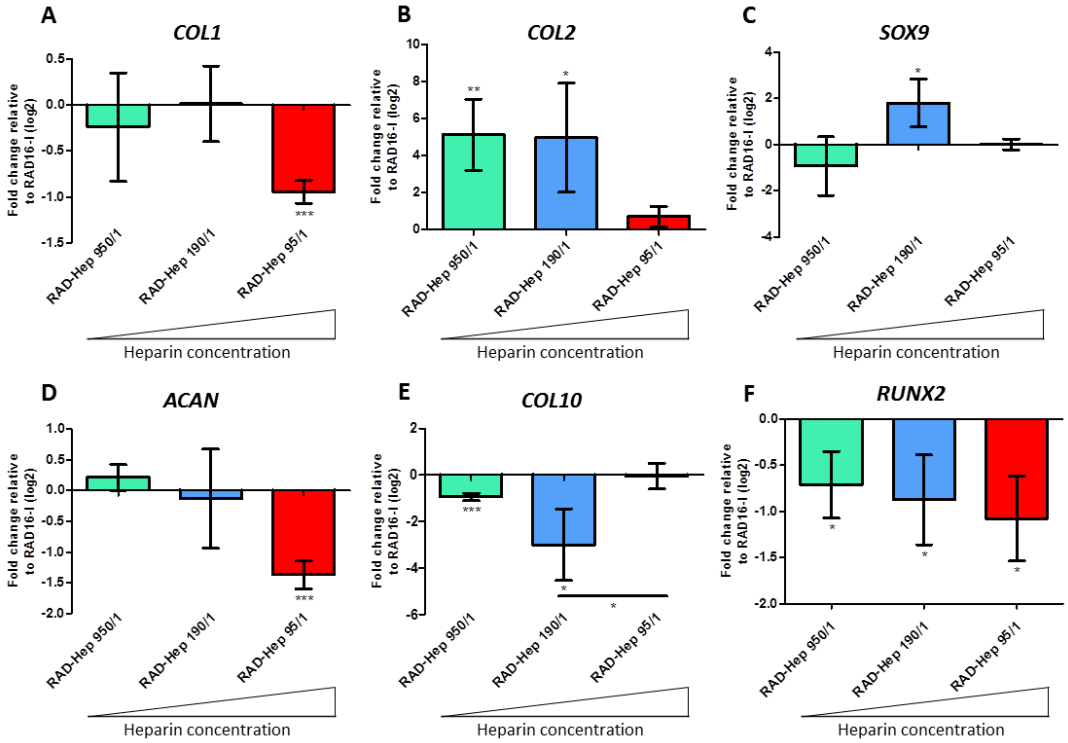

Figure 3.4.14. Gene expression levels of chondrogenic and hypertrophic markers of ADSCs cultured with induction medium during 4 weeks. RAD/Heparin composites (950/1, 190/1 and 95/1) were compared to RAD16-I. Collagen type I (*COL1*, A), collagen type II (*COL2*, B), *SOX9* (C), aggrecan (*ACAN*, D), collagen type X (*COL10*, E) and *RUNX2* (F) were determined through real time RT-PCR. Ct values relative to ribosomal protein L22 (*RPL22*) were obtained and reported as fold increase (ΔΔCt) relative to 3D constructs without heparin (RAD16-I). (Statistical differences are indicated as:* for $p<0.05$, ** for $p<0.01$, and *** for $p<0.001$, Two-way ANOVA, n=3).

Moreover, the synthesis of PGs by the cells was analyzed qualitatively by staining the constructs with toluidine blue (Figure 3.4.15 A). Constructs cultured with chondrogenic medium became highly stained with strong blue coloration, indicating a significant production of PGs. This staining was homogenous across the entire construct. In contrast, constructs cultured with the control medium stained relatively weakly for PGs and was probably caused by the heparin initially present in the scaffold, which suggest that ADSCs do not commit to cartilage tissue under control medium conditions. These results correlate with the expression patterns obtained by RT-PCR and western blot. In particular, aggrecan gene expression was only detected in constructs cultured with chondrogenic medium (Figure 3.4.15 B). Besides aggrecan, other PGs such as versican, syndecan and perlecan could be stained by toluidine blue.

Furthermore, von Kossa staining was performed to 3D constructs cultured with the chondrogenic medium in order to analyze the possible calcifications characteristic of osteogenic differentiation (Figure 3.4.15 C). Calcium mineral deposits should appear black or brown–black; however, as expected, constructs stained negative for von Kossa in external and internal sections. This clearly indicates that the chondrogenic medium did not promote mineralization in ADSCs cultured in the 3D system after 4 weeks of culture, while rendering a homogeneous PGs-containing matrix.

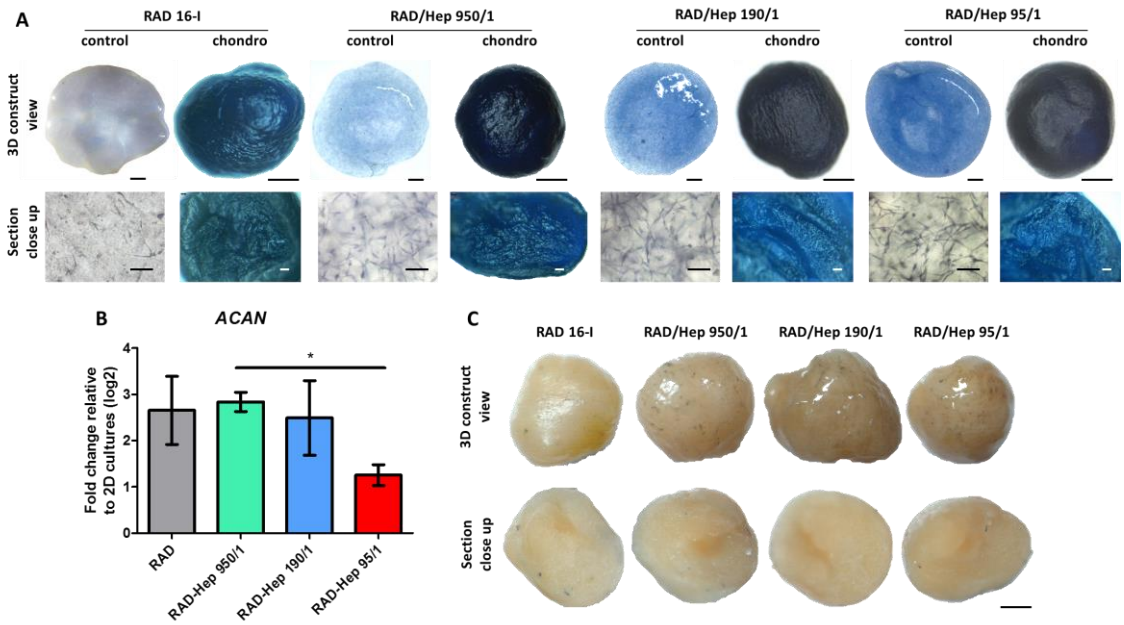

Figure 3.4.15. Chondrogenic characterization of ADSCs cultured in RAD16-I and composites scaffolds for 4 weeks. (A) Toluidine blue staining (sulfated glycosaminoglycans) of 3D ADSCs constructs cultured in control and chondrogenic media (3D construct view scale bars= 500µm and section close up scale bars= 100µm). (B) Gene expression levels of aggrecan of ADSCs cultured with induction medium. Constructs cultured with control medium did not express aggrecan after 4 weeks of culture. Ct values relative to ribosomal protein L22 (*RPL22*) were obtained and reported as fold increase (ΔΔCt) relative to 2D cultures. (Statistical differences are indicated as:* for $p<0.05$, ** for $p<0.01$, and *** for $p<0.001$, Two-way ANOVA, n=3). (C) Von Kossa staining (calcium mineralization) of 3D ADSCs constructs cultured in chondrogenic media (Scale bars= 500µm).

3.4.4 MECHANICAL CHARACTERIZATION OF 3D CONSTRUCTS

Finally, an additional insight is provided by mechanical measurement of the 3D constructs cultured with the chondrogenic medium (Figure 3.4.16). Regarding the elastic component (storage modulus, G'), the composite with higher heparin content (RAD/Heparin 95/1) presented higher values (G' around 250 kPa) than the other composites and RAD16-I (G' around 150 kPa) (Figure 3.4.16 A). Moreover, the G' values of RAD/Heparin 95/1 were closely related to that found in chicken and calf native cartilage (measured in same conditions as our samples). Moreover, the loss modulus (G'') and the complex modulus (G*) have a similar tendency than the storage modulus (G') described above (Figure 3.4.16 B&C). Interestingly, tan(delta) indicates that all constructs dissipate energy equally, suggesting that regardless of the initial combinations of the hydrogels there is an intrinsic property of the hydrogel system in maintaining its viscoelastic nature (tan(delta) = viscosity/elasticity) (Figure 3.4.16 D). Nevertheless, the full viscoelastic behavior still differs from native cartilage, as demonstrated by tan(delta) values.

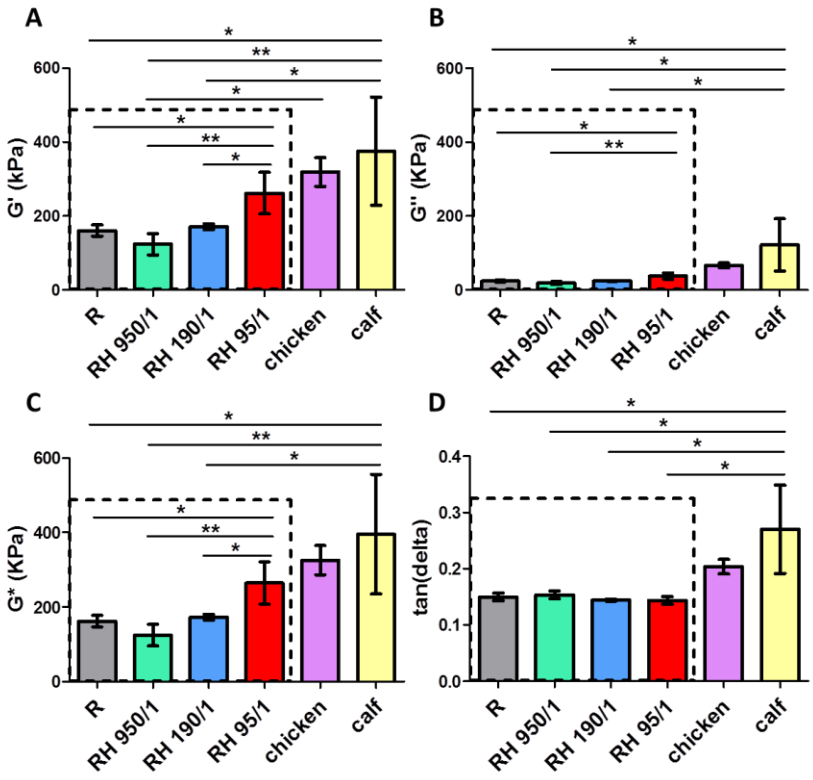

Figure 3.4.16. Mechanical characterization of ADSCs 3D constructs cultured in chondrogenic medium after 4 weeks of culture. Storage modulus (G') measures the sample's elastic behavior. (B) Loss modulus (G'') measures the viscous response of the material. (C) Complex modulus (G*) is the sum of storage and loss modulus. (D) Tan(delta) is the ratio of the loss to the storage. 3D ADSCs constructs cultured in chondrogenic medium and chicken and calf articular cartilage were measured in the same conditions. R refers to RAD16-I and RH to RAD/Heparin composites. Samples boxed in dashed line were analyzed statistically separated. (Statistical differences are indicated as:* for $p<0.05$, ** for $p<0.01$, and *** for $p<0.001$, Two-way ANOVA, n=3).

3.5 DISCUSSION

Heparin molecules are all over the body, in different forms, meaning sizes and degree of sulfation. Heparins interact with hundreds of different molecular entities, GFs, cytokines, chemokines, proteins of the ECM, etc. Moreover, heparin is present in all culture media containing serum and is interacting with components of the serum, the surface of the cell, the ECM of the cell components, etc. Meaning that, at any given moment *in vivo* we have heparin molecules doing hundreds of different interactions. When cells were embedded in self-assembling peptides in presence of serum, heparin molecules will interact in diverse manners. Mainly, by binding at the peptide matrix structure and somehow modifying the GF-cell receptor interaction in a more physiological way.

In this chapter, the RAD/Heparin bi-component scaffold was used for a specific TE strategy: in cartilage regeneration. Previously, the mechanical and structural stability at physiological conditions was corroborated, indicating that the nanofiber formation was not interfered by the presence of heparin at chosen working concentrations (Figure 3.4.2). In addition, the composite could be used as a drug delivery system to bind and release physiologically significant quantities of GFs containing HBD such as $VEGF_{165}$, FGFβ and TGFβ1. Interestingly; a different binding affinity of heparin to the three GFs studied was observed. In the case of $VEGF_{165}$, the binding was very specific and the composite gradually released the growth factor over the course of the experiment (36 h) (Figure 3.2.3 A). It seems that the presence of heparin enhanced the binding specificity of $VEGF_{165}$. However, although FGFβ presented a similar release profile it was not significantly different from the control RAD16-I (Figure 3.2.3 B). Finally, to our surprise, considering that TGFβ1 is described to have HBD, in our condition tested it did not show any specific affinity when comparing to the control scaffold RAD16-I without heparin (Figure 3.4.1). These results altogether could indicate that heparin from the source we used (porcine intestine), presents good specific capacity for binding $VEGF_{165}$ but not so specific for FGFβ or TGFβ1. We speculate that the study of heparin from different origins or other GAGs such as chondroitin sulfate, heparan sulfate or dermatan sulfate could present different affinities to respective GFs.

Importantly, this new biomaterial could be used in different tissue engineering applications due to the ability of heparin to bind different GFs. According to the literature, heparinized scaffolds seem to induce and enhance chondrogenic differentiation and it is well-known that TGFβ1 is a chondrogenic inductor with heparin binding affinity[47]. This effect could be explained due to the unique bioactivities of heparin moieties that can hold various GFs (including TGFβ1) and protect them from denaturation[48]. Taking all this into account, the new biomaterial was evaluated as a scaffold to support *in vitro* chondrogenic differentiation using human ADSCs). They were maintained for 4 weeks in the presence or absence of standard chondrogenic medium. Remarkably, the media used was defined (without FBS), which could help in the translation of future *in vivo* studies. After 4 weeks of culture cell viability was compromised when using the control medium in the scaffold without heparin. This suggests that the

presence of heparin in the scaffold has cell survival properties, maybe due to local retention and presentation of cell secreted GFs, which is not happening in control scaffolds (RAD16-I). This effect is very important since the signal obtained in this way is different to the signal obtained by the interaction of the GF-receptor with the soluble ligand. Heparin apparently will stay associated very stable to the nanofiber. We have obtained peptide matrices modified with heparin that after days of washing are still containing high amounts of heparin. We think that micro-mechanics (stiffness values around the cell) should change when heparin is present. The fact that in presence of heparin some cells have better survival in absence of serum indicates that somehow heparin is complementing a basic function, probably in helping to present GF to the specific cell receptor.

In the context of molecular markers, the first approach was to study protein levels of three types of collagens involved in chondrogenesis, collagen types I, II and X. The presence of collagen type I and X expression in ADSCs growing on classical plates with complete culture media was really evident, but there was no the expression of collagen type II (Figure 3.4.12). Surprisingly, cells growing in 3D scaffolds with heparin with control medium did not show expression of any of the collagens tested, which suggest that the 3D environment *per se* is less instructive in inducing protein expression than 2D cultures. Interestingly, in the presence of the chondrogenic medium all collagens were upregulated compared to 3D control cultures. In particular, collagen type II was expressed only in 3D chondrogenic cultures. Subsequently, we proceed to analyze gene expression of chondrogenic markers in more detail by real time RT-PCR (Figure 3.4.14). In particular, the expression of collagen types I, II and X as previously studied by western blot and additionally *RUNX2*, *SOX9* and aggrecan was studied. Levels of expression between the three heparin quantities in comparison with the control scaffold without heparin were assessed only for those constructs cultured with the chondrogenic medium. By looking at the results it was a clear upregulation of *COL2* in lower and medium RAD/Heparin composites and some decrease in *COL10* in the medium content of heparin. For the rest of the markers, no differences seem to be observed among the heparin range studied. These results suggest a contribution of heparin promoting cells to undergo a chondrogenic lineage commitment. Nevertheless, since this is a gene expression snapshot at 4 weeks of culture, we cannot conclude about the general differentiation process which was undergone by the constructs. Hence, more precise evaluation of time dependent changes on gene expression should be performed. Moreover, we speculate on an effective heparin concentration associated to the matrix responsible for generating certain signals that, as a consequence, we detected in a differential gene expression. The synthesis of PGs, typical components of articular cartilage ECM, was confirmed by positive toluidine blue staining across the entire constructs cultured with chondrogenic medium (Figure 3.4.15 A). Furthermore, coincidently with the strong toluidine blue staining the constructs presented a storage modulus (G') in the same order of magnitude to chicken or calf articular cartilage(150–250 kPa); however, the full mechanical response of the material was quite different from native cartilage as evidenced by tan(delta) (see Figure 3.4.16). The elastic property of the

constructs might be due to a combination of simultaneous processes including a drastic reduction in the size of the structures by condensation and the synthesis of ECM components by the cells, such as collagens and PGs. Moreover, an interesting behavior of these hydrogels is that regardless of the initial components and the following evolution of each hydrogel the viscoelastic nature (tan(delta) = viscosity/elasticity) is clearly maintained (Figure 3.4.16 D), which could indicate an intrinsic property of these types of self-assembling peptide materials

Finally, we confirmed the absence of calcium mineralization by von Kossa staining which indicates that during the time period studied the system did not undergo cartilage hypertrophy. In these later experiments on chondrogenesis, the addition of heparin improves cell survival as well as cell differentiation which can be explained by the specific binding characteristics of TGFβ1 to this new bimolecular matrix. The 3D microenvironment could provide other signaling processes, for instance, secreted GFs by the cells (in addition to added GFs, such as TGFβ1) could be captured and stabilized by scaffold associated heparin assisting in their presentation to the proper cellular receptors. In other words, the presentation of growth factors secreted by the cells as well as TGFβ1 to the particular receptor could be fundamentally different in the presence or absence of heparin associated to the scaffolds. It is well known that most of these receptors can be clustered by the presence of the GFs associated to ECM and, as a consequence, its signaling would be different from the typical soluble GF binding to the receptor. Therefore, we hypothesize that this could be one of the reasons that the presence of heparin significantly enhances chondrogenesis in our system. Although a preliminary chondrogenic phenotype was obtained it is important to mention that these cells did not present a chondrocyte-like shape, suggesting an early chondrogenic stage recreating a pre-cartilage condensation without undergoing a terminal differentiation.

Altogether, considering both previous results and the results presented in this work, the new composite is a promising material for different tissue engineering applications. It is, therefore, interesting that depending on the conditions provided: cellular type, peptide concentration or culture media composition – between others – the new bi-component material can enhance different cellular processes. This demonstrates, in part, the potentiality of the material and the versatility of the system to study chondrogenesis, vasculogenesis or cardiogenesis, as well as, other future applications. Moreover, it is an ‘‘easy to prepare’’ material made by a simple combination of two commercial products: self-assembling peptide RAD16-I (PuraMatrix™) and heparin sodium salt solution. Remarkably, the commercial availability of clinical grade PuraMatrix™ and heparin enables its future use in *in vivo* studies.

3.6 CONCLUDING REMARKS

- The TGFβ1 releasing pattern of RAD16-I and RAD/Heparin composite were evaluated and no significant differences were observed by the presence of heparin moieties in the scaffold.

- New blended ratios of the RAD/Heparin bi-component scaffold were performed and used to perform 3D cultures with ADSCs. In the provided microenvironment cells elongate, interconnect and extend different cellular processes.

- Viability of ADSCs was compromised after 4 weeks of culture in RAD16-I scaffold under control medium conditions. Interestingly, chondrogenic medium and the presence of heparin in the scaffold enhance cell survival.

- The expression of chondrogenic and hypertrophic markers evidenced a favored microenvironment for chondrogenic differentiation by the presence of heparin in the scaffold. Results suggested that the presence of heparin molecules promote chondrogenesis by the heparin-GF complex receptor recognition rather that GF release.

- Viscoelastic properties of 3D constructs in chondrogenic medium after 4 weeks of culture were in the same order of magnitude than chicken or calf articular cartilage, evidencing the potential of this constructs to be used in cartilage tissue engineering applications.

3.7 REFERENCES

1. Semino, C. E. Self-assembling Peptides: From Bio-inspired Materials to Bone Regeneration. *J. Dent. Res.* **87,** 606–616 (2008).
2. Zhang, S. & Semino, C. E. Design peptide scaffolds for regenerative medicine. *Adv. Exp. Med. Biol.* **534,** 147–63 (2003).
3. Sieminski, a. L., Was, a. S., Kim, G., Gong, H. & Kamm, R. D. The Stiffness of Three-dimensional Ionic Self-assembling Peptide Gels Affects the Extent of Capillary-like Network Formation. *Cell Biochem. Biophys.* **49,** 73–83 (2007).
4. Genove, E., Shen, C., Zhang, S. & Semino, C. E. The effect of functionalized self-assembling peptide scaffolds on human aortic endothelial cell function. *Biomaterials* **26,** 3341–3351 (2005).
5. Zhang, S. *et al.* Self-complementary oligopeptide matrices support mammalian cell attachment. *Biomaterials* **16,** 1385–93 (1995).
6. Kisiday, J. *et al.* Self-assembling peptide hydrogel fosters chondrocyte extracellular matrix production and cell division: implications for cartilage tissue repair. *Proc. Natl. Acad. Sci. U. S. A.* **99,** 9996–10001 (2002).
7. Semino, C. E., Kasahara, J. & Hayashi, Y. Entrapment of Migrating Hippocampal Neural Cells in Three-Dimensional Peptide Nanofiber Scaffold. *Tissue Eng Part* **10,** (2004).
8. Borro, S., Garreta, E., Ph, D. & Genove, E. Osteogenic Differentiation of Mouse Embryonic Stem Cells. 1–14 (2006).
9. Quintana, L. *et al.* Early tissue patterning recreated by mouse embryonic fibroblasts in a three-dimensional environment. *Tissue Eng. Part A* **15,** 45–54 (2009).
10. Semino, C. E. Can We Build Artificial Stem Cell Compartments? *J. Biomed. Biotechnol.* **2003,** 164–169 (2003).
11. Holmes, T. C. *et al.* Extensive neurite outgrowth and active synapse formation on self-assembling peptide scaffolds. *Proc. Natl. Acad. Sci. U. S. A.* **97,** 6728–33 (2000).
12. Puig-Sanvicens, V. A. C. & Semino, C. E. Self-assembling peptide scaffolds as innovative platforms for drug and cell delivery systems in cardiac regeneration. *Drug Deliv. Transl. Res.* **3,** 330–335 (2013).
13. Lin, Y.-D. *et al.* Instructive nanofiber scaffolds with VEGF create a microenvironment for arteriogenesis and cardiac repair. *Sci. Transl. Med.* **4,** 146ra109 (2012).
14. Griffith, L. G. & Swartz, M. a. Capturing complex 3D tissue physiology in vitro. *Nat. Rev. Mol. Cell Biol.* **7,** 211–24 (2006).
15. Dvir, T., Timko, B. P., Kohane, D. S. & Langer, R. Nanotechnological strategies for engineering complex tissues. *Nat. Nanotechnol.* **6,** 13–22 (2011).
16. Guo, H. *et al.* Sustained delivery of VEGF from designer self-assembling peptides improves cardiac function after myocardial infarction. *Biochem. Biophys. Res. Commun.* **424,** 105–11 (2012).
17. Kim, J. *et al.* The enhancement of mature vessel formation and cardiac function in infarcted hearts using dual growth factor delivery with self-assembling peptides.

Biomaterials **32,** 6080–8 (2011).

18. Rajangam, K. *et al.* Heparin binding nanostructures to promote growth of blood vessels. *Nano Lett.* **6,** 2086–90 (2006).
19. Sakiyama-Elbert, S. E. & Hubbell, J. a. Development of fibrin derivatives for controlled release of heparin-binding growth factors. *J. Control. Release* **65,** 389–402 (2000).
20. Wissink, M. J. *et al.* Binding and release of basic fibroblast growth factor from heparinized collagen matrices. *Biomaterials* **22,** 2291–9 (2001).
21. Tanihara, M., Suzuki, Y., Yamamoto, E., Noguchi, a & Mizushima, Y. Sustained release of basic fibroblast growth factor and angiogenesis in a novel covalently crosslinked gel of heparin and alginate. *J. Biomed. Mater. Res.* **56,** 216–21 (2001).
22. Fernández-Muiños, T. *et al.* Bimolecular based heparin and self-assembling hydrogel for tissue engineering applications. *Acta Biomater.* **16,** 35–48 (2015).
23. Semino, C. E., Merok, J. R., Crane, G. G., Panagiotakos, G. & Zhang, S. Functional differentiation of hepatocyte-like spheroid structures from putative liver progenitor cells in three-dimensional peptide scaffolds. *Differentiation.* **71,** 262–70 (2003).
24. Hari, G., Thompson, B. T. & Hales, C. A. invited review. **1111,** 779–789 (2000).
25. Ono, K., Hattori, H., Takeshita, S., Kurita, A. & Ishihara, M. Structural features in heparin that interact with VEGF165 and modulate its biological activity. *Glycobiology* **9,** 705–711 (1999).
26. Muñoz, E. M. & Linhardt, R. J. Heparin-binding domains in vascular biology. *Arterioscler. Thromb. Vasc. Biol.* **24,** 1549–57 (2004).
27. Hirsh, J., Anand, S. S., Halperin, J. L. & Fuster, V. Mechanism of Action and Pharmacology of Unfractionated Heparin. 1094–1097 (2001).
28. Benoit, D. S. W. & Anseth, K. S. Heparin functionalized PEG gels that modulate protein adsorption for hMSC adhesion and differentiation. *Acta Biomater.* **1,** 461–70 (2005).
29. Ou, Y. *et al.* Inhibition of Urinary Macromolecule Heparin on Aggregation of Nano-COM and Nano-COD Crystals. 1626–1642 (2015). doi:10.3390/molecules20011626
30. Castells-Sala, C. *et al.* Three-Dimensional Cultures of Human Subcutaneous Adipose Tissue-Derived Progenitor Cells Based on RAD16-I Self-Assembling Peptide. *Tissue Eng. Part C. Methods* **22,** 1–12 (2016).
31. Recha-Sancho, L. & Semino, C. E. Heparin based self-assembling peptide scaffold reestablish chondrogenic phenotype of expanded de-differentiated human chondrocytes. *J. Biomed. Mater. Res. Part A* **104,** 1694–1706 (2016).
32. Khan, W. S., Johnson, D. S. & Hardingham, T. E. The potential of stem cells in the treatment of knee cartilage defects. *Knee* **17,** 369–374 (2010).
33. Freyria, A. Chondrocytes or adult stem cells for cartilage repair : The indisputable role of growth factors. **43,** 259–265 (2012).
34. Longo, U. G. *et al.* Stem cells and gene therapy for cartilage repair. *Stem Cells Int.* **2012,** 168385 (2012).
35. Krampera, M., Pizzolo, G., Aprili, G. & Franchini, M. Mesenchymal stem cells for bone , cartilage , tendon and skeletal muscle repair. **39,** 678–683 (2006).

36. Benders, K. E. M. *et al.* Extracellular matrix scaffolds for cartilage and bone regeneration. *Trends in Biotechnology* **31,** 169–176 (2013).

37. Terry, D. E., Chopra, R. K., Ovenden, J. & Anastassiades, T. P. Differential use of Alcian blue and toluidine blue dyes for the quantification and isolation of anionic glycoconjugates from cell cultures: application to proteoglycans and a high-molecular-weight glycoprotein synthesized by articular chondrocytes. *Anal. Biochem.* **285,** 211–9 (2000).

38. Klunk, W. E., Pettegrew, J. W. & Abraham, D. J. Quantitative evaluation of congo red binding to amyloid-like proteins with a beta-pleated sheet conformation. *J. Histochem. Cytochem.* **37,** 1273–1281 (1989).

39. Daura, X. *et al.* Circular dichroism spectra of beta-peptides: sensitivity to molecular structure and effects of motional averaging. *Eur. Biophys. J.* **32,** 661–70 (2003).

40. Kelly, S. M. & Price, N. C. The use of circular dichroism in the investigation of protein structure and function. *Curr. Protein Pept. Sci.* **1,** 349–84 (2000).

41. Greenfield, N. J. Using circular dichroism spectra to estimate protein secondary structure. *Nat. Protoc.* **1,** 2876–2890 (2006).

42. Hellingman, C. A., Koevoet, W. & Osch, G. J. V. M. Van. Can one generate stable hyaline cartilage from adult mesenchymal stem cells ? A developmental approach. (2011). doi:10.1002/term

43. Cals, F. L. J., Hellingman, C. A., Koevoet, W., Baatenburg de Jong, R. J. & van Osch, G. J. V. M. Effects of transforming growth factor-β subtypes on in vitro cartilage production and mineralization of human bone marrow stromal-derived mesenchymal stem cells. *J. Tissue Eng. Regen. Med.* **6,** 68–76 (2012).

44. Bianca M. Bussmann, Sven Reiche, Núria Marí-Buyé, Cristina Castells-Sala, H. J. M. and C. E. S. Chondrogenic potential of human dermal fibroblasts in a contractile, soft, self-assembling, peptide hydrogel. *J. Tissue Eng. Regen. Med.* (2013). doi:10.1002/term

45. Marí-Buyé, N., Luque, T., Navajas, D. & Semino, C. Development of a three-dimensional bone-like construct in a soft self-assembling peptide matrix. *Tissue Eng Part A* **19,** 870–881 (2013).

46. Fernández-Muiños, T., Suárez-Muñoz, M., Sanmartí-Espinal, M. & Semino, C. E. Matrix dimensions, stiffness, and structural properties modulate spontaneous chondrogenic commitment of mouse embryonic fibroblasts. *Tissue Eng. Part A* **20,** 1145–55 (2014).

47. Hubbell, J. a. Matrix-bound growth factors in tissue repair. *Swiss Med. Wkly.* **137 Suppl ,** 72S–76S (2007).

48. Kim, M., Kim, S. E., Kang, S. S., Kim, Y. H. & Tae, G. The use of de-differentiated chondrocytes delivered by a heparin-based hydrogel to regenerate cartilage in partial-thickness defects. *Biomaterials* **32,** 7883–96 (2011).

CHAPTER 4

EVALUATION OF THE CHONDROGENIC POTENTIAL OF THE RAD/HEPARIN BI-COMPONENT SCAFFOLD IN THE REDIFFERENTIATION PROCESS OF DEDIFFERENTIATED ARTICULAR CHONDROCYTES

Recha-Sancho L and Semino CE. Heparin based self-assembling peptide scaffold reestablish chondrogenic phenotype of expanded de-differentiated human chondrocytes. *J Biomed Mater Res Part A*. **104**, 1694-706 (2016).

4.1 INTRODUCTION

Adult articular cartilage is an avascular, highly specialized tissue with a limited intrinsic capacity for regeneration in response to injury or disease[1]. Therefore, treatments to assist cartilage repair and restore their function are challenging in regenerative medicine. Tissue engineering (TE) strategies have emerged as a potential source to address cartilage lesions combining cells, biomaterials based-scaffolds and bioactive molecules[2–4]. Chondrocytes represent an ideal cell source for cartilage TE. They are the unique cellular type resident in cartilage tissue and have the role of producing, maintaining and remodeling the extracellular matrix (ECM), which is composed of a highly complex network of collagen fibrils and proteoglycans (PGs)[5]. However, they are available in very limited quantities[6]. For this reason, multiple passages in *in vitro* monolayer culture are required to increase the amount of cells. Once they are isolated from their native surrounding ECM and cultured into traditional flat and rigid surfaces, they undergo dedifferentiation losing the expression of cartilage markers[7]. They acquire a fibroblast-like phenotype, down-regulating the expression of cartilage ECM proteins over passages[8].

Three-dimensional (3D) cultures are a more realistic approach, aiming to recreate the complex and hierarchical cellular microenvironment found in the native tissue[9,10]. 3D pellet culture system has been extensively used as a model to study chondrogenesis, since the high seeding density resembles the mesenchymal condensation that occurs *in vivo* during hyaline cartilage formation[11]. Moreover, it has been reported that the pellet culture of dedifferentiated chondrocytes stimulates their re-differentiation and up-regulation of cartilage matrix proteins[12]. First studies with biomaterials showed that dedifferentiated chondrocytes cultured into agarose[13] or alginate beads[14,15] then re-expressed chondrogenic markers. Moreover, attempts were also performed in collagen[16,17] or fibrin[18] matrices and successful results were obtained. Therefore, the dedifferentiation phenotype can be reversed, at least in part, using proper conditions in 3D cultures demonstrating the plasticity of chondrocytes. In native cartilage, they are surrounded by an abundant ECM in all directions and constantly exposed to cell-matrix interactions. Bioactive and biomimetic scaffolds resembling the natural microenvironment are desirable to drive cell proliferation and differentiation[19,20]. Hydrogels can be good candidates for cartilage TE scaffolds since they possess highly hydrated 3D networks mimicking the native cartilage ECM[21]. Some studies showed promising results culturing chondrocytes in 3D hydrogel scaffolds[22,23] and comparing natural to synthetic hydrogels[24].

In this study, our 3D culture was based on the self-assembling hydrogel RAD16-I (AcN-$(RADA)_4$-CNH_2)[20]. It is a synthetic scaffold that provides a reproducible and custom-tailored microenvironment, compared to natural biomaterials (as agarose and alginate). In particular, it is composed by repeating units of hydrophilic-hydrophobic amino acids, which self-assemble under physiological conditions into a network of interweaving nanofibers of around 10nm

diameter, a pore size of 50 to 200nm and over 99% water content[25]. This nanoscale architecture mimics the natural ECM, allowing cells to truly experiment the three dimensions. Mechanical properties can be modulated by changing peptide concentration and it is defined as a "non-instructive" from the point of view of cell receptor recognition/activation. Several publications showed that RAD16-I *per se* could promote growth and proliferation of multiple cell types, including endothelial cells, hepatocytes, neuronal cells, fibroblasts, osteoblasts, as well as embryonic and somatic stem cells[26–33].

In the present work, human articular chondrocytes (ACs), previously expanded in monolayer, were cultured in the RAD16-I self-assembling peptide in order to analyze the intrinsic effect of the 3D microenvironment provided by the scaffold in adult chondrocytes[34]. Moreover, we took advantage of the versatility of this hydrogel to specifically add molecular cues for guiding the differentiation process of the cultured cells. For this reason, heparin moieties were added to the scaffold by a simple mixture forming a stable heparin based self-assembling hydrogel. Previous study (see Chapter 3) showed promising results using this composed hydrogel fostering chondrogenic commitment with adipose-derived stem cells (ADSCs)[35]. Moreover, other groups have worked with heparinized scaffolds for cartilage regeneration[36–38]. In addition, this composite material is capable of retaining growth factors (GFs) with heparin binding domain, either endogenous secreted by the cells or exogenous added to the medium, protecting them from degradation[35]. Therefore, the RAD16-I peptide provides the 3D environment and heparin the binding affinity to GFs. These attractive qualities motivated to encapsulate human chondrocytes into the heparinized self-assembling scaffold attempting to recreate the native ECM.

4.2 MOTIVATIONS AND SPECIFIC AIMS

Previous studies reinforce the potential advantage of decorating non-instructive scaffolds with heparin moieties with aim of developing a microenvironment for different cellular types as well as TE purposes. The goal of the present chapter is to recover the chondrogenic phenotype of dedifferentiated ACs using chemical induction and the RAD/Heparin composite. The specific objectives of this chapter are the following:

(1) To corroborate the dedifferentiation process of human ACs under monolayer expansion.

(2) To study the cellular behavior and viability of dedifferentiated ACs in RAD16-I based 3D scaffolds (RAD16-I and RAD/Heparin composites).

(3) To assess the recovery of the chondrogenic phenotype thorough the analysis of mature cartilage markers at gene and protein level.

(4) To evaluate the evolution of the viscoelastic behavior of the 3D constructs and to compare their mechanical properties to native articular cartilage.

4.3 RESULTS

4.3.1 DEDIFFERENTIATION PROCESS OF HUMAN CHONDROCYTES EXPANDED IN MONOLAYER

First, we wanted to study whether the selected chondrocytes underwent dedifferentiation under monolayer culture conditions. For this purpose, human ACs were cultured until passage 6 in traditional 2D culture flasks and chondrogenic and hypertrophic markers were quantitatively analyzed at gene level in each passage (passages 3, 4, 5 and 6 were compared to passage 2).

All studied markers were down-regulated along the passages (Figure 4.3.1). Particularly, collagen type I (*COL1*) suffers downregulation from passage 4 and over (Figure 4.3.1 A). The expression of collagen type II (*COL2*), a specific ECM component for chondrocytes, was initially downregulated from passage 3 and over. Statistical differences could be observed from the passage 3 to the following passages indicating a higher degree of downregulation in increasing passages (Figure 4.3.1 B). Although both *COL1* and *COL2* were downregulated, the fold change relative to passage 2 was approximately 10 times more decreased in *COL2* than in *COL1*. *SOX9* was progressively downregulated along the passages (Figure 4.3.1 C). Aggrecan (*ACAN*) showed a similar expression pattern to *COL1*; no differences at passage 3 and a significant downregulation in the following passages (Figure 4.3.1 D). In the case of collagen type X (*COL10*), present in hypertrophic areas, it was downregulated up to passage 5 (Figure 4.3.1 E). Finally, *RUNX2* was drastically downregulated from passage 3 and the expression levels were maintained until passage 6 (Figure 4.3.1 F). These results suggest that ACs were losing the expression of chondrogenic and hypertrophic markers during monolayer expansion.

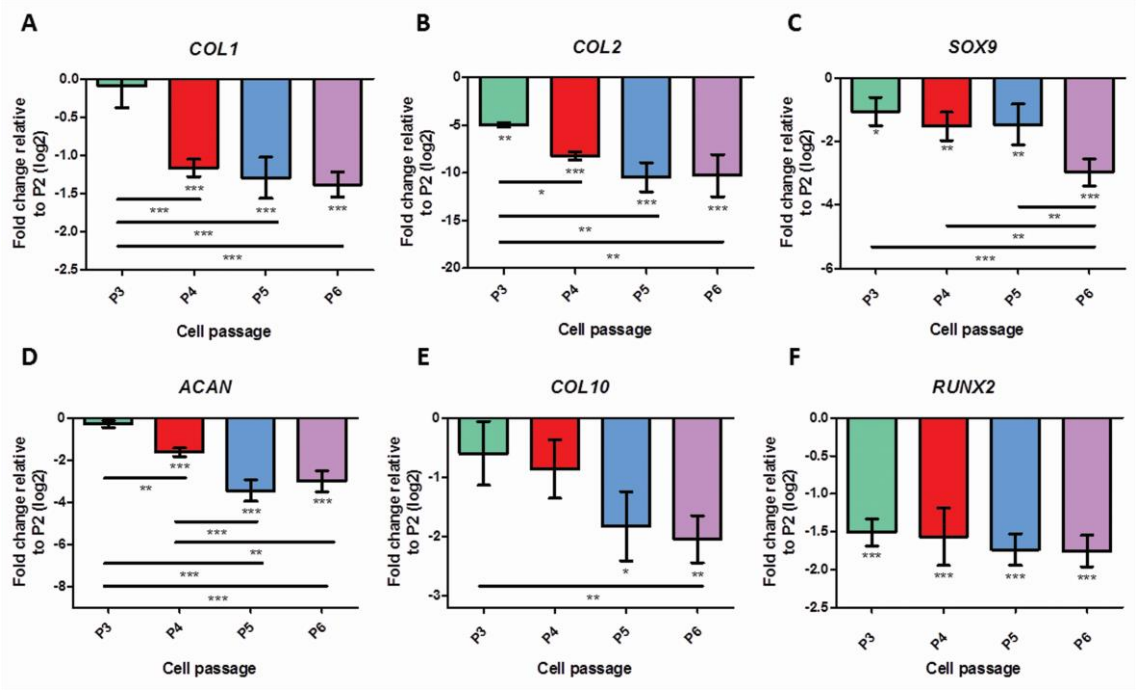

Figure 4.3.1. Gene expression levels of chondrogenic and hypertrophic markers of human articular chondrocytes (AC) cultured in monolayer at different passages. Passages 3, 4, 5, and 6 were compared with Passage 2. Collagen type I (*COL1*, A), collagen type II (*COL2*, B), SOX9 (C), aggrecan (*ACAN*, D), collagen type X (*COL10*, E), and *RUNX2* (F) were determined through real time RT-PCR. Ct values relative to ribosomal protein L22 (*RPL22*) were obtained and reported as fold increase (ΔΔCt) relative to Passage 2 (Statistical differences are indicated as: * for $p<0.05$, ** for $p<0.01$, and *** for $p<0.001$, One-way ANOVA, n=4).

4.3.2 EVALUATION OF ACs BEHAVIOUR AND VIABILITY IN 3D CULTURES

RAD16-I hydrogel and three different blending ratios of RAD/Heparin composites with increasing amounts of heparin (950/1, 190/1 and 95/1) were used to culture dedifferentiated ACs at passage 6 obtained above (see Figure 4.3.1).

Regarding cellular morphology, cells remained round shape when embedded within the 3D scaffold, as observed in phase-contrast microscopy images at day 1 of culture (Figure 4.3.2 A). Then, they started to elongate and connect to neighboring cells as observed in images at 2 and 4 weeks of culture (Figure 4.3.2 A). Macroscopically, only scaffolds cultured in chondrogenic conditions underwent condensation, where the diameter of the structure was reduced approximately 60% compared to the initial size. This event was independent of the presence of heparin in the scaffolds and was reached it maximum effect at 2 weeks of culture. Next, fluorescence microscopy images at 4 weeks (of nuclei and actin filaments staining) showed that cells formed clusters when culture in control medium (Figure 4.3.2 B). In contrast, a dense cellular network could be observed in constructs cultured with chondrogenic medium, correlating with the condensation of the structure described above (see Figure 4.3.2 A). In

both media composition, cells seemed to be more elongated and interconnected in the presence of heparin in the scaffold independently of the polysaccharide concentration.

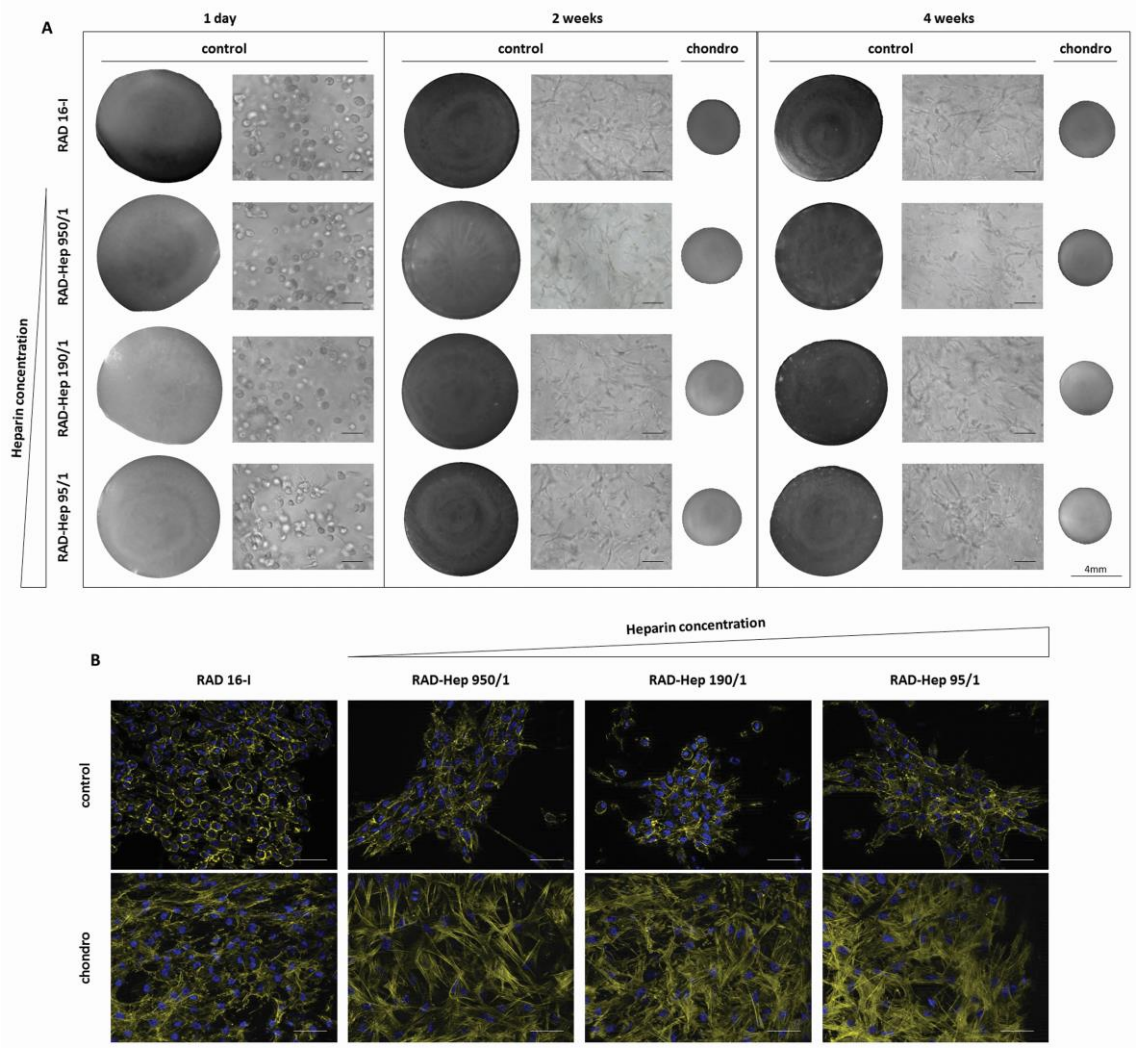

Figure 4.3.2. Human Articular Chondrocytes (ACs) cultured with control and chondrogenic media in self-assembling peptide scaffold RAD16-I and in the different RAD/Heparin composites. (A) ACs were cultured at Passage 6 in the different hydrogels (RAD16-I, RAD-Hep 950/1, RAD-Hep 190/1, and RAD-Hep 95/1), maintained for 4 weeks and evaluated along the culture for cell and construct morphology by phase contrast images. Control refers to control medium and chondro to chondrogenic medium. 3D constructs images showed a contracted structure of constructs cultured with chondrogenic medium (Scale bars=50 µm). (B) Fluorescent images of nuclei (DAPI, blue) and actin microfilaments (phalloidin, pseudo-colored in yellow) at 4 weeks of culture of the different composites in both culture media (Scale bars=50 µm).

Viability of ACs in the 3D scaffolds was evaluated with two methods: the qualitative live and dead staining and the quantitative MTT assay (Figure 4.3.3). Fluorescent images showed that the majority of the cells were alive in the 3D scaffolds after 5 days of culture in all the conditions tested (Figure 4.3.3 A). However, some differences could be observed between culture media at the end of the experiment (4 weeks). Clusters of live cells were observed in

control medium, while cells appeared more packed, creating a more homogeneous distribution in the 3D construct under chondrogenic conditions.

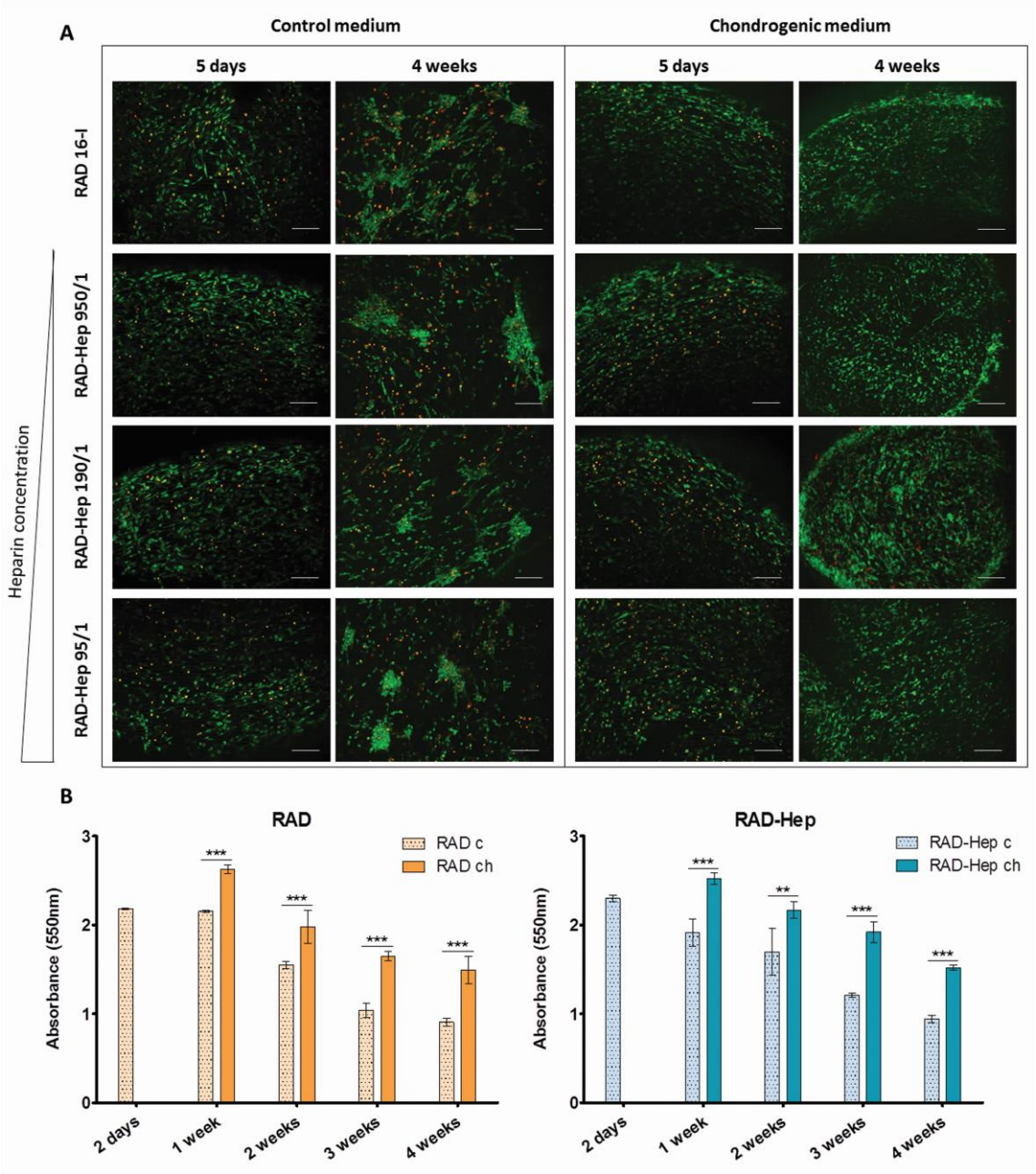

Figure 4.3.3. Viability of human Articular Chondrocytes (ACs) cultured with control and chondrogenic media in the self-assembling peptide scaffold RAD16-I and in the different RAD/Heparin composites. (A) Fluorescent images of live and dead staining at 5 days and 4 weeks of culture. Live cells were stained in green and dead cells in red (Scale bars=200 µm). (B) MTT absorbance values of 3D ACs constructs growing in control and chondrogenic media at different time points of the culture. RAD-Hep refers to the composite with the intermediate concentration of heparin (RAD/Heparin 190/1) (Statistical differences are indicated as: * for $p<0.05$, ** for $p<0.01$, and *** for $p<0.001$, Two-way ANOVA, N=2, n=3).

Survival patterns along the 4 weeks of culture were assessed by MTT assay (Figure 4.3.3 B). The intermediate concentration of heparin (RAD/Heparin 190/1) was used in composites to compare to RAD16-I hydrogel alone. It could be observed a similar absorbance decreasing rate in both scaffold types along culture time. However, more cells were alive in constructs under chondrogenic medium compared to control medium, because significantly higher absorbance values were detected at each week of culture.

4.3.3 ANALYSIS OF THE CHONDROGENIC PHENOTYPE IN ACs 3D CULTURES

Chondrogenic and hypertrophic markers were studied at protein and gene levels in order to characterize their expression profiles. Some of the collagens constituents of articular cartilage ECM (collagens type I, II and X) were first analyzed by western blot assays in ACs cultured in monolayers (2D cultures) and in 3D scaffolds (Figure 4.3.4). Regarding collagen type I (COL1), a band of high molecular weight (~220kDa), probably a pro-collagen intermediate, was observed in 2D cultures and in 3D constructs under chondrogenic conditions. Faint COL1 bands were detected in 3D constructs cultured in control medium. Moreover, collagen type II (COL2), characteristic of articular cartilage, was only detected in 3D constructs cultured in chondrogenic conditions. ACs at passage 6 in 2D cultures were not synthetizing this specific protein of articular cartilage ECM. Collagen type X (COL10) protein expression was detected in 2D cultures and in 3D constructs cultured with chondrogenic medium after 4 weeks. Faint bands could be also observed in the 3D cultures composed by RAD16-I and heparin with control medium. These results suggest a positive effect of the 3D system and the chondrogenic medium stimulating the production of collagens type I, II and X and, importantly, collagen type II was not detected in 2D cultures under the conditions tested.

Subsequently, gene expression patterns of ACs 3D constructs cultured with chondrogenic medium were quantitatively compared to expanded ACs in monolayer (Figure 4.3.5). *COL1* expression was upregulated in all 3D constructs. However, less levels of upregulation were detected in the presence of heparin (Figure 4.3.5 A). Interestingly, the expression of *COL2* was upregulated in RAD/Heparin composites, obtaining values that were directly related to heparin quantity and, therefore, indicating a heparin dose-response. The highest value could be observed in the scaffold with higher heparin quantity (RAD/Heparin 95/1), compared to scaffolds with the lowest heparin quantity (RAD/Heparin 950/1) and without heparin (Figure 4.3.5 B). The expression of the transcription factor *SOX9* was also significantly upregulated in composites with high quantities of heparin (RAD/Heparin 190/1 and 95/1) (Figure 4.3.5 C), as expected being correlated with the expression of collagen type II at protein and gene levels (see Figure 4.3.4 and Figure 4.3.5 B, respectively). In the case of aggrecan (*ACAN*), an upregulation was observed in all RAD/Heparin composites, detecting differences between 3D constructs with and without heparin (RAD/Heparin 950/1 and 95/1) (Figure 4.3.5 D). In terms of hypertrophic markers, *COL10* expression was maintained to 2D cultures levels in RAD16-I and in composites RAD/Heparin 950/1 and 190/1, but it was upregulated in the presence of

high quantity of heparin in the scaffold (RAD/Heparin 95/1) (Figure 4.3.5 E). Finally, *RUNX2* was upregulated in constructs without heparin (RAD16-I scaffolds) and with the lowest heparin quantity (composites RAD/Heparin 950/1) (Figure 4.3.5 F).

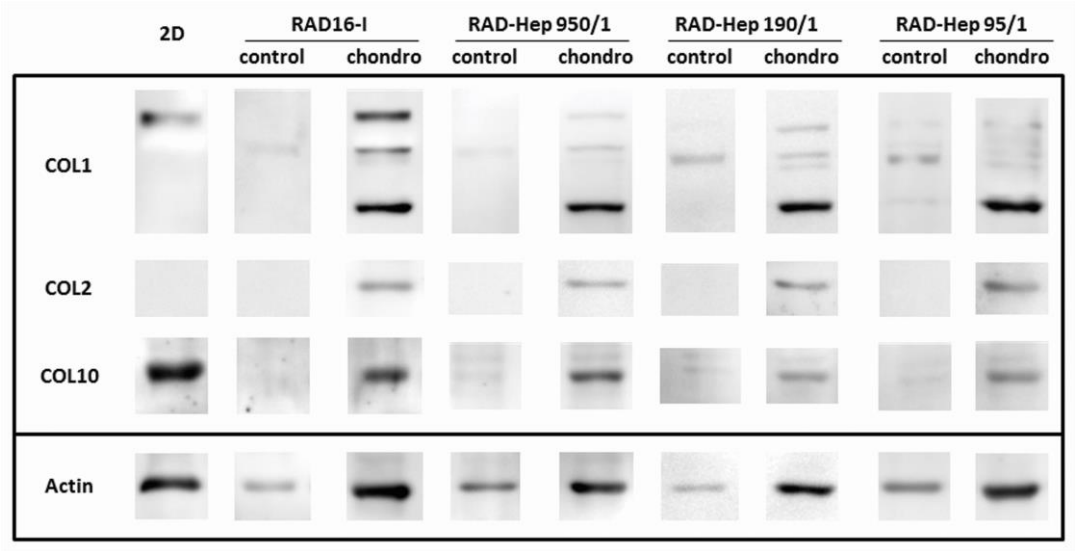

Figure 4.3.4. Protein expression characterization of ACs cultured in monolayer and in RAD16-I and composites scaffolds after 4 weeks of culture. Western blot results of collagen type I (COL1), collagen type II (COL2), and collagen type X (COL10) of ACs cultured in control and chondrogenic media in RAD16-I and in the three RAD/Heparin composites (950/1, 190/1, and 95/1). Actin expression was used as an internal control. Samples were prepared in triplicate.

Toluidine blue staining, which is indicative of PGs production, indicated that 3D constructs cultured with control medium stained relatively weakly for PGs (Figure 4.3.6). As expected, samples showing upregulation of aggrecan at gene level (see above Figure 4.3.5 D) stained positive for toluidine blue, especially RAD/Heparin composites compared to RAD16-I alone.

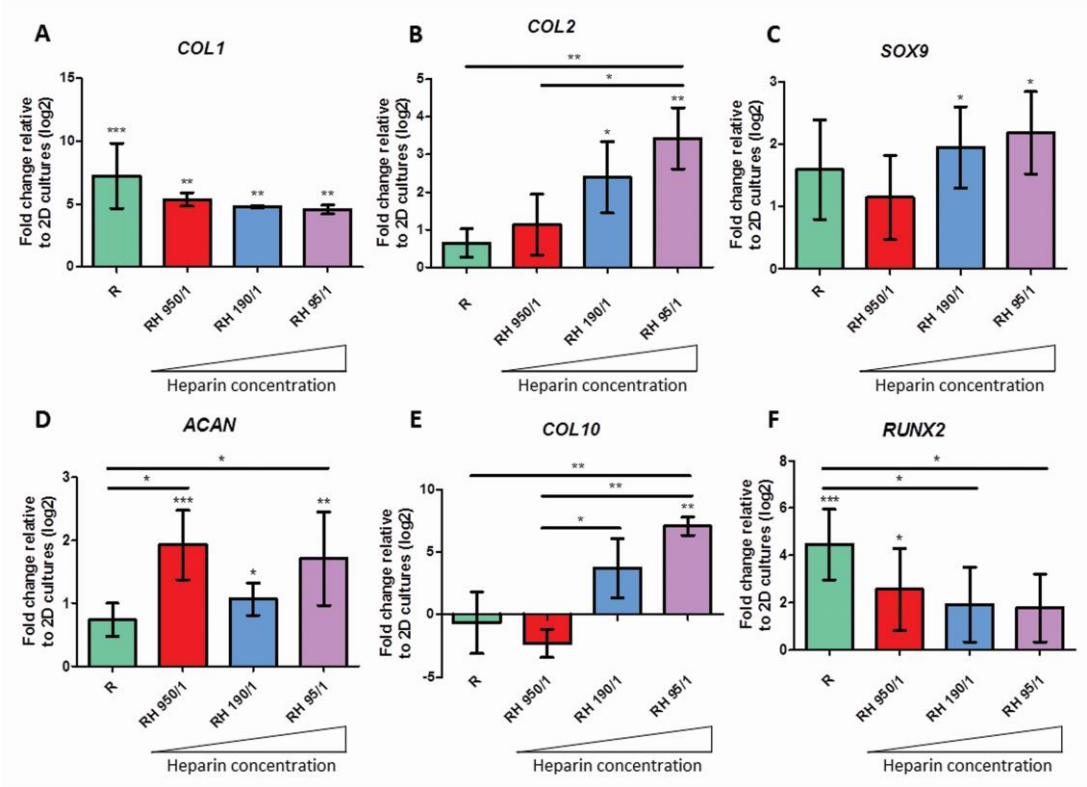

Figure 4.3.5. Gene expression levels of chondrogenic and hypertrophic markers of ACs 3D constructs cultured with induction medium after 4 weeks. RAD16-I and RAD/Heparin composites (950/1, 190/1, and 95/1) were compared with 2D cultures at the corresponding passage from where 3D cultures were performed (Passage 6). R refers to RAD16-I and RH to RAD/Heparin composites. Collagen type I (*COL1*, A), collagen type II (*COL2*, B), *SOX9* (C), aggrecan (*ACAN*, D), collagen type X (*COL10*, E), and *RUNX2* (F) were determined through real time RT-PCR. Ct values relative to ribosomal protein L22 (*RPL22*) were obtained and reported as fold increase (ΔΔCt) relative to monolayer (Statistical differences are indicated as: * for $p<0.05$, ** for $p<0.01$, and *** for $p<0.001$, One-way ANOVA, N=2, n=3).

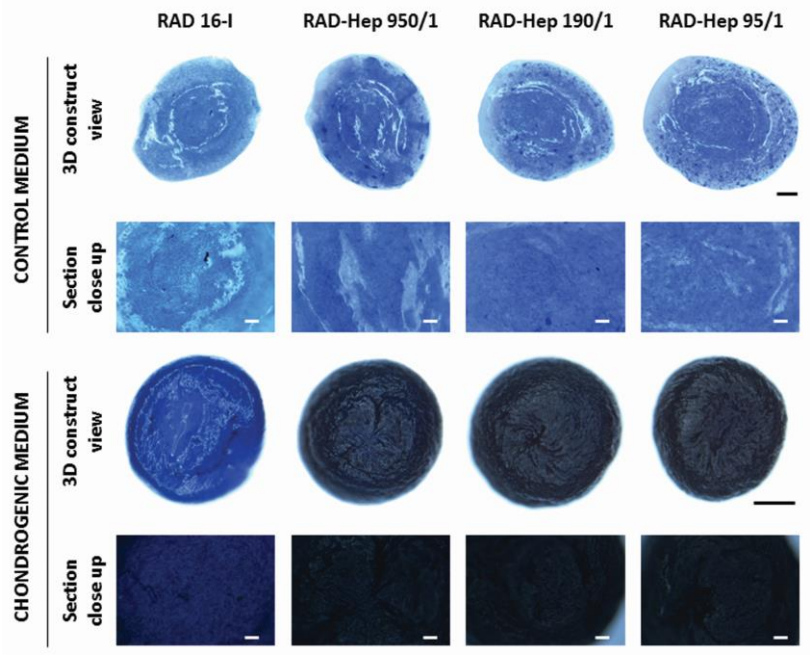

Figure 4.3.6. Proteoglycans synthesis characterization of human Articular Chondrocytes (ACs) cultured in RAD16-I and in the different RAD/Heparin composites for 4 weeks. Toluidine blue staining (sulfated glycosaminoglycans) of 3D ACs constructs cultured in control and chondrogenic media (3D construct view scale bars=500 µm, control medium section close up scale bars=400 µm and chondrogenic medium section close up scale bars=100 µm).

Additionally, possible calcifications characteristic of osteogenic differentiation were analyzed by von Kossa staining in 3D constructs cultured with chondrogenic medium (Figure 4.3.7). Importantly, samples stained negatively both at the surface as well as inside, demonstrating the absence of calcium minerals deposits, as indicative of a hypertrophy process and/or bone commitment.

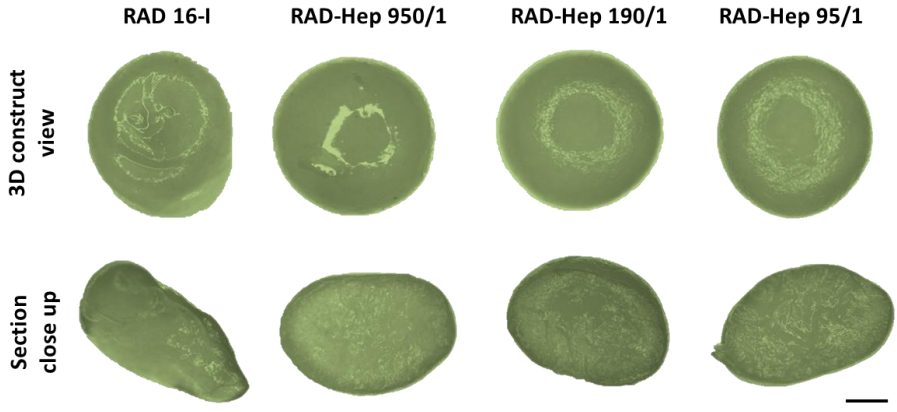

Figure 4.3.7. Calcium mineral deposits characterization of human Articular Chondrocytes (ACs) cultured in RAD16-I and in the different RAD/Heparin composites at the end of the culture (4 weeks). Von Kossa staining of 3D ACs constructs cultured in chondrogenic media (Scale bars= 500µm).

4.3.4 MECHANICAL PROPERTIES OF THE 3D CONSTRUCTS

Finally, we characterized the viscoelastic behavior of 3D constructs in chondrogenic medium at the end of the culture (Figure 4.3.9). After 4 weeks of culture, the mechanical properties of this constructs were comparable to calf and chicken native cartilage, since all samples could be measured under the same conditions (see Chapter 2, Materials and Methods). On the other hand, the soft nature of 3D constructs under control medium, constructs at few days of culture or the scaffold alone did not allow the mechanical measurement under the same conditions. Therefore, only chondrogenic 3D constructs could be compared to native cartilage under the experimental conditions tested.

As previously reported (see Figure 4.3.2), 3D cultures under chondrogenic medium experienced a spontaneous contraction process ending in a compacted structure with different mechanical properties from the initial days. In particular, ACs were initially seeded in RAD16-I hydrogel at a concentration of 0.15% (w/v), which correspond to 100Pa, as previously described[39]. During culture time, they evolve into a stiffer structure in the order of 50-80 KPa values (Figure 4.3.8).

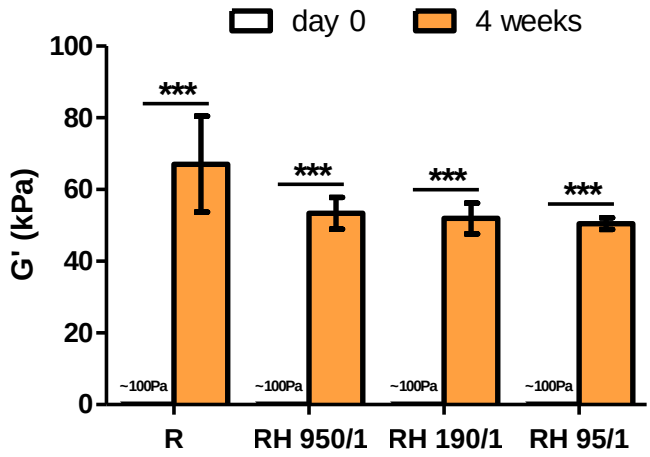

Figure 4.3.8. Mechanical characterization of human Articular Chondrocytes (ACs) cultured in RAD16-I and in the different RAD/Heparin composites at day 0 and at the end of the culture (4 weeks). Elastic component, represented by storage modulus (G'), of 3D ACs constructs cultured in chondrogenic medium. R refers to RAD16-I and RH to RAD/Heparin composites (Statistical differences are indicated as:* for $p<0.05$, ** for $p<0.01$, and *** for $p<0.001$, One-way ANOVA, N=2 n=3).

Moreover, an overview of the sample viscoelastic behavior were provided by 4 different parameters: storage modulus (G'), loss modulus (G''), complex modulus (G*) and tan(delta). Regarding elastic component (Figure 4.3.9 A), chondrogenic 3D constructs presented significantly lower G' values than chicken or calf articular cartilage. The G'' (Figure 4.3.9 B) and G* (Figure 4.3.9 C) modulus showed a similar tendency between 3D constructs and cartilage controls, compared to G'. When analyzing a same sample, values of G' were higher than values

of G'', indicating that constructs were more elastic than viscous. Tan(delta), which gives an idea of full viscoelastic properties of the constructs, showed that all 3D constructs were closely related to chicken cartilage, but still differ from calf cartilage (Figure 4.3.9 D). Moreover, no differences were observed between 3D constructs, indicating that the presence of heparin was not influencing the mechanical behavior of the cultures.

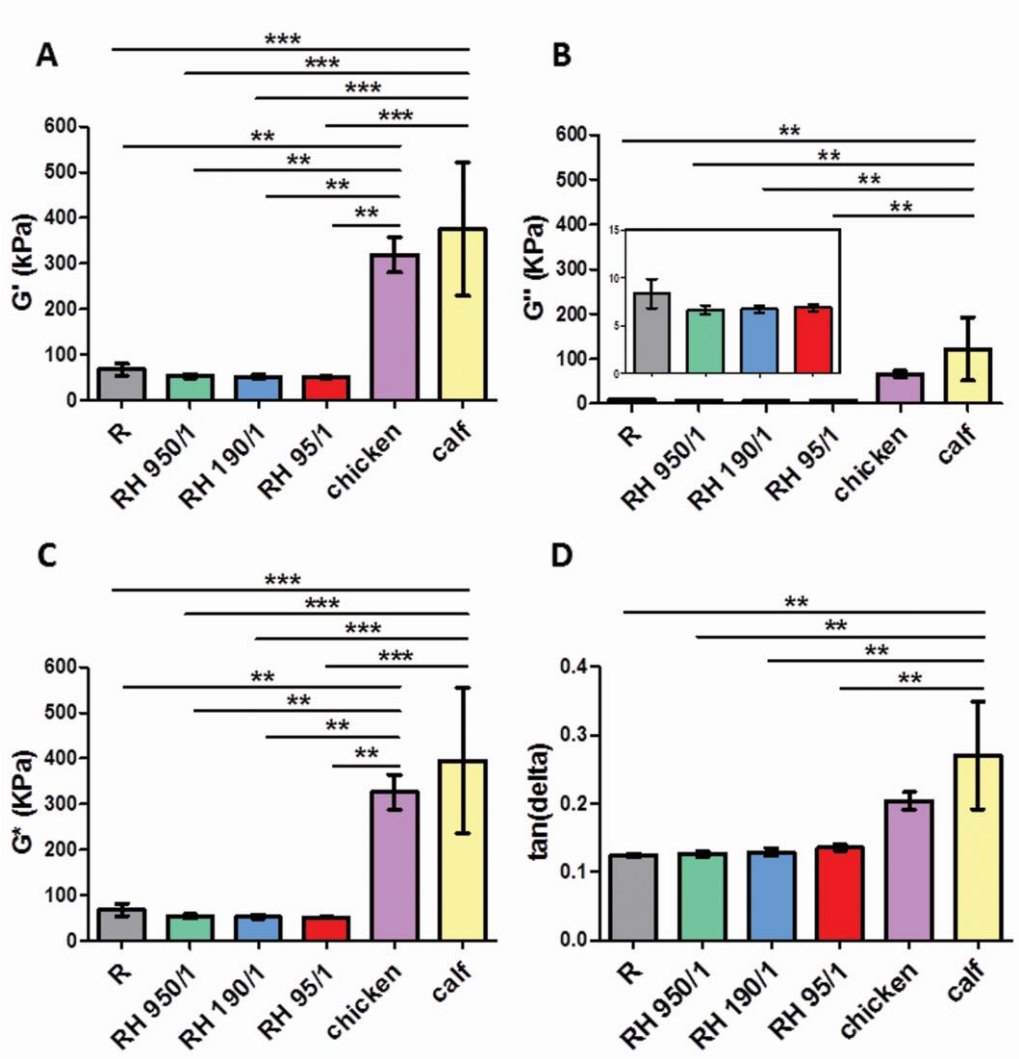

Figure 4.3.9. Mechanical characterization of 3D human Articular Chondrocytes (ACs) constructs after 4 weeks of culture. (A) Storage modulus (G') measures the sample's elastic behavior. (B) Loss modulus (G'') measures the viscous response of the material. (C) Complex modulus (G*) is the sum of storage and loss modulus. (D) Tan(delta) is the ratio of the loss to the storage. 3D constructs cultured in chondrogenic medium and chicken and calf articular cartilage were measured in the same conditions. R refers to RAD16-I and RH to RAD/Heparin composites (Statistical differences are indicated as: * for $p<0.05$, ** for $p<0.01$, and *** for $p<0.001$, One-way ANOVA, N=2, n=3).

4.4 DISCUSSION

It has been reported that chondrocytes dedifferentiate when expanded in monolayer and, therefore, different culture techniques to maintain their phenotype have been attempted[40–42]. In the present work, expanded dedifferentiated ACs, at passage 6, were cultured within a 3D synthetic scaffold in order to study the influence of this microenvironment in the chondrogenic lineage re-commitment. The proposed 3D scaffold was previously characterized (see Chapter 3) and consists of the simple combination of the self-assembling RAD16-I peptide and the heparin polysaccharide[35]. The mixture forms a stable composite scaffold with enhanced properties from the point of view of cell survival and differentiation[35,43]. Therefore, in this work, we aimed to evaluate the potential of the RAD/Heparin composites as a 3D culture system in a different scenario: redifferentiating expanded human chondrocytes. We hypothesize that heparin moieties might act as functional elements recruiting/presenting GFs to enhance the reengagement of the chondrogenic commitment[44–46]. This idea is supported by previous results (see Chapter 3) that demonstrates that the presence of heparin in the scaffold enhanced survival of adipose-derived stem cells (ADSCs)[35]. In addition, the expression of specific markers of mature cartilage tissue including collagen type II and the specific proteoglycan aggrecan was confirmed. Moreover, previous *in vitro* studies with other mammalian cells types have shown the ability of the RAD16-I nanometric scaffold to support cell attachment, maintenance, proliferation and differentiation[31,47–49]. During the culture time, morphological changes of the seeded cells as well as the entire 3D construct were observed[43,50,51]. In the work presented here, initial seeded scaffolds with cells undergo dramatic morphological changes ending in a cartilage-like structure from the point of view of the biological and biomechanical phenotype (see Figure 4.3.2). These results suggest that ACs were undergoing different cellular processes such as elongation, cell-cell and cell-matrix interactions. Moreover, the chondrogenic medium causes condensation of the 3D system (volume reduction) probably due to cell-cell and cell-matrix interaction as well as matrix remodeling. The interplay between the cells, the provided matrix and the inductors into the medium is a dynamic event changing the cellular microenvironment over time, fostering cellular lineage commitment, to chondrogenic phenotype in this case.

In the present work, in terms of viability, the majority of the cells were alive after 4 weeks of culture in the different scaffolds combination and culture media (Figure 4.3.3 A). Quantitative results revealed a similar tendency in both scaffold types (RAD16-I and RAD/Heparin composite) along culture time, suggesting that cells performed their re-differentiation process without experienced significant cell dead (Figure 4.3.3 B). Cellularity decays at the same rate in both control and chondrogenic media over time, but higher absorbance values were detected in constructs maintained in chondrogenic medium. We propose that the presence of GFs in chondrogenic medium induce certain cell proliferation at the beginning of the culture, not detected in control medium. Moreover, live cells in control medium were probably grouped in

order to take advantage of endogenous GFs secreted by neighboring cells, which could have a paracrine effect.

Regarding molecular markers, ACs at passage 6 in monolayer expressed collagens type I and X (at protein level), but no collagen type II synthesis was detected (Figure 4.3.4), suggesting that cell culture on flasks are not appropriated for cell differentiation conditions under the conditions tested. Interestingly, when they were cultured in the 3D scaffolds under chondrogenic conditions the studied collagens were expressed, including collagen type I, II and X. Curiously, COL1 protein profile showed different molecular weight species (from 220 to 130kDa), suggesting a possible protein maturation process (mainly observed in chondrogenic condition)[11]. Its presence could indicate that COL1 protein is probably undergoing processing to reach its final mature product of about 130-140kDa (the expected molecular weight for mature α1 chain is 139kDa and α2 chain 129kDa). These results suggest that only in 3D cultures under chondrogenic conditions and favored by the presence of heparin, COL1 protein is properly processed contributing to the formation of a physiological matrix structure. This is particularly interesting since the proper secretion and self-assembling of collagen type I at the ECM is important for the biomechanical and signaling function of these proteins. Gene expression profiles revealed that the presence of heparin in the scaffold, in general, improves the expression of chondrogenic markers (i.e. up-regulation of *COL2*, *SOX9* and *ACAN*) (Figure 4.3.5). Moreover, at intermediate amounts of heparin (RAD/Heparin 190/1) better performance seems to be observed by downregulation of the expression of hypertrophic markers (*COL10* and *RUNX2*).

Furthermore, the strong toluidine blue staining obtained in chondrogenic constructs was indicative of a PG-rich matrix containing aggrecan and other possible PGs such as versican, syndecan and perlecan also present in cartilaginous tissue (Figure 4.3.6). The absence of calcium mineral deposits confirmed by von Kossa staining indicates that constructs did not undergo final cartilage hypertrophy. Again here, the importance of having a chondrogenic system where cells undergo lineage differentiation without engaging into hypertrophy, which would be non-beneficial for the potential cartilage graft development.

Regarding mechanical properties, ACs were initially seeded into a compliant hydrogel that provides a soft and permissiveness microenvironment for the cells, allowing to extend cellular processes as elongation and network formation, being able to self-organize[25]. Therefore, our 3D culture was dynamic and the mechanical properties were evolving during the culture days, ending with a stiffer structure. This event was also previously observed with other cellular types[32,50,51]. For this reason, we decided to select the end of the culture as our time point to compare the mechanical properties with chicken and calf native articular cartilage and similarities in tan(delta) chicken cartilage were found. Moreover, no differences between 3D constructs in the mechanical parameters analyzed were observed, suggesting that the presence of heparin and, therefore, the composition of the hydrogels do not influence the viscoelastic nature of the cultures.

Taken together, these results propose a 3D scaffold that promotes the redifferentiation of dedifferentiated human ACs. Cells in 3D cultures changed their shape from round to elongated, extended processes and increased cell-cell and cell-matrix interactions. Consequently, different ECM components naturally present in cartilage (collagens and PGs) were synthetized along the culture, producing a more physiological matrix. Moreover, a global condensation of the scaffold structure was observed under chondrogenic conditions leading into a stiffer 3D construct, which better mimics the mechanical properties of native cartilage tissue compared to constructs under control conditions. Although cells did not present the characteristic round morphology of mature chondrocytes, a pre-cartilage condensation could explain an early chondrogenic stage.

On the other hand, the presence of heparin in the scaffold seems to stimulate the chondrogenic differentiation as evidenced by quantitative gene expression analysis. As mentioned above, the possible role of heparin could be in capturing endogenous and exogenous GFs, secreted by the cells and added to the medium, respectively, which would activate signaling processes to engage expanded chondrocytes to redifferentiate back cartilage-like tissue. The studied 3D scaffold used to culture human chondrocytes aim to mimic the native ECM and represent an *in vitro* and synthetic approximation of the complex microenvironment of native cartilage. Moreover, this 3D model can allow researchers to analyze the biological and biomechanical signals present *in vitro* which are responsible to maintain chondrogenic phenotype. Finally, it opens the possibility to develop an efficient and stable chondrocytes-based platform for CTE for repair or regeneration purposes.

4.5 CONCLUDING REMARKS

- Human ACs dedifferentiated after monolayer expansion, downregulating progressively (over passages) the expression of chondrogenic and hypertrophic specific markers.

- ACs cultured in soft 3D scaffolds (RAD16-I and RAD/Heparin composites) elongated, created a cellular network and remodeled the matrix over culture time changing the construct morphology. Moreover, good viability results were observed after 4 weeks of culture.

- The expression of specific mature cartilage markers at both protein and gene expression levels suggests a recovery of the original cartilage phenotype in the studied 3D matrices. Moreover, heparin seems to help in the chondrogenic lineage re-commitment based on gene expression results.

- The mechanical properties of 3D constructs evolve during culture time ending in a compacted and stiffer structure that more closely resemble native cartilage.

4.6 REFERENCES

1. Chiang, H. & Jiang, C. Repair of articular cartilage defects: review and perspectives. *J. Formos. Med. Assoc.* **108,** 87–101 (2009).
2. Castells-sala, C. *et al.* Current Applications of Tissue Engineering in Biomedicine. *Biochips & Tissue chips* **S2:004,** (2013).
3. Zhao, C., Tan, A., Pastorin, G. & Ho, H. K. Nanomaterial scaffolds for stem cell proliferation and differentiation in tissue engineering. *Biotechnol. Adv.* **31,** 654–68 (2012).
4. Johnstone, B. *et al.* TISSUE ENGINEERING FOR ARTICULAR CARTILAGE REPAIR – THE STATE OF THE ART. **25,** 248–267 (2013).
5. Freyria, A. Chondrocytes or adult stem cells for cartilage repair : The indisputable role of growth factors. **43,** 259–265 (2012).
6. Chung, C. & Burdick, J. Engineering Cartilage Tissue. *Adv Drug Deliv Rev.* **60,** 243–62 (2008).
7. Darling, E. M. & Athanasiou, K. A. Rapid phenotypic changes in passaged articular chondrocyte subpopulations. *J. Orthop. Res.* **23,** 425–432 (2005).
8. Hong, E. & Reddi, a H. Dedifferentiation and redifferentiation of articular chondrocytes from surface and middle zones: changes in microRNAs-221/-222, -140, and -143/145 expression. *Tissue Eng. Part A* **19,** 1015–22 (2013).
9. Alemany-Ribes, M. & Semino, C. E. Bioengineering 3D environments for cancer models. *Adv. Drug Deliv. Rev.* **79-80,** 40–49 (2014).
10. Griffith, L. G. & Swartz, M. a. Capturing complex 3D tissue physiology in vitro. *Nat. Rev. Mol. Cell Biol.* **7,** 211–24 (2006).
11. Bobick, B. E., Chen, F. H., Le, A. M. & Tuan, R. S. Regulation of the chondrogenic phenotype in culture. *Birth Defects Res. Part C - Embryo Today Rev.* **87,** 351–371 (2009).
12. Tallheden, T. *et al.* Gene expression during redifferentiation of human articular chondrocytes. *Osteoarthritis Cartilage* **12,** 525–35 (2004).
13. Benya, P. D. & Shaffer, J. D. Dedifferentiated chondrocytes reexpress the differentiated collagen phenotype when cultured in agarose gels. *Cell* **30,** 215–224 (1982).
14. Bonaventure, J. *et al.* Reexpression of cartilage-specific genes by dedifferentiated human articular chondrocytes cultured in alginate beads. *Exp. Cell Res.* **212,** 97–104 (1994).
15. Stevens, M. A rapid-curing alginate gel system: utility in periosteum-derived cartilage tissue engineering. *Biomaterials* **25,** 887–894 (2004).
16. Chaipinyo, K., Oakes, B. W. & Van Damme, M.-P. I. The use of debrided human articular cartilage for autologous chondrocyte implantation: maintenance of chondrocyte differentiation and proliferation in type I collagen gels. *J. Orthop. Res.* **22,** 446–55 (2004).
17. Takahashi, T. *et al.* Three-dimensional microenvironments retain chondrocyte phenotypes during proliferation culture. *Tissue Eng.* **13,** 1583–1592 (2007).

18. Ting, V. *et al.* In vitro prefabrication of human cartilage shapes using fibrin glue and human chondrocytes. *Ann. Plast. Surg.* **40,** 413–421 (1998).

19. Benders, K. E. M. *et al.* Extracellular matrix scaffolds for cartilage and bone regeneration. *Trends in Biotechnology* **31,** 169–176 (2013).

20. Gelain, F., Horii, A. & Zhang, S. Designer self-assembling peptide scaffolds for 3-D tissue cell cultures and regenerative medicine. *Macromol. Biosci.* **7,** 544–551 (2007).

21. Semino, C. E. Can we build artificial stem cell compartments? *J. Biomed. Biotechnol.* **3,** 164–169 (2003).

22. Mhanna, R. *et al.* Chondrocyte Culture in 3D Alginate Sulfate Hydrogels Promotes Proliferation While Maintaining Expression of Chondrogenic Markers. *Tissue Eng. Part A* 1–38 (2013). at <http://www.ncbi.nlm.nih.gov/pubmed/24320935>

23. Kisiday, J. *et al.* Self-assembling peptide hydrogel fosters chondrocyte extracellular matrix production and cell division: implications for cartilage tissue repair. *Proc. Natl. Acad. Sci. U. S. A.* **99,** 9996–10001 (2002).

24. Yamaoka, H. *et al.* Cartilage tissue engineering using human auricular chondrocytes embedded in different hydrogel materials. *J. Biomed. Mater. Res. A* **81,** 771–780 (2006).

25. Semino, C. E. Self-assembling Peptides: From Bio-inspired Materials to Bone Regeneration. *J. Dent. Res.* **87,** 606–616 (2008).

26. Sieminski, a L., Semino, C. E., Gong, H. & Kamm, R. D. Primary sequence of ionic self-assembling peptide gels affects endothelial cell adhesion and capillary morphogenesis. *J. Biomed. Mater. Res. A* **87,** 494–504 (2008).

27. Wu, J. *et al.* Nanometric self-assembling peptide layers maintain adult hepatocyte phenotype in sandwich cultures. *J. Nanobiotechnology* **8,** 29 (2010).

28. Semino, C. E., Kasahara, J. & Hayashi, Y. Entrapment of Migrating Hippocampal Neural Cells in Three-Dimensional Peptide Nanofiber Scaffold. *Tissue Eng Part* **10,** (2004).

29. Alemany-Ribes, M., García-Díaz, M., Busom, M., Nonell, S. & Semino, C. E. Toward a 3D Cellular Model for Studying In Vitro the Outcome of Photodynamic Treatments: Accounting for the Effects of Tissue Complexity. *Tissue Eng. Part A* **19,** 1665–74 (2013).

30. Dégano, I. R. *et al.* The effect of self-assembling peptide nanofiber scaffolds on mouse embryonic fibroblast implantation and proliferation. *Biomaterials* **30,** 1156–65 (2009).

31. Quintana, L. *et al.* Early tissue patterning recreated by mouse embryonic fibroblasts in a three-dimensional environment. *Tissue Eng. Part A* **15,** 45–54 (2009).

32. Marí-Buyé, N., Luque, T., Navajas, D. & Semino, C. Development of a three-dimensional bone-like construct in a soft self-assembling peptide matrix. *Tissue Eng Part A* **19,** 870–881 (2013).

33. Castells-Sala, C. *et al.* Influence of electrical stimulation on 3D-cultures of adipose tissue derived progenitor cells (ATDPCs) behavior. *Conf. Proc. ... Annu. Int. Conf. IEEE Eng. Med. Biol. Soc. IEEE Eng. Med. Biol. Soc. Annu. Conf.* **2012,** 5658–61 (2012).

34. Recha-Sancho, L. & Semino, C. E. Heparin based self-assembling peptide scaffold reestablish chondrogenic phenotype of expanded de-differentiated human

chondrocytes. *J. Biomed. Mater. Res. Part A* **104,** 1694–1706 (2016).

35. Fernández-Muiños, T. *et al.* Bimolecular based heparin and self-assembling hydrogel for tissue engineering applications. *Acta Biomater.* **16,** 35–48 (2015).

36. Kim, M., Kim, S. E., Kang, S. S., Kim, Y. H. & Tae, G. The use of de-differentiated chondrocytes delivered by a heparin-based hydrogel to regenerate cartilage in partial-thickness defects. *Biomaterials* **32,** 7883–96 (2011).

37. Xu, X., Jha, A. K., Duncan, R. L. & Jia, X. Acta Biomaterialia Heparin-decorated , hyaluronic acid-based hydrogel particles for the controlled release of bone morphogenetic protein 2. *Acta Biomater.* **7,** 3050–3059 (2011).

38. Park, J. S. *et al.* Heparin-bound transforming growth factor-beta3 enhances neocartilage formation by rabbit mesenchymal stem cells. *Transplantation* **85,** 589–96 (2008).

39. Sieminski, a. L., Was, a. S., Kim, G., Gong, H. & Kamm, R. D. The Stiffness of Three-dimensional Ionic Self-assembling Peptide Gels Affects the Extent of Capillary-like Network Formation. *Cell Biochem. Biophys.* **49,** 73–83 (2007).

40. Tew, S. R., Murdoch, A. D., Rauchenberg, R. P. & Hardingham, T. E. Cellular methods in cartilage research: primary human chondrocytes in culture and chondrogenesis in human bone marrow stem cells. *Methods* **45,** 2–9 (2008).

41. Coates, E. E. & Fisher, J. P. Phenotypic variations in chondrocyte subpopulations and their response to in vitro culture and external stimuli. *Annals of Biomedical Engineering* **38,** 3371–3388 (2010).

42. Demoor, M. *et al.* Cartilage tissue engineering: Molecular control of chondrocyte differentiation for proper cartilage matrix reconstruction. *Biochim. Biophys. Acta - Gen. Subj.* **1840,** 2414–2440 (2014).

43. Castells-Sala, C. *et al.* Three-Dimensional Cultures of Human Subcutaneous Adipose Tissue-Derived Progenitor Cells Based on RAD16-I Self-Assembling Peptide. *Tissue Eng. Part C. Methods* **22,** 1–12 (2016).

44. Rajangam, K. *et al.* Heparin binding nanostructures to promote growth of blood vessels. *Nano Lett.* **6,** 2086–90 (2006).

45. Tanihara, M., Suzuki, Y., Yamamoto, E., Noguchi, a & Mizushima, Y. Sustained release of basic fibroblast growth factor and angiogenesis in a novel covalently crosslinked gel of heparin and alginate. *J. Biomed. Mater. Res.* **56,** 216–21 (2001).

46. Sakiyama-Elbert, S. E. & Hubbell, J. a. Development of fibrin derivatives for controlled release of heparin-binding growth factors. *J. Control. Release* **65,** 389–402 (2000).

47. Genové, E. *et al.* Functionalized self-assembling peptide hydrogel enhance maintenance of hepatocyte activity in vitro. *J. Cell. Mol. Med.* **13,** 3387–97 (2009).

48. Genove, E., Shen, C., Zhang, S. & Semino, C. E. The effect of functionalized self-assembling peptide scaffolds on human aortic endothelial cell function. *Biomaterials* **26,** 3341–3351 (2005).

49. Garreta, E., Genové, E., Borrós, S. & Semino, C. E. Osteogenic Differentiation of Mouse Embryonic Stem Cells and Mouse Embryonic Fibroblasts in a Three-Dimensional. *Tissue Eng Part A* **12,** 2215–2227 (2006).

50. Bianca M. Bussmann, Sven Reiche, Núria Marí-Buyé, Cristina Castells-Sala, H. J. M. and C. E. S. Chondrogenic potential of human dermal fibroblasts in a contractile, soft, self-assembling, peptide hydrogel. *J. Tissue Eng. Regen. Med.* (2013). doi:10.1002/term

51. Fernández-Muiños, T., Suárez-Muñoz, M., Sanmartí-Espinal, M. & Semino, C. E. Matrix dimensions, stiffness, and structural properties modulate spontaneous chondrogenic commitment of mouse embryonic fibroblasts. *Tissue Eng. Part A* **20,** 1145–55 (2014).

CHAPTER 5

DEVELOPMENT OF CHONDROITIN SULFATE- AND DECORIN-BASED SELF-ASSEMBLING SCAFFOLDS AND EVALUATION OF THEIR POTENTIAL TO FOSTER CHONDROGENIC COMMITMENT OF ADIPOSE DERIVED STEM CELLS AND DEDIFFERENTIATED ARTICULAR CHONDROCYTES

Recha-Sancho L and Semino CE. Chondroitin Sulfate- and Decorin-based self-assembling scaffolds for cartilage tissue engineering. *Plos One*. **11**(6):e0157603. (2016).

5.1 INTRODUCTION

Adult articular cartilage lacks an intrinsic capacity to regenerate after trauma or injury due to its avascularity and low biosynthetic activity[1]. Consequently, cartilage defects are degenerative, thus contributing to the development of compromised tissue function and joint disability[2,3]. Current clinical approaches for repairing cartilage defects include a variety of surgical options, such as autologous chondrocyte implantation and microfracture techniques[4–6]. However, these treatments often result in the formation of fibrocartilage tissue with inferior biomechanical properties compared to the original cartilage[7]. Therefore, the development of new strategies to restore and repair damaged areas is of growing interest[8]. In this regard, cartilage tissue engineering (CTE) attempts to create functional substitutes through the appropriate combination of cells, scaffolds and stimulatory factors[9,10].

Candidate cell types for cartilage repair include articular chondrocytes (ACs) and mesenchymal stem cells (MSCs) because chondrocytes already possess the desired phenotype and MSCs present lineage potential to differentiate into mature chondrocytes[11]. In principle, ACs are the only resident cell type in mature articular cartilage and are therefore responsible for the synthesis and remodeling of the extracellular matrix (ECM). Once they are isolated from their natural surrounding matrix and cultured in a monolayer for cell expansion, they undergo dedifferentiation and lose the expression of specific chondrogenic markers, including collagens and glycosaminoglycans (GAGs)[12,13]. Consequently, they acquire a fibroblast-like phenotype, which compromises their use in CTE applications. Nevertheless, promising results have been obtained with different three-dimensional (3D) culture platforms to restore and maintain the chondrogenic phenotype[14–17]. In contrast, MSCs are multipotent progenitor cells that possess the ability to proliferate *in vitro* and differentiate into lineages of mesodermal origin, including bone, cartilage and fat[18,19]. They can be isolated from different sources, such as bone marrow, muscle, adipose tissue and the umbilical cord[20]. In particular, MSCs of adipose origin are easy to acquire and allow an abundant supply of cells with minimally invasive surgery[21]. Along with these reasons, the plasticity of MSCs makes them a promising source of adult stem cells in CTE applications. In this work, expanded dedifferentiated ACs and adipose-derived MSCs, both from human origin, were selected for evaluation in a comparative study of chondrogenic differentiation using specific culture conditions and biomimetic scaffolds[22].

The composition and structure of the ECM govern the physical, biochemical and biomechanical signals that are continuously received by cells[23]. Therefore, biomaterials are designed to mimic the complex cellular microenvironment while providing cells with the appropriate cues[24,25]. Hydrogels are attractive candidates as tissue engineering scaffolds because they are biocompatible and possess a unique hydrated 3D network, thus recreating the nano-architectural pattern of the natural ECM[8]. Importantly, self-assembling peptides provide a network of interweaving nanofibers (50 to 200 nm pore size), which allow cells to experience a truly 3D environment. The self-assembly process is driven by noncovalent interactions (e.g.,

hydrogen bonds, electrostatic interactions) under physiological conditions, allowing cells to freely extend processes for intercellular interactions, migration and proliferation[26,27]. Moreover, self-assembling peptides are synthetic hydrogels with reproducible, controllable and customizable properties. For these reasons, in the present work 3D cultures were based on the self-assembling RAD16-I peptide (AcN-$(RADA)_4$-CNH_2), which has been widely used to culture various mammalian cell types for their growth and differentiation[28–35]. The mechanical properties of the cultured cells can be controlled by changing the peptide concentration, which enables their use in different tissue engineering applications[36]. The RAD16-I scaffold lacks the intrinsic capacity to instruct cells through receptor/ligand interactions, but it can be modified to incorporate specific signaling motifs or functional molecules[37,38]. In this regard, we have previously shown that noncovalent interactions between the RAD16-I nanofibers and heparin moieties can form a stable bi-component scaffold with growth factor (GF) binding affinity (Chapter 3)[39]. This finding demonstrates a potential use in vascular and CTE applications because the biomaterial could promote different cellular processes, depending on the conditions provided (cell type, culture media and peptide concentration)[39,40]. To expand on our previous work, the aim of this chapter was to develop novel biomaterials to support chondrogenesis by taking advantage of the ability of the RAD16-I scaffold to interact with other biomolecules. Our approach was based on mimicking the native articular cartilage ECM while providing bioactive signals to the non-instructive RAD16-I peptide scaffold. GAGs and proteoglycans (PGs) are important structural components of cartilage that influence the regulation of cell proliferation, migration and differentiation[41]. Among them, Chondroitin Sulfate (CS) and Decorin were selected in this work and were separately combined with the self-assembling peptide RAD16-I.

Chondroitin, a kind of GAG, is a anionic polysaccharide chain of alternating units of N-acetylgalactosamine (GalNAc) and glucuronic acid (GlcA) that can be sulfated on the either or both GalNAc and GlcA units (Figure 5.1.1 A)[42]. Its molecular weight ranges from 10,000 to 50,000 Da[41]. Chondroitin and its sulfates are frequently attached to proteins to form PGs. Decorin is a member of the family of small leucine-rich proteoglycan (SLRP) and is characterized by the presence of a leucine-rich repeat motif that dominates the structure of the core protein[43,44]. It contains a core protein bound to one chain of CS and is able to bind collagen fibrils and regulate the diameter of forming fibrils (Figure 5.1.1 B)[45].

These molecules play several important roles in regulating different cellular responses[46–48]. For instance, they bind to GFs, such as transforming growth factor-β (TGF-β), which interacts with both the protein core and the side chain of CS[49,50]. We hypothesize that the presence of CS or Decorin in combination with the RAD16-I scaffold could modulate chondrogenesis under different experimental conditions. Two different cell types were cultured with our novel bi-component scaffolds in order to redifferentiate expanded human chondrocytes and guide MSCs from adipose tissue to cartilage commitment.

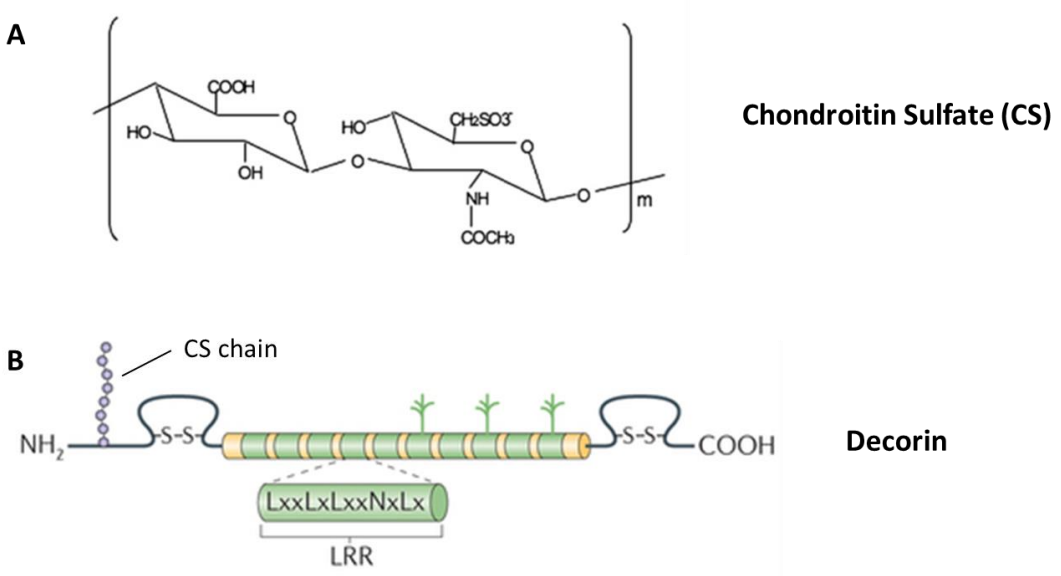

Figure 5.1.1. Chondroitin Sulfate (CS) and Decorin molecules. (A) Chemical structure of CS. (B) Decorin is a small leucine-rich proteoglycan (SLRP) characterized by highly conserved leucine rich repeats (LRR) in the core molecule. It is composed of one CS chain attached to a 40kDa core protein. Image adapted from Varghese *et al.*[42] and Mouw *et al*.[51]

5.2 MOTIVATIONS AND SPECIFIC AIMS

The general aim of this chapter is to develop novel biomaterials for CTE and to evaluate their chondrogenic potential in different scenarios: redifferentiating expanded human articular chondrocytes (ACs) and guiding adipose-derived stem cells (ADSCs) to cartilage commitment. Previous studies (Chapters 3 and 4) reported the potential of self-assembling RAD16-I peptide to be functionalized with molecular entities present in cartilage ECM (heparin polysaccharide). This finding motivated the incorporation of other ECM components (CS and Decorin) to create new scaffolds and to study their effects on chondrogenic differentiation. Therefore, the specific objectives of this chapter are the following:

(1) To develop and characterize novel bi-component scaffolds for CTE purposes by combining the self-assembling peptide RAD16-I with CS or Decorin molecules.

(2) To study the general cellular behavior of dedifferentiated ACs and ADSCs in the bi-component scaffolds by inducing the chondrogenic differentiation process.

(3) To characterize the expression patterns at gene and protein level of specific cartilage markers under chondrogenic conditions in bi-component scaffolds.

(4) To evaluate the mechanical properties of ADSCs and ACs 3D constructs at the end of 3D cultures comparing to native articular cartilage.

5.3 RESULTS

5.3.1 DEVELOPMENT AND CHARACTERIZATION OF THE BI-COMPONENT SCAFFOLDS

In the present chapter, CS and Decorin were combined separately with the self-assembling peptide RAD16-I to develop novel scaffolds for CTE applications. Building from previous work with a RAD/Heparin bi-component scaffold (Chapter 3 and Chapter 4)[39,40], the chemical and structural stability of the new composites were evaluated by combining different ratios of RAD/CS and RAD/Decorin. As expected, mixtures ranging from 950/1 to 9.5/1 for each composite type were structurally stable at a physiological pH and formed nanofiber composite self-assembling scaffolds (Figure 5.3.1 A&B). Toluidine blue staining was performed to detect highly anionic charged molecules in CS and Decorin[52]. The homogeneous blue color observed in the composite gels after staining confirmed that both CS and Decorin were stably associated to the self-assembling nanofiber network in a dose-dependent manner. As expected, the RAD/Decorin composite showed a less intense blue staining because Decorin is composed of only one single chain of CS covalently bound to a small protein. Moreover, congo red staining showed the formation of β-sheet secondary structures for all scaffolds, thus indicating the proper formation of nanofibers. Therefore, CS and Decorin did not interfere in the self-assembling process, regardless of the concentration. In view of these results, we selected the intermediate ratio of 47.5/1 for both scaffolds (RAD/CS and RAD/Decorin) for further characterization and *in vitro* analysis.

In addition, the effect of CS and Decorin in the nanofiber formation was studied by atomic force microscopy (AFM). AFM is an imaging tool for determining surface topographies and is able to measure 3D topography information at sub-nanometer resolution[53]. Together with CS and Decorin, we also aimed to study the effect of heparin moieties in the nanofiber formation, since the RAD/Heparin composite was previously used as scaffold in Chapters 3 and 4. The presence of nanofibers in aqueous solutions was observed in all the composites and AFM images revealed similar nanofiber results (30-50 nm wide fibers) (Figure 5.3.2). Interestingly, in the case of heparin some differences at structural level could be observed without changing the nanofiber structure. We hypothesize that this finding could be associated to different effects from the point of view of biomechanics, chemical recognition or electrostatic interactions. In sum, AFM results confirmed the previous observation of nanofiber formation by visual inspection (Figure 5.3.1) and therefore, their potential use as scaffolds for tissue culture.

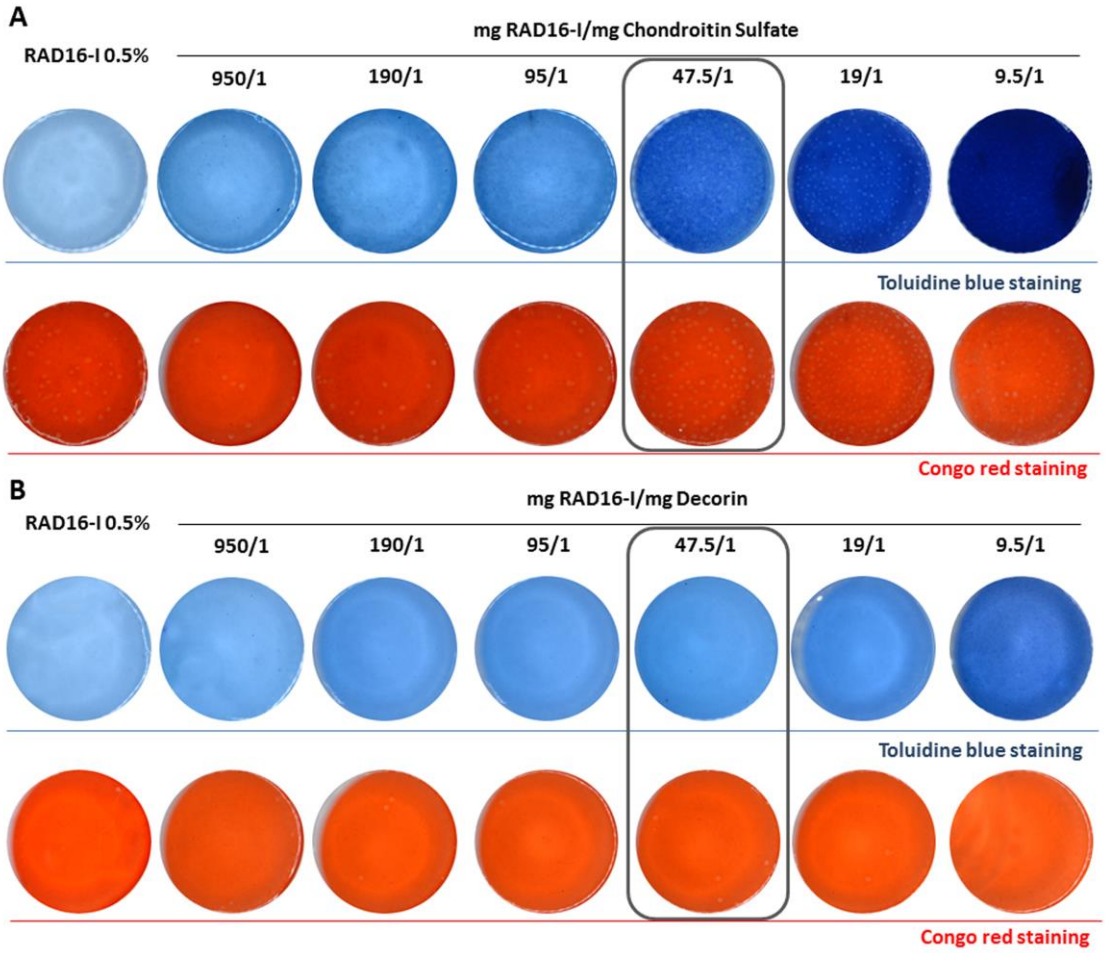

Figure 5.3.1. Characterization of the bi-component scaffolds. (A) Toluidine blue and congo red staining of RAD16-I and RAD/CS composites with increasing quantities of CS. Ratios of mg RAD16-I/mg CS ranging from 950/1 to 9.5/1. (B) Toluidine blue and congo red staining of RAD16-I and RAD/Decorin composites with increasing quantities of Decorin. Ratios of mg RAD16-I/mg Decorin ranging from 950/1 to 9.5/1.

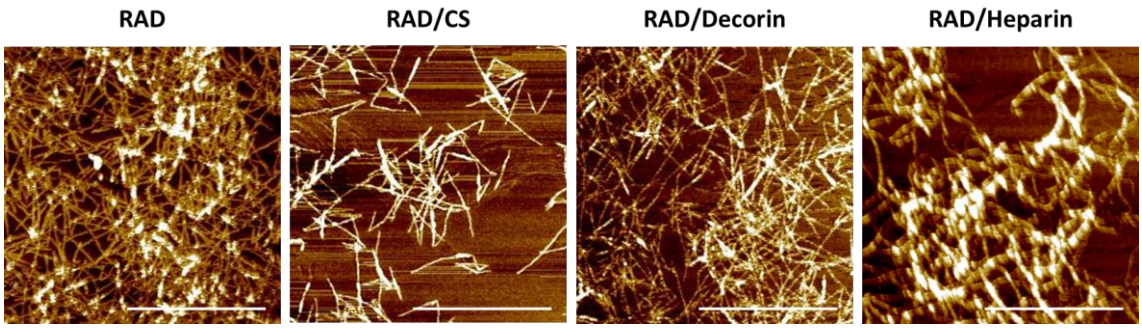

Figure 5.3.2. AFM topographical micrographs of the bi-component scaffolds. Composites RAD/CS, RAD/Decorin and RAD/Heparin (ratios 47.5/1) and the control RAD16-I were prepared in aqueous solutions. Scale bars = 1 μm.

Our next step was focused on studying the GF binding affinity of our biomaterial composites. We selected TGFβ1 as a model GF to evaluate its release profile by the different scaffolds because this GF has an important role in chondrogenic differentiation[54]. To this end, we incubated the new composites (RAD/CS, RAD/Decorin) and the previous described RAD/Heparin composite[39,40] in the presence of TGFβ1 to study its binding and release over time (Figure 5.3.3 A-C). In general, the release pattern of TGFβ1 was similar for all tested composites, and these composite scaffolds showed a release pattern similar to that of the control RAD16-I scaffold. However, we observed some differences between the composites. Interestingly, in the case of RAD/CS, more TGFβ1 was released at 24 and 36 hours compared to the control scaffold (Figure 5.3.1 A), but no differences in GF release were detected between the RAD/Decorin and control RAD16-I scaffold over time (Figure 5.3.1 B). Finally, as previously reported, a similar TGFβ1 release profile was observed between RAD16-I and the composite RAD/Heparin scaffold, as indicated by the overlapping curves (Figure 5.3.1 C).

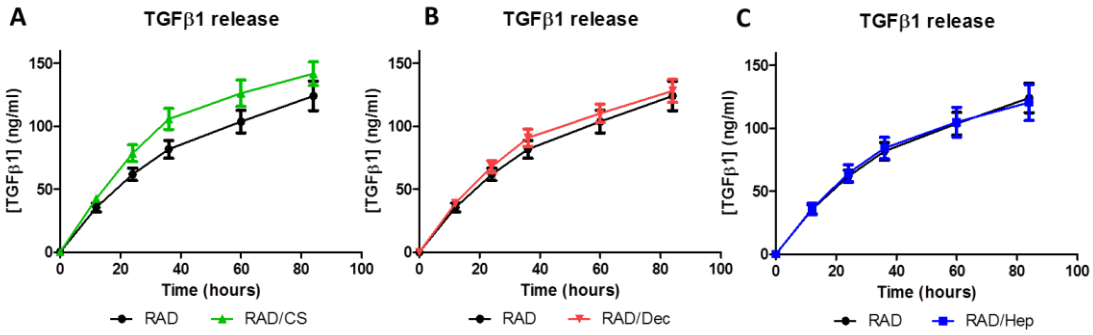

Figure 5.3.3. Characterization of the TGFβ1 release pattern in the bi-component scaffolds. (A) Quantification of TGFβ1 released by RAD16-I and the composite RAD/CS (ratio 47.5/1) after 12, 24, 36, 60 and 84 hours of delivery (mean ± SD, n=3). (B) Quantification of TGFβ1 released by RAD16-I and the composite RAD/Decorin (ratio 47.5/1) after 12, 24, 36, 60 and 84 hours of delivery (mean ± SD, n=3). (C) Quantification of TGFβ1 released by RAD16-I and composite RAD/Heparin (ratio 47.5/1) after 12, 24, 36, 60 and 84 hours of delivery (mean ± SD, n=3).

5.3.2 INDUCTION OF CHONDROGENIC DIFFERENTIATION BY THE BI-COMPONENT SCAFFOLDS

The capacity for inducing chondrogenic differentiation was assessed for RAD/CS, RAD/Decorin and the RAD16-I scaffold alone using two different human cell types: expanded de-differentiated ACs and ADSCs. The aim of the work was to corroborate the versatility of the scaffolds in two different tissue engineering scenarios: differentiation of expanded ACs to their original phenotype and induction of ADSCs to a chondrogenic lineage commitment. Cells were seeded in the two different composite scaffolds and maintained for 4 weeks in control or chondrogenic medium (see Chapter 2, Materials and Methods). Moreover, ACs were cultured

in a third medium containing GFs (expansion medium used in monolayer cultures, see Materials and Methods) because this culture condition could affect the fate of the 3D culture.

First, cell morphology was evaluated by DAPI-Phalloidin staining of the cells cultured under the different experimental conditions (Figure 5.3.4). In general, good performance was observed in the two cell types for all conditions (with the exception of control), as evidenced by the formation of cellular networks. ADSCs possessed a round morphology under control conditions and were elongated and aligned under chondrogenic conditions. In contrast, ACs were elongated and interconnected in all cases, but lower density cells were observed in control conditions. In addition, construct morphologies were similar between the scaffold types cultured in the same medium; representative images for each condition are shown in Figure 5.3.4. Chondrogenic medium causes the most relevant morphological change in both cell types; a reduction in diameter of approximately 70% (compared to diameter at day 0) was observed after 4 weeks of culture. This event correlated with a dense and compacted cellular network observed by DAPI-Phalloidin staining. In contrast, when cultured in control medium, the diameter of constructs was reduced by only a marginal amount from the initial state. A reduction of approximately 50% was observed when ACs were cultured under expansion medium. Therefore, depending on the culture medium, cells developed different construct morphologies.

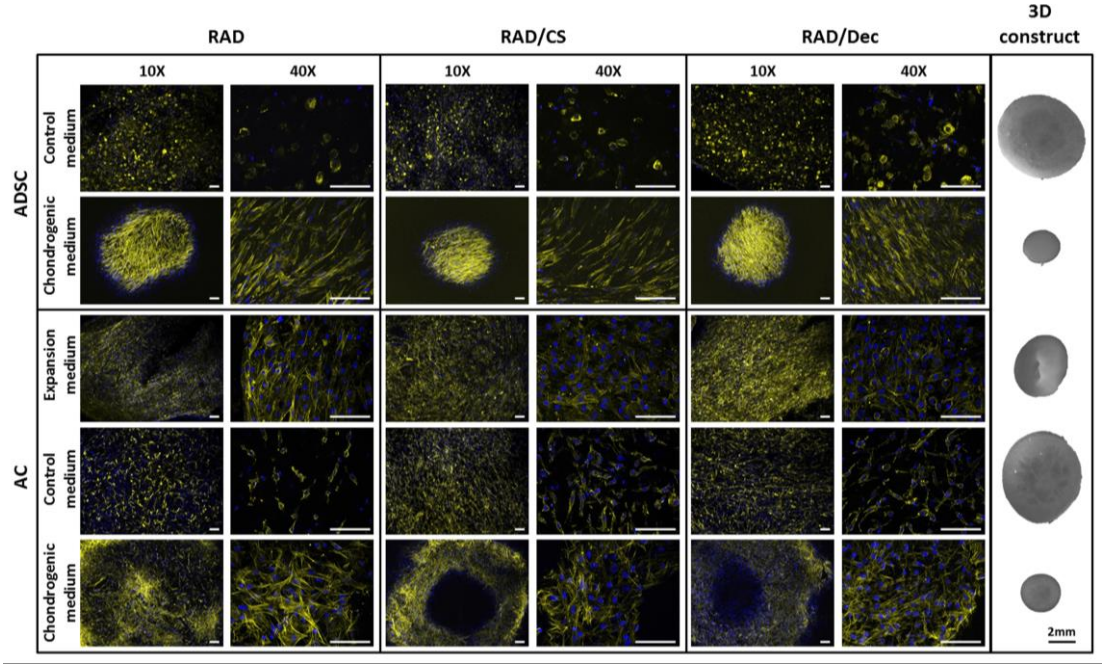

Figure 5.3.4. Human ADSCs and ACs cultured under different media conditions with the self-assembling RAD16-I peptide scaffold and bi-component composites. ADSCs and ACs were encapsulated in the control scaffold (RAD16-I) and in the composites (RAD/CS and RAD/Decorin), maintained for 4 weeks in the different media compositions and evaluated throughout the culture period for cell and construct morphology by phase contrast images. Images of 3D constructs show a contracted structure under chondrogenic culture conditions. Fluorescent images of nuclei (DAPI, blue) and actin microfilaments (phalloidin, pseudo-colored in yellow) of the three scaffolds after 4 weeks of culture in different culture media (Scale bars = 100 µm).

Cellular viability in the 3D cultures was assessed by a quantitative MTT assay at different time points throughout the culture period and by qualitative live/dead staining at the end of the culture (Figure 5.3.5 and Figure 5.3.6).

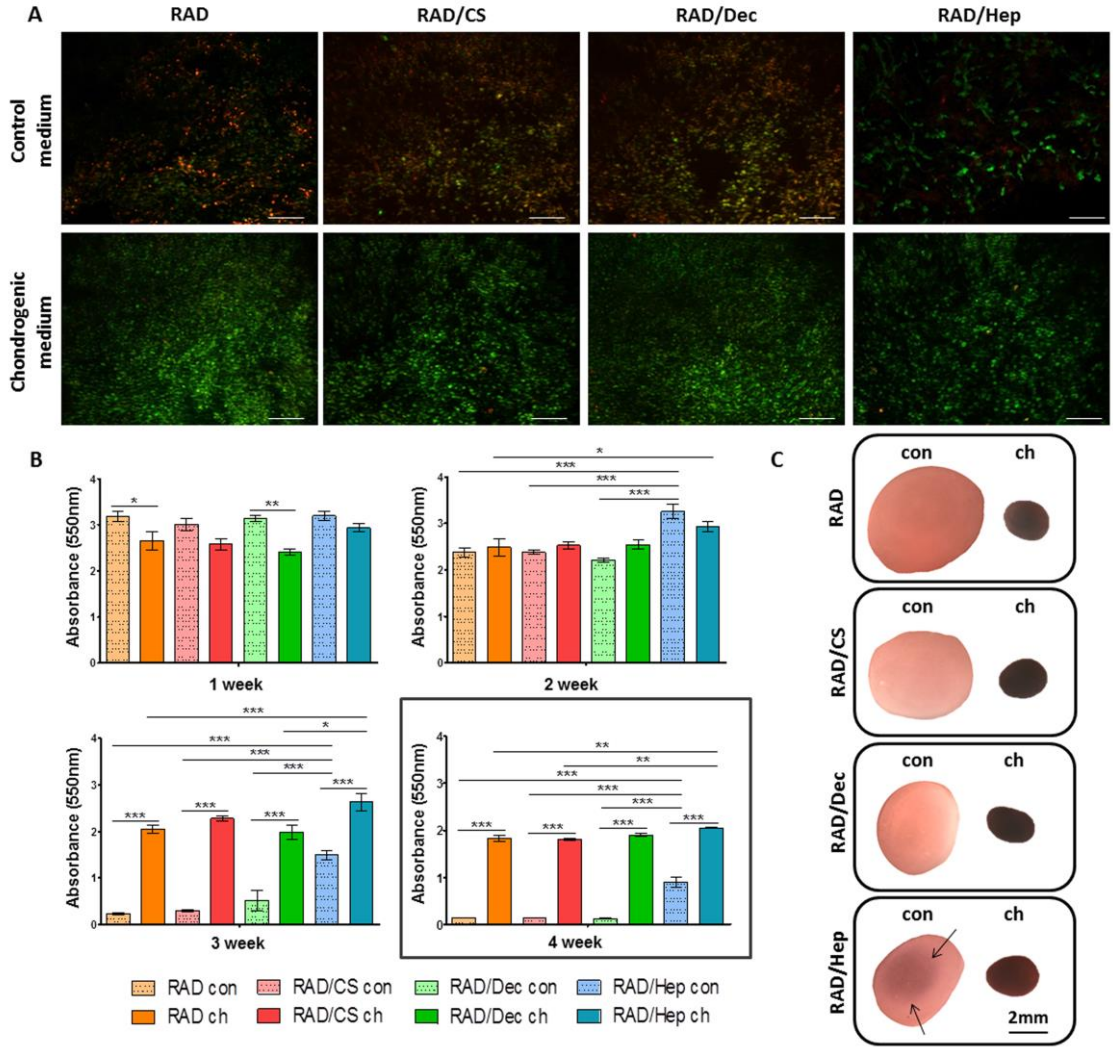

Figure 5.3.5. Viability of human ADSCs cultured with control and chondrogenic media in the self-assembling RAD16-I peptide scaffold and in RAD/CS, RAD/Decorin and RAD/Heparin composites. (A) Fluorescent images of live/dead staining at week 4 of culture. Live cells are stained in green and dead cells in red (Scale bars = 200 µm). (B) MTT absorbance values of 3D constructs in both control and chondrogenic culture media in the four scaffold types at different weeks of culture (Significant differences are indicated as * for $p<0.05$, ** for $p<0.01$, and *** for $p<0.001$, One-way ANOVA, N=2 n=3). (C) Construct appearance after MTT incubation at week 4 of culture with the different culture media (Con, control medium; ch, chondrogenic medium). Constructs under chondrogenic medium were completely purple after MTT incubation, and constructs under control medium were faintly stained. In the case of RAD/Heparin constructs, live cells were detected in the inner part of the construct (fine arrows).

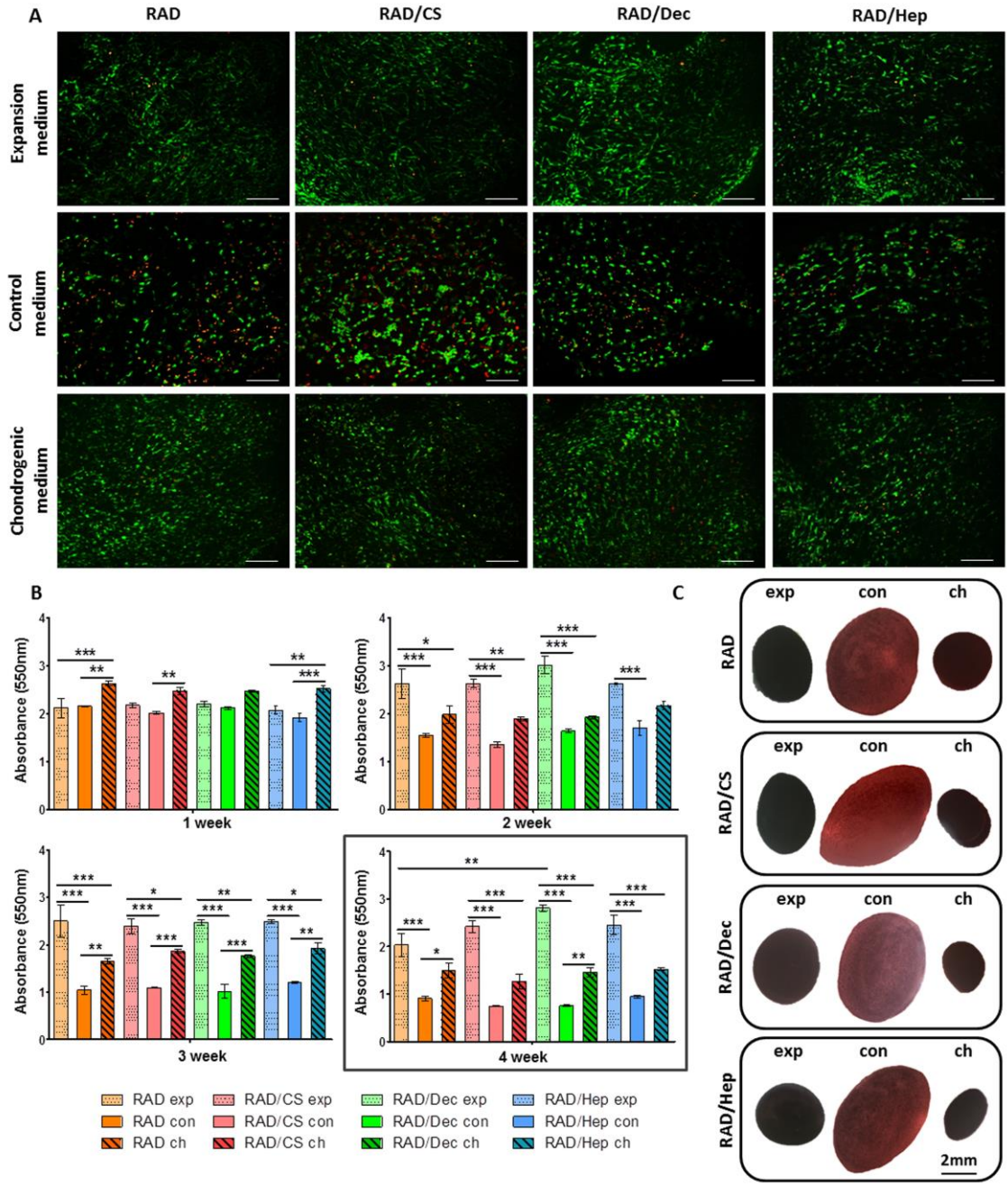

Figure 5.3.6. Viability of human ACs cultured with expansion, control and chondrogenic media in the self-assembling RAD16-I peptide scaffold and in RAD/CS, RAD/Decorin and RAD/Heparin composites. (A) Fluorescent images of live/dead staining at week 4 of culture. Live cells are stained in green and dead cells in red (Scale bars = 200 µm). (B) MTT absorbance values of 3D constructs in the three culture media in the four scaffold types at different weeks of culture (Significant differences are indicated as * for $p<0.05$, ** for $p<0.01$, and *** for $p<0.001$, One-way ANOVA, N=2 n=3). (C) Construct appearance after MTT incubation at week 4 of culture with the different culture media: expansion (exp), control (con) and chondrogenic (ch) media.

Interestingly, ADSCs that were cultured in chondrogenic medium remained alive until the end of the culture period, whereas the majority of ADSCs cultured in control medium died by the end of the culture period, with the exception of those cultured with RAD/Heparin composites (Figure 5.3.5 A). This finding is consistent with a previous study of this thesis (see Chapter 3)[39] in which the presence of heparin in the scaffold promoted ADSCs viability, but this phenomenon was not observed in the case of the CS or Decorin scaffolds. Furthermore, the viability of cells cultured with different constructs was similar during the first 2 weeks of culture, but drastic cell death occurred during the third week for samples incubated in control medium (Figure 5.3.5 B&C). Remarkably, constructs cultured with RAD/Heparin composites showed significantly higher viability over the experimental timeframe. Viable cells cultured in control medium with RAD/Heparin composites were detected mainly in the inner area of the constructs (Figure 5.3.5 C).

A different behavior was observed for ACs cells in the 3D constructs. Cells remained predominantly alive in all experimental conditions by week 4 of culture, regardless of the culture medium or scaffold type (Figure 5.3.6 A). Although some dead cells could be detected in constructs cultured in control medium, the majority of cells were alive. In the two other culture media (expansion and chondrogenic), cells appeared more compact compared to control medium. Moreover, viability profiles along the culture showed increasing differences between culture media over time (Figure 5.3.6 B). At week 1 of culture, viability was maintained at similar levels between construct types, and some differences could be detected between chondrogenic constructs compared to the other culture media conditions. Through 2 weeks of culture, constructs under expansion medium presented significantly higher viability than did those under control and chondrogenic media. A similar tendency was observed at 3 weeks of culture; however, in addition, significant differences were detected between control and chondrogenic constructs. Therefore, at the end of the culture period, the constructs in expansion medium showed the highest absorbance values, those cultured in control medium showed the lowest values, and those under chondrogenic medium showed intermediate values between those of control and expansion media. These differences are also indicated by the construct's appearance after MTT incubation at week 4 (Figure 5.3.6 C). In this case, the presence of heparin in the scaffold did not lead to a significant enhancement in viability of ACs[40].

SEM images were collected to more precisely assess cell morphology and the appearance of the surface constructs at week 4 of culture (Figure 5.3.7). ADSCs cultured in chondrogenic medium appeared elongated and well-anchored to the scaffold surface. However, SEM images of ADSCs constructs in control medium showed nanofibers and other possible ECM components synthesized by the cells during the culture period. In contrast, ACs cultured in expansion medium possessed a spherical shape with possible cell-matrix interactions and thorough ECM components. Similar to ADSCs, nanofibers and putative matrix components could be observed on the surface of constructs cultured in control medium. Additionally, grooves with visible fibers were detected on the entire surface of constructs cultured in

chondrogenic medium, suggesting the presence of secreted matrix components. Although cells were not visualized on the surface of the scaffold in all experimental conditions, we hypothesize that they were present in the inner area of the scaffold, as observed by DAPI-Phalloidin staining (Figure 5.3.4).

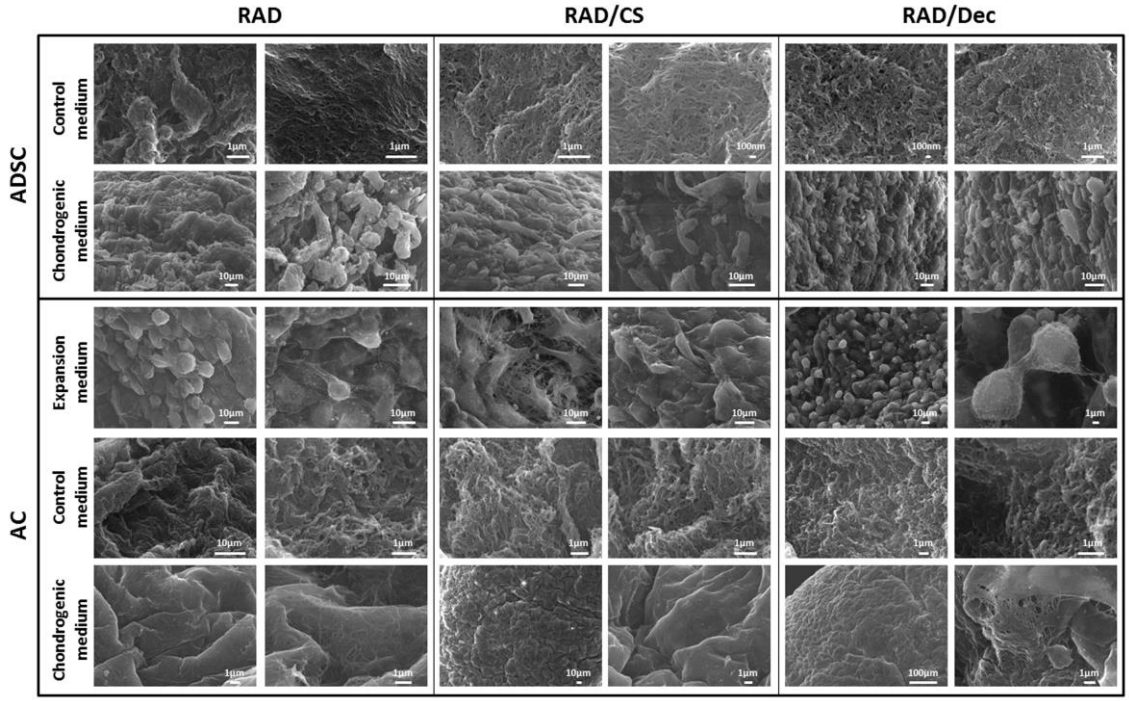

Figure 5.3.7. SEM images of ADSCs and ACs 3D constructs after 4 weeks of culture. Cells were seeded into RAD16-I, RAD/CS or RAD/Decorin scaffolds. ADSCs were cultured with control or chondrogenic media; ACs were cultured with expansion, control or chondrogenic media.

5.3.3 EXPRESSION OF CHONDROGENIC MARKERS

Because no significant differences in cell morphology and viability were detected between CS or Decorin scaffold types, further assessments of gene and protein expression were performed for both cell types. Chondrogenic markers were studied in ADSCs constructs cultured in chondrogenic medium and in ACs constructs cultured in chondrogenic and expansion media (cell viability was compromised under control medium). Gene expression analyses of different ECM components and transcription factors were analyzed quantitatively, and 3D cultures were compared with their 2D counterparts (Figure 4.3.3). In the case of ADSCs constructs cultured under chondrogenic medium, the expression of collagen type I (*COL1*) was significantly downregulated in RAD16-I scaffolds and maintained at 2D culture levels in RAD/CS and RAD/Decorin composites (Figure 4.3.3 A). Collagen type II (*COL 2*) appeared to be upregulated in 3D cultures, but no significant differences were detected (Figure 4.3.3 B). In contrast, the transcription factor *SOX9*, a regulator of *COL2* expression, was clearly upregulated for all composites (Figure 4.3.3 C). The characteristic proteoglycan of articular cartilage, aggrecan,

was significantly upregulated in the RAD16-I scaffold and the RAD/CS composite (Figure 4.3.3 D). In our analysis of hypertrophic markers, we found that the expression levels of collagen type X (*COL10*) and the transcription factor *RUNX2* in 3D cultures were maintained at levels comparable to 2D culture conditions (Figure 4.3.3 E&F).

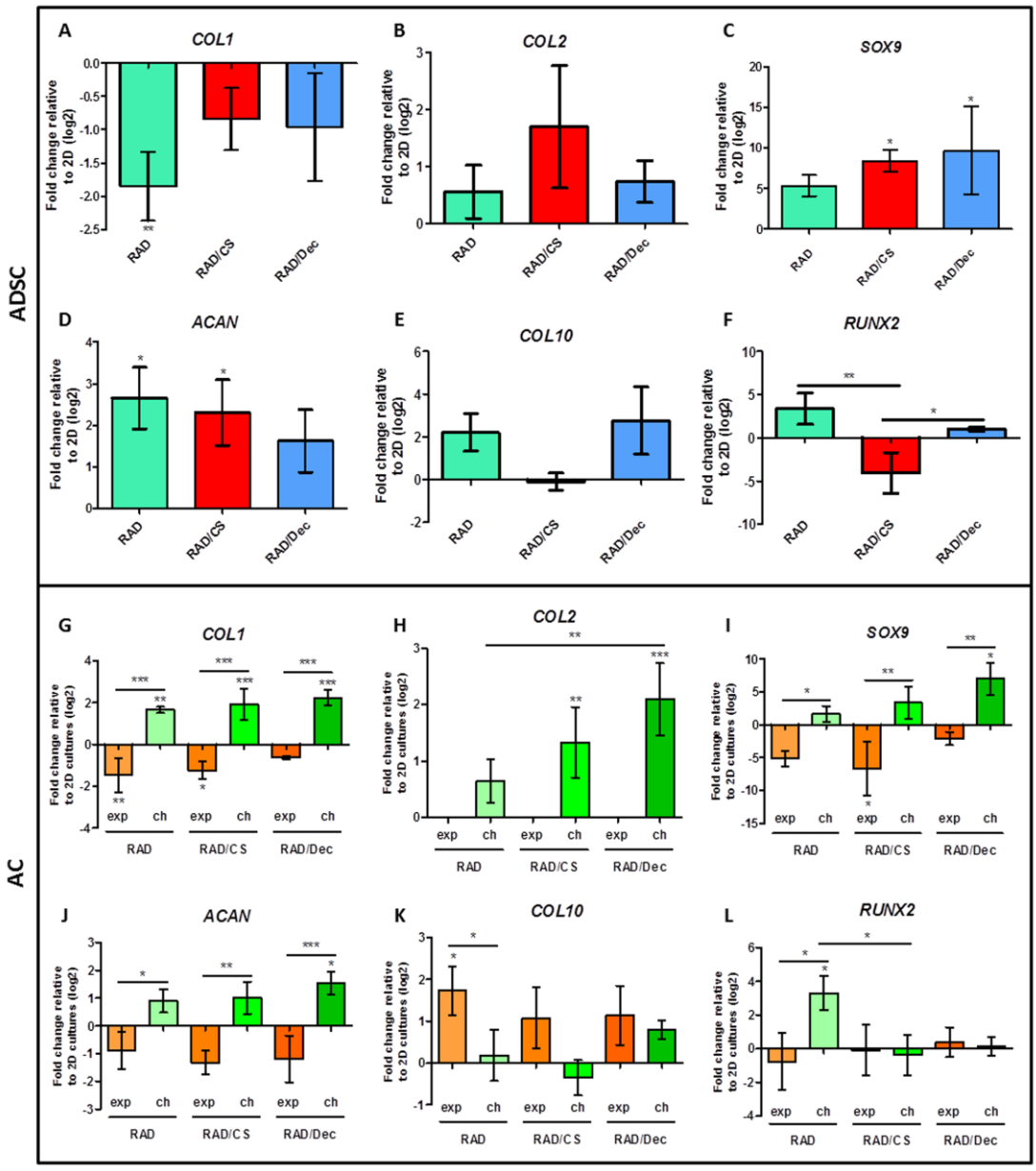

Figure 5.3.8. Gene expression levels of chondrogenic and hypertrophic markers of ADSCs and ACs cultured in 3D scaffolds for 4 weeks. ADSCs cultured with RAD16-I, RAD/CS and RAD/Decorin scaffolds in chondrogenic medium were analyzed by real time RT-PCR for collagen type I (*COL1*, A), collagen type II (*COL2*, B), *SOX9* (C), aggrecan (*ACAN*, D), collagen type X (*COL10*, E) and *RUNX2* (F). ACs cultured with RAD16-I, RAD/CS and RAD/Decorin scaffolds in expansion (exp) and chondrogenic (ch) medium were analyzed by real time RT-PCR for *COL1* (G), *COL2* (H), *SOX9* (I), *ACAN* (J), *COL10* (K) and *RUNX2* (L). Ct values relative to ribosomal protein L22 (*RPL22*) were obtained and reported as the fold increase (ΔΔCt) relative to 2D cultures (Significant differences are indicated as * for $p<0.05$, ** for $p<0.01$, and *** for $p<0.001$, One-way ANOVA, N=2 n=3).

On the other hand, ACs constructs were analyzed in expansion and chondrogenic media, and significant differences could be observed between them. *COL1* was upregulated in 3D constructs under chondrogenic medium and downregulated under expansion medium (Figure 4.3.3 G). Remarkably, the expression of *COL2* was only upregulated in RAD/CS and RAD/Decorin scaffolds under chondrogenic medium (Figure 4.3.3 H). As expected, this finding correlates with the expression of *SOX9*, which was significantly upregulated in chondrogenic constructs when compared to 3D constructs cultured in expansion medium (Figure 4.3.3 I). The expression of *ACAN* was higher in constructs cultured in chondrogenic medium than in constructs cultured in expansion medium (Figure 4.3.3 J). No significant differences were detected in the expression of hypertrophic markers between 3D constructs compared to monolayer growth conditions, except in the case of the RAD16-I scaffold, in which *COL10* and *RUNX2* expression was upregulated in expansion and chondrogenic media, respectively (Figure 4.3.3 K&L). Therefore, as expected, chondrogenic medium is more effective than expansion medium at promoting chondrogenesis in ACs constructs.

The protein expression profiles of different collagen constituents of the ECM (collagen type I, II and X) were analyzed by western blot in 2D and 3D cultures of ADSCs and ACs at week 4 of culture (Figure 4.3.4).

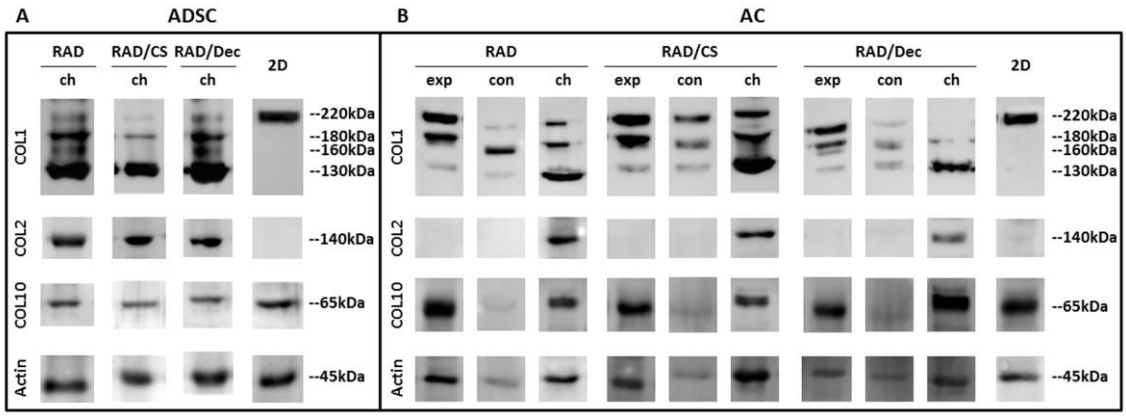

Figure 5.3.9. Characterization of protein expression in ADSCs and ACs cultured as monolayers and in 3D cultures after 4 weeks of culture. Western blot results of collagen type I (COL1), collagen type II (COL2) and collagen type X (COL10) from ADSCs (A) and ACs (B) cultured in RAD16-I alone, RAD/CS or RAD/Decorin. Actin was used as an internal control. Samples were prepared in triplicate. Exp, expansion medium; con, control medium; ch, chondrogenic medium.

In the case of ADSCs, only the constructs cultured in chondrogenic medium were analyzed because ADSCs cultured in control medium were dead by the end of the culture period (Figure 5.3.5). COL1 was detected in both cell types when grown as monolayers or in 3D constructs, but interestingly, different band patterns were observed. In 2D cultures, only a single band of high molecular weight was detected (~220 kDa), which was likely generated by a pro-collagen intermediate. In addition, more bands of lower molecular weight (ranging from 180 to 130 kDa) were observed in 3D cultures. Nevertheless, the intensities of the bands were different

between culture medium; for instance, the ~130 kDa band was predominant in 3D constructs cultured in chondrogenic medium. In the case of ACs constructs cultured in expansion medium, higher molecular weight bands (~220 kDa and ~180 kDa) presented as more intense than the ~130 kDa band. Importantly, COL2 was detected only in 3D constructs cultured with chondrogenic medium for both ADSCs and ACs, which is consistent with the gene expression results (Figure 4.3.3 B&H). COL10 protein expression was observed in all of the analyzed samples, including the 2D and 3D cultures of both cell types; however, only faint bands were detected in constructs cultured in control medium.

Furthermore, entire 3D constructs were stained with toluidine blue to qualitatively assess the production of GAGs by the cells (Figure 4.3.5 A&B). In both cell types, constructs cultured in chondrogenic medium showed intense blue staining, indicating a significant production and accumulation of GAGs. In the case of ACs, constructs cultured in expansion media showed less GAG staining than did those cultured in chondrogenic medium, whereas constructs cultured with control medium showed only relatively weak staining.

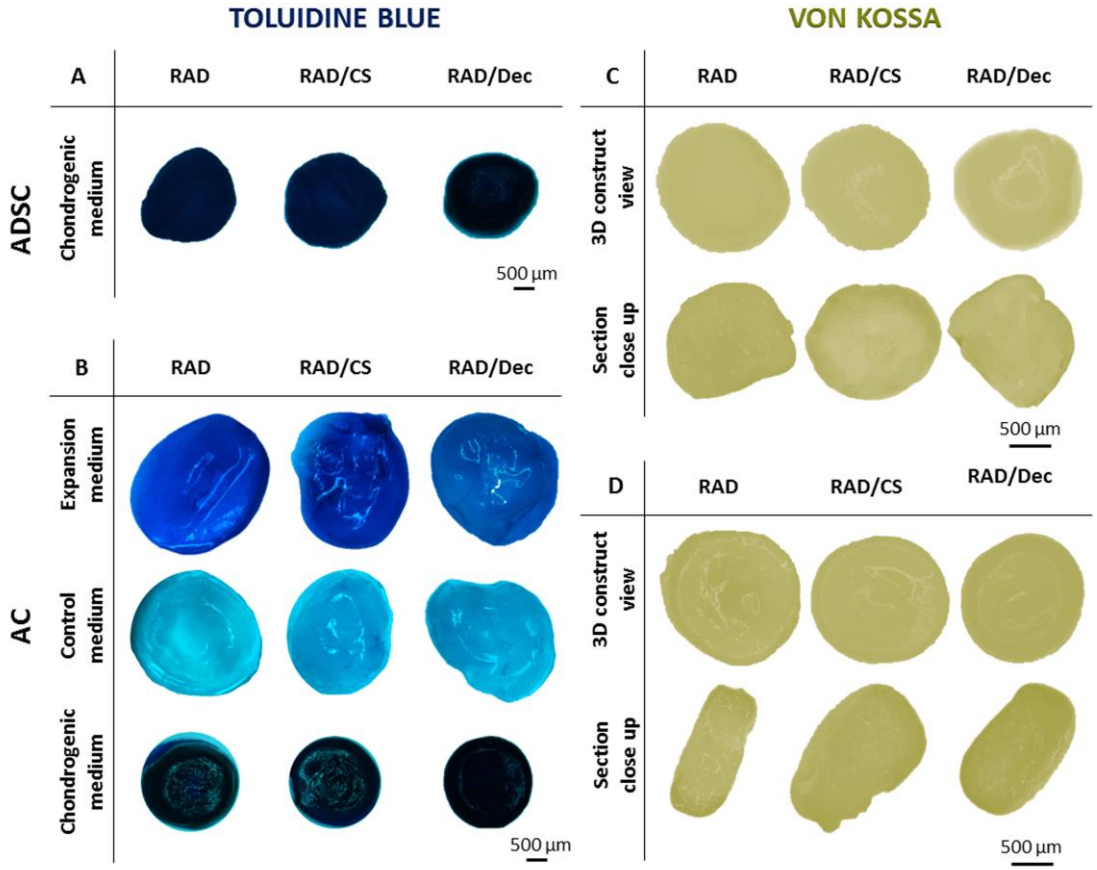

Figure 5.3.10. Characterization of chondrogenic phenotypes of ADSCs and ACs cultured with RAD16-I, RAD/CS, or RAD/Decorin composite scaffolds for 4 weeks. (A) Toluidine blue staining (sulfated GAGs) of 3D ADSCs constructs cultured in chondrogenic medium. (B) Toluidine blue staining of 3D ACs constructs cultured in expansion, control and chondrogenic media. (C) Von Kossa staining (indicating calcium mineralization) of 3D ADSCs constructs cultured in chondrogenic medium. (D) Von Kossa staining of 3D ACs constructs cultured in chondrogenic medium.

Moreover, Von Kossa was performed to assess the production of calcium mineral deposits characteristic of osteogenic differentiation in 3D ADSCs and ACs constructs cultured in chondrogenic medium (Figure 4.3.5 C&D). As expected, constructs showed no calcification, as indicated by a lack of dark spots detected in external and internal sections.

5.3.4 MECHANICAL CHARACTERIZATION OF TISSUE CONSTRUCTS

The mechanical properties of both 3D ADSCs and ACs constructs cultured in chondrogenic medium at the end of the culture period were assessed by DMA (Figure 4.3.6). Natural calf and chicken articular cartilage samples were also measured under the same assay conditions, allowing us to compare these tissues with the synthetic constructs after 4 weeks of culture. To provide a complete profile of the viscoelastic behavior of the samples, different parameters were studied: storage modulus (G'), loss modulus (G''), complex modulus (G*) and tan(delta).

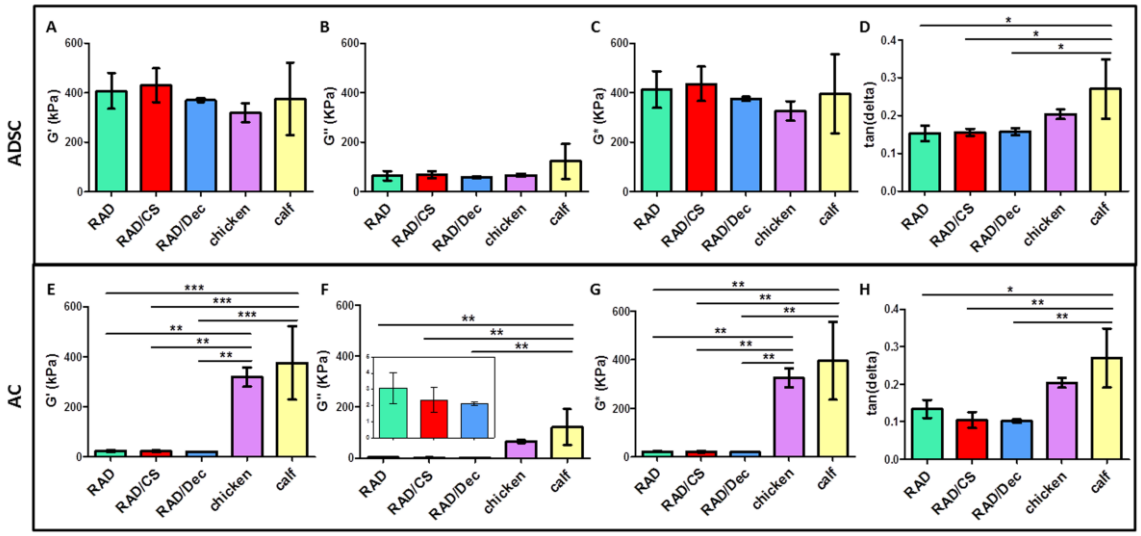

Figure 5.3.11. Mechanical characterization of 3D constructs cultured for 4 weeks in chondrogenic medium compared to chicken and calf articular cartilage. ADSCs cultured with RAD16-I, RAD/CS and RAD/Decorin scaffolds were analyzed for storage modulus (G', A), loss modulus (G'', B), complex modulus (G*, C) and tan(delta) (D). ACs cultured with RAD16-I, RAD/CS and RAD/Decorin scaffolds were analyzed for storage modulus (G', E), loss modulus (G'', F), complex modulus (G*, G) and tan(delta) (H). (Significant differences are indicated as * for $p<0.05$, ** for $p<0.01$, and *** for $p<0.001$, One-way ANOVA, N=2 n=3).

The elastic component (represented by G') showed a different profile between cell types. In the case of ADSCs constructs, the values of G' were comparable to chicken and calf articular cartilage (Figure 4.3.6 A). In contrast, ACs constructs displayed significantly lower G' values than did the native cartilage samples (Figure 4.3.6 E). Moreover, no significant differences were detected between scaffold types. The viscous component (G'') and the complex modulus (G*) for both cell types showed a more similar tendency than G' between 3D constructs and cartilage controls (Figure 4.3.6 B-C&F-G). However, all samples presented with G' values that

were much higher than the G'' values, indicating that the constructs were more elastic than viscous. Tan(delta) values, which gives an idea of the full mechanical response of the material, showed that all 3D constructs were comparable to chicken cartilage and differ from calf cartilage (Figure 4.3.6 D&H). Thus, we conclude that the mechanical behavior of our ADSCs constructs is more similar to chicken and calf native articular cartilage (Figure 4.3.6 A-D) than is the mechanical behavior of our ACs constructs (Figure 4.3.6 E-H).

5.4 DISCUSSION

In the work presented in this chapter, CS and Decorin molecules were combined with the self-assembling RAD16-I peptide to develop new scaffolds for CTE applications. RAD16-I hydrogel alone was previously used to support chondrogenesis with different cell types[34,35]. Moreover, RAD16-I was combined with heparin moieties to generate a bi-component scaffold with bioactive signals to promote capillary morphogenesis of endothelial cells and enhance the chondrogenesis of ADSCs and chondrocytes (Chapters 3 and 4)[39,40]. In this study, CS and Decorin molecules were selected based on their ability to mimic the natural ECM of articular cartilage and generate chondro-favorable biochemical cues in the 3D microenvironment. In fact, prior CTE strategies have evaluated the combination of CS with different hydrogel scaffolds, such as chitosan[55], poly(ethylene glycol) (PEG)[42] or collagen type I[56]. Although several studies have explored the influence of CS on chondrogenesis, less is known about the ability of Decorin to guide chondrogenic commitment. Therefore, in the present work, we studied the influence of both CS and Decorin on chondrogenesis in a nanometric 3D system. As in the case of RAD/Heparin composites[39,40], CS and Decorin-based self-assembling scaffolds were generated with a simple mixture of the two components (see Chapter 2, Material and Methods). The bi-component scaffolds exhibited structural stability at physiological pH, wherein β–sheet structural characteristics of the self-assembling peptide were maintained (Figure 5.3.1). Moreover, CS and Decorin molecules were homogenously distributed in the nanofiber network, as evidenced by toluidine blue staining. We suggest that the hydrophilic, negatively charged nature of CS molecules (and Decorin PGs containing a CS chain) allows the interaction of CS and Decorin molecules with the positive residues of the amphiphilic RAD16-I peptide via the electrostatic interactions that occur during the self-assembling process. In addition, AFM results confirmed the nanofiber formation in all cases, which correlates with previous studies with self-assembling peptides[36,37,57].

Our TGFβ1 release studies revealed that the RAD/CS composite released more TGFβ1 within the first 24 hours compared to the control scaffold. Although we could not calculate the quantity of TGFβ1 initially bound to the hydrogel, we believe that this difference was likely due to a differential GF binding affinity to the scaffold. Thus, we reason that more TGFβ1 could be initially bounded to the RAD/CS scaffold compared to the RAD16-I scaffold. This slow release process suggests that TGFβ1 may be bound to the carbohydrate moiety and presented to the cell's surface GF receptor, thereby promoting a signal cascade comparable to that which occurs physiologically. The development of this type of bi-component scaffold (structural-signaling integrated) could be applied towards deconstructing the complex signaling network to which cells are exposed during differentiation (ADSCs) or reengagement of lineage commitment (dedifferentiated ACs). In fact, the present work was aimed at promoting cartilage tissue development *in vitro* using the above-mentioned paradigm: two cell types (multipotent ADSCs and dedifferentiated ACs) in a 3D bi-component scaffold with chondrogenic induction media (i.e., containing TGFβ1).

Cells embedded in the nanometric RAD16-I scaffold experience a truly 3D environment, as demonstrated in previous studies[29,30,35,58], where they can elongate, interconnect with neighboring cells and matrix, proliferate and extend different cellular processes. Hence, this 3D culture system models the *in vivo* environment, and depending on the conditions provided (culture medium, cell type, scaffold functionalization, etc.), could evolve into different cellular microenvironments[59]. In particular, our work revealed differences between the behavior of ADSCs and ACs cultured in the same scaffolds. ADSCs became elongated and formed a cellular network only under chondrogenic conditions, whereas ACs appeared elongated in all culture conditions (Figure 5.3.4). However, ACs were more compacted and established connections in both expansion and chondrogenic medium. Indeed, it appears that the control medium did not promote cellular spreading and interconnectivity. For both cell types, the diameter of constructs cultured in control medium was reduced by only a small amount from the initial state. In contrast, constructs cultured in chondrogenic medium underwent a significant scaffold condensation during the culture timeframe, resulting in a compacted structure after 4 weeks. This morphological change was likely prompted by forces exerted by the cells and the matrix, a remodeling process stimulated by the chondro-inductive factors contained in the medium (e.g., TGFβ1).

Differences in cell viability were also observed between cell types. ADSCs were only alive after 4 weeks of culture under chondrogenic conditions or in the presence of the heparin scaffold (Figure 5.3.5 and Figure 5.3.6). In contrast, ACs were found to be viable in all experimental conditions, but their relative viability in control medium was reduced compared to expansion and chondrogenic media. Therefore, we suggest that the presence of GAGs in the scaffold enhanced cell viability and their general performance during the 4 weeks of culture (Figure 5.3.5 B and Figure 5.3.6 B).

The expression of important chondrogenic markers, including *COL2*, *SOX9* and *ACAN,* in 3D ADSCs constructs was increased compared to monolayer cultures (Figure 4.3.3). Similarly, in ACs constructs, the expression of these markers was stimulated under chondrogenic conditions and was decreased in expansion medium. Therefore, the combination of scaffold GAGs and chemical inducers present in chondrogenic medium led to the activation of signaling pathways that are important for the chondrogenic commitment. The mechanism underlying this activation, however, remains poorly understood. At the protein level, western blot results revealed a possible increased COL1 maturation process in 3D cultures of both cell types when compared to the COL1 detected in 2D cultures[43]. In particular, a pattern of four main bands was detected (220 kDa, 180 kDa, 160 kDa and 130 kDa). The final mature COL1 product corresponds to the lower molecular weight band (Figure 4.3.4). Moreover, mature COL1 was predominant in constructs cultured in chondrogenic medium, suggesting that COL1 was only properly processed in 3D constructs cultured in chondrogenic medium and, therefore, contributes to the formation of a more physiologically representative matrix. Importantly, the expression of COL2 was confirmed in 3D cultures under chondrogenic conditions and was not previously detected in 2D cultures. Additionally, toluidine blue staining revealed the

production of GAGs by both 3D ADSCs and 3D ACs cultured in chondrogenic medium (Figure 4.3.5). These results indicate the synergistic effect of the 3D culture system and the chondrogenic medium in stimulating the production of collagen and GAG components of the ECM, which could play an important role in matrix remodeling. Moreover, these constructs did not mineralize the scaffold, as indicated by von Kossa staining, suggesting that 3D constructs did not undergo cartilage hypertrophy during the culture period.

Finally, mechanical characterization showed that the viscoelastic behavior of ADSCs constructs more closely resembled native cartilage than did the viscoelastic behavior of ACs constructs (Figure 4.3.6). In both cell types, no significant differences were detected between CS- or Decorin-scaffold constructs. This finding suggests that the initial composition of the hydrogels did not influence the resultant mechanical properties of the constructs. As previously mentioned, constructs cultured in chondrogenic medium experienced a contraction process during the culture period that resulted in a compacted structure (Figure 5.3.4) with mechanical properties that changed from day 0 to the end of the culture period. In contrast, the diameter of constructs cultured in control medium was reduced by only a small amount from the initial state, and the mechanical properties at the end of the culture differed greatly from those of the chondrogenic constructs. Control constructs formed softer structures that could not be measured under the same conditions as chondrogenic constructs, owing to the disparity in mechanical properties among construct types. Similarly, the initial mechanical characteristics of the RAD16-I scaffold alone could not be measured under the same conditions as the chondrogenic constructs due to the soft nature of the peptide. However, previous studies report that the initial peptide concentration at which cells were embedded (0.15% (w/v) RAD16-I) corresponds to 100 Pa[36]. This soft microenvironment and the nature of the hydrogel allows cells to freely migrate, interconnect and extend different cellular processes in a dynamic and permissiveness milieu[27]. Therefore, as a consequence of the matrix remodeling process by the cells, constructs evolve into stiffer structures which better mimic the mechanical properties of native cartilage.

In summary, the present study reports promising results for different chondrogenic scenarios, revealing the functionality and versatility of novel bi-component scaffolds, depending on the conditions provided. Moreover, the availability and the ease of preparation of our novel biomaterials make them suitable for future *in vivo* applications.

5.5 CONCLUDING REMARKS

- Two novel biomaterials for CTE applications were developed: the CS- and Decorin-based self-assembling peptides. They presented good chemical and structural stability forming nanofiber composite self-assembling scaffolds.

- The bi-component materials could be used to bind and release significant quantities of TGFβ1, an essential GF present in the chondrogenic medium composition.

- ADSCs and dedifferentiated ACs cultured in the bi-component scaffolds (RAD/CS and RAD/Decorin) elongated, created a cellular network and remodeled the matrix over culture time changing the construct morphology.

- Regarding viability results, different cell behaviors were observed depending on cell type. ADSCs viability was compromised under control conditions after 4 weeks of culture. In contrast, ACs viability was similar between culture conditions at the end of the experiment.

- The expression of specific mature cartilage markers at protein and gene levels evidenced a favored microenvironment by the effect of the chondrogenic medium and the new bi-component scaffolds in both cell types: ADSCs and ACs.

- ADSCs constructs induced with chondrogenic medium were more similar mechanically to native articular cartilage than ACs constructs under the same conditions. In both cases, the 3D structures evolved during culture time into a compacted and stiffer structure, but only in the case of ADSCs viscoelastic values were in the same order of magnitude than chicken and calf articular cartilage.

5.6 REFERENCES

1. Keeney, M., Lai, J. H. & Yang, F. Recent progress in cartilage tissue engineering. *Curr. Opin. Biotechnol.* **22,** 734–740 (2011).
2. Hunziker, E. B. Articular cartilage repair: basic science and clinical progress. A review of the current status and prospects. *Osteoarthr. Cartil.* **10,** 432–463 (2002).
3. Jeng, L., Ng, F. & Spector, M. *Chapter 42 - Articular Cartilage*. *Principles of Regenerative Medicine* (Elsevier Inc., 2011). doi:10.1016/B978-0-12-381422-7.10042-2
4. Laporta, T. F., Richter, A., Sgaglione, N. A. & Grande, D. A. Clinical relevance of scaffolds for cartilage engineering. *Orthop Clin North Am* **43,** 245–254 (2012).
5. Chiang, H. & Jiang, C. Repair of articular cartilage defects: review and perspectives. *J. Formos. Med. Assoc.* **108,** 87–101 (2009).
6. Brittberg, M. *et al.* Treatment of deep cartilage defects in the knee with autologous chondrocyte transplantation. *N Engl J Med* **331,** 889–895 (1994).
7. Ochi, M., Uchio, Y., Tobita, M. & Kuriwaka, M. Current concepts in tissue engineering technique for repair of cartilage defect. *Artif. Organs* **25,** 172–9 (2001).
8. Johnstone, B. *et al.* Tissue engineering for articular cartilage repair--the state of the art. *Eur. Cell. Mater.* **25,** 248–67 (2013).
9. Castells-sala, C. *et al.* Biochips & Tissue chips Current Applications of Tissue Engineering in Biomedicine. (2013). doi:10.4172/2153-0777.S2-004
10. Lee, S.-H. & Shin, H. Matrices and scaffolds for delivery of bioactive molecules in bone and cartilage tissue engineering. *Adv. Drug Deliv. Rev.* **59,** 339–59 (2007).
11. Hubka, K. M., Dahlin, R. L., Meretoja, V. V, Kasper, K. & Mikos, A. G. Enhancing Chondrogenic Phenotype for Cartilage Tissue Engineering: Monoculture and Co-culture of Articular Chondrocytes and Mesenchymal Stem Cells. *Tissue Eng. Part B* **20,** 1–50 (2014).
12. Lefebvre, V., Peeters-Joris, C. & Vaes, G. Production of collagens, collagenase and collagenase inhibitor during the dedifferentiation of articular chondrocytes by serial subcultures. *Biochim Biophys Acta* **1051,** 266–275 (1990).
13. Darling, E. M. & Athanasiou, K. A. Rapid phenotypic changes in passaged articular chondrocyte subpopulations. *J. Orthop. Res.* **23,** 425–432 (2005).
14. Girotto, D. *et al.* Tissue-specific gene expression in chondrocytes grown on three-dimensional hyaluronic acid scaffolds. *Biomaterials* **24,** 3265–3275 (2003).
15. Miot, S. *et al.* Effects of scaffold composition and architecture on human nasal chondrocyte redifferentiation and cartilaginous matrix deposition. *Biomaterials* **26,** 2479–2489 (2005).
16. Kim, M., Kim, S. E., Kang, S. S., Kim, Y. H. & Tae, G. The use of de-differentiated chondrocytes delivered by a heparin-based hydrogel to regenerate cartilage in partial-thickness defects. *Biomaterials* **32,** 7883–96 (2011).
17. Grad, S., Ph, D., Gogolewski, S. & Sci, D. Effects of Simple and Complex Motion Patterns on Gene Expression of Chondrocytes Seeded in 3D Scaffolds. **12,** (2006).

18. Vater, C., Kasten, P. & Stiehler, M. Acta Biomaterialia Culture media for the differentiation of mesenchymal stromal cells. *Acta Biomater.* **7,** 463–477 (2011).

19. Pittenger, M. F. Multilineage Potential of Adult Human Mesenchymal Stem Cells. *Science* **284,** 143–147 (1999).

20. Eslaminejad, M. B. & Poor, E. M. Mesenchymal stem cells as a potent cell source for articular cartilage regeneration. **6,** 344–354 (2014).

21. Merceron, C., Vinatier, C. & Clouet, J. Adipose-derived mesenchymal stem cells and biomaterials for cartilage tissue engineering. *Joint, bone, …* **75,** 672–674 (2008).

22. Semino, C. E. Can we build artificial stem cell compartments? *J. Biomed. Biotechnol.* **3,** 164–169 (2003).

23. Vanderkraan, P. *et al.* Interaction of chondrocytes, extracellular matrix and growth factors: relevance for articular cartilage tissue engineering. *Osteoarthr. Cartil.* **10,** 631–637 (2002).

24. Alemany-Ribes, M. & Semino, C. E. Bioengineering 3D environments for cancer models. *Adv. Drug Deliv. Rev.* **79-80,** 40–49 (2014).

25. Griffith, L. G. & Swartz, M. a. Capturing complex 3D tissue physiology in vitro. *Nat. Rev. Mol. Cell Biol.* **7,** 211–24 (2006).

26. Kopesky, P. W. *et al.* Self-Assembling Peptide Hydrogels Modulate In Vitro. **16,** (2010).

27. Semino, C. E. Self-assembling Peptides: From Bio-inspired Materials to Bone Regeneration. *J. Dent. Res.* **87,** 606–616 (2008).

28. Alemany-Ribes, M., García-Díaz, M., Busom, M., Nonell, S. & Semino, C. E. Toward a 3D Cellular Model for Studying In Vitro the Outcome of Photodynamic Treatments: Accounting for the Effects of Tissue Complexity. *Tissue Eng. Part A* **19,** 1665–74 (2013).

29. Marí-Buyé, N., Luque, T., Navajas, D. & Semino, C. Development of a three-dimensional bone-like construct in a soft self-assembling peptide matrix. *Tissue Eng Part A* **19,** 870–881 (2013).

30. Quintana, L. *et al.* Early tissue patterning recreated by mouse embryonic fibroblasts in a three-dimensional environment. *Tissue Eng. Part A* **15,** 45–54 (2009).

31. Wu, J. *et al.* Nanometric self-assembling peptide layers maintain adult hepatocyte phenotype in sandwich cultures. *J. Nanobiotechnology* **8,** 29 (2010).

32. Semino, C. E., Kasahara, J. & Hayashi, Y. Entrapment of Migrating Hippocampal Neural Cells in Three-Dimensional Peptide Nanofiber Scaffold. *Tissue Eng Part* **10,** (2004).

33. Garreta, E., Genové, E., Borrós, S. & Semino, C. E. Osteogenic Differentiation of Mouse Embryonic Stem Cells and Mouse Embryonic Fibroblasts in a Three-Dimensional. *Tissue Eng Part A* **12,** 2215–2227 (2006).

34. Bussmann, B. M. *et al.* Chondrogenic potential of human dermal fibroblasts in contractile solft self-assembling peptide hydrogel. *J. Tissue Eng. Regen. Med.* (2013).

35. Fernández-Muiños, T., Suárez-Muñoz, M., Sanmartí-Espinal, M. & Semino, C. E. Matrix dimensions, stiffness, and structural properties modulate spontaneous chondrogenic commitment of mouse embryonic fibroblasts. *Tissue Eng. Part A* **20,** 1145–55 (2014).

36. Sieminski, a. L., Was, a. S., Kim, G., Gong, H. & Kamm, R. D. The Stiffness of Three-

dimensional Ionic Self-assembling Peptide Gels Affects the Extent of Capillary-like Network Formation. *Cell Biochem. Biophys.* **49,** 73–83 (2007).

37. Genove, E., Shen, C., Zhang, S. & Semino, C. E. The effect of functionalized self-assembling peptide scaffolds on human aortic endothelial cell function. *Biomaterials* **26,** 3341–3351 (2005).

38. Genové, E. *et al.* Functionalized self-assembling peptide hydrogel enhance maintenance of hepatocyte activity in vitro. *J. Cell. Mol. Med.* **13,** 3387–97 (2009).

39. Fernández-Muiños, T. *et al.* Bimolecular based heparin and self-assembling hydrogel for tissue engineering applications. *Acta Biomater.* **16,** 35–48 (2015).

40. Recha-Sancho, L. & Semino, C. E. Heparin based self-assembling peptide scaffold reestablish chondrogenic phenotype of expanded de-differentiated human chondrocytes. *J. Biomed. Mater. Res. Part A* **104,** 1694–1706 (2016).

41. Chen, W., Yao, C., Chu, I. & Wei, Y. Compare the effects of chondrogenesis by culture of human mesenchymal stem cells with various type of the chondroitin sulfate C. *JBIOSC* **111,** 226–231 (2011).

42. Varghese, S. *et al.* Chondroitin sulfate based niches for chondrogenic differentiation of mesenchymal stem cells. **27,** 12–21 (2008).

43. Bobick, B. E., Chen, F. H., Le, A. M. & Tuan, R. S. Regulation of the chondrogenic phenotype in culture. *Birth Defects Res. Part C - Embryo Today Rev.* **87,** 351–371 (2009).

44. Ladanyi, A. *et al.* Expression of a decorin-like moleculein human melanoma. *Pathol. Oncol. Res.* **7,** 260–266 (2001).

45. Knudson, C. B. & Knudson, W. Cartilage proteoglycans. *Semin. Cell Dev. Biol.* **12,** 69–78 (2001).

46. Seidler, D. G. & Dreier, R. Decorin and its galactosaminoglycan chain: Extracellular regulator of cellular function? *IUBMB Life* **60,** 729–733 (2008).

47. Trowbridge, J. M. & Gallo, R. L. Dermatan sulfate: new functions from an old glycosaminoglycan. *Glycobiology* **12,** 117R–25R (2002).

48. Tayalia, P. & Mooney, D. J. Controlled growth factor delivery for tissue engineering. *Adv. Mater.* **21,** 3269–85 (2009).

49. Tiedemann, K. *et al.* Regulation of the chondroitin / dermatan fine structure by transforming growth factor- ␤1 through effects on polymer-modifying enzymes. **15,** 1277–1285 (2005).

50. Hildebrand, a *et al.* Interaction of the small interstitial proteoglycans biglycan, decorin and fibromodulin with transforming growth factor beta. *Biochem. J.* **302 (Pt 2,** 527–534 (1994).

51. Mouw, J. K., Ou, G. & Weaver, V. M. Extracellular matrix assembly: a multiscale deconstruction. *Nat. Rev. Mol. Cell Biol.* **15,** 771–785 (2014).

52. Terry, D. E., Chopra, R. K., Ovenden, J. & Anastassiades, T. P. Differential use of Alcian blue and toluidine blue dyes for the quantification and isolation of anionic glycoconjugates from cell cultures: application to proteoglycans and a high-molecular-weight glycoprotein synthesized by articular chondrocytes. *Anal. Biochem.* **285,** 211–9 (2000).

53. Radmacher, M. Measuring the elastic properties of biological samples with the AFM. *IEEE Engineering in Medicine and Biology Magazine* **16,** 47–57 (1997).

54. Cals, F. L. J., Hellingman, C. A., Koevoet, W., Baatenburg de Jong, R. J. & van Osch, G. J. V. M. Effects of transforming growth factor-β subtypes on in vitro cartilage production and mineralization of human bone marrow stromal-derived mesenchymal stem cells. *J. Tissue Eng. Regen. Med.* **6,** 68–76 (2012).

55. Sechriest, V. F. *et al.* GAG-augmented polysaccharide hydrogel: A novel biocompatible and biodegradable material to support chondrogenesis. *J. Biomed. Mater. Res.* **49,** 534–541 (2000).

56. Mullen, L. M. *et al.* Bioactive IGF-1 release from collagen–GAG scaffold to enhance cartilage repair in vitro. *J. Mater. Sci. Mater. Med.* **26,** 2 (2015).

57. Zhang, S. Designer Self-Assembling Peptide Nanofiber Scaffolds for Study of 3-D Cell Biology and Beyond. *Adv. Cancer Res.* **99,** 335–362 (2008).

58. Castells-Sala, C. *et al.* Influence of electrical stimulation on 3D-cultures of adipose tissue derived progenitor cells (ATDPCs) behavior. *Conf. Proc. ... Annu. Int. Conf. IEEE Eng. Med. Biol. Soc. IEEE Eng. Med. Biol. Soc. Annu. Conf.* **2012,** 5658–61 (2012).

59. Semino, C. E. Can We Build Artificial Stem Cell Compartments? *J. Biomed. Biotechnol.* **2003,** 164–169 (2003).

CHAPTER 6

DEVELOPMENT OF A POLY(Ɛ-CAPROLACTONE)/SELF-ASSEMBLING PEPTIDE COMPOSITE SCAFFOLD TO PROMOTE THE REDIFFERENTIATION PROCESS OF DEDIFFERENTIATED ARTICULAR CHONDROCYTES

Recha-Sancho L, Moutos FT, Abellà J, Guilak F and Semino CE. Dedifferentiated human articular chondrocytes redifferentiate to a cartilage-like tissue phenotype in a poly(ε-caprolactone)/self-assembling peptide composite scaffold. *Materials*. **9** (6), 472 (2016).

6.1 INTRODUCTION

Articular cartilage is an avascular tissue with a highly specialized extracellular matrix (ECM) architecture and composition that allows it to withstand the mechanical requirements of the diarthrodial joint[1]. The principal function of cartilage is to withstand mechanical loads while allowing low friction movements of joints over millions of cycles of loading[2]. Chondrocytes are the only resident cells in articular cartilage and, therefore, are responsible for synthesizing and maintaining the complex ECM[3]. However, cartilage shows little or no capacity for self-repair, and cartilage defects generated by trauma or injury can result in long-term pain and loss of joint function. Moreover, due to lack of a healing response, such focal injuries can often lead to progressive degenerative changes that compromise joint function[4]. While several surgical methods are currently used to enhance cartilage repair[5], these procedures have not shown long-term clinical success. Therefore, new strategies for cartilage repair are required and tissue engineering has emerged as a potential source to generate cartilage-like structures through the use of cells and biomaterials[6,7].

One approach of cartilage tissue engineering (CTE) is based on mimicking the natural tissue environment in order to stimulate the formation of new cartilage[8,9]. In this case, biomimetic materials which are similar structurally and mechanically to ECM and recreate *in vivo* conditions are of high interest[10,11]. A wide variety of scaffolds have been explored so far in CTE and they can be classified into natural or synthetic biomaterials[12]. Natural materials include collagen, fibrin, alginate or hyaluronan among others, and they possess a variety of properties, such as biocompatibility and biodegradability. However, they present variability from batch to batch and possible modifications to improve them are limited. In contrast, the main advantages of synthetic biomaterials are their reproducibility and their design with specific mechanical, structural, and biological properties. Some examples include polyethylene glycol (PEG), polyurethanes, polycaprolactone, and self-assembling peptides[6]. Additionally, composites scaffolds consisting of two or more biomaterials with different properties have been studied to provide enhanced properties that cannot be achieved with a single material[13]. In the present work, a new composite was generated by combining two different synthetic biomaterials: the three-dimensional (3D) woven poly (ε-caprolactone) (PCL) scaffold and the RAD16-I self-assembling peptide. 3D weaving can be used to create porous structures arranged in multiple layers of continuous fibers in three orthogonal directions, as previously described (Figure 6.1.1)[14]. Such scaffolds were engineered with predetermined properties aiming to reproduce the anisotropy, viscoelasticity, and tension–compression non-linearity of native articular cartilage. Moreover, PCL is a FDA approved biomaterial, biocompatible and biodegradable with extended experience medical use[15,16]. RAD16-I self-assembling peptide is commercially available under the name of PuraMatrix™[17]. It is a water soluble peptide that self-assembles into a network of nanofibers when the ionic strength increases or when the pH is adjusted to neutrality forming a soft hydrogel[18]. The cells can be embedded in a truly 3D matrix during the self-assembling process driven by weak non-covalent interactions including

hydrogen bonds, ionic bonds, electrostatic interactions, van der Waals interactions, etc.)[19]. Importantly, these weak interactions enable cells to freely migrate, interact and extend different cellular processes. Therefore, this nanofiber network promotes cell–cell and cell–matrix interactions allowing cells to grow, proliferate and differentiate under specific experimental conditions[18,20]. Previous studies showed the ability of RAD16-I to support cell maintenance in a variety of cell types, including endothelial cells, hepatocytes, neural cells, fibroblasts, osteoblasts, embryonic, and somatic stem cells[21–27]. It is a biocompatible and biodegradable peptide that can be defined as "non-instructive" from the point of view of cell receptor recognition/activation, since it does not contain specific motifs in their native sequence[28]. Moreover, it can be functionalized with specific signaling motifs (or molecules) to promote different cellular responses[29–31].

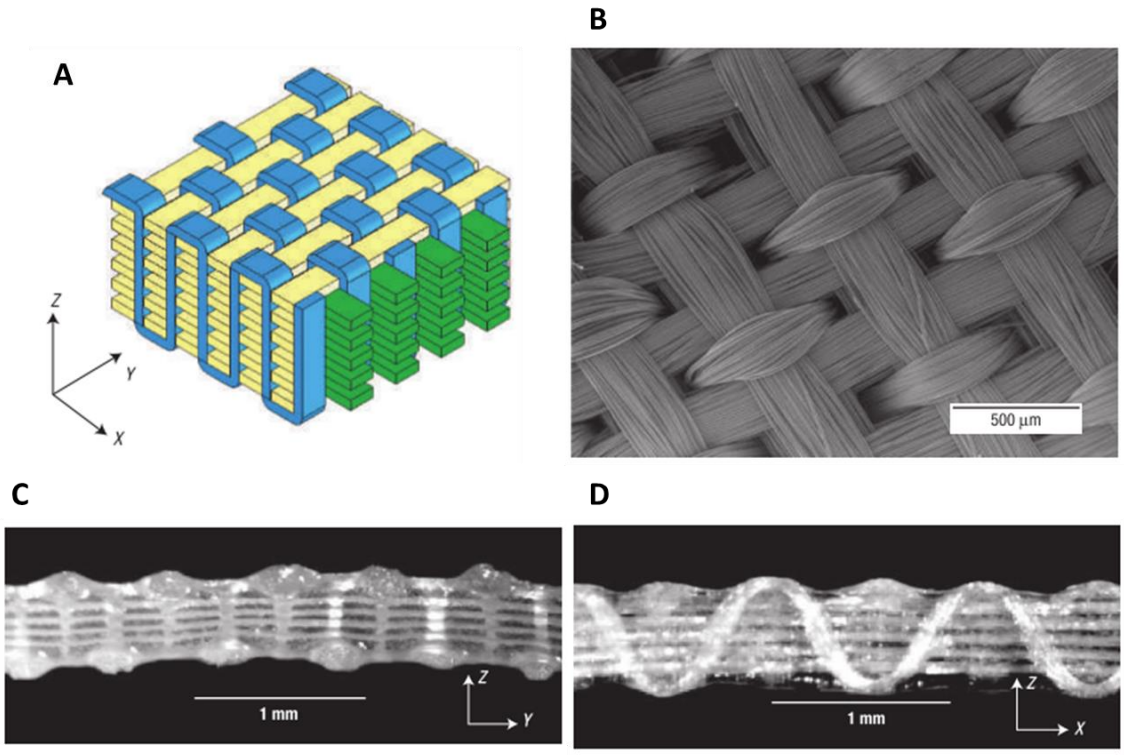

Figure 6.1.1. Fiber architecture of a 3D orthogonally woven structure. 3D structures were woven by interlocking multiple layers of two perpendicularly oriented sets of in-plane fibres (x- or warp direction, and y- or weft direction) with a third set of fibres in the z-direction. (A) Schematic diagram. (B) Surface view of the X–Y plane (scanning electron microscope). (C) Cross-sectional view of the Y–Z plane. (D) Cross-sectional view of the X–Z plane. Image adapted from Moutos *et al.*[14]

The strategy in this chapter was to combine these two dissimilar materials in order to facilitate the attachment, proliferation and differentiation of embedded cells, while simultaneously providing a biomimetic mechanical environment of the native tissue[32]. The use of both biomaterials in CTE applications was already reported. In previous studies, PCL scaffolds have been combined with other hydrogels, such as agarose, fibrin, Matrigel®, or interpenetrating network (IPN) gels to mimic the functional properties of cartilage while providing a cellular

environment that was conducive to chondrogenesis for different cellular types[14,33–35]. As each type of hydrogel may possess significantly different biological and biomechanical properties (e.g., matrigel vs. IPN), the 3D composite of a woven fiber scaffold infiltrated with a gel matrix can be tailored to provide different properties at the macroscopic as well as the cellular scale. RAD16-I, for example, has been shown to induce spontaneous chondrogenic commitment of mouse embryonic fibroblasts that were cultured in the peptide scaffold[36,37]. Moreover, RAD16-I can also promote cartilage differentiation of human dermal fibroblasts under chemical induction[38]. Although the stiffness of the scaffold can be modulated by changing the peptide concentration, this hydrogel provides a soft and permissive environment where cells can act remodeling the surrounding matrix. Therefore, cells are embedded in a dynamic microenvironment and the mechanical properties of the entire construct can evolve during the culture time, ending in a stiffer structure[27].

Besides the scaffold, determining the optimal cell source for CTE is still a challenge. Adult human chondrocytes represent a potential cell source, because they are found in native cartilage and have the original chondrogenic phenotype. Since they are isolated from patients, the main drawback is to obtain a sufficient cell number for their use in clinics. For this reason, an *ex vivo* expansion often is required to overcome the limited supply[39]. However, chondrocytes dedifferentiate in monolayer cultures losing their ability to express articular cartilage ECM specific markers[40,41]. Therefore, the recovery of the chondrogenic phenotype is an essential step prior to further application. 3D matrices providing environmental support and mimicking the native tissue architecture have emerged as a potential toolbox in CTE platforms[42]. Several studies showed the use of 3D cultures to enable the *in vitro* maintenance of chondrocyte phenotype[43–46]. The goal of the present study is to stimulate the redifferentiation of human expanded chondrocytes into functional cartilage-like tissue using a new PCL/RAD composite. It has been previously demonstrated the dedifferentiation of articular chondrocytes (ACs) during monolayer expansion[47]. Therefore, the idea was to promote the recovery of the chondrogenic phenotype under specific culture conditions during 4 weeks of culture (Figure 6.1.2). We hypothesize that the biochemical and biomechanical signals provided by the composite scaffold could guide chondrocytes commitment to reestablish and maintain its mature cartilage phenotype.

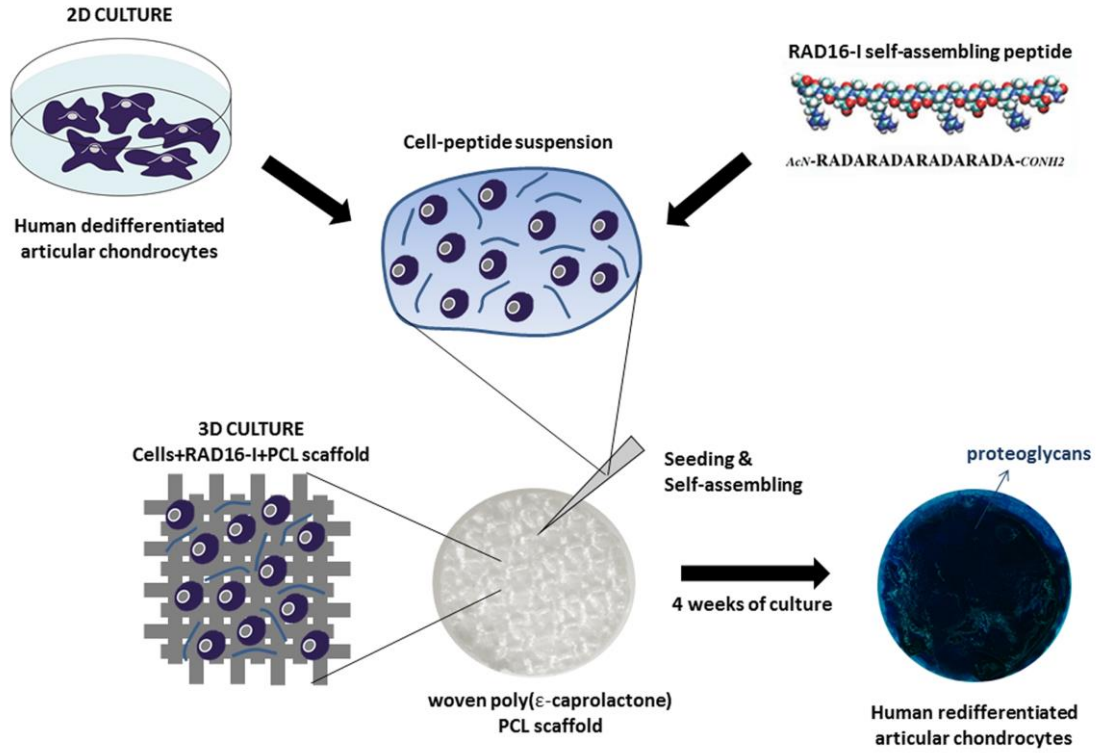

Figure 6.1.2. Schematic process to obtain 3D cultures of chondrocytes in PCL/RAD composite scaffolds. Human dedifferentiated articular chondrocytes were cultured into PCL/RAD composite scaffolds during 4 weeks under chondrogenic conditions to promote the redifferentiation process of articular chondrocytes.

6.2 MOTIVATIONS AND SPECIFIC AIMS

Previous studies reported the successful use of either woven PCL scaffolds or RAD16-I self-assembling peptide for CTE applications. These biomaterials possess different chemical, structural and biological properties, which motivated their combination in a novel composite scaffold. In order to evaluate the potential of this new composite scaffold the goal of the present chapter is to promote the redifferentiation process of expanded human ACs (also used in Chapters 4 and 5). The specific objectives of this chapter are the following:

(1) To develop a novel composite scaffold consisting on woven PCL scaffold and RAD16-I self-assembling peptide.

(2) To assess the viability of dedifferentiated ACs in the composite scaffold at different time points.

(3) To characterize the recovery of the chondrogenic phenotype of dedifferentiated ACs thorough the analysis of mature cartilage markers at gene and protein level.

(4) To study the mechanical properties of the composite scaffold and the 3D constructs at the end of the culture comparing with native articular cartilage.

6.3 RESULTS

6.3.1 PCL/RAD COMPOSITE DEVELOPMENT

As a previous step a simple wettability assay was performed on PCL scaffold measuring the contact angle formed with water (Figure 4.3.1 A) and RAD16-I at 0.5% (w/v) (Figure 4.3.1 B). In both cases, the liquid drop was totally absorbed by the PCL scaffold (contact angle <<90º) indicating high wettability. Then, the fiber architecture of the woven PCL scaffold and PCL/RAD composite scaffold were assessed by scanning electron microscope (SEM) (Figure 4.3.1 C-F). In the case of the composite, areas of RAD16-I peptide deposition could be observed within the highly organized woven morphology of the fiber scaffold (Figure 4.3.1 E&F). Moreover, the grooves observed in the woven PCL scaffold surface can be easily filled with water and RAD16-I peptide solution, as evidenced by the 3D view on stereoscopic microscope (Figure 4.3.1 G-I). Altogether, these results showed the infiltration of the peptide solution into the 3D structure of PCL scaffold.

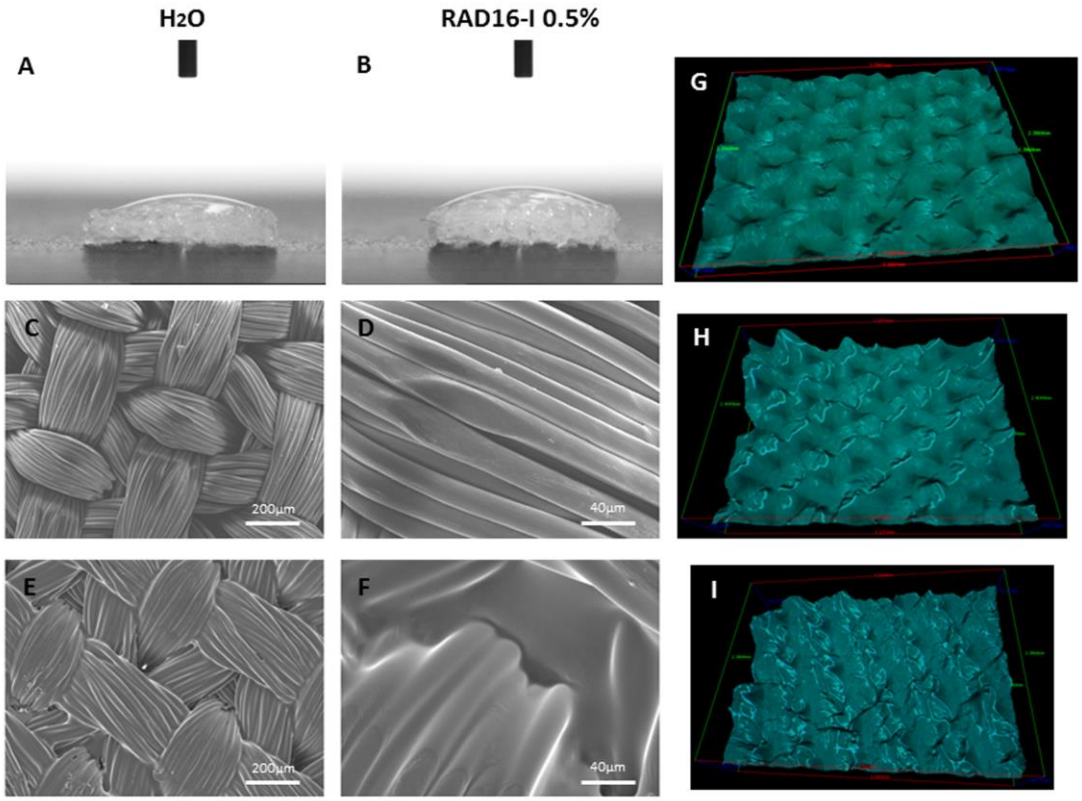

Figure 6.3.1. Wettability and fiber architecture of woven poly (ε-caprolactone) (PCL) scaffold and PCL/RAD16-I self-assembling peptide composite scaffold. (A) Water contact angle (B) RAD16-I 0.5% (w/v) solution contact angle. (C) Surface view of PCL structure by scanning electron microscope (SEM). (D) Close up of panel C of microfiber detail. (E) Surface view of composite PCL/RAD by SEM. RAD16-I 0.5% was lyophilized within the PCL scaffold. (F) Close up of panel E. (G) Three-dimensional (3D) view of PCL scaffold surface. (H) 3D view of PCL scaffold surface wet with water. (I) 3D view of PCL/RAD composite scaffold surface.

6.3.2 CHONDROCYTE VIABILITY DURING CULTURE IN 3D SCAFFOLDS

Next, we evaluated the seeding capacity of ACs into three different scaffolds: PCL, RAD16-I and its combination (composite PCL/RAD). The composite scaffold was studied in parallel with the simple scaffolds (PCL and RAD16-I) to compare the different platforms and to ascertain if the mixture implies an improvement from the point of view of cellular behavior and chondrogenic differentiation.

ACs were expanded and dedifferentiated in monolayer, as published in a previous work[47]. Then, cells were seeded into each scaffold system to obtain the corresponding constructs. First, MTT was performed to assess cellular viability in each construct at two different time points: 4 days and 4 weeks (Figure 4.3.2). At 4 days of culture in expansion media, cells remained alive inside the constructs. Moreover, ACs were equally distributed as observed by the homogeneity of the purple color among the constructs (Figure 4.3.2 A). However, the experiment at 4 weeks was more complex since two more culture media (control and chondrogenic) were added to perform further chondrogenic evaluation assays. Then, each construct type was cultured in three different culture media: expansion, control and chondrogenic (see Chapter 2, Materials and Methods). Viability results after 4 weeks of culture indicated a good cell survival for all construct and media tested (Figure 4.3.2 B). Nevertheless, higher values of absorbance were observed for PCL and PCL/RAD constructs cultured with chondrogenic medium compared to expansion and control media (Figure 4.3.2 C). In contrast, for RAD construct no differences were observed between expansion and chondrogenic media but control medium presented the lowest values (Figure 4.3.2 C). As observed by color distribution at 4 weeks of culture, the distribution of cells in the construct was homogeneous for all cases (Figure 4.3.2 B). This event was also before observed at 4 days of culture (Figure 4.3.2 A). Moreover, the intensity of the purple color was higher in the case of expansion and chondrogenic media compared to control medium, which correlates with the absorbance values.

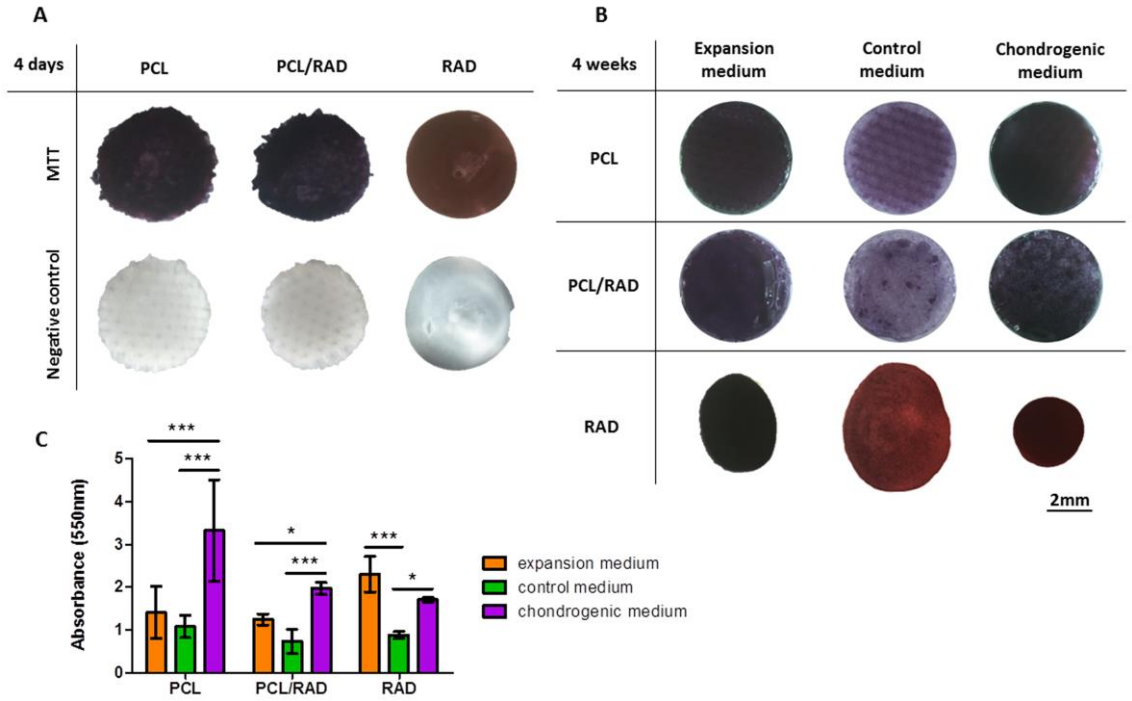

Figure 6.3.2. Viability of Articular Chondrocytes (ACs) cultured in 3D scaffolds at different time points. PCL, PCL/RAD composite and RAD scaffolds were seeded with ACs and incubated with MTT to assess cell viability and distribution. (A) Construct appearance after MTT incubation at 4 days of culture with expansion medium. The same constructs were incubated in the absence of MTT reagent as a negative control. (B) Construct appearance after MTT incubation at 4 weeks of culture with the different culture media: expansion, control and chondrogenic media. (C) MTT values at 4 weeks of culture were expressed of formazan (product) absorbance at 550 nm. (Statistical differences are indicated as: * for $p<0.05$, ** for $p<0.01$, and *** for $p<0.001$, Two-way ANOVA, N=2 n=3).

6.3.3 CHONDROGENIC DIFFERENTIATION OF ACs IN 3D SCAFFOLDS

Further analysis was focused on assessing the potential of the three construct types to support chondrogenic differentiation with ACs. It is important to note the basic composition differences among the media used, since we aimed to chemically induce the chondrogenic differentiation process through inducers (TGF-β1, L-ascorbic acid 2-phosphate and dexamethasone) contained in the chondrogenic medium[48]. Additionally, the expansion medium containing FBS and different growth factors used to culture ACs in monolayer was also employed in the culture of the 3D constructs.

Gene expression pattern studies were performed from the point of view of protein and gene expression. Regarding gene expression profiles, collagens type I, II and X, aggrecan, *SOX9* and *RUNX2* and *RPL22* as housekeeping gene were analyzed by real time RT-PCR at 4 weeks of culture (Figure 4.3.3). In the case of constructs cultured with control medium, RNA levels were not enough to perform the analysis. *COL1* expression, as a marker of dedifferentiation, was reduced in PCL constructs cultured with expansion medium, maintained equal to 2D cultures levels (used to normalize expressions levels, baseline) in PCL/RAD and RAD scaffolds cultured

with expansion medium and increased in all scaffolds cultured with chondrogenic medium (Figure 4.3.3 A). Interestingly, the expression of *COL2*, one of the main components of articular cartilage, was only slightly increased in PCL/RAD and RAD scaffolds cultured with chondrogenic medium; however, only for RAD scaffold significance difference was detected (Figure 4.3.3 B). The expression of the transcription factor *SOX9*, as a marker of chondrogenesis, was down-regulated in PCL cultured with both media and in PCL/RAD constructs cultured with expansion medium. However, it was maintained similar to 2D baseline levels in PCL/RAD constructs cultured with chondrogenic medium and in RAD constructs (Figure 4.3.3 C). In the case of *ACAN*, its expression was reduced in all constructs cultured with expansion medium and increased in all constructs cultured with chondrogenic medium, but no significant differences were detected relative to baseline. Nevertheless, differences could be observed between expansion and chondrogenic medium in PCL/RAD scaffolds and in RAD constructs (Figure 4.3.3 D). Regarding hypertrophic markers, *COL10* and *RUNX2* expression was up-regulated in some of the constructs with respect to baseline, but, importantly, no significant increase was detected in RAD constructs and in PCL/RAD constructs cultured with chondrogenic media in the case of *COL10* expression (Figure 4.3.3 E&F).

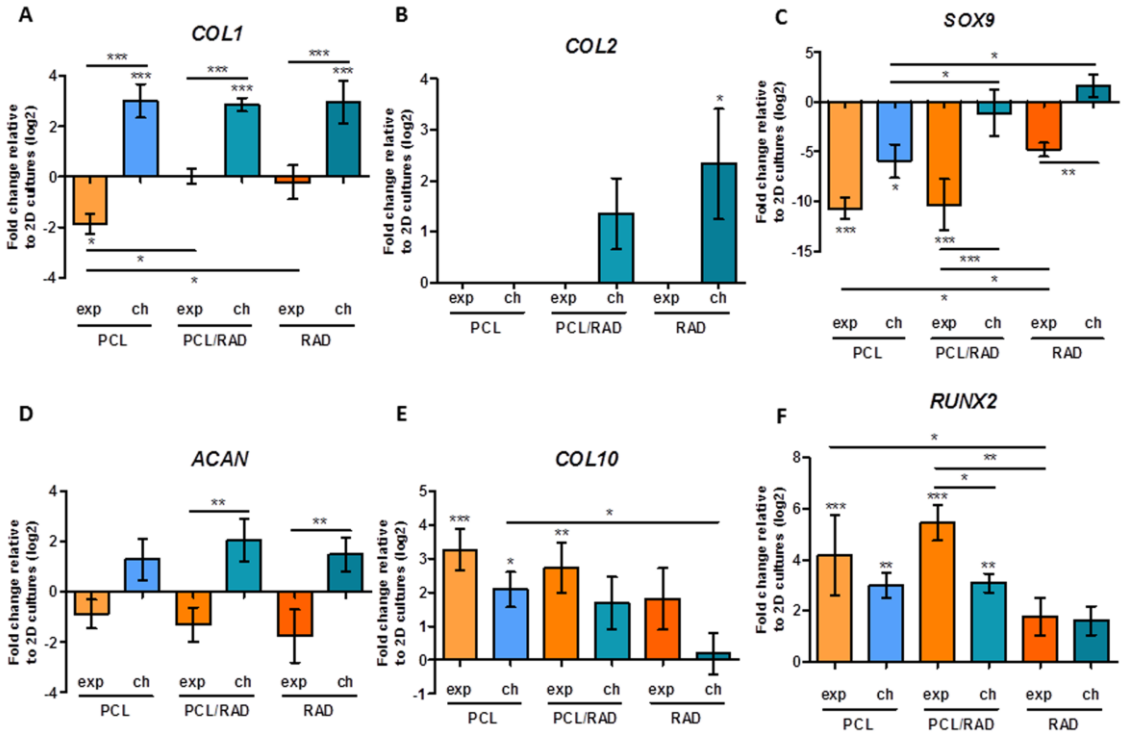

Figure 6.3.3. Gene expression levels of chondrogenic and hypertrophic markers of Articular Chondrocytes (ACs) cultured in 3D scaffolds during 4 weeks. ACs in PCL, PCL/RAD and RAD scaffolds were analyzed for gene expression in expansion (exp) and chondrogenic (ch) media. Collagen type I (*COL1*, A), collagen type II (*COL2*, B), *SOX9* (C), aggrecan (*ACAN*, D), collagen type X (*COL10*, E) and *RUNX2* (F) were determined through real time RT-PCR. Ct values relative to ribosomal protein L22 (*RPL22*) were obtained and reported as fold increase (ΔΔCt) relative to 2D cultures in expansion medium (baseline) (Statistical differences are indicated as:* for $p<0.05$, ** for $p<0.01$, and *** for $p<0.001$, One-way ANOVA, N=2 n=3).

Moreover, collagens type I, II and X were analyzed by western blot in monolayer (2D) and in the different 3D systems (Figure 6.3.4). COL1 was observed in the 2D cultures and in all 3D constructs; except for the case of PCL constructs cultured with expansion medium. This results correlates with the down-regulation detected by real time RT-PCR (see Figure 4.3.3 A). Interestingly, the bands pattern was different between samples producing COL1. A band of high molecular weight (~220kDa), probably a pro-collagen intermediate, was detected in 2D and in 3D cultures positive samples. In addition, more bands of lower molecular weight (ranging from 180 to 130kDa) were observed in 3D cultures of PCL/RAD and RAD (in all media composition) and PCL in chondrogenic conditions. Remarkably, COL2 was only detected in PCL/RAD and RAD construct cultured with chondrogenic medium, correlating with gene expression results (see Figure 4.3.3 B). COL10 protein expression was detected in all samples, both 2D cultures and 3D constructs, which correlates with the expression patterns obtained by real time RT-PCR (see Figure 4.3.3 E).

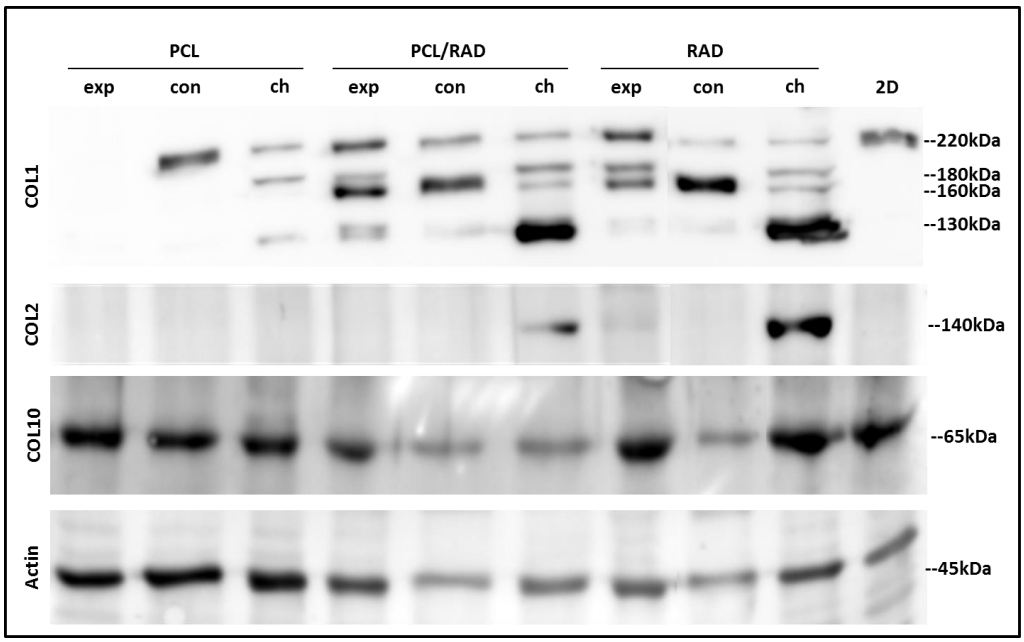

Figure 6.3.4. Protein expression characterization of articular chondrocytes (ACs) cultured in monolayer and in the 3D scaffolds after 4 weeks of culture. Western blot results of collagen type I (COL1), collagen type II (COL2), and collagen type X (COL10) when ACs were maintained in expansion (exp), control (con) and chondrogenic (ch) media in the different scaffolds (PCL, PCL/RAD and RAD) and in monolayer (2D). Actin expression was used as an internal control. Samples were prepared in triplicate.

Furthermore, ACs constructs were stained with toluidine blue to asses qualitatively the production of glycosaminoglycans (GAGs) by the cells (Figure 4.3.4). Constructs cultured with chondrogenic medium became highly blue stained, indicating a significant production and accumulation of GAGs. Constructs cultured with expansion media showed less staining for GAGs than previous ones and finally, those cultured in control media were relatively weak stained.

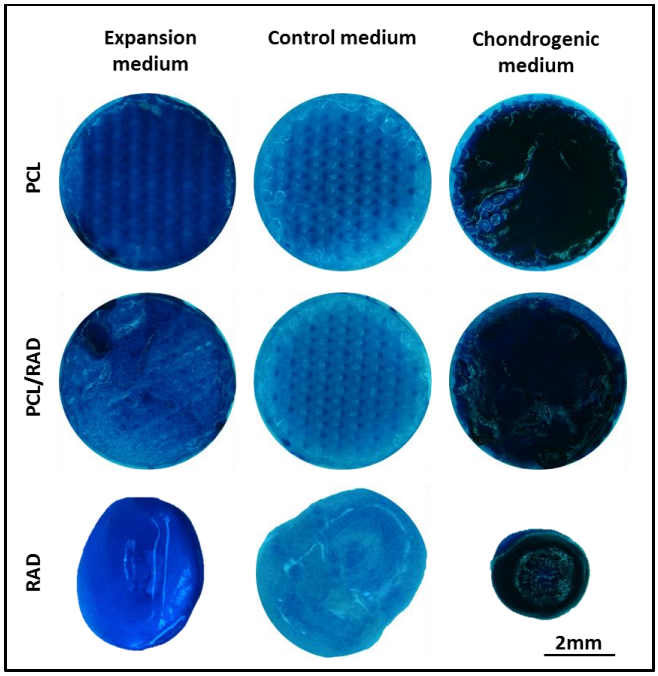

Figure 6.3.5. Toluidine blue staining of articular chondrocytes (ACs) 3D constructs after 4 weeks of culture. ACs seeded into PCL, PCL/RAD and RAD scaffolds cultured in expansion, control and chondrogenic media.

An additional insight was provided at microscopic level by scanning electron microscopy (SEM). SEM images from the different culture conditions of ACs were obtained in order to evaluate the morphology of the cells and their interaction with the different scaffolds (Figure 4.3.5). ACs in PCL scaffolds appeared elongated, growing onto the surface of PCL fibers and, interestingly, more fibers were observed under chondrogenic conditions probably due to an increase in the ECM components secretion. Regarding PCL/RAD constructs, cells appeared to be well attached to the PCL fibers, with a more spherical shape than PCL alone. Finally, ACs cultured in RAD scaffolds present in general a spherical morphology and more cellular density due to the construct condensation occurred during the culture (see Figure 4.3.2 B).

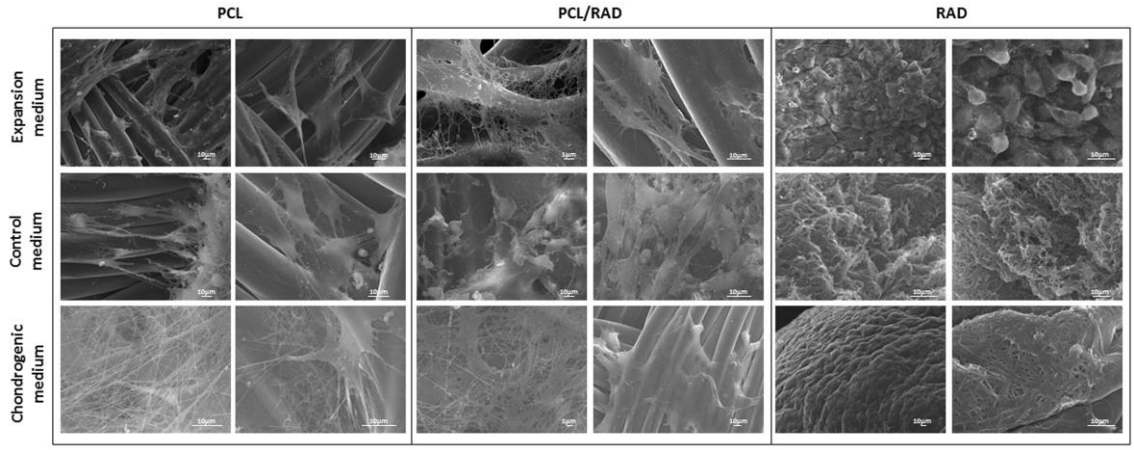

Figure 6.3.6. Scanning Electron Microscopy (SEM) images of Articular Chondrocytes (ACs) cultured in 3D scaffolds after 4 weeks. ACs were seeded into PCL, PCL/RAD and RAD scaffolds and cultured with expansion, control and chondrogenic media. Two images per condition were shown.

6.3.4 MECHANICAL CHARACTERIZATION

Viscoelastic properties of the scaffolds alone and its ACs seeded constructs were assessed by dynamic mechanical analysis (DMA) (see Chapter 2, Materials and Methods). Moreover, 3D constructs at 4 weeks of culture were compared to native articular cartilage (Figure 4.3.6). Regarding the elastic component (G', storage modulus), native articular cartilage from chicken and calf displayed significantly higher storage values than the 3D scaffolds and constructs studied (Figure 4.3.6 A). No significant differences were observed in G' between scaffolds and constructs groups. The viscous component (G'', loss modulus) presented a similar tendency as G': calf native cartilage differed from all the studied 3D scaffolds and chicken articular cartilage only presented differences with cellular PCL scaffolds (Figure 4.3.6 B). All samples presented G' values much higher than G'' values meaning that the measured material was more elastic than viscous. Therefore, as the complex modulus (G*) is the sum of both components, in this case, G* basically corresponds to the elastic component and, therefore, presented the same pattern as the G' (Figure 4.3.6 C). Finally, a different tendency was observed in tan(delta), which gives us an idea of the full mechanical response of the material (Figure 4.3.6 D). The studied scaffold and constructs were closely related to native articular cartilage; except in the case of RAD chondrogenic constructs with calf articular cartilage where differences exist. Moreover, statistical differences could be observed between PCL/RAD and RAD constructs when the same medium was used. Therefore, the combination of PCL scaffolds and RAD16-I hydrogel changed their viscoelastic nature after 4 weeks of culture with ACs, as reflected in the increase of tan(delta) values of the composite PCL/RAD compared to RAD scaffolds alone. This effect was not present between the composites PCL/RAD and the PCL scaffolds groups. Moreover, there were no differences between cellularized and acellular PCL scaffolds, but surprisingly, there were significant differences between PCL/RAD scaffold and PCL/RAD with cells in expansion

and chondrogenic media. Moreover, cellularized PCL/RAD scaffolds reached equivalent tan(delta) values to native articular cartilage. This fact might indicate that the combination of scaffolds and cells provide the optimal working conditions in this particular configuration.

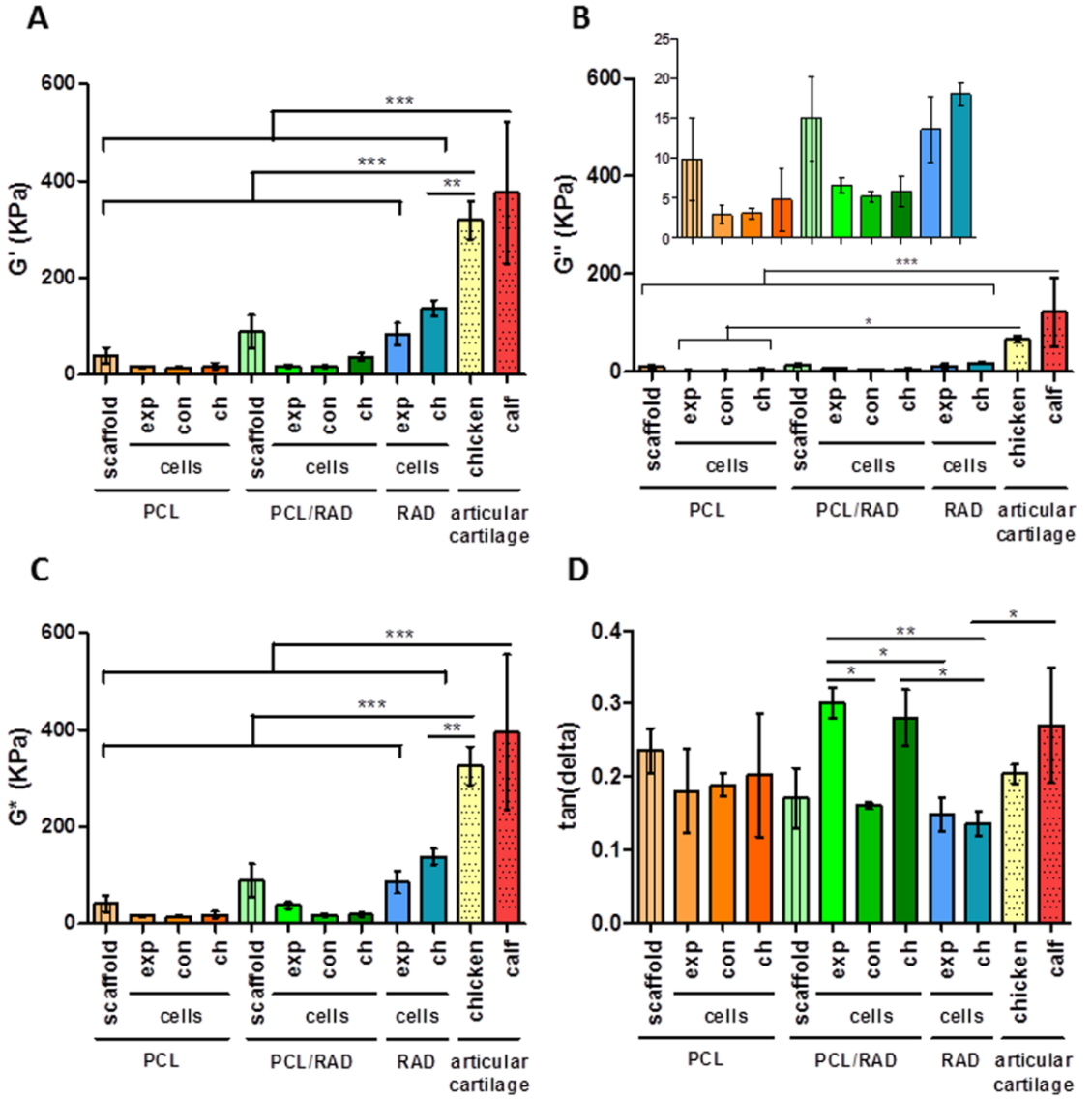

Figure 6.3.7. Mechanical characterization of PCL-based scaffolds and articular chondrocytes (ACs) 3D constructs after 4 weeks of culture. (A) Storage modulus (G') measures the sample's elastic behavior. (B) Loss modulus (G'') measures the viscous response of the material. (C) Complex modulus (G*) is the sum of storage and loss modulus. (D) Tan(delta) is the ratio of the loss to the storage. PCL scaffold and PCL/RAD composite scaffold refers to the acellular scaffold. 3D ACs constructs cultured in expansion (exp), control (con) and chondrogenic (ch) media. Small pieces of articular cartilage of chicken and calf were measured in the same conditions (Statistical differences are indicated as: * for $p<0.05$, ** for $p<0.01$, and *** for $p<0.001$, One-way ANOVA, N=2 n=3).

6.4 DISCUSSION

In the work presented in this chapter, two well-established scaffolds were combined to create a new composite biomaterial with novel biomechanical and biological properties for CTE applications. A 3D woven PCL scaffold and the RAD16-I self-assembling peptide nanofiber hydrogel were selected based on their reported properties in extended 3D culture studies[14,18]. This approach provides biomimetic mechanical properties from the PCL scaffold and biological/chemical stimulation from the hydrogel RAD16-I in the composite matrix. In particular, the developed PCL/RAD scaffold was used to assess the capacity of the composite to reestablish the chondrogenic phenotype of expanded dedifferentiated human ACs. Chondrocyte dedifferentiation following monolayer expansion has been a perpetual limitation in the use of primary chondrocytes for tissue engineering, but has not been tested in PCL scaffolds previously. In earlier studies, both biomaterials were used independently as scaffolds for *in vitro* culture studies[49,50]. Moreover, the woven PCL scaffold has been previously infiltrated with other biomaterials, such as fibrin or Matrigel, to enhance its functionality[13,35,51]. However, it is important to note that different gel matrices may have different biological or biomechanical properties, particularly in combination with a 3D fiber structure. For example, Matrigel has been shown to be conducive to chondrogenic induction of mesenchymal stem cells (MSCs), but may contain components that induce an immunogenic response[52]. Conversely, IPN hydrogels possess extremely tough mechanical properties and their composition is well-defined, but may influence cell proliferation and metabolic activity[53]. Therefore, using this general approach, a new composite scaffold incorporating both micro- and nano-scale features was developed and evaluated to foster chondrogenesis.

Due to high wettability properties of the PCL scaffold (Figure 4.3.1 A&B), RAD16-I peptide combined with cells was easily introduced between the interweaving fibers of the scaffold. A comparative study was performed in order to contrast the properties of each scaffold alone (3D woven PCL scaffold or RAD16-I self-assembling peptide) and the corresponding composite (PCL/RAD). Moreover, three culture media compositions were evaluated (expansion, control and chondrogenic) to study the response of ACs to different conditions. In general, good performance was observed in all the conditions studied, but some important differences were detected. Viability results showed the lowest values in constructs cultured in control medium (Figure 4.3.2), which is expected due to the lack of growth factors or serum in the medium (see Chapter 2, Materials and Methods). In terms of gene expression profile, significant differences were observed between expansion and chondrogenic media (Figure 4.3.3). As expected, the chondrogenic factors added to the medium induced an apparently chondrogenic phenotype with combined expressions of the different collagens studied[54]. Regarding the scaffold system, the presence of RAD16-I peptide (in the composite or alone) enhanced the expression of cartilage markers as evidenced by up-regulation of *COL2* and *ACAN* and maintenance of *SOX9* compared to 2D culture levels. However, *COL1* and *COL10* were also upregulated which could indicate a partial redifferentiation and a possible mechanism of presumptive hypertrophy. In

terms of protein expression, COL1 presented different band patterns between samples, suggesting a possible protein maturation process[55]. Considering the expected size for mature COL1 (139kDa for α1 chain and 129kDa for α2 chain), the scaffolds containing RAD16-I (composite or alone) under chondrogenic induction expressed higher quantity of the mature COL1 (130-140kDa) compared to other conditions tested (Figure 6.3.4). This result indicates that COL1 protein was processed differentially by influence of the medium composition and the scaffold system, and only under specific conditions the final mature product was obtained contributing to the formation of a more physiological matrix composition/structure. It should be emphasized that COL2, characteristic of chondrogenic differentiation, was only detected in PCL/RAD and RAD scaffolds cultured with chondrogenic medium, which suggest that the expression of this characteristic cartilage protein expression was due to the presence of RAD16-I hydrogel in the matrix. Curiously, these two construct systems also present the most severe degraded profile of COL1, which could indicate the presence of some mechanism to increase the ratio of COL2/COL1, a characteristic of cartilage tissue. Toluidine blue staining evidenced the synthesis and accumulation of some considerable amounts of proteoglycans, presumably aggrecan (or others unidentified), favored under chondrogenic conditions (Figure 4.3.4). Expansion and control media did not promote such level of staining, which suggest that dedifferentiated ACs do not rexpress the differentiated phenotype without chondrogenic inducers in the medium[30].

Further, the mechanical testing revealed that PCL-based constructs (PCL and PCL/RAD with cells) after 4 weeks of culture retained the same viscoelasticity displayed by PCL scaffolds alone (Figure 4.3.6). Previous work has clearly shown that this 3D woven PCL scaffold demonstrates multidirectional biomechanical behavior that mimics the anisotropy of native articular cartilage, whereas typical scaffolds used for cartilage tissue engineering are limited to isotropic biomechanical properties[13,14,33,34]. Furthermore, mechanical characterization of these scaffolds has shown that key compressive, tensile, and shear properties closely match the reported values of native cartilage. In contrast, initial values of the RAD16-I scaffold alone could not be measured under the same conditions due to the soft nature of the peptide. However, previous studies described that the concentration at which ACs were seeded initially (0.15% (w/v) RAD16-I) corresponds to 100Pa[56]. This indicates that the mechanical properties of the constructs were evolving during culture time, ending with a stiffer and compacted structure (~100kPa). RAD16-I scaffold provides a soft and permissive microenvironment where cells can extend different cellular processes as they elongate and form networks, leading to the spontaneous contraction of the 3D construct and changing the initial viscoelastic properties. Finally, due to the disparity in mechanical properties presented among constructs types at 4 weeks of culture (PCL, PCL/RAD and RAD), the measurement conditions settings were adjusted to obtain comparable data from different scaffold platforms (see Chapter 2, Materials and Methods). Interestingly, at the end of the culture, all the constructs tested seems to present a behavior compatible to systems undergoing chondrogenesis, since the viscoelastic nature (tan(delta)=G''/G') was similar to native articular cartilage. However,

significant differences exists in the elastic component (G'), since the obtained values in the 3D cultures differ several folds from measured native cartilage. It is known that the surrounding microenvironment determines cell growth and differentiation, since cells have the ability to actively sense and react to the properties of the ECM[57,58]. Therefore, mechanical properties of 3D scaffolds have significant influence on regulating cell activities and controlling these properties has a key role in future applications of engineered constructs[59,60]. We consider the composite scaffold to be biomimetic because the inclusion of the PCL reinforcement provides functional mechanical properties closer to cartilage than RAD16-I hydrogel alone. It is true that the PCL does prevent the interpenetrating RAD16-I from cell-mediated contraction, which could be one reason why in RAD16-I alone cells condensate mimicking mesenchymal condensation and, as a consequence, increasing cell density and ECM concentration which ends in higher G' and G'' values.

These results propose a novel 3D composite scaffold, which is designed to mimic the cartilage matrix, to promote redifferentiation of dedifferentiated human ACs under induction conditions. The nanoscale microenvironment provided by RAD16-I scaffold and the microscale mechanical properties provided by fibers of PCL represent a realistic approach, aiming to recreate a transient complex 3D architecture found in native cartilage. Previous studies have reported the successful combination of PCL with other materials such as fibrin, alginate and poly-acrylamide[33–35]. Here, we hypothesized that the synergistic properties obtained by the combination of the woven PCL scaffolds with the self- assembling peptides for CTE would significantly improve the biological as well as biomechanical properties of engineered cartilage constructs. Moreover, the developed composite could have advantages when used in the context of defect implant in an acute injure scenario, basically due to the biomimetic initial mechanical properties provided by the reinforcing PCL component.

6.5 CONCLUDING REMARKS

- A new synthetic composite scaffold was obtained by infiltrating a 3D woven PCL scaffold with the RAD16-I self-assembling peptide hydrogel containing cells (ACs). While the woven microfiber PCL scaffold provides mechanical support, the nanofibers of RAD16-I peptide facilitate cell attachment and growth, resulting into a multi-scale biomimetic scaffold for CTE applications.

- The *in vitro* 3D culture of dedifferentiated human ACs demonstrated that the new composite supports cell survival and promotes the reestablishment of the chondrogenic lineage commitment.

- The expression of specific mature cartilage markers at both protein and gene expression levels suggested that the presence of RAD16-I enhanced chondrogenic lineage commitment (composite PCL/RAD and RAD16-I). The microenvironment provided to the embedded chondrocytes aims to resemble the native ECM by mimicking mechanical and biological requirements of cartilage tissue.

- The mechanical properties at the end of the culture of 3D constructs were closely related to native cartilage. Therefore, this composite scaffold may provide a 3D culture platform for future therapeutic applications for cartilage repair or regeneration.

6.6 REFERENCES

1. Hunziker, E. B. Articular cartilage repair: basic science and clinical progress. A review of the current status and prospects. *Osteoarthr. Cartil.* **10,** 432–463 (2002).
2. Chiang, H. & Jiang, C. Repair of articular cartilage defects: review and perspectives. *J. Formos. Med. Assoc.* **108,** 87–101 (2009).
3. Chung, C. & Burdick, J. Engineering Cartilage Tissue. *Adv Drug Deliv Rev.* **60,** 243–62 (2008).
4. Kock, L., Van Donkelaar, C. C. & Ito, K. Tissue engineering of functional articular cartilage: The current status. *Cell Tissue Res.* **347,** 613–627 (2012).
5. Hunziker, E. B., Lippuner, K., Keel, M. J. B. & Shintani, N. An educational review of cartilage repair: precepts & practice - myths & misconceptions - progress & prospects. *Osteoarthritis Cartilage* **23,** 334–350 (2014).
6. Johnstone, B. *et al.* Tissue engineering for articular cartilage repair--the state of the art. *Eur. Cell. Mater.* **25,** 248–67 (2013).
7. Asnaghi, M. A. *et al.* Trends in biomedical engineering: focus on Regenerative Medicine. *J. Appl. Biomater. Biomech.* **9,** 73–86 (2011).
8. Castells-sala, C. *et al.* Current Applications of Tissue Engineering in Biomedicine. *Biochips & Tissue chips* **S2:004,** (2013).
9. Cucchiarini, M. *et al.* A vision on the future of articular cartilage repair. *Eur. Cell. Mater.* **27,** 12–6 (2014).
10. Griffith, L. G. & Swartz, M. a. Capturing complex 3D tissue physiology in vitro. *Nat. Rev. Mol. Cell Biol.* **7,** 211–24 (2006).
11. Guilak, F., Butler, D. L., Goldstein, S. A. & Baaijens, F. P. T. Biomechanics and mechanobiology in functional tissue engineering. *J. Biomech.* **47,** 1933–1940 (2014).
12. Yoon, D. M. & Fisher, J. P. Chondrocyte signaling and artificial matrices for articular cartilage engineering. *Adv. Exp. Med. Biol.* **585,** 67–86 (2006).
13. Moutos, F. T. & Guilak, F. Composite scaffolds for cartilage tissue engineering. *Biorheology* **45,** 501–512 (2008).
14. Moutos, F. T., Freed, L. E. & Guilak, F. A biomimetic three-dimensional woven composite scaffold for functional tissue engineering of cartilage. *Nat. Mater.* **6,** 162–167 (2007).
15. Huang, M. H., Li, S., Hutmacher, D. W., Coudane, J. & Vert, M. Degradation characteristics of poly(E-caprolactone)-based copolymers and blends. *J. Appl. Polym. Sci.* **102,** 1681–1687 (2006).
16. Rohner, D., Hutmacher, D. W., Cheng, T. K., Oberholzer, M. & Hammer, B. In vivo efficacy of bone-marrow-coated polycaprolactone scaffolds for the reconstruction of orbital defects in the pig. *J. Biomed. Mater. Res. B. Appl. Biomater.* **66,** 574–580 (2003).
17. Zhang, S. Fabrication of novel biomaterials through molecular self-assembly. *Nat. Biotechnol.* **21,** 1171–8 (2003).

18. Semino, C. E. Self-assembling Peptides: From Bio-inspired Materials to Bone Regeneration. *J. Dent. Res.* **87,** 606–616 (2008).

19. Matson, J. B. & Stupp, S. I. Self-assembling peptide scaffolds for regenerative medicine. *Chem. Commun.* **48,** 26 (2012).

20. Semino, C. E. Can We Build Artificial Stem Cell Compartments? *J. Biomed. Biotechnol.* **2003,** 164–169 (2003).

21. Garreta, E., Genové, E., Borrós, S. & Semino, C. E. Osteogenic Differentiation of Mouse Embryonic Stem Cells and Mouse Embryonic Fibroblasts in a Three-Dimensional. *Tissue Eng Part A* **12,** 2215–2227 (2006).

22. Wu, J. *et al.* Nanometric self-assembling peptide layers maintain adult hepatocyte phenotype in sandwich cultures. *J. Nanobiotechnology* **8,** 29 (2010).

23. Semino, C. E., Kasahara, J. & Hayashi, Y. Entrapment of Migrating Hippocampal Neural Cells in Three-Dimensional Peptide Nanofiber Scaffold. *Tissue Eng Part* **10,** (2004).

24. Sieminski, a L., Semino, C. E., Gong, H. & Kamm, R. D. Primary sequence of ionic self-assembling peptide gels affects endothelial cell adhesion and capillary morphogenesis. *J. Biomed. Mater. Res. A* **87,** 494–504 (2008).

25. Dégano, I. R. *et al.* The effect of self-assembling peptide nanofiber scaffolds on mouse embryonic fibroblast implantation and proliferation. *Biomaterials* **30,** 1156–65 (2009).

26. Alemany-Ribes, M., García-Díaz, M., Busom, M., Nonell, S. & Semino, C. E. Toward a 3D Cellular Model for Studying In Vitro the Outcome of Photodynamic Treatments: Accounting for the Effects of Tissue Complexity. *Tissue Eng. Part A* (2013). doi:10.1089/ten.TEA.2012.0661

27. Marí-Buyé, N., Luque, T., Navajas, D. & Semino, C. Development of a three-dimensional bone-like construct in a soft self-assembling peptide matrix. *Tissue Eng Part A* **19,** 870–881 (2013).

28. Semino, C. E. Can we build artificial stem cell compartments? *J. Biomed. Biotechnol.* **3,** 164–169 (2003).

29. Genové, E. *et al.* Functionalized self-assembling peptide hydrogel enhance maintenance of hepatocyte activity in vitro. *J. Cell. Mol. Med.* **13,** 3387–97 (2009).

30. Fernández-Muiños, T. *et al.* Bimolecular based heparin and self-assembling hydrogel for tissue engineering applications. *Acta Biomater.* **16,** 35–48 (2015).

31. Genove, E., Shen, C., Zhang, S. & Semino, C. E. The effect of functionalized self-assembling peptide scaffolds on human aortic endothelial cell function. *Biomaterials* **26,** 3341–3351 (2005).

32. Freed, L. E., Engelmayr, G. C., Borenstein, J. T., Moutos, F. T. & Guilak, F. Advanced Material Strategies for Tissue Engineering Scaffolds. *Adv. Mater.* **21,** 3410–3418 (2009).

33. Valonen, P. K. *et al.* In vitro generation of mechanically functional cartilage grafts based on adult human stem cells and 3D-woven poly(ε-caprolactone) scaffolds. *Biomaterials* **31,** 2193–2200 (2010).

34. Moutos, F. T. & Guilak, F. Functional properties of cell-seeded three-dimensionally woven poly(epsilon-caprolactone) scaffolds for cartilage tissue engineering. *Tissue Eng. Part A* **16,** 1291–1301 (2010).

35. Liao, I. C., Moutos, F. T., Estes, B. T., Zhao, X. & Guilak, F. Composite three-dimensional woven scaffolds with interpenetrating network hydrogels to create functional synthetic articular cartilage. *Adv. Funct. Mater.* **23,** 5833–5839 (2013).

36. Fernández-Muiños, T., Suárez-Muñoz, M., Sanmartí-Espinal, M. & Semino, C. E. Matrix dimensions, stiffness, and structural properties modulate spontaneous chondrogenic commitment of mouse embryonic fibroblasts. *Tissue Eng. Part A* **20,** 1145–55 (2014).

37. Quintana, L. *et al.* Early tissue patterning recreated by mouse embryonic fibroblasts in a three-dimensional environment. *Tissue Eng. Part A* **15,** 45–54 (2009).

38. Bussmann, B. M. *et al.* Chondrogenic potential of human dermal fibroblasts in contractile solft self-assembling peptide hydrogel. *J. Tissue Eng. Regen. Med.* (2013).

39. Brittberg, M. *et al.* Treatment of deep cartilage defects in the knee with autologous chondrocyte transplantation. *N Engl J Med* **331,** 889–895 (1994).

40. Lefebvre, V., Peeters-Joris, C. & Vaes, G. Production of collagens, collagenase and collagenase inhibitor during the dedifferentiation of articular chondrocytes by serial subcultures. *Biochim Biophys Acta* **1051,** 266–275 (1990).

41. Darling, E. M. & Athanasiou, K. A. Rapid phenotypic changes in passaged articular chondrocyte subpopulations. *J. Orthop. Res.* **23,** 425–432 (2005).

42. Lee, S.-H. & Shin, H. Matrices and scaffolds for delivery of bioactive molecules in bone and cartilage tissue engineering. *Adv. Drug Deliv. Rev.* **59,** 339–59 (2007).

43. Girotto, D. *et al.* Tissue-specific gene expression in chondrocytes grown on three-dimensional hyaluronic acid scaffolds. *Biomaterials* **24,** 3265–3275 (2003).

44. Miot, S. *et al.* Effects of scaffold composition and architecture on human nasal chondrocyte redifferentiation and cartilaginous matrix deposition. *Biomaterials* **26,** 2479–2489 (2005).

45. Kim, M., Kim, S. E., Kang, S. S., Kim, Y. H. & Tae, G. The use of de-differentiated chondrocytes delivered by a heparin-based hydrogel to regenerate cartilage in partial-thickness defects. *Biomaterials* **32,** 7883–96 (2011).

46. Grad, S., Ph, D., Gogolewski, S. & Sci, D. Effects of Simple and Complex Motion Patterns on Gene Expression of Chondrocytes Seeded in 3D Scaffolds. **12,** (2006).

47. Recha-Sancho, L. & Semino, C. E. Heparin based self-assembling peptide scaffold reestablish chondrogenic phenotype of expanded de-differentiated human chondrocytes. *J. Biomed. Mater. Res. Part A* **104,** 1694–1706 (2016).

48. Cals, F. L. J., Hellingman, C. A., Koevoet, W., Baatenburg de Jong, R. J. & van Osch, G. J. V. M. Effects of transforming growth factor-β subtypes on in vitro cartilage production and mineralization of human bone marrow stromal-derived mesenchymal stem cells. *J. Tissue Eng. Regen. Med.* **6,** 68–76 (2012).

49. N. Garcia-Giralt, R. Izquierdo, X. Nogués, M. Perez-Olmedilla, P. Benito, J. L. G.-R. & M. A. Checa, J. Suay, E. Caceres, J. C. M. A porous PCL scaffold promotes the human chondrocytes redifferentiation and hyaline-specific extracellular matrix protein synthesis. *J. Biomed. Mater. Res. A* **85,** 1082–9 (2008).

50. Kisiday, J. *et al.* Self-assembling peptide hydrogel fosters chondrocyte extracellular matrix production and cell division: implications for cartilage tissue repair. *Proc. Natl.*

Acad. Sci. U. S. A. **99,** 9996–10001 (2002).

51. Moutos, F. T., Estes, B. T. & Guilak, F. Multifunctional Hybrid Three-dimensionally Woven Scaffolds for Cartilage Tissue Engineering. *Macromol. Biosci.* **10,** 1355–1364 (2010).

52. Li, Q. *et al.* Proteomic analysis of naturally-sourced biological scaffolds. *Biomaterials* **75,** 37–46 (2016).

53. Darnell, M. *et al.* Performance and Biocompatibility of Extremely Tough Alginate/ Polyacrylamide Hydrogels. *Biomaterials* **34,** 8042–8048 (2013).

54. Baugé, C., Girard, N., Lhuissier, E., Bazille, C. & Boumediene, K. Regulation and Role of TGFβ Signaling P athway in Aging and Osteoarthritis Joints. *Aging Dis.* **5,** 394–405 (2014).

55. Bobick, B. E., Chen, F. H., Le, A. M. & Tuan, R. S. Regulation of the chondrogenic phenotype in culture. *Birth Defects Res. Part C - Embryo Today Rev.* **87,** 351–371 (2009).

56. Sieminski, a. L., Was, a. S., Kim, G., Gong, H. & Kamm, R. D. The Stiffness of Three-dimensional Ionic Self-assembling Peptide Gels Affects the Extent of Capillary-like Network Formation. *Cell Biochem. Biophys.* **49,** 73–83 (2007).

57. Discher, D. E., Janmey, P. & Wang, Y.-L. Tissue cells feel and respond to the stiffness of their substrate. *Science* **310,** 1139–43 (2005).

58. Engler, A. J., Sen, S., Sweeney, H. L. & Discher, D. E. Matrix elasticity directs stem cell lineage specification. *Cell* **126,** 677–89 (2006).

59. Nava, M. M., Raimondi, M. T. & Pietrabissa, R. Controlling Self-Renewal and Differentiation of Stem Cells via Mechanical Cues. **2012,** (2012).

60. Nava, M. M. *et al.* Interactions between structural and chemical biomimetism in synthetic stem cell niches. *Biomed. Mater.* **10,** 015012 (2015).

CONCLUSIONS

Bi-component scaffolds

- Two novel biomaterials for cartilage tissue engineering (CTE) applications were developed: the RAD/CS and RAD/Decorin bi-component scaffolds. They showed good chemical and structural stability forming nanofiber composite self-assembling scaffolds.

- These new biomaterials together with the previous developed RAD/Heparin composite scaffold could be used to bind and release significant quantities of TGFβ1, an essential growth factor (GF) present in the chondrogenic medium composition. Nevertheless, no significant differences were observed between bi-component scaffolds and the control scaffold RAD16-I.

- In terms of GF presentation to the specific cell membrane receptor, we suggest that GF-receptor interaction is more physiological when the polysaccharide/proteoglycan (heparin, CS and Decorin) are present in the scaffold. This could explain why in the bi-component scaffolds better chondrogenesis performance was obtained.

- The chondrogenic potential of the three bi-component scaffolds (RAD/Heparin, RAD/CS and RAD/Decorin) was studied with two different cell lines from human origin: adipose-derived stem cells (ADSCs) and dedifferentiated articular chondrocytes (ACs) and interesting differences were observed between cell types.

- ACs dedifferentiated after monolayer expansion, downregulating progressively (over passages) the expression of chondrogenic and hypertrophic specific markers.

- ADSCs and dedifferentiated ACs cultured in the bi-component scaffolds elongated, created a cellular network and remodeled the matrix over culture time changing the construct morphology.

- Viability of ADSCs was compromised after 4 weeks of culture under control medium conditions; however, chondrogenic medium and the presence of heparin in the scaffold enhanced cell survival. In contrast, ACs presented good viability in the three bi-component scaffolds and in the different culture conditions.

- The expression of specific mature cartilage markers at protein and gene levels evidenced a favored microenvironment for chondrogenesis in the three bi-component scaffolds. The redifferentiation process of expanded dedifferentiated ACs and the chondrogenic commitment of ADSCs were enhanced under inductive conditions and by the presence of heparin, CS or Decorin molecules in the scaffold.

- 3D constructs under chondrogenic medium conditions evolved during culture time into a compacted and stiffer structures, showing viscoelastic properties compatible to a system undergoing chondrogenesis. Interestingly, ADSCs constructs were more closely related to chicken or calf native articular cartilage than ACs constructs.

PCL/RAD composite scaffolds

- A new synthetic composite scaffold was obtained by infiltrating a 3D woven poly (ε-caprolactone) (PCL) scaffold with the RAD16-I self-assembling peptide hydrogel containing cells (ACs). While the woven microfiber PCL scaffold provides mechanical support, the nanofibers of RAD16-I peptide facilitate cell attachment and growth, resulting into a multi-scale biomimetic scaffold for CTE applications.

- The *in vitro* 3D culture of dedifferentiated human ACs demonstrated that the new composite supports cell survival and promotes the reestablishment of the chondrogenic lineage commitment.

- The expression of specific mature cartilage markers at both protein and gene expression levels suggested that the presence of RAD16-I enhanced chondrogenic lineage commitment (composite PCL/RAD and RAD16-I). The microenvironment provided to the embedded chondrocytes aims to resemble the native extracellular matrix by mimicking mechanical and biological requirements of cartilage tissue.

- The mechanical properties at the end of the culture of 3D constructs were closely related to native cartilage. Therefore, this composite scaffold may provide a 3D culture platform for future therapeutic applications for cartilage repair or regeneration.

CONCLUSIONES

Matrices bi-compuestas

- Se han desarrollado dos nuevos biomaterials para aplicaciones de ingeniería de tejidos en la reparación de cartílago: las matrices bi-compuestas de RAD/condroitin sulfato y RAD/decorina. Estas matrices muestran buena estabilidad química y estructural, de modo que se forman nanofibras en matrices auto-ensamblantes compuestas.

- Se ha demostrado que tanto los nuevos biomaterials como la matriz compuesta de RAD/Heparina previamente desarrollada, unen y liberan cantidades significativas de TGFβ1, un factor de crecimiento esencial presente en el medio condrogénico. Sin embargo, no se detectaron diferencias significativas entre las matrices compuestas y la matriz control de RAD16-I.

- Sugerimos que la presencia del polisacárido/proteoglicano (heparina, condroitin sulfato y decorina) en la matriz aporta una presentación de factores de crecimiento mucho más parecida a la fisiológica que conlleva una mejora en la interacción con el receptor de membrana, obteniendo por tanto una mejor respuesta condrogénica en las matrices compuestas.

- El potencial condrogénico de las tres matrices bi-compuestas (RAD/Heparina, RAD/CS y RAD/Decorina) fue estudiado en dos líneas celulares diferentes de origen humano (células madre derivadas de tejido adiposo y condrocitos articulares) y se observaron diferencias interesantes entre los tipos celulares.

- Se ha demostrado que los condrocitos articulares humanos se desdiferencian después de una expansión en monocapa, dado que la expresión de marcadores condrogénicos e hipertróficos disminuye progresivamente (con los pasajes).

- Las células madre derivadas de tejido adiposo y los condrocitos desdiferenciados cultivados en las matrices bi-compuestas se alargan, crean redes interconectadas y remodelan la matriz a lo largo del cultivo cambiando su morfología y la del constructo.

- La viabilidad de las células madre derivadas de tejido adiposo se ve comprometida después de 4 semanas de cultivo en medio control; sin embargo, el medio condrogénico y la presencia de heparina en la matriz promueven la supervivencia celular. En cambio, los condrocitos articulares presentan buena viabilidad en las tres matrices bi-compuestas y en las diferentes condiciones de cultivo.

- La expresión de marcadores específicos de cartílago a nivel génico y proteico evidencian que las tres matrices bi-compuestas aportan un microambiente favorecedor para la condrogénesis. La presencia de moléculas de heparina, CS o decorina en la matriz y el medio de inducción favorecen el proceso de rediferenciación de los condrocitos articulares y la diferenciación condrogénica de células madre derivadas de tejido adiposo.

- Los constructos tridimensionales cultivados en medio condrogénico evolucionan, durante el tiempo de cultivo, a estructuras más rígidas y compactas, mostrando unas propiedades viscoelásticas compatibles con un sistema condrógenico. De forma interesante, los constructos de células madre derivadas de tejido adiposo se semejan más a nivel mecánico a tejido de cartílago articular que los constructos de condrocitos.

Matrices compuestas por PCL/RAD

- Se ha desarrollado un nuevo material compuesto introduciendo el hidrogel RAD16-I con células en el interior de los poros de una matriz 3D de policaprolactona (PCL). Mientras que las microfibras entrelazadas de PCL confieren soporte mecánico, las nanofibras del péptido auto-ensamblante RAD16-I facilitan la adhesión y el crecimiento celular. El resultado es un material biomimético que puede ser utilizado para aplicaciones de ingeniería de tejidos en el área de cartílago.

- El nuevo material es capaz de mantener la viabilidad celular y promover el restablecimiento del linaje condrogénico en condrocitos humanos, proporcionando por tanto un material prometedor para el desarrollo de una estrategia para la regeneración de cartílago.

- La expresión de marcadores específicos de cartílago tanto a nivel génico como proteico sugiere que la presencia del péptido RAD16-I mejora la diferenciación de las células a un linaje condrogénico. El microambiente proporcionado a los condrocitos pretende mimetizar el tejido nativo de la matriz extracelular de los condrocitos.

- La combinación de PCL con el RAD16-I permite el mantenimiento del fenotipo celular y el desarrollo de unas propiedades mecánicas muy parecidas al tejido nativo de cartílago. Así pues, este material compuesto resulta ser prometedor para el desarrollo de una plataforma de cultivo 3D para futuras aplicaciones terapéuticas en la reparación o regeneración de cartílago.

PUBLICATIONS

RESEARCH ARTICLES FROM THIS THESIS

- Fernández-Muiños T*, Recha-Sancho L*, Lopez-Chicon P, Castells-Sala C, Mata A, Semino CE. Bimolecular based heparin and self-assembling hydrogel for tissue engineering applications. *Acta Biomaterialia*. **16**, 35-48 (2015).

- Recha-Sancho L and Semino CE. Heparin based self-assembling peptide scaffold reestablish chondrogenic phenotype of expanded de-differentiated human chondrocytes. *J Biomed Mater Res Part A*. **104**, 1694-706 (2016).

- Recha-Sancho L and Semino CE. Chondroitin Sulfate- and Decorin-based self-assembling scaffolds for cartilage tissue engineering. *Plos One*. **11**(6):e0157603 (2016).

- Recha-Sancho L, Moutos FT, Abellà J, Guilak F and Semino CE. Dedifferentiated human articular chondrocytes redifferentiate to a cartilage-like tissue phenotype in a poly(ε-caprolactone)/self-assembling peptide composite scaffold. *Materials*. **9**(6), 472 (2016).

OTHER RESEARCH ARTICLES

- Castells-Sala C*, Sanchez B*, Recha-Sancho L, Puig V, Bragos R, Semino CE. Influence of electrical stimulation on 3D-cultures of adipose tissue derived progenitor cells (ATDPCs) behavior. *Conf Proc IEEE Eng Med Biol Soc*. 5658–61 (2012).

- Castells-Sala C*, Recha-Sancho L*, Llucià-Valldeperas A, Soler-Botija C, Bayes-Genis A, Semino CE. Three-Dimensional Cultures of Human Subcutaneous Adipose Tissue-Derived Progenitor Cells Based on RAD16-I Self-Assembling Peptide. *Tissue Eng Part C Methods*. **22**, 1–12 (2016).

REVIEW

- Castells-Sala C*, Alemany-Ribes M*, Fernández-Muiños T, Recha-Sancho L, López-Chicón P, Aloy-Reverté C, Caballero-Camino J, Márquez-Gil A, Semino CE. Current Applications of Tissue Engineering in Biomedicine. *J Biochip Tissue Chip*. **S2**, 1–14 (2013).

*Both authors contributed equally to this work